



Developing a Human-Machine Control Interface for the Detection of Motion Intentions in a Self-Balanced Lower-Limb Exoskeleton

Omar Mounir Alaoui

► To cite this version:

Omar Mounir Alaoui. Developing a Human-Machine Control Interface for the Detection of Motion Intentions in a Self-Balanced Lower-Limb Exoskeleton. Robotics [cs.RO]. Sorbonne Université, 2021. English. NNT : 2021SORUS534 . tel-03866856

HAL Id: tel-03866856

<https://theses.hal.science/tel-03866856>

Submitted on 23 Nov 2022

HAL is a multi-disciplinary open access archive for the deposit and dissemination of scientific research documents, whether they are published or not. The documents may come from teaching and research institutions in France or abroad, or from public or private research centers.

L'archive ouverte pluridisciplinaire **HAL**, est destinée au dépôt et à la diffusion de documents scientifiques de niveau recherche, publiés ou non, émanant des établissements d'enseignement et de recherche français ou étrangers, des laboratoires publics ou privés.

WANDERCRAFT



THÈSE

présentée pour obtenir

le titre de docteur délivré par Sorbonne Université

École doctorale: Science Mécanique, Acoustique, Électronique et Robotique de Paris

par

Omar MOUNIR ALAOUI

Developing a Human-Machine Control Interface for the Detection of Motion Intentions in a Self-Balanced Lower-Limb Exoskeleton

Catherine ACHARD
Samer MOHAMMED
Hélène PILLET
Domen NOVAK
Guillaume MOREL
Nathanaël JARRASSÉ
Fabien EXPERT

Professeure des Universités à Sorbonne Université
Professeur des Universités à l'Université Paris-Est Créteil
Professeure des Universités à Arts et Métiers ParisTech
Associate Professor à University of Cincinnati
Professeur des Universités à Sorbonne Université
Chargé de Recherche CNRS à Sorbonne Université
Directeur du Département Mécatronique à Wandercraft

Présidente
Rapporteur
Rapporteuse
Examinatrice
Directeur de thèse
Encadrant
Encadrant

Institut des Systèmes Intelligents et de Robotique (ISIR)
Pyramide Tour 55, 4 place Jussieu
UMR CNRS 7222, Paris, France

Abstract

In the recent years, advancements in robotics-related fields accompanied the development of exoskeletal devices that enhance the physical capabilities of the wearer, or assist impaired individuals in performing specific body movements. In particular, assistive lower-limb exoskeletons can be proposed to impaired people as a possible alternative to wheelchairs, or as rehabilitation medical devices. However, while existing ones can perform a variety of movements – such as walking, turning in place, steering, etc. – the intention detection interfaces are often based on basic solutions that lack intuitiveness, partly monopolize the use of hands, or prevent seamless transitions between the available activity modes.

In this context, this doctoral work investigates natural and intuitive movement-based solutions to robustly detect motion intentions in a marketed assistive lower-limb exoskeleton. It focuses on walking-related intentions – namely gait initiation, gait termination, and steering – and evaluates novel implementations of high-level controllers based on acceleration and angular velocity signals recorded from upper-body-worn Inertial Measurement Units. Signals from these sensors can be analyzed, so that descriptive features of the exhibited movements are extracted, and serve as inputs to a classification architecture: they can either be compared to training data in a supervised learning approach, or to empirically derived thresholds.

For gait initiation, an intention detection interface was built upon a Linear Discriminant Analysis classifier, based on experimental training data recorded from unimpaired individuals exhibiting anticipatory postural adjustments prior to initiating gait. For gait termination, maintained arm swing movements were used to keep the exoskeleton walking. Amplitude and coordination-based features were derived to indicate the state of arm movements, and compared to specific thresholds to detect whether walking should be stopped. An alteration to these movements – by exhibiting an asymmetry in the arm swing amplitude – was used to detect the intention and direction of steering.

Experimental results of these algorithms were obtained from different groups of unimpaired participants using the exoskeleton, along with qualitative results from preliminary tests of the gait termination interface conducted with two impaired patients. These first results indicate that the developed methods could be a viable alternative for intention detection in medical lower-limb exoskeletons, and could greatly enhance their usability.

Keywords: Wearable Robotics, Assistive Exoskeletons, Intention Detection, High-Level Control Interface, Classification Architecture, Inertial Sensors

Résumé

Des avancées technologiques récentes dans les domaines liés à la robotiques ont permis le développement de dispositifs exosquelettes pour l'augmentation des capacités physiques humaines, ou l'assistance aux gestes. En particulier, dans le cas de handicaps moteurs, des exosquelettes d'assistance pour les jambes peuvent être utilisés comme une alternative aux fauteuils roulants, ou pour la rééducation des membres inférieurs. Mais si de tels appareils sont déjà capables de réaliser plusieurs types de mouvements – marche, demi-tours, virages, etc. – les interfaces permettant la détection des intentions sont souvent basées sur des solutions qui ne permettent pas un contrôle intuitif des dispositifs, monopolisent l'usage des mains, et entraînent des transitions d'états non fluides.

Dans ce contexte, ce travail s'appuie sur des solutions naturelles et intuitives basées sur les mouvements du haut du corps, afin de détecter de manière robuste et efficace les intentions de mouvement dans un exosquelette d'assistance à la marche. Il se focalise notamment sur des intentions relatives à la marche – l'initiation, l'arrêt, et les virages – et évalue l'implémentation de contrôleurs haut-niveau basés sur les signaux de centrales inertielles portées au niveau du haut du corps. Ces signaux peuvent être analysés de sorte à ce que des caractéristiques descriptives des mouvements puissent en être extraites, puis utilisées en entrée de diverses architectures de classification – selon des approches d'apprentissage supervisé, ou au travers de comparaisons avec des seuils définis empiriquement.

Pour l'initiation de la marche, une interface de détection d'intentions a été développée sur la base d'un classificateur LDA (*Linear Discriminant Analysis*), et de données d'entraînement issues d'expériences de marche pendant lesquelles des individus ne souffrant pas de handicap moteur ont exhibé des ajustements posturaux anticipatoires avant d'initier le mouvement. Pour l'arrêt de la marche, le maintien d'un mouvement de balancier des bras a été utilisé pour maintenir l'exosquelette en marche. Des caractéristiques indicatives de l'amplitude et de la coordination de ces mouvements ont été calculées, puis comparées à des seuils empiriques pour déterminer si le robot devait être arrêté ou non. Une altération de ces mouvements, définie par une asymétrie de l'amplitude entre les deux bras, a été utilisée pour détecter l'intention de tourner pendant la marche, ainsi que la direction des virages.

Ces algorithmes ont pu être testés expérimentalement, et des résultats ont été obtenus pour des groupes de participants ne présentant pas de handicap moteur. Des résultats qualitatifs avec patients ont également été obtenus pour l'interface d'arrêt de la marche, sur la base d'essais préliminaires. Ces premiers résultats indiquent que les méthodes développées au cours de ce travail de thèse pourraient être utilisées comme une solution efficace et ergonomique pour la détection d'intentions dans un exosquelette de jambes à usage médical.

Mots-Clés: Robotique Wearable, Exosquelettes d'Assistance, Détection d'Intentions, Interface de Contrôle Haut Niveau, Architecture de Classification, Capteurs Inertiels

Acknowledgements

Les quelques mots qui vont suivre sont dédiés à toutes celles et à tous ceux qui m'ont soutenu pendant les quatre années que ma thèse a duré. Car aussi solitaire qu'un tel travail puisse parfois être, il ne se réalise réellement que grâce à l'accompagnement précieux de ceux et celles qui nous entourent. Et parce que statistiquement, les mots les plus lus dans un manuscrit de thèse sont ceux dédiés aux remerciements, je voudrais maintenant m'appliquer à adresser les miens à toutes ces personnes.

Je commence tout naturellement par ceux qui m'ont encadré pendant ces quatre ans. Tout d'abord Guillaume, qui a su me faire confiance, et a accepté de prendre la direction de mes travaux. Bien qu'ayant surtout suivi mes avancements de loin, tu as toujours cru au potentiel de mon sujet, et à ses implications pour le monde de la robotique médicale et des exosquelettes. Merci donc pour tes conseils avisés et pour ton soutien. Merci également à Fabien, qui a pris en charge mon encadrement à Wandercraft. Tu ne savais pas vraiment où tu mettais les pieds quand tu as accepté de m'accompagner sur ce sujet, mais poussé par ta curiosité et ton fort intérêt pour la thématique, tu n'as pas hésité à te lancer dans cette aventure, et à la poursuivre jusqu'au bout avec moi. Merci encore pour ton écoute et ton dévouement. Et enfin, Nathanaël. Je crois que tu dois maintenant savoir tout le plaisir que j'ai eu à travailler avec toi. Tu m'as toujours traité comme un pair avec lequel tu pouvais partager de véritables discussions et réflexions techniques et scientifiques. Tes précieux conseils m'ont toujours guidé pour m'aider à forger mon travail, et à en faire ce qui est présenté tout au long des pages suivantes. Merci pour tout, travailler avec toi va certainement beaucoup me manquer !

Je tiens également à remercier l'ensemble des membres du jury pour leur disponibilité, et pour les précieux échanges que nous avons pu avoir le jour de ma soutenance. Je peux sincèrement dire que j'ai pris plaisir à discuter avec vous, et à répondre à vos nombreuses questions.

Evidemment, quatre années de thèse ne pourraient s'être aussi bien déroulées sans compter sur la présence et le soutien de mes collègues de travail, à Wandercraft, comme en équipe AGATHE.

Aux premi-er-ère-s, je voudrais dire un grand merci de m'avoir accueilli dans une si belle entreprise, où la joie et la bonne humeur vont de pair avec un grand dévouement au travail et au sérieux. Merci notamment à Mathieu Masselin, président de Wandercraft, de m'avoir fait confiance lorsque je l'ai contacté pour la première fois avec l'idée de mon sujet de thèse. Merci également à mes compagnons du lundi gaspacho, Yoann, Adrien, Max, Pierre, et Guillaume, qui ont fini par maîtriser à la perfection le dosage idéal entre une soupe froide, du pain, du fromage, au moins deux types de tartinables, des yaourts Laitière, et des fruits. Enfin, mon passage à Wandercraft n'aurait jamais été le même sans la présence de trois personnes en particulier. Des collègues devenus de véritables amis, sans qui

toute cette expérience eût été bien différente. Merci à vous, Raphy, Guillaume, et Clémence. J'ai hâte de vivre de nouvelles aventures 3b1c avec vous !

Vient donc maintenant le tour de toutes les personnes qui m'ont entouré en équipe AGATHE, à l'ISIR. Merci, bien évidemment, à tou-te-s les permanent-e-s – et je pense notamment à Ludo et Fabien – mais surtout à ceux et celles qui ont fait – ou font encore – partie de la famille nombreuse des non-permanent-e-s. On dit très souvent que le plus important pour un travail de thèse, ça n'est pas tant le sujet, que l'équipe que l'on rejoint. Et vous étiez sans nulle doute la meilleure équipe sur laquelle je pouvais espérer tomber. Merci à vous tou-te-s, Jésus, Jimmy, Éléonore, Étienne, Josh, Charlotte, Clémence, Alexis, Saman, Antoine, Félix, Delphine, et Lucas, et j'adresse une pensée toute particulière pour Rémi, Mathilde, Angelina, Mario, et Mégane, qui ont été les toutes premières personnes que j'ai croisées au laboratoire. Je pens qu'on peut dire qu'avec vous, se sont noués ces liens si particuliers qui unissent des doctorant-e-s ayant embarqué à bord de la même galère. Alors merci d'avoir été là pour cette belle traversée, et d'avoir toujours montré votre soutien à la moindre petite vaguelette.

Après les collègues, il est évidemment temps de remercier tou-te-s mes ami-e-s. Il m'est difficile de citer tout le monde, et je panique à l'idée de pouvoir oublier qui que ce soit si je me lance dans une liste exhaustive. Mais je tiens malgré tout à mentionner deux groupes en particulier, parce qu'ils ont été très présents ces quatre dernières années. Merci, donc, à mes ami-e-s d'enfance : Meryem, Rym, Imane, Nawal, Marouane, Tatim, Yasmine, Zineb, et Adam ; et merci à mes ami-e-s d'École – qui m'ont par ailleurs aidé à relire mon manuscrit pour identifier et corriger les quelques coquilles qui s'y étaient glissées : Pierre, Clara, Alix, Antoine, Diane, Antoine, Dany, Eliot, Émilien, Kevin, Laurane, Marie, Lucas, Momo, Sarah, et Vincent. Merci à toutes ces personnes que j'ai citées, qui m'ont toujours entouré avec un talent incroyable, mêlant des formes variées d'attention et de raillerie à une amitié profonde et sincère. Vous tenez une place importante dans ma vie, il était donc tout naturel que vous puissiez également tenir une place importante dans ces quelques lignes.

D'autres personnes encore tiennent une place très (très) importante dans ma vie. Merci à mes parents et à mon frère, qui m'ont toujours soutenu, et ont toujours cru en moi. Vous n'avez jamais douté un seul instant de mes capacités à mener ce projet à bout, et avoir eu le plaisir de vous voir à ma soutenance, malgré les conditions difficiles liées à la pandémie (il fallait bien que je la cite, elle aussi) restera à jamais l'un de mes plus grand bonheurs. Mille fois merci, vous avez tout mon amour.

Enfin, la dernière personne à qui sont dédiées les lignes restantes sait déjà beaucoup de ce que mon coeur a à lui dire. Elle m'a toujours poussé à donner le meilleur de moi-même, à me dépasser, et à persévére jusqu'au bout pour produire ce travail et ce manuscrit. Merci Eva. Merci pour ta patience et ton soutien sans faille. Merci pour tes mots et tes encouragements face à mes doutes et à mes remises en question. Merci pour tout. Merci pour toi.

Contents

| | |
|--|-------------|
| Abstract | i |
| Résumé | ii |
| Acknowledgements | iii |
| List of Figures | xi |
| List of Tables | xiii |
| Introduction | 1 |
| 1 Lower-limb exoskeletons and the challenges of motor intention detection | 5 |
| 1.1 Lower-limb exoskeletons | 6 |
| 1.1.1 The origins of exoskeleton devices | 6 |
| 1.1.2 Lower-limb exoskeletons: design aspects and applications . . | 10 |
| 1.1.2.1 General design considerations for the development of active lower-limb exoskeletons | 11 |
| 1.1.2.2 Augmentation LLEs for military and industrial applications | 12 |
| 1.1.2.3 Medical exoskeletons for assistance | 14 |
| 1.1.2.4 Medical exoskeletons for rehabilitation | 16 |
| 1.2 Detecting the user's intentions in medical LLEs: existing solutions . | 18 |
| 1.2.1 Control framework of medical LLEs | 18 |
| 1.2.2 The different input modalities to the high-level controller . . | 20 |
| 1.2.2.1 Discrete switching inputs | 20 |
| 1.2.2.2 Electrophysiological signals | 21 |
| 1.2.2.3 Kinematics and interaction signals | 23 |
| 1.2.2.4 Drawbacks of these modalities | 24 |
| 1.3 Towards more intuitive interfaces for intention detection: using natural body coordination | 27 |
| 1.3.1 Understanding human locomotion | 27 |

| | | |
|----------|---|-----------|
| 1.3.2 | Relying on natural body coordination | 27 |
| 1.3.3 | Objective of the thesis | 28 |
| 2 | Technical framework for the development of a high-level control interface | 29 |
| 2.1 | Atalante: a self-balanced assistive lower-limb exoskeleton for im- paired patients | 30 |
| 2.1.1 | An overview of the Atalante exoskeleton | 30 |
| 2.1.2 | 12 Dofs and no crutches: a technical description of Atalante | 32 |
| 2.1.2.1 | The mechanical conception of Atalante | 32 |
| 2.1.2.2 | The sensing capabilities of Atalante | 33 |
| 2.1.3 | From Datagen to Wanderbrain: the software of Atalante . . | 33 |
| 2.1.3.1 | Generating trajectories | 33 |
| 2.1.3.2 | Controlling the robot | 34 |
| 2.1.4 | Detecting the user intent: a brief summary on how to navi- gate the Finite State Machine | 34 |
| 2.1.4.1 | An overview of Atalantes's Finite State Machine . | 34 |
| 2.1.4.2 | Inputs to the control interface: intention detection methods | 36 |
| 2.2 | An experimental framework for the exploration of intention detec- tion methods | 36 |
| 2.2.1 | A generic experimental procedure for the detection of walking- related intentions | 36 |
| 2.2.1.1 | Focusing on three different intentions | 36 |
| 2.2.1.2 | Exploration and validation: a two-steps generic framework | 37 |
| 2.2.2 | Hardware tools: using IMUs to analyze upper-body kinematics | 37 |
| 2.2.2.1 | From MoCap to body-worn sensors: methods for analyzing human movement | 37 |
| 2.2.2.2 | IMU sensors used in this work | 38 |
| 2.2.3 | A unified process for detecting intentions based on IMU data | 40 |
| 2.2.3.1 | A brief summary on the common classification frame- work | 40 |
| 2.2.3.2 | A unified software implementation | 41 |
| 3 | Detecting the Gait Initiation Intention | 43 |
| 3.1 | Gait initiation: definition and characteristics | 45 |
| 3.1.1 | The mechanisms of gait initiation | 45 |
| 3.1.2 | Velocity and duration considerations | 46 |
| 3.1.3 | Gait initiation in impaired groups | 47 |
| 3.1.4 | Gait initiation in the Atalante exoskeleton | 47 |

| | | |
|---------|--|----|
| 3.2 | The detection of gait initiation intention | 48 |
| 3.2.1 | Current solutions | 48 |
| 3.2.2 | Using training data from a free setting to detect the gait initiation intention in Atalante | 49 |
| 3.3 | Exploring upper-body kinematics during gait initiation in a free walking setting | 49 |
| 3.3.1 | The experimental setup | 49 |
| 3.3.2 | Data processing | 50 |
| 3.3.3 | Data analysis and classification | 50 |
| 3.3.3.1 | Linear Discriminant Analysis | 50 |
| 3.3.3.2 | Labeling the training data | 53 |
| 3.3.3.3 | Selecting relevant features | 54 |
| 3.3.3.4 | Training and testing the data | 56 |
| 3.3.4 | Results of the study | 57 |
| 3.3.4.1 | Upper-body kinematics during Gait Initiation in the Free Setting experiment | 57 |
| 3.3.4.2 | Offline classification of the Free Setting signals | 57 |
| 3.3.5 | Discussion | 60 |
| 3.3.5.1 | Qualitative analysis of upper-body kinematic signals | 60 |
| 3.3.5.2 | Evaluation of Gait Initiation detection in the Free Setting (FS) based on an offline classification architecture | 61 |
| 3.4 | Using generic upper-body kinematics data from the Free Setting to detect Gait Initiation Intention in the Atalante exoskeleton | 62 |
| 3.4.1 | The experimental setup | 62 |
| 3.4.1.1 | The Constrained Setting experiment | 62 |
| 3.4.1.2 | The False Positives experiment | 64 |
| 3.4.2 | Data processing | 64 |
| 3.4.3 | Data analysis and classification | 64 |
| 3.4.3.1 | Constrained Setting experiment | 64 |
| 3.4.3.2 | False Positives experiment | 65 |
| 3.4.4 | Results of the study | 65 |
| 3.4.4.1 | Upper-body kinematics during Gait Initiation in the Constrained Setting experiment | 65 |
| 3.4.5 | Online classification of the CS signals | 67 |
| 3.4.6 | Testing the classifier for false Gait Initiation Intention (GII) positives induced by everyday movements | 71 |
| 3.4.7 | Discussion | 72 |
| 3.4.7.1 | Qualitative analysis of upper-body kinematic signals | 72 |

| | | |
|----------|---|-----------|
| 3.4.7.2 | Experimental evaluation of gait initiation detection in the exoskeleton based on a free setting training set | 72 |
| 3.4.7.3 | Experimental evaluation of the robustness of the global classifier to false Gait Initiation Intention (GII) positives | 73 |
| 3.5 | Limitations and prospects of the study | 74 |
| 3.6 | Conclusion | 74 |
| 4 | Detecting the Gait Termination Intention | 77 |
| 4.1 | Gait termination: definition and characteristics | 80 |
| 4.1.1 | The mechanisms of gait termination | 80 |
| 4.1.2 | Effects of walking speed | 80 |
| 4.1.3 | Upper-body behaviour during gait termination | 82 |
| 4.1.4 | Gait termination in the Atalante exoskeleton | 82 |
| 4.2 | Arm swing movements during gait | 83 |
| 4.2.1 | The mechanisms of arm swing | 83 |
| 4.2.2 | The function of arm swing | 84 |
| 4.2.3 | Arm swing in impaired individuals | 84 |
| 4.2.4 | Walking detection rather than gait termination detection: a dead-man switch approach based on arm swing | 85 |
| 4.3 | Exploring arm swing during walk in the exoskeleton: a preliminary experiment | 85 |
| 4.3.1 | The experimental setup | 86 |
| 4.3.1.1 | No forced arm movements configuration | 87 |
| 4.3.1.2 | Explicit arm swing configurations with varying amplitudes | 87 |
| 4.3.2 | Data analysis | 87 |
| 4.3.2.1 | Signal analysis | 87 |
| 4.3.3 | The dynamics of arm swing during walk in the exoskeleton | 89 |
| 4.3.3.1 | Time-domain analysis of the arm swing | 89 |
| 4.3.3.2 | Frequency-domain analysis of the arm swing | 92 |
| 4.3.4 | Deriving distinctive features of arms swing during walk in the exoskeleton | 92 |
| 4.3.4.1 | Amplitude-based features | 95 |
| 4.3.4.2 | Coordination-based features | 97 |
| 4.3.4.3 | Frequency-based features | 98 |
| 4.3.4.4 | Choosing adequate threshold values | 100 |
| 4.3.5 | A threshold-based classification architecture as the walking control interface | 102 |

| | | |
|----------|---|------------|
| 4.4 | Using arm swing movements to walk in the exoskeleton: a validation experiment | 105 |
| 4.4.1 | The experimental setup | 105 |
| 4.4.2 | Data and statistical analyses | 105 |
| 4.4.3 | Results of the study | 106 |
| 4.4.3.1 | Accuracy of the classification architecture | 106 |
| 4.4.3.2 | Analysis of gait termination detection time delays | 108 |
| 4.4.3.3 | Analysis of arm swing amplitude | 108 |
| 4.4.3.4 | Analysis of the classifier features | 109 |
| 4.4.4 | Discussion | 112 |
| 4.4.4.1 | Effectiveness of the threshold-based classifier architecture | 112 |
| 4.4.4.2 | Lowering the time delay for gait termination | 113 |
| 4.5 | Preliminary testing with patients | 115 |
| 4.6 | Limitations and prospects of the study | 115 |
| 4.7 | Conclusion | 116 |
| 5 | Detecting the Steering Intention | 119 |
| 5.1 | Steering during gait: definition and characteristics | 120 |
| 5.1.1 | The different steering strategies | 120 |
| 5.1.2 | The mechanisms of turning | 122 |
| 5.1.3 | Upper-body movements and the anticipation of steering | 123 |
| 5.1.4 | Steering in the Atalante exoskeleton: detection and implementation | 123 |
| 5.2 | The detection of the steering intention | 124 |
| 5.2.1 | Steering detection: existing solutions | 124 |
| 5.2.2 | A steering detection method compatible with arm swing controlled walking | 125 |
| 5.3 | Exploring upper-body-based steering strategies in the exoskeleton | 127 |
| 5.3.1 | The experimental setup | 127 |
| 5.3.2 | Data analysis | 127 |
| 5.3.2.1 | Asymmetric arm swing | 128 |
| 5.3.2.2 | Repeated trunk motion | 130 |
| 5.3.2.3 | Comparing the feature performances | 130 |
| 5.3.3 | Results of the study | 132 |
| 5.3.3.1 | Repeated Trunk Motion | 132 |
| 5.3.3.2 | Abandoning the repeated trunk motion strategy | 134 |
| 5.3.3.3 | Asymmetric arm swing | 135 |
| 5.3.4 | Discussion on the asymmetric arm swing strategy | 138 |
| 5.3.4.1 | Amplitude of movements | 138 |

| | | |
|---------------------|--|------------|
| 5.3.4.2 | Features analysis | 139 |
| 5.4 | Preliminary online validation with one participant | 142 |
| 5.4.1 | Experimental setup | 142 |
| 5.4.2 | Results and Discussion | 143 |
| 5.5 | Limitations and prospects of the study | 144 |
| 5.6 | Conclusion | 145 |
| Conclusion | | 147 |
| Bibliography | | 165 |

List of Figures

| | | |
|------|--|----|
| 1.1 | Drawings from Nicholas Yagn’s patents | 8 |
| 1.2 | Photos of exoskeletons | 10 |
| 1.3 | Augmentation exoskeletons for military and industrial applications . | 13 |
| 1.4 | Medical exoskeletons for assistance | 15 |
| 1.5 | The Lokomoat device | 17 |
| 1.6 | Generalized control framework for active lower-limb prostheses and orthoses | 19 |
| 1.7 | The different input modalities for intention detection in LLEs . . . | 26 |
| 2.1 | The Atalante exoskeleton | 31 |
| 2.2 | The anatomical planes | 32 |
| 2.3 | FSM and input controls of Atalante | 35 |
| 2.4 | IMUs used during the experimental protocols | 39 |
| 2.5 | Generic high-level controller process | 42 |
| 3.1 | Trajectories of the CoM and CoP during gait initiation | 46 |
| 3.2 | Illustration of the FS condition protocol | 51 |
| 3.3 | Illustration of Fisher’s Linear Discriminant | 52 |
| 3.4 | Variation of the features extracted from accelerometer signals . . . | 55 |
| 3.5 | Results from the FS experiment | 58 |
| 3.6 | Representation of the intra classifiers in the 2D LDA-generated sub- space | 59 |
| 3.7 | IDNN for each participant for the intra classifiers | 60 |
| 3.8 | Illustration of the CS experiment | 63 |
| 3.9 | Results from the CS experiment | 66 |
| 3.10 | Typical AP acceleration pattern during the CS experiment | 66 |
| 3.11 | General gait initiation strategy during the CS experiment | 68 |
| 3.12 | Classification results for the CS experiment | 69 |
| 3.13 | LDA-generated subspace based on FS data from one participant . . | 70 |
| 3.14 | 3D LDA-generated subspace based on FS data and MM recordings | 71 |
| 4.1 | Results from the study by Jian et al. (1993) | 81 |
| 4.2 | Exploratory Experiment setup | 86 |
| 4.3 | Arm angular velocities signals | 90 |
| 4.4 | Mean angular ranges during the EE | 91 |

| | | |
|------|---|-----|
| 4.5 | Inter-arms coordination during the EE | 93 |
| 4.6 | Frequency-domain representations of the left arm angular velocities | 94 |
| 4.7 | RMS feature of the arm angular velocities | 96 |
| 4.8 | Normalized cross-correlation feature of the arm angular velocities | 97 |
| 4.9 | Angle feature of the arm angular velocities | 99 |
| 4.10 | Representation of the EE data in the feature space | 101 |
| 4.11 | Offline results of the classifier on the EE data | 104 |
| 4.12 | Results from an FN trial and a successful trial | 107 |
| 4.13 | Average gait termination detection delays during the VE | 108 |
| 4.14 | Mean angular ranges during the VE | 109 |
| 4.15 | Mean averages and standard deviations of the feature values during the VE | 110 |
| 4.16 | Distribution of wrong outputs per feature during the VE | 111 |
| 4.17 | Average gain in time delays | 114 |
| 5.1 | Steering strategies | 121 |
| 5.2 | Steering experimental setup | 128 |
| 5.3 | Example of a direction detection method with the repeated trunk motion strategy | 131 |
| 5.4 | Relevant values for the computation of the $F_{f,\alpha}$ ratio | 132 |
| 5.5 | Results from repeated trunk motion trials from two participants | 133 |
| 5.6 | Angular ranges during the repeated trunk motion trials | 134 |
| 5.7 | Maximum angular velocities during the repeated trunk motion trials | 135 |
| 5.8 | Example results from an AASL trial | 136 |
| 5.9 | Angular ranges during the asymmetric arm swing trials | 137 |
| 5.10 | Evaluation of the performance of the different features during the asymmetric arm swing trials | 139 |
| 5.11 | Results from an offline implementation of the asymmetric arm swing based steering detection method | 141 |
| 5.12 | Results from a preliminary online test of the steering detection in- terface | 143 |

List of Tables

| | | |
|-----|---|-----|
| 1.1 | List of exoskeletons with discrete switching inputs | 21 |
| 1.2 | List of exoskeletons with electrophysiological signals as inputs . . . | 22 |
| 1.3 | List of exoskeletons with kinematics or interaction signals as inputs | 25 |
| 3.1 | Set of features used in classifiers construction | 54 |
| 3.2 | Peak average GII accelerations and angular velocities during the FS experiment | 57 |
| 3.3 | Classification rates from the offline classification of the FS data. . . | 58 |
| 3.4 | Distance metrics in the feature space for all classes and participants | 61 |
| 3.5 | Peak average GII accelerations and angular velocities during the CS experiment | 67 |
| 3.6 | Distance metrics in the feature space between data clusters from the CS intra trials and the four class clusters | 70 |
| 4.1 | Rates of wrong window outputs during the VE | 111 |
| 5.1 | Average values for the left and right arm angular ranges during the AAS trials | 137 |
| 5.2 | Window classification rates and delays for the offline implementa- tion of the steering detection method on the AAS trials | 142 |

Introduction

| Context of the thesis.

Over the last decades, developments in the fields of robotics and mechatronics have made it possible to design lower-limb assistive devices, such as exoskeletons and active orthoses, that could be used for physical augmentation or as an alternative to wheelchairs for physically impaired individuals such as Spinal Cord Injury patients. In popular culture, exoskeletons are often referred to as robotic armors that surround a person's limbs to assist their movements or enhance the capabilities of their body.

Although such devices still face important challenges – many of which revolve around actuation, cost, weight, and human-machine interfaces – a certain number of companies and research teams have been able to bring out what was once considered a science fiction technology to real life. In particular, more and more devices have been marketed in the recent years, with a focus on assisting workers achieve demanding and complex tasks, making patients suffering from Spinal Cord Injury (SCI) able to walk again, or helping with the rehabilitation of stroke patients.

However, most of the medical exoskeletons targeted at impaired patients still rely on constraining control strategies that fail in providing the users with natural and intuitive control interfaces. The motion intentions of users are usually detected through state-triggering buttons, or based on stereotyped upper-body gestures that serve as inputs to movement sensors. Most devices also need the use of a walking aid or crutches, which can be equipped with additional sensors to trigger specific movements, but highly impede the use of the upper limbs during walking.

In a context where patients wish for such assistive devices to become physical extensions of their own bodies, it is necessary to develop control interfaces that are not only robust, efficient, and safe, but feel natural and intuitive as well. While it is possible to think of electrophysiological signals (such as electromyograms – EMGs – or electroencephalograms – EEGs) as effective means to decode human motor intentions and provide an external device with input control signals, the complexity of correct training, as well as the variability and the lack of robustness of the decoding schemes make it difficult to apply such methods in an uncontrolled setting.

It is in this context that in 2012, the french start-up company Wandercraft (Paris, France) has taken up the challenge to develop a dynamically stable lower-limb exoskeleton for patients with lower-limb impairments. Their robot, named Atalante, is the first self-balanced device capable of dynamic walking without relying on crutches for stabilization. However, it still makes use of remote buttons to switch between its different states, and an Inertial Measurement Unit (IMU) to trigger specific movements based on upper-trunk kinematics.

The objective of this thesis was to develop novel intention detection methods for the Atalante exoskeleton, that would rely on naturally exhibited upper-body movements, and use acceleration and angular velocity signals recorded from body-worn IMUs as inputs.

| Main Contributions.

The thesis focused on three motion intentions: gait initiation, gait termination, and steering while walking. For each of these intentions, an analysis of corresponding upper-body movements was conducted based on experimental data, and allowed to develop novel IMU-based high-level control interfaces.

For gait initiation, it was shown that anticipatory postural adjustments that are exhibited before heel-off of the swing leg in unimpaired individuals can be recorded to serve as training data for a supervised learning classification architecture. By additionally recording IMU signals from typical everyday movements that can be performed while standing, the classifier was made robust enough to correctly detect the gait initiation intention, without triggering the walking state of the robot when unrelated upper-body movements are exhibited.

The gait termination interface was constructed based on the dead man switch paradigm: instead of detecting a short transitioning pattern in the kinematic inputs, the walking state of the exoskeleton is rather maintained as long as natural arm swing movements are exhibited. A set of descriptive features of such movements has been derived, and was used as part of a threshold-based classifier to detect when the arm swing ceases, and the exoskeleton should stop.

The steering intention was preliminarily explored, and the detection interface was based on an alteration of the arm swing movements described above: by creating an asymmetry in the amplitude of swing between both arms, the intention and direction of turning can be detected.

All solutions were tested both offline on recorded data, and online. Software implementation of the gait termination and steering detection methods were done directly in the embedded system of the exoskeleton through a unified signal observer architecture. The gait initiation detection solution was only implemented in a separate computer.

Lastly, as part of this work, a novel IMU-embedded jacket was designed for the Wandercraft company. It is equipped with one sensor on the back, and one on the side of each arm. It can be directly attached to the exoskeleton, and is directly interfaced with its hardware.

| Outline of the thesis.

This dissertation is divided into five chapters:

Chapter 1 This chapter presents a brief history of exoskeletal devices, and provides a state of the art of existing exoskeletons, and the detection methods used in the medical ones.

Chapter 2 This chapter presents the Atalante exoskeleton, and the hardware used throughout this thesis. It additionally describes the experimental framework for the exploration and validation of the different intention detection solutions.

Chapter 3 This chapter focuses on the gait initiation intention, and presents the experimental work conducted to explore predictive kinematic patterns of the upper-body during anticipatory postural adjustments. It then describes the supervised learning method used to detect the gait initiation intention, as well as its online implementation.

Chapter 4 This chapter focuses on the evaluation of a method to terminate gait when arm swing movements during walking cease. The online implementation is based on a threshold-based classifier.

Chapter 5 This chapter focuses on the detection of the steering intention. It is preliminary work that explored how an asymmetry in the arm swing movements exhibited for the gait termination interface could be used to indicate the intention and direction of turning.

| Publications.

During this thesis, the study around the detection of the gait initiation intention was published in a journal paper:

- O. Mounir Alaoui, F. Expert, G. Morel and N. Jarrassé, "Using Generic Upper-Body Movement Strategies in a Free Walking Setting to Detect Gait Initiation Intention in a Lower-Limb Exoskeleton," in *IEEE Transactions on Medical Robotics and Bionics*, vol. 2, no. 2, pp. 236-247, May 2020, doi: 10.1109/TMRB.2020.2982004.

A French patent for the arm-swing-based gait termination interface and the steering detection layer is also pending (n°FR2109174). The corresponding studies could not be submitted for publication before the patent was filed, but have now been submitted.

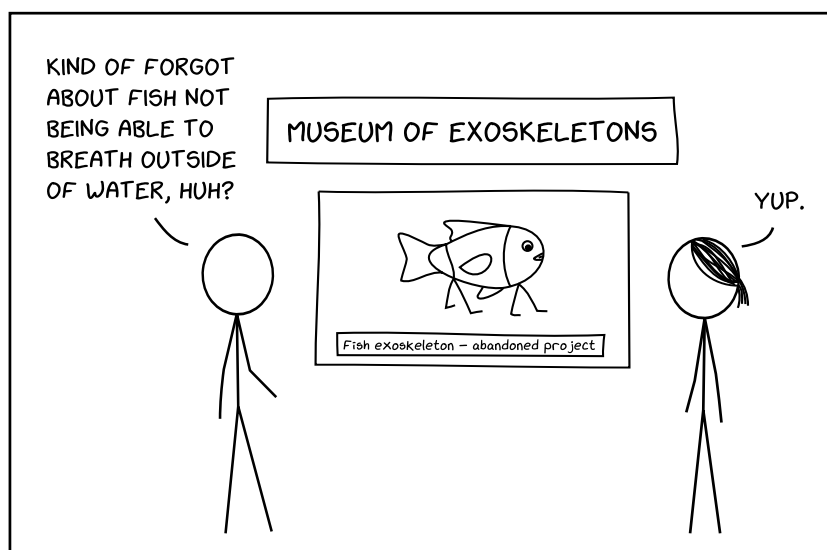
Work from this thesis was also presented during the *Ma thèse en 180s* competition, and during two conference workshops:

- *IEEE International Conference on Robotics and Automation 2020*, Integrating Multidisciplinary Approaches to Advance Physical Human-Robot Interaction.
- *IEEE International Conference on Intelligent Robots and Systems 2021*, Challenges and Opportunities of Human-robot Symbiosis: from Wearable Robots to Neurorobotics.

Chapter 1

Lower-limb exoskeletons and the challenges of motor intention detection

After a brief history of the development of exoskeletons from the late 19th century up to the past few decades, this chapter introduces the main different types of lower-limb devices and their applications: military, industrial, or medical. It then focuses on the general control framework associated with medical exoskeletons, and reviews the existing detection methods for the patients' motor intentions. These are mainly based on three types of input modalities: discrete switching inputs, electrophysiological signals, and kinematic or interaction signals. However, these existing solutions are hardly well-integrated with the users' sensory-motor control system, and generally suffer from a lack of intuitiveness. Therefore, the objective of this thesis is to try and build more natural interfaces based on existing body coordinations, and to provide users with seamless controls for medical exoskeletal devices.



Chapter Contents

| | | |
|------------|---|-----------|
| 1.1 | Lower-limb exoskeletons | 6 |
| 1.1.1 | The origins of exoskeleton devices | 6 |
| 1.1.2 | Lower-limb exoskeletons: design aspects and applications | 10 |
| 1.2 | Detecting the user’s intentions in medical LLEs: existing solutions | 18 |
| 1.2.1 | Control framework of medical LLEs | 18 |
| 1.2.2 | The different input modalities to the high-level controller | 20 |
| 1.3 | Towards more intuitive interfaces for intention detection: using natural body coordination | 27 |
| 1.3.1 | Understanding human locomotion | 27 |
| 1.3.2 | Relying on natural body coordination | 27 |
| 1.3.3 | Objective of the thesis | 28 |



1.1 | Lower-limb exoskeletons.

1.1.1 The origins of exoskeleton devices

The term “exoskeleton” comes from the Greek words ἐξω (exo, meaning outside) and σκελετός (skeletos, meaning dried up) (Harper 2021). It was first used in Biology to define “a hard outer layer that protects the bodies of certain animals, such as insects” (Oxford University Press 2021). However, its meaning has been further extended to refer to robotic exoskeletons, which are external mechatronical devices attached in parallel to a user’s body or body parts to – actively or passively – provide help with their movements or extend their physical capabilities. The term “orthosis” can also be used to refer to similar devices. In his 2009 review, Herr provided a general terminology to distinguish between exoskeletons and orthoses based on their end application: while exoskeletons are usually designed for performance augmentation of able-bodied users, orthoses more often describe devices developed for the assistance of impaired individuals (Herr 2009). However, the word “exoskeleton” is often used interchangeably with “orthosis” in many works of the field, and will be the preferred term used in this thesis.

The first technological concept of an exoskeleton can be traced back to the late 19th century, in 1889-1890, when Russian inventor Nicholas Yagn filed multiple

patents for an apparatus for facilitating walking, running, and jumping (Yagn 1889, 1890a–c). His inventions relied on the use of springs or bow-springs attached to the legs to support the body weight and assist walking, running, and jumping movements. He also proposed a method based on a compressed-fluid accumulator for energy storage. The drawings from his patents can be seen in figure 1.1.

Around the same time, in December 1889, the St. Paul Daily Globe, a Minnesotan journal, reported that an inventor from Minneapolis named Ira C.C. Rinehart was able to come up with a Walking Machine that relied on wheels placed underneath the feet of the user to take longer strides than a pedestrian (St. Paul Daily Globe 1889).

In the following years, and throughout the first half of the 20th century, many other patents were granted for similar devices (Skorzewski 1904; Kelley 1919; Cobb 1935). In 1942, Italian inventor Pietro Filippi patented a knee orthotic device that could be controlled by the means of a hydraulic system (Filippi 1942). Operation of the orthosis could be achieved through a tension fixation to the torso of the wearer, in a way that either deliberate or natural movements (for example when trying to regain balance) allowed for the blocking and release of the knee joint. Later, in a 1951 patent, American inventor John Murphy claimed a passive orthotic brace that could adapt to the gait phase, and rely on a spring mechanism to automatically activate or deactivate walking motions of the legs based on weight shifts of the wearer (Murphy 1951). However, it remains unclear whether any of these inventions were ever really made.

Similar powered orthotic (and prosthetic) structures for the upper body and arms were also investigated in the late 1950s and early 1960s. Reswick and Vodovnik drew a comprehensive review where many examples from different research teams were presented, many of which already made use of electrical actuation, and some even used electromyography (EMG) signals as control inputs (Reswick et al. 1967). Two notable examples of such devices are the Case Research Arms Aid-Mark I & II and the Rancho Los Amigos Hospital Electric Arm Systems, both of which are further described by Reswick (1972).

In the early 1960s, Zaroodny, a researcher from the U.S. Army Exterior Ballistics Laboratory, published a report about his work on a strength-augmentation device for able-bodied users, and reportedly built a 3 Degrees of Freedom (DoFs) pneumatically powered prototype (Dollar et al. 2008). During the same time, the Cornell Aeronautical Laboratory (Buffalo, NY, USA) was sponsored by the Office of Naval Research of the Department of the Navy to develop a wearable full-body powered exoskeleton for strength and endurance amplification (Mizen 1963). While the full powered structure, dubbed the Man Amplifier, was never actually built, a preliminary unpowered concept was tested to assess the feasibility of wearing an exoskeleton, and its effects on human ranges of motion and dynamic responses (Mizen 1964). The work eventually led to a patent, filed in 1966 and granted in 1969 (Mizen 1969).

However, the first occurrence of a fully-powered whole-body exoskeletal structure was developed between 1965 and 1971 by the General Electric Company

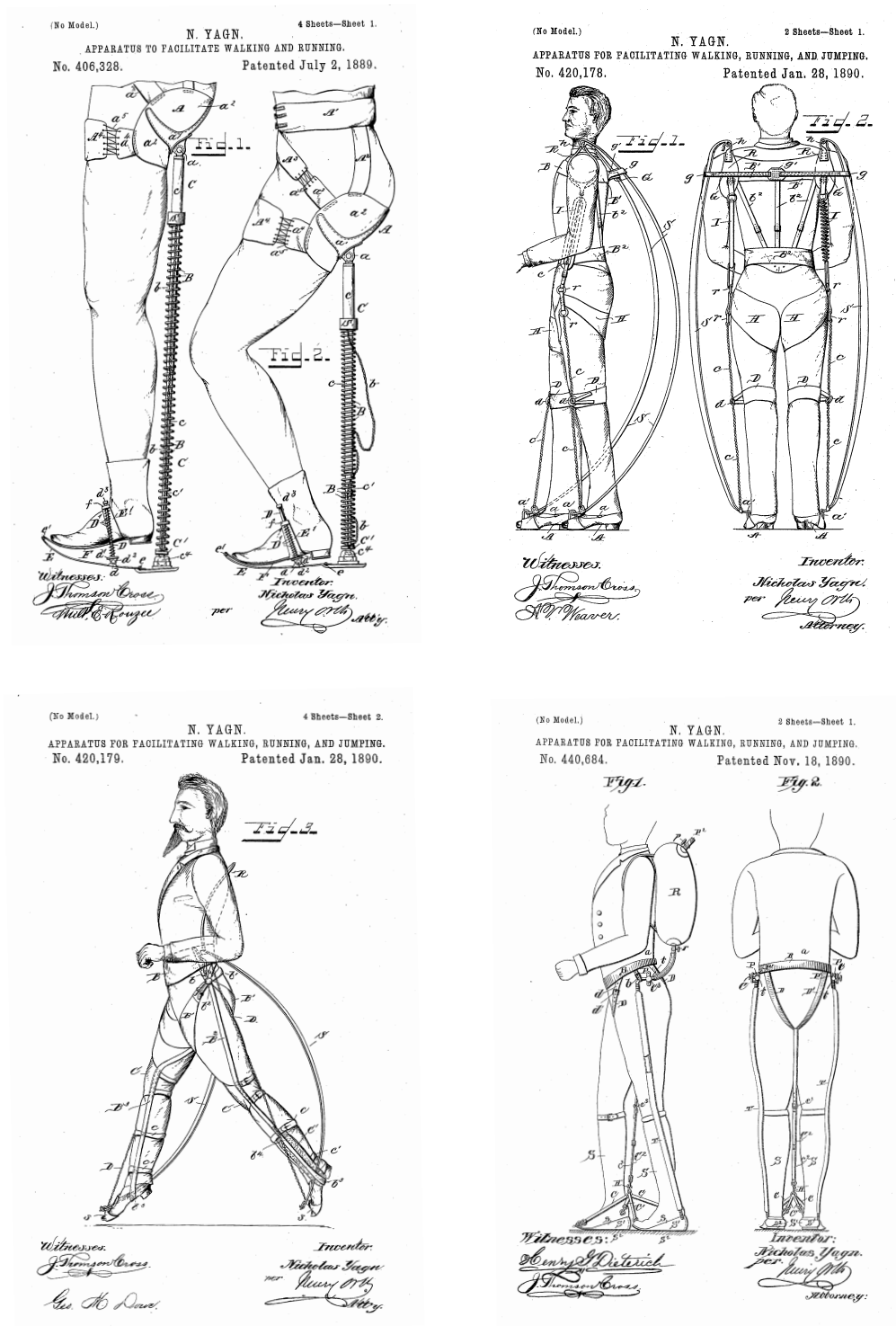


FIGURE 1.1: Drawings from Nicholas Yagn's patents of mutiple devices for facilitating walking, running, and jumping (Yagn 1889, 1890a–c).

(Boston, MA, USA), under a joint sponsorship between the US Army and the US Navy (Mosher 1967; Fick et al. 1971). The powered exoskeleton, called Hardiman, was mainly designed for military and industrial applications. It weighed approximately 680 kg and consisted in 30 powered joints actuated by electrohydraulic servos and hydromechanical actuators (see figure 1.2.A). It was able to support its own weight, and lift additional loads up to 680 kg. However, while the arm subsystems were effectively functional, the leg system only achieved limited performance. Nevertheless, the Hardiman project was a key turnpoint in the development of powered exoskeletons, and allowed for several technological breakthroughs that critically advanced the state-of-the-art in the exoskeleton field.

Around the same time, a research team led by Vukobratović at the Mihailo Pupin Institute (Belgrade, former Yugoslavia) worked on the first lower-limb exoskeletal devices for the assistance of impaired patients (Vukobratović et al. 1990). The project started in 1967 with the development of a passive measuring structure to assess the kinematic characteristics of human gait, closely followed by a hydrolically powered system to model the human legs. In 1969, the research team developed a kinematic walker with passive ankles, and hips and knees actuated by pneumatic cylinders. The device was constrained to the sagittal (or longitudinal) plane, and was tested by unimpaired participants. The first trials with patients later took place in 1971, first with a partial exoskeleton, and then with a complete device, both of which were equipped with active ankles, as well as an additional degree of freedom at the hip level to allow for trunk rotations in the frontal plane. These two exoskeletons still relied on pneumatic actuation, and the patients needed to use crutches or rolling aids to achieve walking. The complete exoskeleton can be seen in figure 1.2.B. Starting from 1974, the research team switched to the use of electromechanical drives, and in the later years, focused its efforts on the development of a modular electrically powered orthosis.

At the beginning of the 1970s, Seireg and Grundman also worked on an exoskeletal device for paraplegic patients at the University of Wisconsin (USA) (Dollár et al. 2008; Viteckova et al. 2013). The exoskeleton was powered with hydraulic power units, and its joints were programmed to follow pre-recorded trajectories from an able-bodied person. It also implemented sitting and standing motions, as well as climbing up and down stairs. While testing with a paraplegic patient might not have been conducted, it is reported that an unimpaired individual succeeded in operating it, with the help of crutches.

While the development of many exoskeletons presented in this section was greatly impeded by the technological maturity at the time, and could not reach stages advanced enough as to become truly effective devices, the many research teams involved in these projects demonstrated the feasibility of equipping the human body with a powered external structure for either strength augmentation or medical assistance and rehabilitation. Their investigations addressed many fundamental difficulties inherent to the development of exoskeletal devices, such as control systems, body-machine interfacing, portable power supplies, or sensing capabilities. Their work undoubtedly enriched the state-of-the-art for the field,

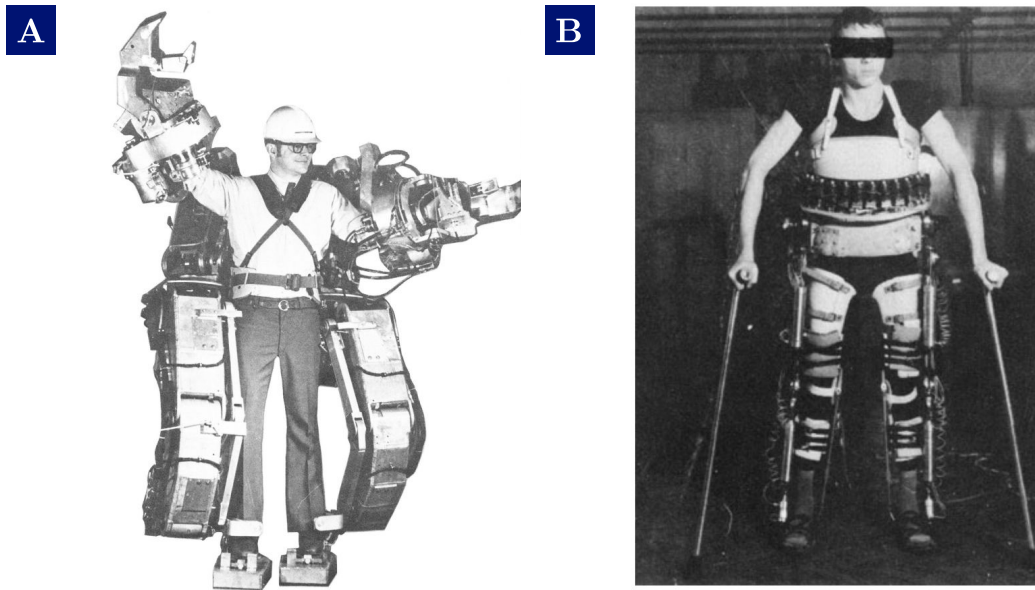


FIGURE 1.2: A. The Hardiman exoskeleton by the General Electric Company (Makinson 1971). B. Complete exoskeleton by Vukobratovic's research team (Vukobratović et al. 1990).

and paved the way towards more effective and technologically mature devices in the following years.

1.1.2 Lower-limb exoskeletons: design aspects and applications

Lower-limb exoskeletons (LLEs) are one particular category of exoskeletal devices that specifically target the lower body. They can also be seen as a specific type of bipedal robot, with added complexity emerging from the coupling dynamics between the user and the device. In the recent years, great improvements were made that allowed for the design of LLEs with better capabilities. While many challenges still remain, advances in such fields as robotics, computer technology, processing techniques, and hardware components and electronics, have accompanied the emergence of exoskeletons from various research teams and industrials. They can be active or passive, and mainly fall into one of three application categories: augmentation devices for military or industrial purposes, assistive exoskeletons for the compensation of physical weaknesses or mobility loss, and rehabilitation exoskeletons for gait training and recovery (Viteckova et al. 2013; Chen et al. 2016; Young et al. 2017; Lee et al. 2020). In the following sections, only active devices will be considered.

1.1.2.1 General design considerations for the development of active lower-limb exoskeletons

The main design considerations for the development of lower-limb exoskeletons revolve around the following aspects (Aliman et al. 2017; Young et al. 2017):

Actuation type Actuation plays a major role in the design of exoskeletons and active orthoses, as all other parts and mechanisms of such devices are usually designed according to the choice of actuators. Huo et al. (2016) presented four main actuation designs that can be chosen for LLEs : hydraulic or pneumatic actuators, electrical actuators, Series Elastic Actuators (SEAs), and artificial pneumatic muscles. The first provide high ratio of power to weight, which is why they are mainly used in augmentation exoskeletons. The second are heavier but more power efficient during walking, and are a good choice for gait assistance devices, for which size requirements of motors are less important than for heavy lifting exoskeletons. SEAs allow for shock tolerance, lower reflected inertia, accurate stable force control, and energy storage. Finally, pneumatic muscles can be used in antagonistic form, have a very good power to weight ratio, are relatively light, and are inherently compliant; however, control methods become more complex.

Degrees of freedom Lower-limb exoskeletons are designed to be as anthropomorphic as possible, and target the hip, knee, and ankle joints. The hip can cover up to 3 DoFs (flexion/extension, abduction/adduction, internal/external rotation), the knee joint can cover up to 2 DoFs (flexion/extension and internal/external rotation), and the ankle joint can cover up to 3 DoFs (dorsiflexar/plantar flexion, abduction/adduction, and internal/external rotation). While full devices encompass all three joints, partial LLEs can specifically target a subset of one or two. The total number of DoFs, as well as the number of actuated DoFs and passive ones, entirely depend on the performance that must be achieved, and the end application of the device.

Control strategy Yan et al. (2015) identified seven main control strategies implemented by full lower-limb exoskeletons, depending on their end application:

- Sensitivity amplification, which is usually based on inverse dynamics models. This strategy is mainly used for force augmentation exoskeletons.
- Predefined gait trajectory control, which is usually implemented in assistive exoskeletons used by subjects that suffer from partial or full loss of voluntary movements. The replayed trajectory can either be recorded from unimpaired individuals, or computed from gait analyses data.
- Model-based control, where a human-exoskeleton model is developed based on methods such as gravity compensation, or others. This strategy heavily

relies on sensory information to derive kinematics and dynamics data. Exoskeletons and orthoses falling into this category can be used for different purposes.

- Adaptive oscillators-based control, which was initially developed to synchronize with the instantaneous frequency and phase of periodic inputs. It was then extended to the field of robotics for multiple purposes, and was recently used to capture periodic features of walking or cyclic rehabilitation exercises. A major drawback of this type of control is that it is strongly dependant on the capacity of subjects to deliver periodic and stable signals during locomotion-related activities.
- Fuzzy control, which aims at implementing an intuitive knowledge about the handling of a physical system.
- Predefined action based on gait pattern, which provides assistance based on the activation of elements such as passive springs or pneumatic cylinders depending on the expected gait events.
- Hybrid assistive strategies can be achieved by combining different assistive strategies.

Additional considerations Additional design aspects should also be taken into account when working on the development of LLEs, such as the power transmission methods, the power autonomy, the integrated sensors, and the materials used.

Note that it is also important to be able to assess the performance of exoskeletons based on the physiological effects on the patients and users, rather than just focus on the mechanical design and control strategies. In particular, metabolic cost, gait biomechanics and muscular activity are three main categories of assessment types that researchers can focus on, and keep in mind when working on LLEs (Huo et al. 2016).

1.1.2.2 Augmentation LLEs for military and industrial applications

In many military and industrial applications, the exoskeletal structure is used to enhance the physical capabilities and endurance of able-bodied users. It mainly relies on sensitivity amplification control algorithms and the transfer of loading weight to the ground to help manipulating or lifting heavy objects and tools while walking.

One notorious example is that of the Berkeley Lower Extremity Exoskeleton (BLEEX, see figure 1.3.A), which was developed for heavy load carrying, and was part of a funding initiative by the Defense Advanced Research Project Agency (DARPA). It was equipped with seven Degrees of Freedom (DoFs) per leg, four of which were actuated by linear hydraulic actuators (Zoss et al. 2005). It could

walk at an average speed of 1.3 m/s, and carry 34 kg. The weight of the mechanical structure, as well as the carrying load, could be transferred to the ground through the exoskeleton frame. Its control relied on an inverse dynamics model of the system, used as a positive feedback controller to achieve sensitivity amplification (Kazerooni et al. 2005). The research team responsible for BLEEX was led by Professor Kazerooni at the Berkeley Robotics & Human Engineering Laboratory, and their work led to the Berkeley ExoWorks spin-off company in 2005. The company worked on many other exoskeleton projects, such as ExoHiker, ExoClimber, and the Human Universal Load Carrier (HULC), all three of which were intended for military use (Kazerooni 2021). The latter has been part of a licensing agreement with Lockheed Martin (Bethesda, MD) to be further developed. However, although it was reportedly tested by the army, it was never brought to the field (Army Technology 2021a). In 2007, Berkeley ExoWorks changed its name to Berkeley Bionics, and then again to Ekso Bionics in 2011, and has since shifted its focus towards medical exoskeletons and upper-body structures for industrial applications (Ekso Bionics 2021).



FIGURE 1.3: Augmentation exoskeletons for military and industrial applications: A. BLEEX by the Berkeley Robotics & Human Engineering Laboratory. B. HAL by Cyberdyne.

Sarcos (Salt Lake City, UT) is another company that benefited from the DARPA programme, and developed a full-body exoskeletal suit for military purposes. The device has later evolved as the XOS and XOS 2 exoskeletons after it has been acquired by Raytheon (Waltham, MA) (Army Technology 2021b).

In Japan, the work on the Hybrid Assistive Limb (HAL) exoskeleton series at the University of Tsukuba started out as early as 1992 (Sankai 2010). The

Cyberdyne company was then created as a university venture in 2004 to continue working on the development of the HAL systems for both medical and power augmentation purposes (Cyberdyne 2021a). The HAL-5 exoskeleton in figure 1.3.B was designed in 2005, and was equipped with a total of six DoFs to provide motion in the sagittal plane and augment power and endurance of able-bodied users. Today, Cyberdyne's non-medical device has been renamed HAL for Well-Being, and targeted at users who have difficulties standing, sitting and walking, without suffering from a serious lower-limb impairment.

1.1.2.3 Medical exoskeletons for assistance

Medical assistive exoskeletons can be used by impaired patients or people suffering from physical weaknesses. Notably, many devices in this category are directed towards patients suffering from Spinal Cord Injury (SCI). The most common causes for SCI are traumatic, with a particularly high prevalence of falls and motorized vehicle accidents (Kang et al. 2017). The World Health Organization (2021) estimates that between 250,000 and 500,000 people are affected by SCI in the world each year, with highly varying incidence numbers, ranging from 13 to 220 million people per year depending on the geographical region (Kumar et al. 2018). The severity and symptoms of SCI highly depend on the level of injury, and can encompass partial or total loss of motor and sensory functions of the limbs and body, as well as chronic pain, and the possible dysfunction of multiple organs (Kang et al. 2017; World Health Organization 2021). In the case of paraplegia, the injury specifically affects the lower extremities, and can cause complete paralysis of the limbs. In this context, assistive LLEs aim at restoring lower-limb mobility and perform ambulatory tasks such as walking or climbing stairs. In most cases, the performed movements follow predefined trajectories that have been generated offline.

In Japan, Cyberdyne was one of the precursor companies to work on the development of medical LLEs, by adapting its HAL exoskeleton to be used by impaired patients for walking (Kawamoto et al. 2003; Suzuki et al. 2005), as well as performing sitting and standing motions (Tsukahara et al. 2010). The company now sells its device under the name HAL for Medical Use, which has obtained the CE marking in Europe as a robotic medical device (Cyberdyne 2021b).

Many other LLEs in this category are also developed by industrials, and are already available on the market. Gardner et al. (2017) compared the capabilities of four devices:

- REX, developed by the REX Bionics company in New Zealand (REX Bionics 2021);
- EksoGT (formerly known as eLegs and now evolved as EksoNR) developed by Ekso Bionics (Strausser et al. 2011; Kolakowsky-Hayner 2013; Ekso Bionics 2021);

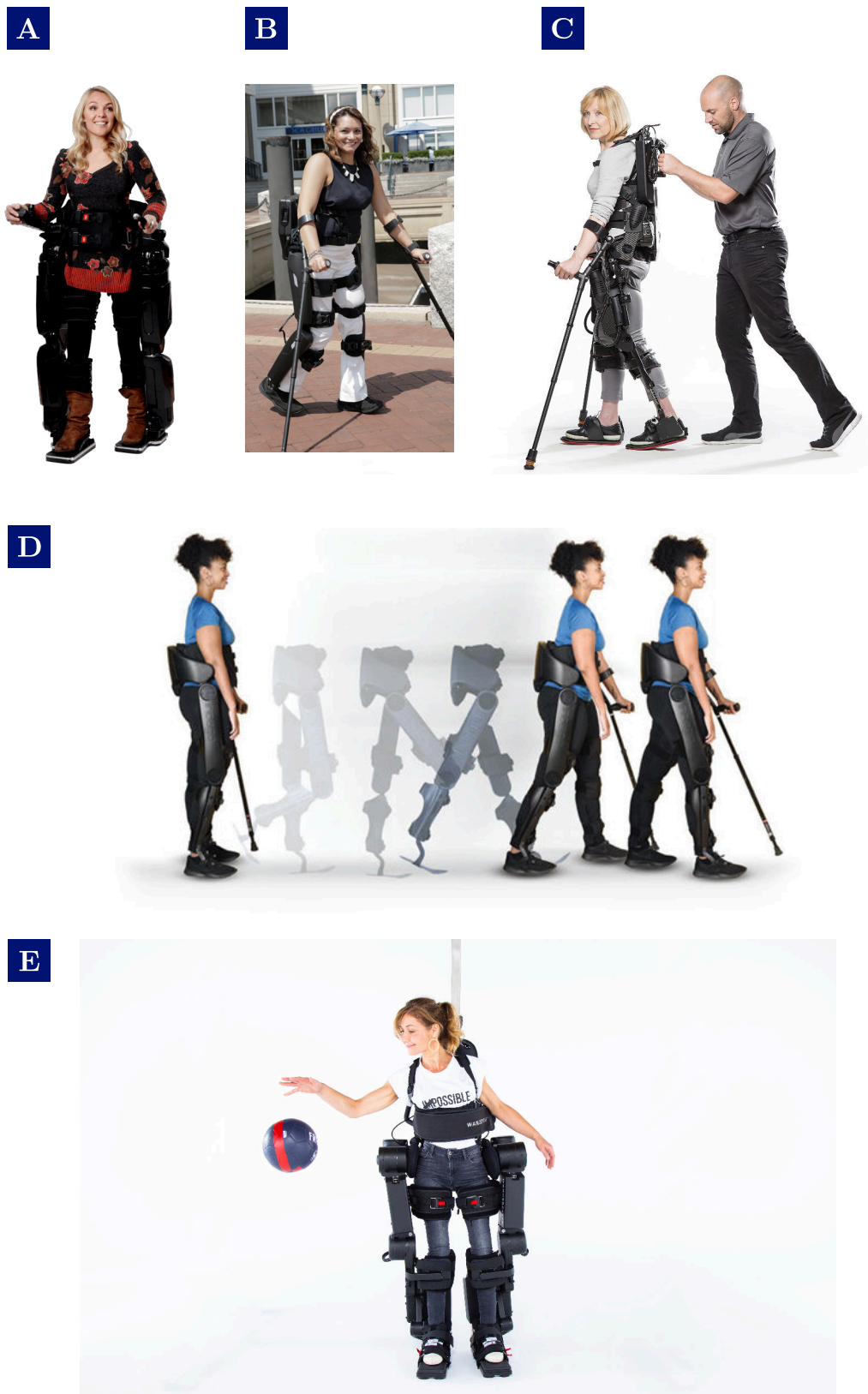


FIGURE 1.4: Medical exoskeletons for assistance: A. REX by REX Bionics. B. ReWalk Personal 6.0 by ReWalk Robotics Ltd. C. EksoNR by Ekso Bionics. D. Indego by Parker Hanifin. E. Atalante by Wandercraft.

- ReWalk (now known as the ReWalk Personal 6.0) developed by ReWalk Robotics Ltd. and originally designed in Israël (Esquenazi et al. 2012; Zeilig et al. 2012; ReWalk Robotics Ltd. 2021);
- Indego, first designed at Vanderbilt University and now developed by the Parker Hanifin Corporation in the US (Farris et al. 2011; Quintero et al. 2011; Parker Hanifin Corporation 2021).

In particular, REX was one of the first commercially-available exoskeletons. It features five DoFs par leg, and weighs 38 kg. It is a self-supporting statically stabilized device, which makes it possible for patients to use without needing crutches or an external walking aid. However, this comes at the price of a slow walking speed (≈ 0.05 m/s), and an unnatural and stereotyped gait pattern (Barbareschi et al. 2015). While the former can be problematic for daily use, the latter is acceptable for an assistive technology aimed at patients who cannot retrieve their lower-limb mobility function. On the contrary, the other three exoskeletons all rely on the use of crutches to stabilize the patient during walk and other gait-related movements. While this allows for higher speeds and lower device weights, it makes it impossible for the patients to freely use their arms and accomplish other tasks. All four devices have been CE marked, and all but REX have received FDA clearance for US commercialization.

In 2018, the Atalante exoskeleton from the French company Wandercraft was the first dynamically stable device to obtain CE marking in Europe as a medical device for the assistance of paraplegic patients. The feedback control algorithms implemented on this exoskeleton rely on the optimal control framework, making it possible to achieve crutchless dynamic gait (Gurriet et al. 2018; Harib et al. 2018). This device was used as the dedicated platform for the work developed during this thesis, and more details on its description and design can be found in chapter 2.

Other assistive LLEs are under development by industrial companies or academic research teams. These include Keeogo by B-TEMIA (Bouyer et al. 2014; Mcleod et al. 2019; B-TEMIA 2021), Quix (formerly known as Mina) by the Institute for Human and Machine Cognition (Kwa et al. 2009; Griffin et al. 2017), MINDWALKER (Gancet et al. 2012; S. Wang et al. 2015), and Arke by Bionik Laboratories Corp. (2017).

1.1.2.4 Medical exoskeletons for rehabilitation

Another category of medical exoskeletons aims at providing assistance with the rehabilitation of patients who suffer from mobility disorders, which is traditionally performed by physiotherapists. Patients – such as stroke survivors, or people with partial loss of motor control due to neurological impairments – can be trained to regain mobility by repeating specific movements with the assistance of an exoskeleton, and taking advantage of the neuroplasticity of the brain (Cramer et al. 2008; Dietz et al. 2013). Usually, the level of assistance can be tuned, and is gradually lowered until the patient correctly recovers from their impairment.

The treadmill-based Lokomat orthosis developed by Hocoma in Switzerland is undoubtedly one of the best-known devices in this category (Riener et al. 2010). Initially known as the Driven Gait Orthosis (DGO), it was designed by the Spinal Cord Injury Center of the University Hospital Balgrist in Zurich starting from 1995 (Colombo et al. 2000). It is equipped with four actuated joints at the hip and knee levels, and is attached to a body-weight support system (Lokolift) that passively allows vertical translations. The ankles are supported by passive foot lifters, and the overall movement of the device is constrained to the sagittal plane. The first control strategy implemented by Lokomat relied on a conventional position PD controller that didn't allow for deviations from the predefined gait trajectories. However, the importance of variability and assisting movements as needed to enhance motor coordination and function was demonstrated by Lewek et al. (2009), which pushed towards the development of a path controller based on impedance control (Duschau-Wicke et al. 2010). The device can be seen in figure 1.5.



FIGURE 1.5: A patient during a rehabilitation exercise using the Lokomat device.

Other treadmill-based exoskeletons include ALEX (Banala et al. 2008; Zanotto et al. 2013) and LOPES (Veneman et al. 2007). However, these devices strongly focus on gait training in the walking plane, with no possibility of performing other movements such as standing or sitting. Additionally, the constraints of using a treadmill and a body-weight support system make it difficult to achieve true ambulation in varying environments, even though Virtual Reality (VR) settings can be used for increased feedback and motivation (Lünenburger et al. 2007).

In this context, most of the industrials responsible for the assistive medical LLEs mentioned in 1.1.2.3 have worked on the integration of rehabilitation capabilities to their existing devices. Some have even made it their primary targeted application, such as Ekso Bionics, who describes its EksoNR device as “a robotic exoskeleton specifically designed to be used in a rehabilitation setting to progress neurorehab patients so they can walk out of the device and back into their communities” (Ekso Bionics 2021), and the REX Bionics company, who seems to have completely dropped the development of an assistive device to solely focus on rehabilitation.

1.2 | Detecting the user’s intentions in medical LLEs: existing solutions.

1.2.1 Control framework of medical LLEs

All the exoskeletons presented in the previous section greatly differ in terms of their design aspects and control algorithms, which are strongly dependant on the targeted application. In particular, it was shown that they can rely on different actuation methods and sensor technologies, may cover different degrees of freedom, and implement various control algorithms. These are all important considerations that must be taken into account for the development of exoskeletal systems that seamlessly extend the users’ capabilities, and can be perceived as integrated parts of their bodies (Seymour 1998). However, one additional key challenge to achieve such an integration is to provide correct interfacing with the users’ sensory-motor control system and to properly convey movement intentions through natural and intuitive control strategies – especially for full medical lower-limb exoskeletons, which are going to be the main focus in all the following sections of this work.

Tucker et al. (2015) proposed a generalized control framework that describes the interactions between the user, the medical orthotic device, and the environment, and their interfacing with a multi-level hierarchical controller. The latter is composed of three layers: a high level controller that estimates the user intent (perception layer), a mid level controller that maps it to a desired device output (translation layer), and a low level controller that implements device-specific controls through error calculation (execution layer). This is summarized in Fig.1.6, reproduced from Tucker et al. (2015).

The high-level and mid-level controllers can sometimes be referred to as the Human-Machine Interface (HMI), or the Body-Machine Interface (BMI). A BMI is presented by Casadio et al. (2012) as a means for interfacing the human body with external devices, and is especially appropriate in assistive and rehabilitation settings. A typical BMI will map the body signals into specific commands for

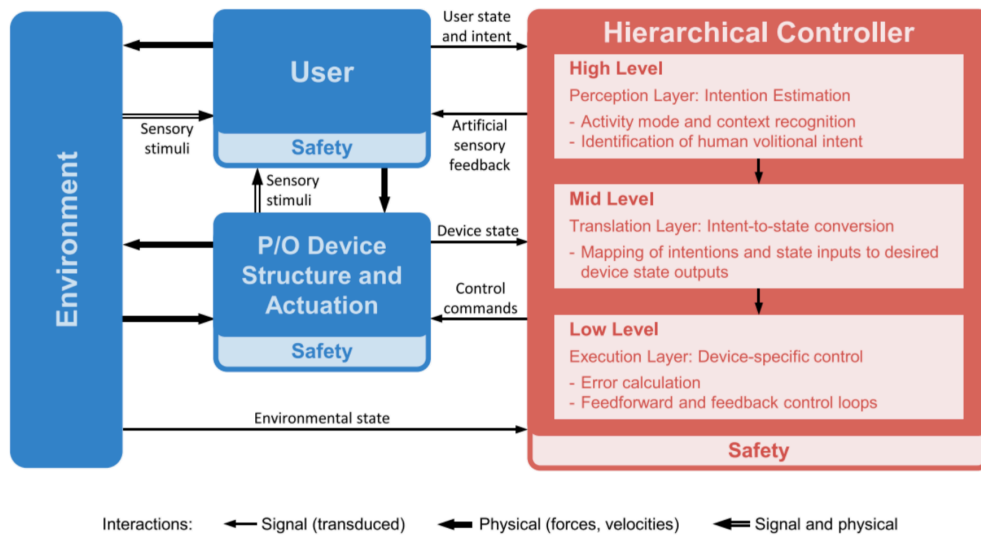


FIGURE 1.6: Generalized control framework for active lower-limb prostheses and orthoses as proposed by Tucker et al. (2015)

controlling a machine. In this context, specific BMI control policies have to be built as intuitive and easy mechanisms to provide for a naturalistic interface between body signals and the control signals for the machine. Such policies can be either discrete or continuous, and some systems can even integrate both control classes. Sensory feedback (usually vision, audio cues, proprioception, etc.) is important to close the control loop and have a better grasp of how to control the machine and effectively use the interface. In the case of LLEs, the movements of the device based on the desired intention can already be considered as an appropriate form of feedback.

Medical lower-limb exoskeletons often implement different gait or activity modes, usually as part of a Finite State Machine (FSM). A FSM consists in a finite number of states through which a machine can navigate, based on predetermined transitions that require specific sets of inputs (J. Wang et al. 2019). In the context of LLEs, it is through the high level layer that the user can switch from one state to another. In some cases, one activity mode can also be divided into a subset of modes, which require additional inputs from the user to operate properly (for example, switching from one leg to the other during walk). The low level layer ultimately takes over, and makes the robot perform a given set of movements corresponding to the recognized mode. Intention detection therefore faces two main challenges:

- The correct detection of transitions between modes, to avoid wrong activity mode detection and unwanted exoskeleton movements;

- The seamless integration of the perception layer to the user’s sensory-motor control system, to make the control interface intuitive and allow for smooth transitions.

1.2.2 The different input modalities to the high-level controller

To correctly achieve its purpose, the high level controller relies on one or multiple types of inputs, which can be mapped to a specific intent from the user. In existing solutions, these can be either discrete switching inputs, electrophysiological signals, or kinematic and interaction signals (Pons 2008; Novak et al. 2015; Tucker et al. 2015; Chen et al. 2016; Huo et al. 2016).

1.2.2.1 Discrete switching inputs

The most straightforward type of input is that of discrete switches. Its ease of implementation and great robustness and reliability make it the method of choice for industrial exoskeletons already available on the market. It simply maps a set of discrete switches (usually tactile, such as buttons on a remote controller) to desired states of the LLE.

It is the case of the Mina v2 exoskeleton from IHMC, which is equipped with a computer screen, a thumb joystick, and a momentary switch (Griffin et al. 2017). These are directly mounted on the right crutch, and allow to switch between different activity modes (using the joystick) and trigger movements (using the switch).

For some devices, discrete switching inputs are the only available high level control modality, as is the case for REX, which relies on a joystick controller (Schütz 2012). However, in a number of LLEs, they are used for global transitions (e.g. from sit to stand, or stand to walk), while other methods are used as a play trigger or for finer control: Ekso Bionics exoskeletons use external buttons or switches on a walking aid (Molteni et al. 2017), ReWalk relies on a wrist pad controller (Esquenazi et al. 2012), the Atalante exoskeleton comes with a remote controller for the patient, and additional buttons on the device to be used by a physiotherapist.

Another type of discrete switching input is that of voice control, which is less common. In a preliminary evaluation of the Vanderbilt exoskeleton, which later became Indego, Farris et al. (2011) asked a paraplegic participant to switch between different states of the device by issuing voice commands. An operator would then enter the command into a host computer to enable the transition. While this is obviously not adapted outside of an experimental setup, recent developments in voice recognition algorithms may provide for automated voice-based switching commands for LLEs. Bionik Laboratories Corp. (2017) recently announced a partnership with Amazon to integrate the Alexa voice-based ecosystem into their Arke exoskeleton.

| Exoskeleton name | Discrete switching input | Reference |
|------------------------|--|---|
| Mina v2 | Joystick, screen and switch button mounted on crutch | Griffin et al. (2017) |
| Twiiice | Crutch remote | Vouga et al. (2017) |
| Ekso | External buttons or buttons on walking aid | Molteni et al. (2017) |
| ReWalk | Wrist pad controller | Esquenazi et al. (2012) |
| Rex | Joystick controller | Schütz (2012) |
| Arke | Computer tablet and voice control | Lemaire et al. (2017) Bionik Laboratories Corp. (2017) |
| MINDWALKER | Pushbutton interface | S. Wang et al. (2015) |
| Auto-LEE | Joystick controller | He et al. (2019) |
| Vanderbilt exoskeleton | Voice commands | Farris et al. (2011) |
| Atalante | User remote and physio buttons | N/A |

TABLE 1.1: List of exoskeletons with discrete switching inputs

Table 1.1 presents a list of exoskeletons that use switching inputs as a high-level control modality.

1.2.2.2 Electrophysiological signals

Numerous studies have focused on the use of electrophysiological signals to decode human motor intentions and provide an external device with input control signals. These are mainly electromyograms – EMGs – or electroencephalograms – EEGs (Lobo-Prat et al. 2014; Benabid et al. 2019; Xu et al. 2019). EMG signals correspond to the electrical activity produced by the muscles as a response to the arriving peripheral nerve signals, and can be recorded using non-invasive techniques such as surface electromyography, based on electrodes placed on the skin (Tucker et al. 2015). Similarly, EEG signals correspond to the electrical activity of the brain, and are usually recorded by a non-invasive array of surface

electrodes placed directly on the scalp through a skull cap (Millán et al. 2010; Tucker et al. 2015). Such electrophysiological signals can serve as a control input for the detection of intentions in medical lower-limb exoskeletons. Note however that the EMG control modality cannot be targeted at people who suffer from total paralysis of the lower extremities, and necessitate that at least some residual motor capabilities are still available.

The HAL exoskeleton series from Cyberdyne implemented EMG-based user control very early on (Kawamoto et al. 2003): a feedback loop based on EMG signals could be used during walking to modulate the level of assistance provided by the device during the different phases of gait.

Tariq et al. (2018) reviewed the potentials of using Brain-Computer Interfaces (BCI) based on EEG data for the control of LLEs. One example is the MIND-WALKER project, funded by the European Commission through the e-Inclusion programme – aiming at the improvement of inclusion of European individuals with lower-limb impairments. This work revolved around the use of a non-invasive BCI for the development of a crutchless assistive exoskeleton, which could be coupled with additional EMG signals from the arms (Gancet et al. 2012). He et al. (2019) also proposed to use EMG and EEG signals to detect user intention in their Auto-LEE exoskeleton, but no experiments relying on this control scheme seem to have been conducted yet.

Another take at using EEG for decoding user intentions in a lower-limb exoskeletal device was made by Kilicarslan et al. (2013) at the University of Houston, TX. They implemented a Gaussian Mixture Model classification scheme to control the REX exoskeleton (renamed NeuroRex during this project) based on EEG inputs.

A summary of devices that rely on detecting the user intent based on electrophysiological signals can be seen in table 1.2.

| Exoskeleton name | Biophysiological signal | Reference |
|------------------|---------------------------|---------------------------|
| HAL | EMG | Kawamoto et al. (2003) |
| MINDWALKER | EEG and complementary EMG | Gancet et al. (2012) |
| Auto-LEE | EEG and EMG | He et al. (2019) |
| NeuroRex | EEG | Kilicarslan et al. (2013) |

TABLE 1.2: List of exoskeletons with electrophysiological signals as inputs

1.2.2.3 Kinematics and interaction signals

Lower-limb exoskeletons can also rely on kinematics or interaction signals derived from sensors such as Inertial Motion Units (IMUs) or force sensors to detect the user intent. Values from such sensors can be used directly, or to provide estimates of the displacement of the Center of Mass of the body (CoM), the Center of Gravity (CoG, usually defined as the horizontal projection of the CoM), or the Center of Pressure of the feet (CoP, defined as the centroid of the ground reaction forces on the feet). In most cases, devices in this category implement this modality in conjunction with discrete input switches, for either finer control during specific events (such as taking additional steps during walk), or for triggering movements after an activity mode has been selected.

Suzuki et al. (2005) worked on a step detection method for HAL based on either floor reaction forces (for patients with residual lower-limb motor control), or on the torso angle in the frontal plane (for paralyzed patients). In both cases, threshold values on the sensor data were used to detect the onset of the following step. However, the patients strongly relied on the use of a walking aid to be able to lean sideways. Similar methods with multiple conditions on the hip angle, the floor reaction forces, and the displacement of the CoP were used to detect the intentions of standing and sitting with HAL (Tsukahara et al. 2010).

Many other crutch-based exoskeletons rely on the detection of leaning motions to control individual steps by the direct measurement of a torso angle: ReWalk takes its steps based on a tilt sensor (Esquenazi et al. 2012), and the Arke device relies on onboard sensors that detect side-to-side movements (Lemaire et al. 2017). Some other LLEs rather rely on the estimation of the projection of the CoM on the floor. Its location can be modulated by upper body movements, and then compared to the position of the feet to decide whether or not a new step should be taken. This estimation is provided by computing the orientation of the exoskeletal segments (using IMUs or potentiometers), and the orientation of the torso. Indego (Quintero et al. 2011) and MINDWALKER (S. Wang et al. 2015) have both implemented this control method, and the former also used it to detect the transitions between its different activity modes, based on different criteria that relied on the robot joint configurations and the pose of the user. This approach takes advantage of the use of crutches, which enable the patient to better use the orientation of their upper-body to control their CoM.

Strausser et al. (2011) developed an intent detection method based on the use of crutches for eLegs, the predecessor of Ekso. IMUs placed on the arms were used to derive the orientation of arms and crutches relative to the body. A threshold value was used to detect when a crutch was swung far in front of the body, meaning that the patient intended to take a step forward. The crutches were additionally equipped with force sensors to make sure that they were both firmly pressed on the ground before initiating any movement of the exoskeleton.

The WPAL exoskeleton by Kagawa et al. (2009) also relied on sensors embedded in an external walker. Accelerometers were used to determine the distance

at which the walker was moved, and derive appropriate joint controls so that the stride length was equal to the estimated distance. The actual steps were triggered based on lateral weight shifts using foot pressure sensors attached to the foot soles of the device.

Another way of relying on interaction forces with an exoskeletal device has been developed by Kong et al. (2006) for the EXPOS exoskeleton. The device was used in conjunction with a caster walker, and the attaching thigh braces were equipped with air bladders and pressure sensors. The device was mainly aimed at individuals with residual motor capabilities, such that muscle contractions of the thighs could induce a pressure change in the air bladders, and be used to derive appropriate torque controls for the exoskeleton.

Lastly, the Atalante exoskeleton from Wandercraft relies on an IMU sensor placed on the back of the patient to trigger specific movements of the robot after a transition has been selected through the remote controller. For example, starting gait from a standstill position first requires the patient to select the walking mode on the remote, and then to lean forwards to actually start walking after a tilt threshold has been reached. The exoskeleton then initiates gait, and does not stop until the patient or a physiotherapist has pushed on the stopping button. More details can be found in chapter 2. Additionally, since Atalante is dynamically stable, it does not need to be used in conjunction with crutches or a walking aid. Therefore, controlling individual steps based on weight shifts initiated by the upper-body can be more difficult for paralyzed patients without being externally stabilized.

Table 1.3 shows a list of the reviewed LLEs which rely on kinematics and interaction signals for the detection of user intention.

1.2.2.4 Drawbacks of these modalities

Figure 1.7 shows a summarized list of exoskeletons using the three input modalities presented above. While these are the most common inputs for high-level controllers in current LLEs, none do simultaneously satisfy both requirements of robustness against false transitions, and the seamless integration to the user's sensory-motor control system for intuitiveness of use.

The main drawback of the switching input modality is that it suffers from a lack of integration to the overall system, and requires the user to manually navigate between the different possible states of an exoskeleton. While it effectively avoids the triggering of unwanted activity modes, it usually requires a handheld external device, which the user needs to learn how to use. In some cases (for example when many different modes are available), this can prove as an extra cognitive burden. Most importantly, discrete switching inputs prevent any form of natural or intuitive control.

| Exoskeleton name | Kinematics / interaction signal | Reference |
|------------------|---|---|
| HAL | Floor Reaction Force for patients with residual lower-limb mobility, torso angle in the lateral plane for other patients. Similar methods for sitting and standing. | Suzuki et al. (2005) Tsukahara et al. (2010) |
| Ekso | Arm IMUs and force sensors on crutches | Strausser et al. (2011) |
| ReWalk | Tilt sensor to trigger the steps | Esquenazi et al. (2012) |
| Indego | CoP estimation based on multiple angle measurements, using accelerometers and potentiometers | Quintero et al. (2011) |
| MINDWALKER | CoM estimation to trigger steps using IMUs | S. Wang et al. (2015) |
| WPAL | Acceleration sensors on a walker, and pressure sensors underneath the feet control individual steps by weight shifting | Kagawa et al. (2009) |
| EXPOS | Pressure sensors around the muscles | Kong et al. (2006) |
| Arke | Onboard sensors to detect leaning motions | Lemaire et al. (2017) |
| Atalante | IMU on the back as a play trigger | N/A |

TABLE 1.3: List of exoskeletons with kinematics or interaction signals as inputs

On the contrary, electrophysiological signals are natural signals that can give direct information on the user's intent. But their variability and the lack of robustness of the decoding schemes make it difficult to apply such methods in an uncontrolled setting, and outside of experimental setups (Wolpaw et al. 2012; Castellini et al. 2014). In particular, the sensors used to capture such signals make it difficult to adapt them to real-world settings (Tucker et al. 2015): to properly measure EMG signals, electrodes have to be correctly calibrated and placed over the skin, and nevertheless remain sensitive to cross-talk from neighbouring muscles, or motion artifacts. Similarly, EEG signals require an electrode-embedded cap that can be difficult to calibrate and properly put on, while remaining susceptible to noise from electrical devices and motion artifacts. They also require long and multiple

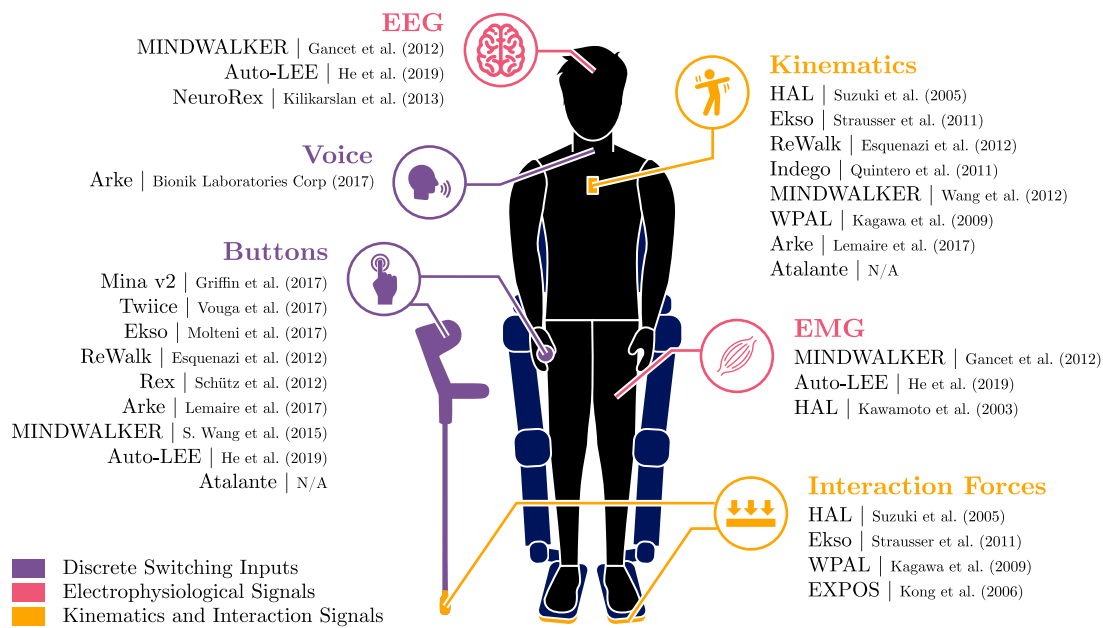


FIGURE 1.7: List of exoskeletons and corresponding references according to the different input modalities used for intention detection. Most exoskeletons use multiple types of inputs in their high-level controller.

training sessions, as well as high levels of concentration from the users, which might be perceived as extra cognitive burden.

Kinematics or interaction signals can be more robust. However, the common paradigm currently adopted by exoskeletons that use these types of signals is based on simple threshold-based approaches that rely on the detection of predefined movements that need to be learned, such as a high amplitude leaning motion and upper-body shifts. These usually serve as play triggers (for example, leaning forwards to start walking), or for fine control of the gait (for example, leaning laterally to start a step). While removing the need for a handheld external device, the required predefined movements can feel unnatural, and in most cases still rely on the use of crutches to help stabilize the upper body when initiating specific movements. Overall, using kinematics or interaction signals as inputs for intention detection is promising, but the current methods can be mainly seen as “gestured” switching inputs.

1.3**Towards more intuitive interfaces for intention detection: using natural body coordination.****1.3.1 Understanding human locomotion**

Human locomotion, which involves the musculoskeletal and neural sensory-motor systems, is controlled by the Central Nervous System (CNS). It is often described to be a result of the superposition of basic motor patterns, which are hypothetically issued by the so-called Central Pattern Generator (CPG) network at the spinal level, and reflex-dependent pathways that are necessary for finer control (Duysens et al. 1998; Pons et al. 2013). The latter also play an important role in maintaining balance during locomotor activities and adapting to external perturbations, as well as integrating afferent sensory feedback from the musculoskeletal system for further modulation of locomotor patterns (Dietz 2002b). Voluntary control can also emerge at the supraspinal level, and interact with the CPG (for example when expecting an obstacle) (Dietz 1997). Additionally, the human body provides a high level of redundancy, which induces multiple solutions for a given motor task. This is supposedly solved by the CNS by recruiting low-dimensional muscle synergies that effectively map motor intentions to actions (Torres-Oviedo et al. 2010). Lastly, there seems to be growing evidence that lower and upper limbs are neurally coupled during specific tasks, such as walking, which gives rise to coordinated muscle activities of the arms and legs (Dietz 2002a).

When suffering from an impairment that directly affects one or more levels of this complex locomotion control loop, the flexibility and redundancy of the musculoskeletal system make it possible to use compensatory strategies to achieve tasks that were dependent on the lost structures (Tucker et al. 2015). Casadio et al. (2012) argue that such redundancies can be taken advantage of for building effective motion-based BMIs that rely on new subsets of movements to interact with an external device. This strategy can also profit from plasticity, which reassigns a given action to new motions.

1.3.2 Relying on natural body coordination

In this context, a different approach to building a relevant high-level controller consists in analyzing upper-body movements that can be predictive of specific motor intentions, or to rely on residual kinematic synergies between different parts of the body that still exist after an injury. For example, by making use of machine learning techniques, it can be possible to reverse the adaptation paradigm, and build more natural control strategies where supervised algorithms can learn from

naturally exhibited human movements, instead of having the users adapt to predefined control patterns. Such a motion-based BMI would therefore take advantage of kinematic inputs derived from the upper-body, and recorded through various wearable sensors, such as Inertial Motion Units.

Similar techniques have already been widely used for IMU-based human activity recognition, such as walking or running (Bao et al. 2004; Karantonis et al. 2006; Preece et al. 2009b; Bartlett et al. 2017), but they can also be applied to classify shorter transitioning predictive movements, such as the intention of initiating gait, or expressing intentions while walking in a LLE. By building robust predictive classifiers, it would therefore be possible to naturally switch between different states of an exoskeleton, while preventing false mode recognition positives.

Analysis of body kinematic signals recorded by sensors such as IMUs can also give more insight into the specificities of movement coordination and patterns, and give way to heuristic methods where descriptive features of the signals can be compared to empirical thresholds through a classification architecture.

1.3.3 Objective of the thesis

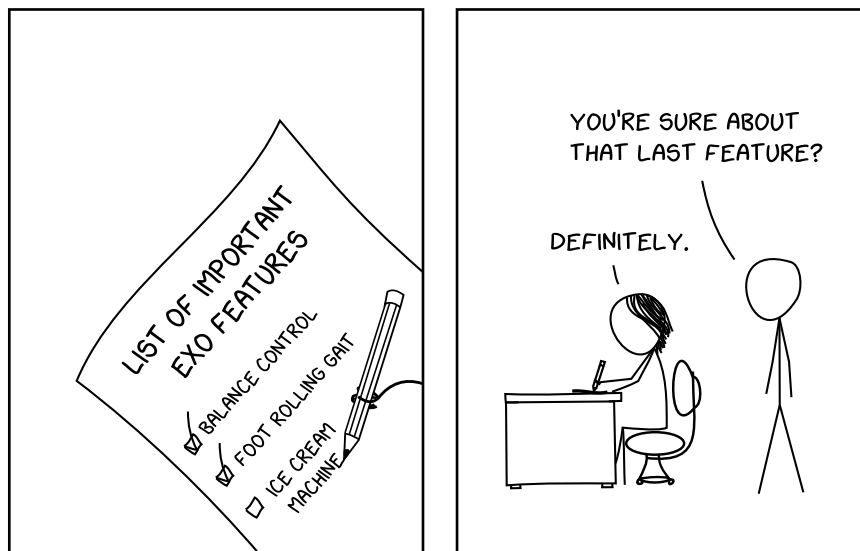
The main objective of this thesis was therefore to build an intuitive motion-based Body-Machine Interface to robustly detect movement intentions in a medical lower-limb exoskeleton, in a way that would feel the most natural possible to the patient. Importantly, such a BMI should rely on upper-body kinematics derived from sensor recordings to robustly switch between different activity modes of an exoskeleton, with minimal false positive occurrences, and no use of discrete switching inputs.

This work was conducted based on the Atalante exoskeleton developed by the Wandercraft company, upon the hypothesis that patients could still show upper-body motor capabilities. This means that these investigations were primarily directed at using the LLE in settings where such patients are involved, but might be extended to a rehabilitative setting involving patients suffering from other impairments, such as post-stroke hemiplegic individuals. The Atalante exoskeleton, as well as the main methods and materials used in this work, will be presented in the next chapter.

Chapter 2

Technical framework for the development of a high-level control interface

This chapter presents the technical framework that was used throughout this thesis. It describes the Atalante exoskeleton, which served as the base exoskeletal platform for the development of intention detection methods and their implementation as a unified high-level control interface. All methods were designed to rely on acceleration and angular velocity signals recorded by three Inertial Motion Units placed on the back and arms of the device users, which in turn served as inputs for a state-dependent classification architecture. In particular, experimental setups were designed to investigate three motion intentions: gait initiation, gait termination, and steering.



Chapter Contents

| | | |
|------------|---|-----------|
| 2.1 | Atalante: a self-balanced assistive lower-limb exoskeleton for im- | 30 |
| | paired patients | |
| 2.1.1 | An overview of the Atalante exoskeleton | 30 |
| 2.1.2 | 12 Dofs and no crutches: a technical description of Atalante | 32 |
| 2.1.3 | From Datagen to Wanderbrain: the software of Atalante | 33 |
| 2.1.4 | Detecting the user intent: a brief summary on how to navigate the Finite State Machine | 34 |
| 2.2 | An experimental framework for the exploration of intention detec- | 36 |
| | tion methods | |
| 2.2.1 | A generic experimental procedure for the detection of walking-related intentions | 36 |
| 2.2.2 | Hardware tools: using IMUs to analyze upper-body kinematics | 37 |
| 2.2.3 | A unified process for detecting intentions based on IMU data | 40 |



2.1 | Atalante: a self-balanced assistive lower-limb exoskeleton for impaired patients.

2.1.1 An overview of the Atalante exoskeleton

The Atalante exoskeleton, shown in figure 2.1, is a full lower-body exoskeletal device developed by the French company Wandercraft (Wandercraft 2021). It has received the CE mark in 2019 as a class IIa medical device, and is mainly targeted for use with paraplegic and stroke patients in rehabilitation centers. To our knowledge, it is the only crutchless and self-balanced exoskeleton capable of moving dynamically. This means it can perform a variety of movements, such as walking, turning in place, or squatting, without ever needing the assistance of external walking aids. However, a safety tether is used preventively to avoid falls that might occur in case of imbalance or exoskeleton failure, and the assistance of a physiotherapist is necessary. A technical description of the robot, as well as its software capabilities, are provided in the following sections.

A



B

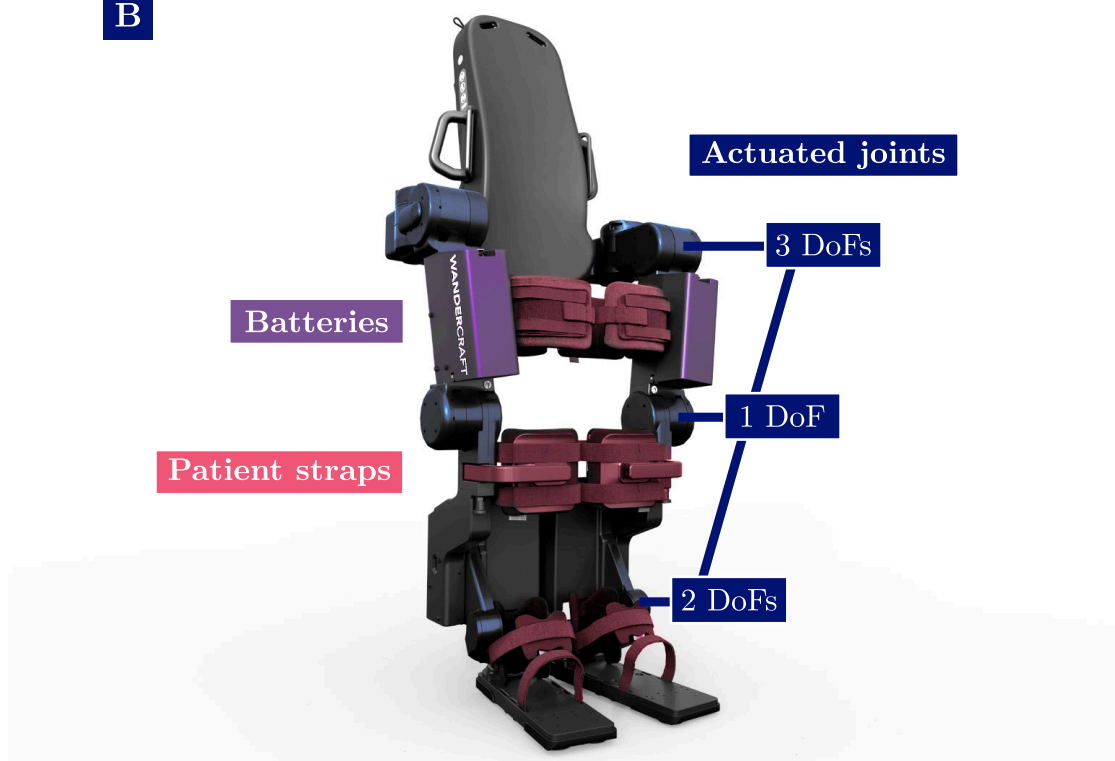


FIGURE 2.1: A. A patient walking in the Atalante exoskeleton during an outside tetherless test. B. The Atalante exoskeleton and some of its features. The blue parts indicate the joint actuators. The pink parts indicate the patient straps. The purple parts indicate the two batteries.

2.1.2 12 Dofs and no crutches: a technical description of Atalante

2.1.2.1 The mechanical conception of Atalante

The Atalante exoskeleton weighs 80 kg, and is comprised of 6 electrically powered Degrees of Freedom (DoFs) per leg, which provide motion in the anatomical planes as presented in figure 2.2:

- 3 at the hips: flexion/extension in the sagittal (or antero-posterior) plane, abduction/adduction in the frontal (or medio-lateral) plane, and internal/external rotation in the transverse plane;
- 1 at the knees: flexion/extension in the sagittal plane;
- 2 at the ankles: dorsiflexar/plantar flexion in the sagittal plane, and inversion/eversion around Henke's axis (Zwipp et al. 1994; Zographos et al. 2001). In the robot, the latter was defined as an oblique axis in the sagittal plane, with a 45° orientation around the medio-lateral direction.

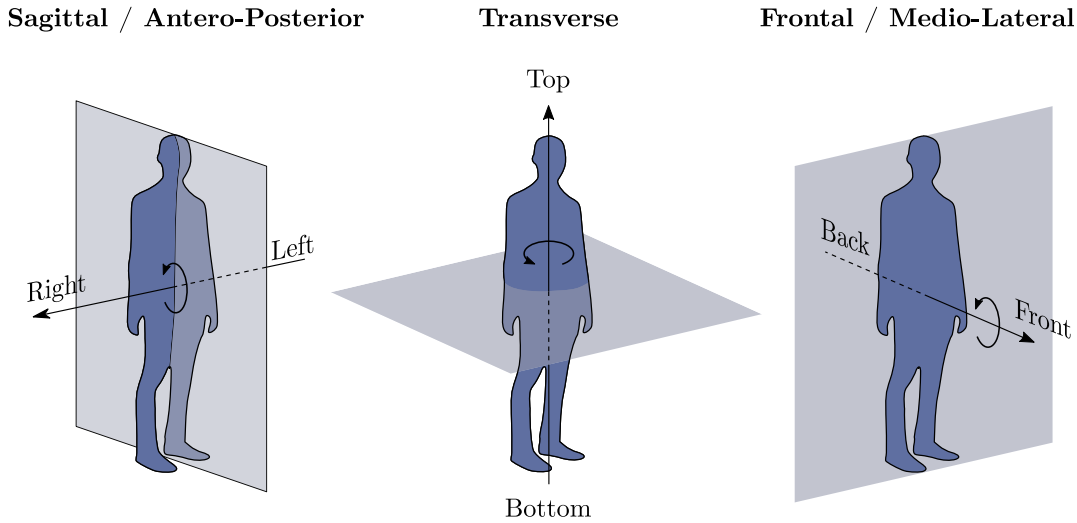


FIGURE 2.2: The anatomical planes in which the Atalante exoskeleton is actuated: the sagittal or antero-posterior plane, the frontal or medio-lateral plane, and the transverse plane.

The femur and tibia segments of the exoskeleton are adjustable in size to accommodate patients with different heights, and its maximum admissible weight is 90 kg. The robot is powered by two removable batteries placed on the femur segments. The patient is attached to the exoskeleton with multiple straps at the foot, knee, and thigh levels, as well as a jacket that is fastened to the robot's back structure. A summary of these features can be seen on figure 2.1.B.

2.1.2.2 The sensing capabilities of Atalante

The Atalante exoskeleton is also equipped with a variety of sensors: encoders are placed on all 12 actuators, and the feet, tibias, and pelvis of the robot are embedded with Inertial Measurement Units (IMUs). Together, these sensors allow the pose of the robot to be estimated in real time. An additional IMU is placed on the back of the patient jacket, and is used for intention detection as part of the high-level control interface. Lastly, force sensors are placed underneath the feet to estimate ground reaction forces and properly switch between the swing and stance legs during gait-related movements.

2.1.3 From Datagen to Wanderbrain: the software of Atalante

2.1.3.1 Generating trajectories

Atalante relies on predefined trajectories for its gait-related movements, which are generated based on the optimal control and direct collocation frameworks described by Gurriet et al. (2018). These trajectories are patient-specific, and depend on morphological parameters. In rehabilitation centers, physiotherapists take the patients' required measurements, and record them in Datagen, a remote server where trajectory generation is handled. Trajectories can then be locally downloaded via dedicated software, and uploaded to the robot before a session starts.

Different types of movements are available on the Atalante exoskeleton, and all are tailored to fit the patients' specific measurements:

- Flat-foot walking trajectories, which allow to perform basic robotic-like gait, where the feet land flat on the floor during walking;
- Foot rolling trajectories (where the feet land with the heel touching the ground first), which are more anthropomorphic, and try to mimic natural human walking;
- Side step trajectories, which allow to walk backwards, or take steps towards the left or right along the medio-lateral direction;
- Sit and stand trajectories;
- In-place turning trajectories, which allow to rotate the robot in place around the vertical axis.

An additional non-trajectory based exercising mode allows to easily move the upper parts of the robot while standing, as well as performing a squatting motion. It relies on the back IMU to derive the orientation of the patient's upper body, and to adapt the movements of the exoskeleton.

2.1.3.2 Controlling the robot

The embedded software system of the Atalante exoskeleton is known as Wander-brain. It handles all calculations, and implements the control interface of the robot. The high-level controller, which deals with detecting the user's intentions, is described in details in 2.1.4.

The mid-level layer contains different controllers, corresponding to different states or modes of the robot. These controllers run at either 200 Hz or 1 kHz. They handle mid-level movement-related variables, joint data, and trajectory tracking.

The low-level controller runs at 1 kHz. It implements PID control over the actuators, and outputs the necessary currents for each joint.

2.1.4 Detecting the user intent: a brief summary on how to navigate the Finite State Machine

2.1.4.1 An overview of Atalantes's Finite State Machine

The different activity modes and transitory states of the Atalante exoskeleton are handled by a Finite State Machine (FSM). Figure 2.3.A shows the main states and transitions of the FSM. Transitions between two states can be either button-enabled, or IMU-enabled. When the exoskeleton is powered on, it is sitting on a chair in the Installation mode, which allows the patient to climb into it. The standard or resting mode when the exoskeleton is standing up is the Standstill state. For movement-related states, the general paradigm adopted by Atalante is to implement a two-step confirmation before initiating the movement: a transition state is first activated by pressing the corresponding button (for example, going into a preparatory state before walking), and an IMU-based confirmation is then necessary to start the actual movement (for example, leaning forward to start walking). This paradigm is used for the standing, sitting, walking (in any direction), and turnaround movements.

In figure 2.3.A, purple boxes represent the preparatory transition states. Solid arrows represent button-enabled transitions, and dotted arrows represent IMU-enabled transitions. Some movements can be based on a generic state with specific modes, such as the Turnaround (or in-place turn), which can be initiated as a left (anti-clockwise) or right (clockwise) rotation. When in the Walk state, the trajectory of the robot can be modulated using a button-based direction controller to slightly veer to the left or right, without altering the actual gait pattern. Lastly, the Pause state is accessible at all times from any other state, and freezes the robot in place with the push of a button. It is also a safety state that is enabled if specific hardware or software errors occur.

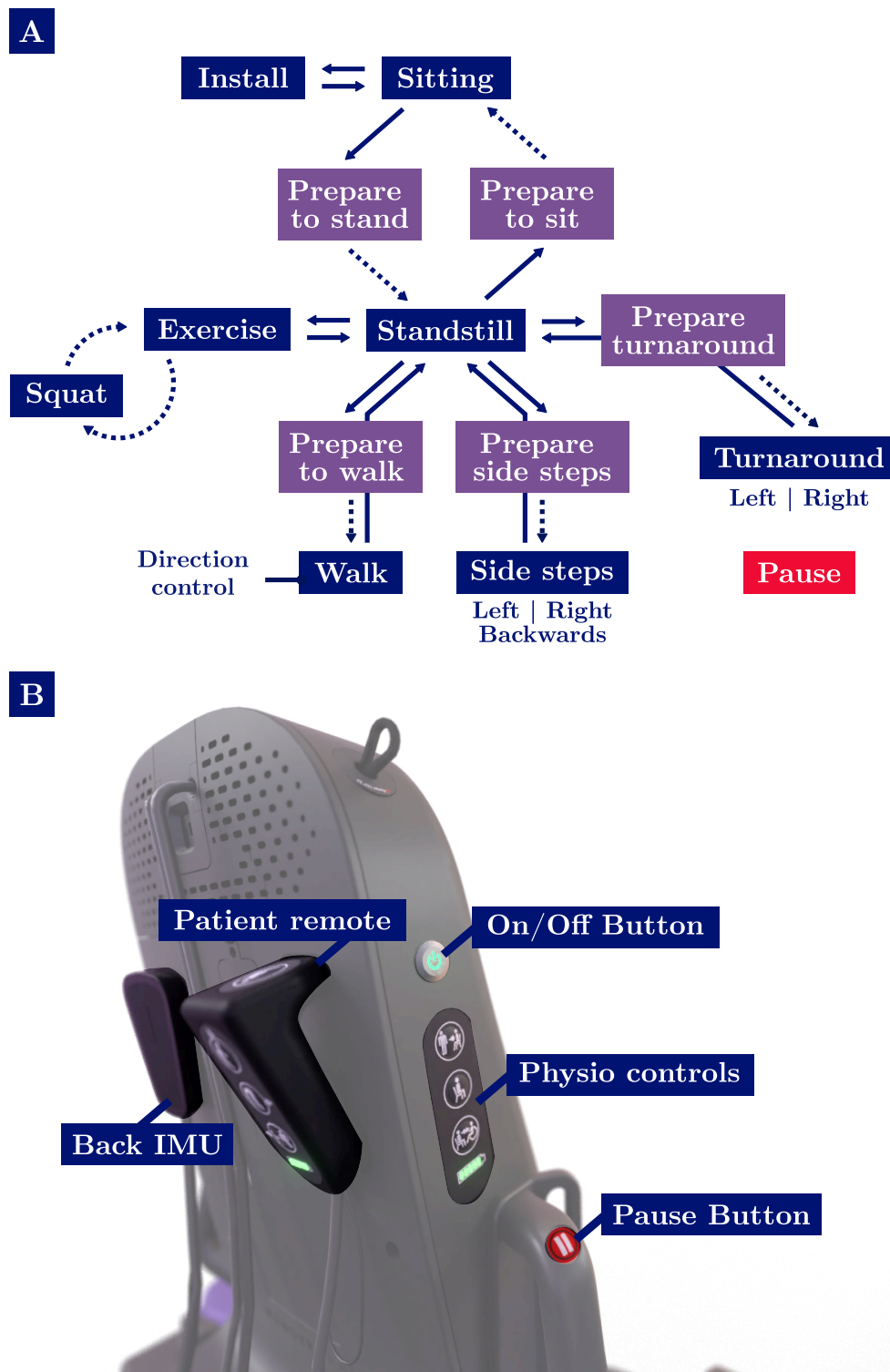


FIGURE 2.3: A. Finite State Machine of the Atalante exoskeleton. Purple boxes represent preparatory transition states. Solid blue lines represent button-enabled transitions. Dotted blue lines represent IMU-enabled transitions. Specific modes of a generic state (for example, left turnaround) are written under the corresponding boxes. Direction control is a button-enabled alteration of the Walk state. The Pause state (in red) is button-enabled, and can be accessed from any other state. B. Hardware control inputs of the Atalante exoskeleton. The patient is equipped with a remote controller, and a back IMU for transition confirmation. Additional buttons are available on the robot for the physiotherapist.

2.1.4.2 Inputs to the control interface: intention detection methods

As described above, the high-level controller of Atalante relies on two types of inputs for detecting the user intent: discrete switching inputs, and kinematic inputs.

The discrete switching inputs are provided by two button interfaces, as shown in figure 2.3.B: a handheld remote controller for the patient, and buttons embedded on the side of the robot for the physiotherapist. Essentially, the remote controller allows the patient to initiate the preparatory states for the standing, walking (in any direction), and turnaround movements, as well as launch the Exercise state, control the direction of walking, and return to the Standstill state. Buttons for the physiotherapist allow to switch between the Install and Sitting states, trigger the preparatory state for sitting down, and pause the robot.

Intended movements are confirmed based on upper-body shifts, as detected by an IMU placed on the back of the patient jacket (fastened to the back of the robot in figure 2.3.B). After having switched to the appropriate preparatory state using the corresponding button, the patient leans forward to stand, sit, or start walking, and leans sideways for side steps or turnarounds. More precisely, the pitch and roll angles are computed based on the complementary filter method as described by Mahony et al. (2008), and thresholds are set depending on the required state transition. The IMU also serves as an input for controlling balance and starting squats in the Exercise state.

2.2 | An experimental framework for the exploration of intention detection methods.

2.2.1 A generic experimental procedure for the detection of walking-related intentions

2.2.1.1 Focusing on three different intentions

As stated in chapter 1, the main objective of this thesis was to build a robust and intuitive high-level control interface for the detection of intentions in patients with upper-body motor capabilities. Lower-limb exoskeletons like Atalante mainly aim at assisting and rehabilitating walking in impaired individuals. Therefore, it was decided to focus the exploration of intent detection methods on three walking-related intentions:

- Gait initiation, or the FSM transition from Standstill to Walk;

- Gait termination, or the FSM transition from Walk to Standstill;
- Turning, or the usage of direction control during Walk.

The main objective was to allow seamless and robust intention detection around the Walk state, without the use of button-based inputs or transitioning preparatory states.

2.2.1.2 Exploration and validation: a two-steps generic framework

For all three intentions, a generic experimental procedure was proposed, consisting of two steps: (1) an exploratory experiment, for the recording and analysis of upper-body kinematics exhibited during intention-related movements, and (2) a validation experiment, to assess the efficiency and accuracy of control interfaces built upon observations from the first step. The experimental protocols presented throughout this work were approved by the Ethical Committee on Research of the Paris Descartes University (IRB number 00012019-47) according to the standards of the Declaration of Helsinki.

The materials and methods for recording movements data during these experiments, which ultimately correspond to the hardware basis of the proposed high-level control interfaces, are presented in the following section. Similarly, a unified software implementation architecture was used for all intention detection methods, and is presented in section 2.2.3.

2.2.2 Hardware tools: using IMUs to analyze upper-body kinematics

2.2.2.1 From MoCap to body-worn sensors: methods for analyzing human movement

As was already pointed out in chapter 1, kinematic inputs used in existing exoskeletons (including Atalante) can be mainly seen as stereotypical gestured switching inputs. However, it was hypothesized that finer analysis of upper-body signals during gait-related movements would provide promising methods for building a more natural interface.

Classical methods for analyzing body kinematics rely on optical Motion Capture (MoCap) systems: retro-reflective markers are attached to the body segments, and tracked with a set of cameras (Bodenheimer et al. 1997). While providing highly accurate measurements, such systems are costly, require long installation times due to marker placement, rely on precise calibration processes, and are constrained to laboratory environments. Moreover, MoCap systems providers usually implement predefined skeleton models for calibration, which offers little flexibility for specific applications (Schönauer et al. 2012).

However, in the recent years, hardware developments allowed for the miniaturization of a variety of sensors, such as inertial units, which can be used to develop body-worn systems for the collection of kinematics data (Brigante et al. 2011; Tadano et al. 2013). Such systems can be less expensive, less complex to handle, and more portable. In particular, many works focused on how body-mounted sensors – mainly IMUs – could be used to develop fully automated frameworks for the detection and identification of daily movement-based human activities (Bao et al. 2004; Karantonis et al. 2006; Bartlett et al. 2017). Tao et al. (2012) drew a comprehensive review on their usage for gait analysis, with applications in sports, rehabilitation, clinical diagnosis, and healthcare monitoring. It was therefore hypothesized that such sensors, worn at the upper-body, would be suitable for the development of movements-based intention detection methods in the Atalante exoskeleton.

2.2.2.2 IMU sensors used in this work

For the purpose of this thesis, two different sets of IMUs, consisting of triaxial accelerometers (for measuring accelerations along three directions) and gyroscopes (for measuring angular velocities around three directions), were used: the Next Generation IMUs (NGIMUs), developed by x-io Technologies (2021), and the Atalante inertial sensor boards, developed by Wandercraft.

The NGIMUs are wireless cased sensors that can send accelerometer and gyroscope data at 400 Hz through a Wi-Fi receiver using the UDP protocol. Three sensors were used during experimental procedures: one was strapped to the back of participants, the other two were strapped to the arms, close to the shoulders (see figure 2.4.A). It was important to limit the number of sensors to improve their practicability and acceptability, while providing informative data about upper-body movements.

However, while NGIMUs were well-suited for movement analyses during exploratory experiments, they were not adapted for interfacing with Atalante’s software. Therefore, a new IMU-embedded patient jacket was developed using the Atalante sensor boards, which can send accelerometer and gyroscope data at 1 kHz. Sensors were placed at the back and arm levels, similarly to the NGIMUs, as seen in figure 2.4.B. The IMU jacket can be directly connected to the exoskeleton using the available back IMU connection, and thus benefit from processing frameworks already implemented on Wanderbrain.

One drawback of the sensors embedded in the jacket is that they are not equipped with magnetometers, which are used to correct for the so-called gyroscope drift in order to derive the yaw angle of the IMU and give its precise orientation (Palermo et al. 2014). One objective of the thesis was therefore to implement high-level control interfaces that would be based on direct measurements from the sensors (accelerations and angular velocities), without requiring precise orientation calculations such as those used by Šlajpah et al. (2014).

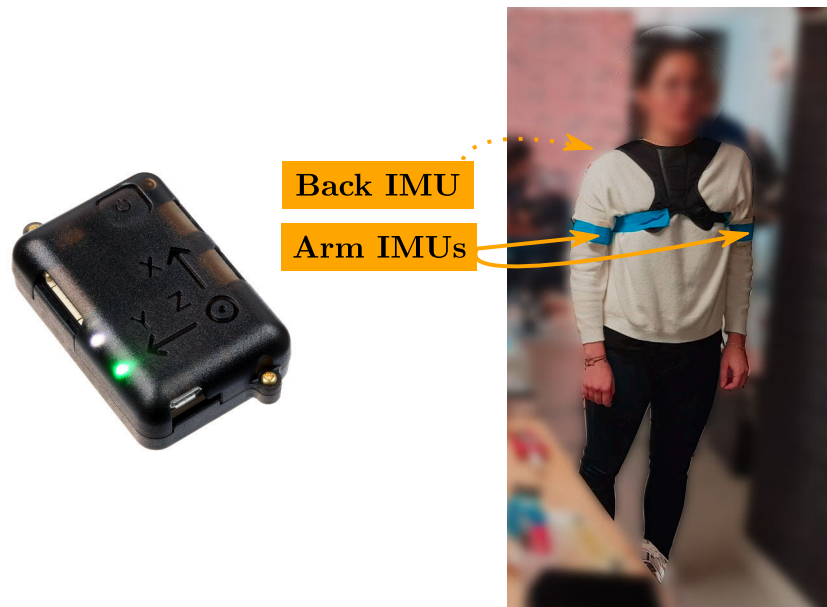
A The NGIMUs**B** The IMU Jacket

FIGURE 2.4: A. Photo of an NGIMU, and placement of the sensors during an experimental procedure. The dashed arrow indicates that the back IMU is not visible on this photo. B. Placement of the IMU sensors in the IMU-embedded jacket.

In the following chapters, the (Back-Front), (Left-Right), and (Bottom-Up) axes represented in figure 2.2 will be respectively referred to as the AP, ML, and vertical axes. AP (or sagittal), ML (or frontal), and vertical accelerations will respectively refer to accelerations along the AP, ML, and vertical axes. Similarly, AP (or sagittal) angular velocities will refer to angular velocities contained in the AP plane around the ML axis, ML (or frontal) angular velocities will refer to angular velocities contained in the ML plane around the AP axis. Vertical angular velocities will refer to angular velocities contained around the vertical axis.

2.2.3 A unified process for detecting intentions based on IMU data

2.2.3.1 A brief summary on the common classification framework

Preece et al. (2009b) provided a comprehensive review of classification techniques in the context of human activity identification based on body-worn sensors. Such methods allow a suitable and portable data collection process. Effective algorithms are then implemented to classify activities based on the collected data, and should correctly overcome the high variability in sensor characteristics and signals to provide robust predictions.

Classification techniques usually follow a multi-stage framework, which consists in dividing the signal into sequential time windows for data collection, extracting the window-related features, and labeling them according to the recognized activity.

Windowing The most commonly used windowing technique for real-time applications is the sliding window. It consists in concatenating data frames into fixed-length time windows. It is important to adapt the window size to the desired application, and an overlap between consecutive windows can improve the results (Bao et al. 2004; Preece et al. 2009a,b). After having been filled with the signals data (which can either come in raw or preprocessed format), the windows are further analyzed through the subsequent steps of the process.

Features extraction Relevant features are extracted from the data windows to serve as inputs for a given classifier. They can be heuristic (i.e. intuitively chosen based on the desired application), or selected from the time, frequency, or time-frequency domains (Preece et al. 2009b). Features in the time domain are directly derived from signal time series. They are often based on statistical metrics, such as the mean, maximum, and minimum values, standard deviation, variance, etc. Features in the frequency domain are usually derived from a Fast Fourier Transform (FFT) of the signals – for example, by combining the frequency components of the signals. Time-frequency features can be obtained from a wavelet analysis, which provides information on both the time and frequency characteristics of a

signal (Hariharan 2019). Further refinement on the choice of features can be done by using feature selection and dimensionality reduction techniques, as described by Preece et al. (2009b).

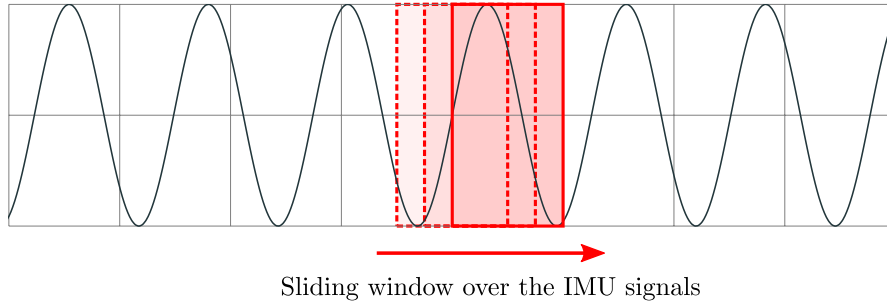
Data classification After the selected features have been extracted from a given window, they are used as input for a classification architecture, which identifies the underlying state or activity. Classification architectures can be as simple as threshold-based classifiers, which output a decision based on comparisons between the extracted features and specified threshold values, or require more complex implementations, such as machine learning-based schemes, where specific algorithms learn to recognize activity patterns based on training data (Preece et al. 2009b). The latter can be either supervised, meaning that training data is explicitly annotated by a human operator, or unsupervised, meaning that the algorithm identifies underlying patterns in the training data to automatically associate them to different classes. Different types of machine-learning models for classification exist, such as linear models, neural networks, or mixture models (C. Bishop 2006; Preece et al. 2009b). However, it is difficult to assess which of these techniques can perform the best given a specific classification problem. This is mainly due to the high variability of conditions through which different studies can be set up. Furthermore, choosing a classifier depends on the specific needs of an application, and classification accuracy cannot be taken as the sole judge for the final choice. Other *criteria*, such as time of training, implementation complexity, or capabilities of on-line processing and real-time performance must be taken into account. It is also possible to propose hybrid approaches, where multiple classifications are performed in parallel using different architectures: the different outputs are combined using techniques such as majority voting (where the majority class output is the overall output) or stacking (where outputs are in turn converted into inputs for a higher classification level).

2.2.3.2 A unified software implementation

An abstract generic process based on the generic classification framework described above was used to build the high-level controller for the detection of intentions in the Atalante exoskeleton. It can be implemented as a unified two-threaded process, as illustrated in figure 2.5:

- Data collection: a thread for buffering the sensors data into a sliding window;
- Data classification: a thread for extracting features from the latest filled window, and classifying the data according to the appropriate classification architecture. Depending on the output of the classifier, a new state of the robot can be triggered.

Thread 1 | Data collection



Thread 2 | Data classification

Specific architecture depends on current state

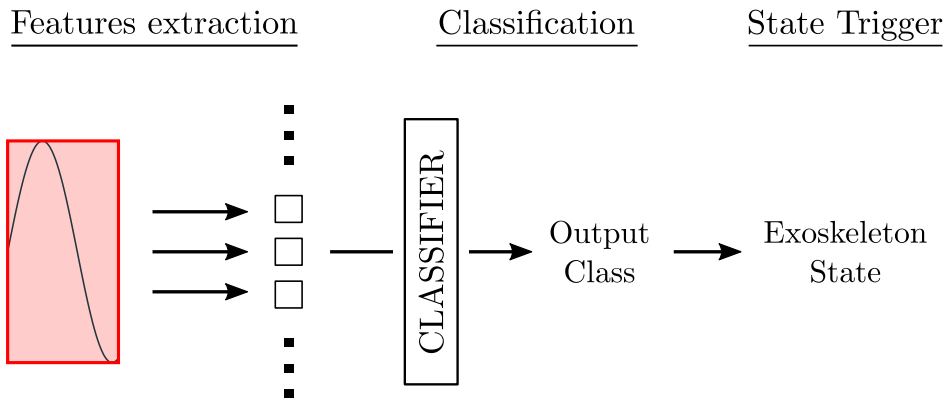


FIGURE 2.5: The unified generic process for the high-level controller. It consists in two tasks, separated into two running threads: one for data collection, and one for data classification.

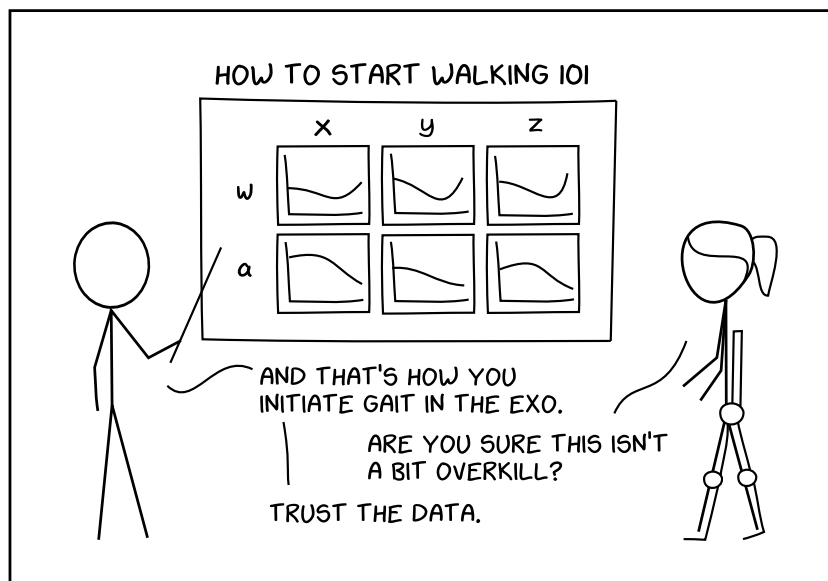
This process can be used for the high-level controller as a whole, with specific implementation adaptations depending on the state of the exoskeleton.

In the following chapters, the two-steps experimental studies of the different walking-related intentions identified in section 2.2 will be presented and discussed. The implementation of the different classification architectures based on the generic high-level controller process will then be described.

Chapter 3

Detecting the Gait Initiation Intention

This chapter focuses on gait initiation, and investigates whether its precursor patterns can still be retrieved through upper body kinematics when unimpaired participants are constrained by an assistive lower-limb exoskeletal structure that prevents free leg movements. A comparison between IMU signals from the upper body during gait initiation out of and in the robot was conducted on a group of healthy unimpaired participants, and data from the free walking setting was used as a training set to build a linear discriminant analysis (LDA) classification architecture that can automatically detect gait initiation intention. This classifier was implemented online as a high-level control interface, and enriched with data recordings from typical everyday movements to increase its robustness against false walk-triggering positives.



Chapter Contents

| | | |
|------------|---|-----------|
| 3.1 | Gait initiation: definition and characteristics | 45 |
| 3.1.1 | The mechanisms of gait initiation | 45 |
| 3.1.2 | Velocity and duration considerations | 46 |
| 3.1.3 | Gait initiation in impaired groups | 47 |
| 3.1.4 | Gait initiation in the Atalante exoskeleton | 47 |
| 3.2 | The detection of gait initiation intention | 48 |
| 3.2.1 | Current solutions | 48 |
| 3.2.2 | Using training data from a free setting to detect the gait initiation intention in Atalante | 49 |
| 3.3 | Exploring upper-body kinematics during gait initiation in a free walking setting | 49 |
| 3.3.1 | The experimental setup | 49 |
| 3.3.2 | Data processing | 50 |
| 3.3.3 | Data analysis and classification | 50 |
| 3.3.4 | Results of the study | 57 |
| 3.3.5 | Discussion | 60 |
| 3.4 | Using generic upper-body kinematics data from the Free Setting to detect Gait Initiation Intention in the Atalante exoskeleton | 62 |
| 3.4.1 | The experimental setup | 62 |
| 3.4.2 | Data processing | 64 |
| 3.4.3 | Data analysis and classification | 64 |
| 3.4.4 | Results of the study | 65 |
| 3.4.5 | Online classification of the CS signals | 67 |
| 3.4.6 | Testing the classifier for false Gait Initiation Intention (GII) positives induced by everyday movements | 71 |
| 3.4.7 | Discussion | 72 |
| 3.5 | Limitations and prospects of the study | 74 |
| 3.6 | Conclusion | 74 |



3.1 | Gait initiation: definition and characteristics.

3.1.1 The mechanisms of gait initiation

Gait initiation is defined as the transition between upright standing and steady-state walking. It can be divided into two distinct phases: the anticipation phase, and the step execution phase, separated by heel-off of the swing limb (Brenière et al. 1992; Brunt et al. 1999). The anticipation phase is characterized by the so-called anticipatory postural adjustments (APA), which come as a centrally preprogrammed compensation for the incoming disturbance to postural balance (Bouisset et al. 1987). During this phase, the Center of Pressure (CoP) moves backwards, and towards the swing limb, which results in a forward movement of the Center of Mass (CoM) towards the stance limb (Jian et al. 1993; Brunt et al. 1999). This reciprocal relationship between the CoP and the CoM is shown in figure 3.1, adapted from Jian et al. (1993). It is initiated 350 – 450 ms before heel-off (Brenière et al. 1992) by specific muscle activity, resulting in momentary loading of the swing leg, and unloading of the stance leg through slight flexion of the hip and knee joints (Jian et al. 1993; Elble et al. 2004).

Brenière et al. (1992) additionally showed that the ipsilateral hip (on the side of the swing leg) begins its forward progression during the anticipation phase to counteract the effects of the perturbation introduced by heel-off: without such an anticipation, the hip joint would provoke a backwards movement instead. The importance of APAs was also suggested by a model of the gait initiation dynamics by Anand et al. (2017), who showed that adding APAs to their model through kinematics of the CoM reduces the net energetic cost, and provides more biologically relevant solutions. Lastly, Brenière et al. (1992) showed that anticipatory movements at the shoulders result in a forward flexion of the trunk, and initiate the forwards progression of the body. Similarly, Ceccato et al. (2009) showed that the trunk presents a general forward inclination in the sagittal plane during the anticipation phase.

This inclination is preserved through the perturbation introduced by heel-off (Brenière et al. 1992; Ceccato et al. 2009), which is characterized by a quick movement of the CoP under the stance limb, as unloading of the swing leg occurs, and the CoM is accelerated forwards (Jian et al. 1993). This starts the step execution phase, which Lepers et al. (1995) compare to a ballistic forward fall around the stance ankle, and during which the forward velocity of the CoM is therefore increased to reach a speed close to that of steady-state gait (Jian et al. 1993; Brunt et al. 1999). By the end of the first step, the progression velocity of the CoM has been shown not to significantly differ from the mean speed of steady-state gait (Breniere et al. 1986), which is generally reached by the second

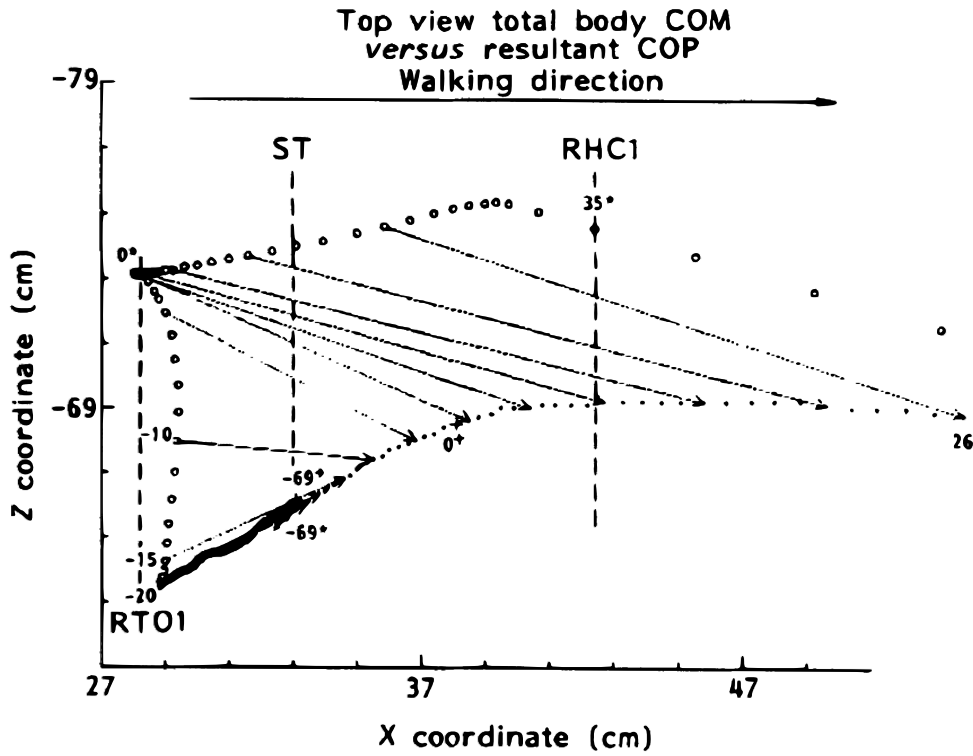


FIGURE 3.1: Adapted from Jian et al. (1993). Trajectories of the CoM (dots) and CoP (circles) during gait initiation. Right leg is the swing limb. Abbreviations: R/L = Right/Left, HC/TO = Heel-Contact/Toe-Off. See original paper for more indications.

step (Yvon Brenière et al. 1991; Jian et al. 1993). Heel-on of the swing limb may therefore indicate the end of the gait initiation motor program (Ceccato et al. 2009). Interestingly, Ceccato et al. (2009) showed that the kinematics and muscular activity of the trunk are similar between the execution phase and steady-state walking, suggesting that the walking motor program probably overlaps with the gait initiation process, and might start as soon as the swing limb leaves the ground.

3.1.2 Velocity and duration considerations

The progression speed achieved by the end of the first step can be modulated during the anticipation phase by increasing the moment around the ankle joint, and therefore the forward inclination of the trunk, which acts on the position of the CoP so that it is more forward in preparation for faster steps: the anticipated control of muscular activity allows to reach a centrally decided speed at the end of the execution phase (Leper et al. 1995). This pre-programming of the gait initiation task is confirmed by the model of Anand et al. (2017), who showed that

a feed-forward law based on an open-loop relationship between velocity and force could predict the net average forces necessary to achieve the required progression speed.

Interestingly, the total duration of gait initiation is independent of progression velocity (Breniere et al. 1986; Yvon Brenière et al. 1987, 1991; Brunt et al. 1999). However, the durations of the anticipation and execution phases are both dependent on speed: the first increases with velocity, while the second decreases (Yvon Brenière et al. 1987). The invariance of the total time between the gait initiation onset and the first step can be explained based on an inverted pendulum model, which suggests that this duration depends solely on biomechanical constants: the body mass, the body moments of inertia, and the distance between the center of gravity and the ground (Breniere et al. 1986; Yvon Brenière et al. 1991). Additionally, during the anticipation phase, the magnitude of APA in the antero-posterior direction is also dependent on the step velocity (Rocchi et al. 2006).

3.1.3 Gait initiation in impaired groups

The mechanisms described above can be affected in aged groups, or in patients with motor disabilities: Halliday et al. (1998) showed that while temporal and spatial patterns during gait initiation are preserved in older groups and patients with Parkinson's Disease (PD), the variables are slower, and propulsive forces smaller. Similarly, M. Mancini et al. (2009) used accelerometers to derive APA characteristics from PD patients, and their results showed lower values for the medio-lateral variables, resulting in smaller lateral dispersion, and suggesting that loading and unloading of the lower limbs are impaired in such a group. Difficulties in the first step execution can also be encountered in aged patients with specific gait disorders, because of limited vertical and antero-posterior forces at the stepping foot (Patchay et al. 2002).

3.1.4 Gait initiation in the Atalante exoskeleton

Initiating gait in the Atalante exoskeleton from the Standstill state is a two-steps process: first, the user needs to push a button on the remote to enter the Prepare to Walk transition state; then the intention is confirmed by tilting the torso forwards, which is detected by the back IMU and initiates the actual gait trajectory. If no movement of the torso is detected after 30 s while in the Prepare to Walk state, the exoskeleton goes back to Standstill.

After initiation of the walk, the exoskeleton performs a first step which characteristics are different from the steady-gait steps: they are computed so that the exoskeleton is properly balanced during this transient period.

3.2 | The detection of gait initiation intention.

3.2.1 Current solutions ---

Many research teams have recently focused on the detection of the gait initiation intention, by proposing different sensor-based methods for the automatic detection of the APA onset. Martinez-Mendez et al. (2011) used Inertial Motion Units (IMUs) placed at the lower-back level and near the ankle to detect APA and derive their characteristic variables. By using a simple threshold-based algorithm, they were able to properly detect the onset of APA. They were also able to evaluate their amplitude and duration using the IMU output signals, with resulting measures similar to those derived from a stabilometer. Similarly, Martina Mancini et al. (2016) used the medio-lateral acceleration from a trunk IMU to identify candidate APA periods based on a threshold, and identified the actual APA using step characteristics derived from the angular velocity outputs from two shank IMUs. Inertial signals were also used to characterize the APA, and results were strongly correlated with measures from a camera and a force plate. However, these methods are only suitable for the analysis of offline data.

Other works have focused on the use of supervised learning techniques to propose automated methods for gait initiation intention detection based on several sensing techniques. Reberšek et al. (2011) compared the performance of a k -nearest neighbor approach, a quadratic discriminant analysis, and a classification tree on three different sources of data: inertial sensors at the legs and trunk, optical markers on the upper and lower body, and force plates. They were able to successfully detect the gait initiation onset well before heel-off. While IMUs did not perform the best, they were still recommended for being the most portable solution. Novak et al. (2013) used more IMUs (placed at the back, arms, thighs, and shanks) in conjunction with instrumented insoles to evaluate the performance of a classification tree at detecting the gait onset at different speed levels. Within-subject classification yielded less than 3% of undetected events, with worse results for subject-independent validation.

Lastly, one team was able to investigate the use of both IMUs and EMGs to detect the onset of gait initiation in transfemoral amputees, using thresholds on the different signals (Wentink et al. 2013, 2014).

3.2.2 Using training data from a free setting to detect the gait initiation intention in Atalante

While some of the solutions described above seem promising for real-time detection of the gait initiation intention, the investigations were limited to unimpaired participants walking freely in an unconstrained environment, and usually partly based on sensors placed at the lower body. The study presented in this chapter investigates whether precursor patterns of gait initiation can still be retrieved through upper body kinematics when unimpaired participants are constrained by an assistive lower-limb exoskeletal structure that prevents free leg movements. In particular, it was hypothesized that generic upper limb movements during APA could be preserved in an exoskeleton-constrained environment, and could therefore be used to predict the user's intention to initiate gait while in the robot. Since no exoskeleton dynamics are present during Standstill, the IMU signals should be correct indicators of the upper-body movements, and therefore of the kinematic patterns of APA. However, simple thresholding techniques can pose the problem of false detections when standing still in the exoskeleton, since any movements with a high-enough amplitude could be perceived as an intent to start walking. Therefore, a supervised learning approach was rather preferred: it was hypothesized that a classification architecture could perform well at robustly detecting the gait initiation onset, while decreasing the risk of false positive detections by adding IMU recordings from typical standing everyday movements to the training data. Such an architecture would allow seamless transitions between standing still and walking, without having to go through a button-induced preparatory state.

Correctly triggering the walking state of Atalante would also confirm that upper body movements that anticipate gait initiation are possibly preserved between the free and constrained settings. They could therefore be used to elaborate more natural and robust control strategies for exoskeletal assistive devices based on classification techniques, with limited to no false positive detections.

3.3 | Exploring upper-body kinematics during gait initiation in a free walking setting.

3.3.1 The experimental setup

Ten participants (7 men and 3 women) took part in a free setting (FS) exploratory experiment. They were aged 29.9 ± 4.3 years old, with an average weight of 67.5 ± 13.32 kg and an average height of 174.7 ± 9.70 cm (mean \pm SD). They had no physical or cognitive disabilities affecting gait, and were not aware of the study's focus on gait initiation. They were equipped with three NGIMUs, as

described in chapter 2. Additionally, they were asked to remove their shoes, and were equipped with a force sensitive resistor (FSR) placed underneath the right heel. The FSR was connected to the back IMU through an analog channel, and the signal was transmitted at 10 Hz. It was used to segment the walking data into left and right steps, and facilitate the training data labeling process.

Instructions were given to the participants after being equipped with the IMUs and the FSR. The experiment consisted of 20 trials, in which the participants performed a straight walk of approximately 4 m at their preferred pace. At the beginning of each trial, they were asked to stand still in a neutral position behind a specified line on the ground, with their arms alongside their body, and their head straight and gazing forwards.

The IMUs were initialized to set the reference frames at the neutral position, after which the recording began. An audio cue was emitted after 3 s, indicating that the participants could start walking. To avoid any startle effects due to the emitted beep, participants were asked to start walking whenever they wanted to after hearing the sound cue. They were also asked to use their right leg as the first swing leg. At the end of the 4 m walk, participants stood still in their neutral position for approximately 2 s, after which they were instructed to go back to the starting position, and wait for the beginning of the following trial. This protocol is illustrated in figure 3.2.

3.3.2 Data processing ---

Data from the FS experiment were processed offline. Accelerometer and gyroscope signals were low-pass filtered using a second-order Butterworth filter with a cutoff frequency of 3 Hz, as used by Martinez-Mendez et al. (2011). Signals were also offset based on their average over the first second of recording, during which the participants were standing still in a neutral position. Trials where indications were not correctly followed, or for which signal waveforms differed significantly from the average ones were considered outliers, and discarded. A total of 170 trials were retained for the subsequent analysis.

3.3.3 Data analysis and classification ---

3.3.3.1 Linear Discriminant Analysis

Data classification was performed using Linear Discriminant Analysis (LDA) (Hastie et al. 2001), which is a supervised learning technique for classification.

One of the earliest formulations of the LDA comes from Fisher (1936), who introduced a criterion F to separate p -dimensional labeled data into two classes

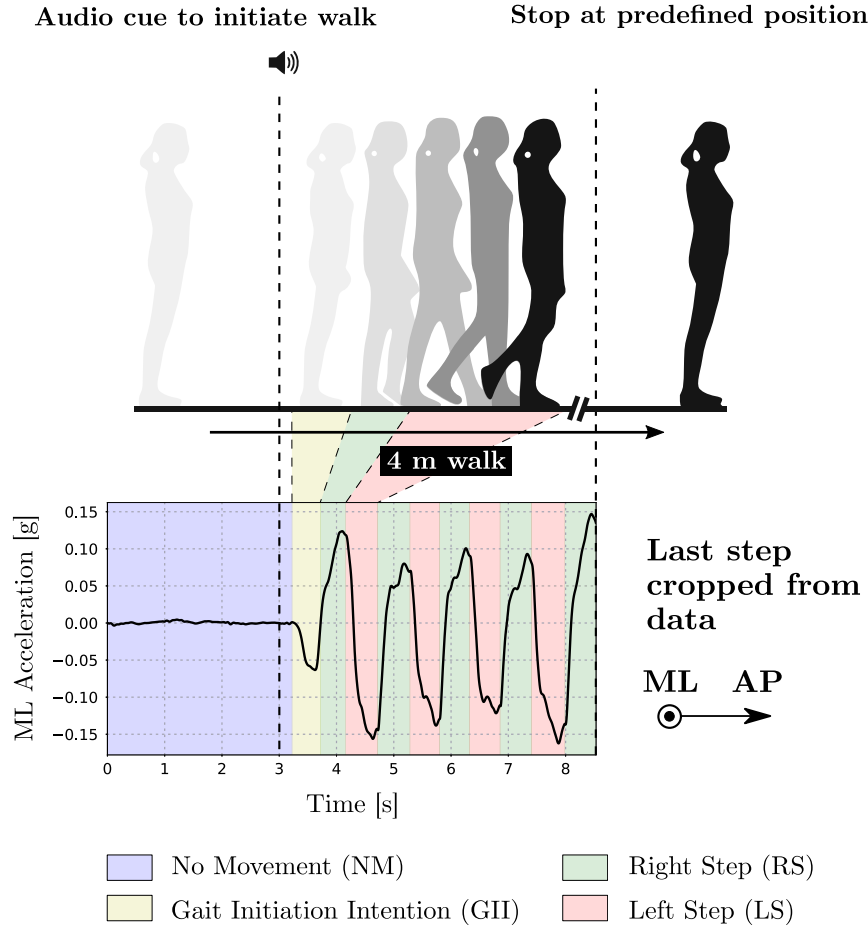


FIGURE 3.2: Illustration of one trial from the FS condition. The signal represents labeled ML acceleration data from the back IMU in [rad/s] after the last step was removed. Blue indicates the NM class, yellow indicates the GII class, green indicates the RS class, and red indicates the LS class.

by maximizing between-class covariance and minimizing within-class covariance using an optimally-defined hyperplane:

$$F = \frac{(m_2 - m_1)^2}{s_1^2 + s_2^2} \quad (3.1)$$

where m_1 (resp. m_2) and s_1 (resp. s_2) are the mean and within-class variance of class 1 (resp. class 2) projected onto the weight vector \mathbf{w} normal to the separation hyperplane. It can be shown that F is maximized when the direction of \mathbf{w} is chosen such that:

$$\mathbf{w} \propto \mathbf{S}_W^{-1} (\mathbf{m}_2 - \mathbf{m}_1) \quad (3.2)$$

where \mathbf{m}_1 (resp. \mathbf{m}_2) is the class 1 (resp. class 2) mean in the original p -dimensional space, and \mathbf{S}_W is the total within-class covariance matrix, defined as the sum of covariance matrices of classes 1 and 2 in the original space. This is illustrated in figure 3.3, adapted from C. Bishop (2006).

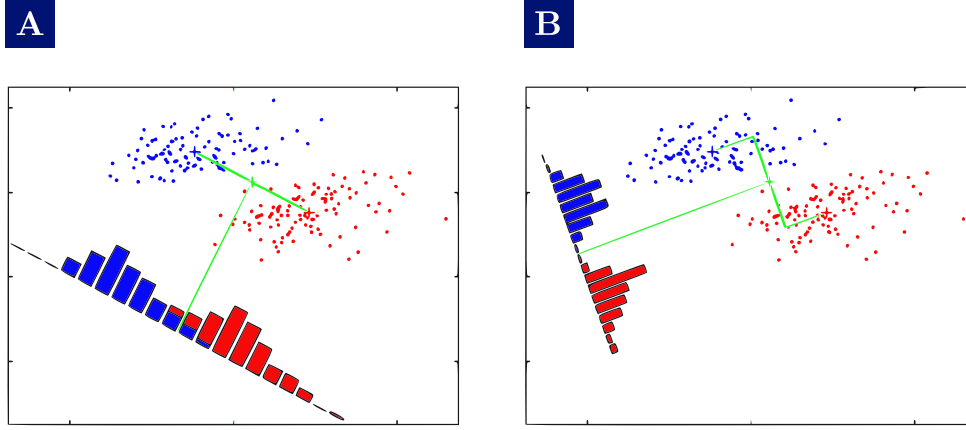


FIGURE 3.3: Adapted from C. Bishop (2006). Two methods for separating two classes in a two-dimensional space. Histograms represent the projections of the data points on the weight vectors normal to the separating hyperplanes. A. The separation between the red and blue classes is based on the weight vector joining the two class means, and leads to considerable overlap. B. The within-class covariance is taken into account through Fisher's criterion, which leads to better class separation.

Extending this method to K classes, the measures of between-class and within-class covariances can be defined as:

$$\mathbf{S}_W = \sum_{k=1}^K \sum_{n \in C_k} (\mathbf{x}_n - \mathbf{m}_k)(\mathbf{x}_n - \mathbf{m}_k)^\top \quad (3.3)$$

$$\mathbf{S}_B = \sum_{k=1}^K N_k (\mathbf{m}_k - \mathbf{m})(\mathbf{m}_k - \mathbf{m})^\top \quad (3.4)$$

where $\mathbf{x}_n, n \in C_k$ is a data point of class k , N_k is the total number of data points in class k , \mathbf{m}_k is the mean of class k , and \mathbf{m} is the total mean of all data points.

It can be shown that the directions of the weight vectors for this multi-class problem are given by the eigenvectors of $\mathbf{S}_W^{-1}\mathbf{S}_B$ corresponding to the $K - 1$ largest eigenvalues (C. Bishop 2006). This additionally allows to project data from the original feature space into subspaces of dimensions at most equal to $K - 1$, which is particularly useful for visualization purposes. Essentially, classification of

a new data point is then performed according to the closest class centroid in the chosen subspace (Hastie et al. 2001).

Hastie et al. (2001) also arrive at the same results, by taking a Bayesian approach, and assuming normally-distributed data with a common covariance matrix for all classes. However, LDA is considered fairly robust to violations to these assumptions (Li et al. 2006).

3.3.3.2 Labeling the training data

Accelerometer and gyroscope signals from the FS experiment were segmented into four different classes: No Movement (NM), Gait Initiation Intention (GII), Right Step (RS), and Left Step (LS). Heel events of the right foot were derived from the FSR data for step labeling. The FSR data during the first three seconds of recording were averaged to set a standing still baseline for each trial. Heel-strike events were then set when the FSR signal was higher than the baseline plus one standard deviation, and heel-off events were set when the FSR signal was lower than the baseline minus one standard deviation. RS was defined as the class covering signal portions going from heel-off to heel-strike, and LS was defined as the class covering signal portions going from heel-strike to heel-off. Data following the last heel-strike event were discarded, as last step dynamics differed from steady-pace walking. The first detected upper-body movements on the IMU data were used to determine the onset time t_{onset} for the GII class. Detection was achieved by setting movement thresholds $T_{+,sig}$ and $T_{-,sig}$ for each accelerometer and gyroscope signal $sig \in \{\ddot{x}, \ddot{y}, \ddot{z}, \omega_x, \omega_y, \omega_z\}$ as:

$$\begin{aligned} T_{+,sig} &= m_{sig} + 10 \times s_{sig} \\ T_{-,sig} &= m_{sig} - 10 \times s_{sig} \end{aligned} \quad (3.5)$$

where m_{sig} (resp. s_{sig}) is the average (resp. standard deviation) of each signal over the 1.5 s preceding the audio cue. For each signal, $t_{min,sig}$ was then defined as the earliest time such that $sig \notin [T_{-,sig}, T_{+,sig}]$, and t_{onset} was defined as:

$$t_{onset} = \min_{sig} t_{min,sig} \quad (3.6)$$

The first heel-off was used as the end of the GII class. The remaining portions of signals, spanning from the beginning of each trial up to the GII onset, were labeled as NM. A final step consisted in manually adjusting the class onsets if outputs from the above steps were incorrect. Figure 3.2 shows an example of labeled accelerometer data.

3.3.3.3 Selecting relevant features

Once accelerometer and gyroscope data from all trials and participants were correctly labeled, they were used as training sets to construct LDA classifiers. Sliding windows with a 25% overlap were used to divide the sensor signals into 500 ms time segments. The choice of window length was motivated by reported values for APA duration by Brenière et al. (1992) and M. Mancini et al. (2009) (350 - 550 ms). The overlap value was chosen to enhance the classifier reaction time. Each window was associated with a given class if at least half of its signal content was labeled as so, based on the labeling step. A set of optimally relevant features were then extracted from each segment to compute labeled feature-space data points. They were selected based on previous research (Preece et al. 2009a,b).

In order to reduce the computational cost for features extraction in real-time, and avoid overfitting, further analyses were conducted to discard features which were not discriminative enough for the classification task. In particular, a single-factor ANOVA between labels and features was conducted to only select features with high variance across the different classes. This allowed to define a subset of 11 features, which were computed from both the time and frequency domains: mean, standard deviation (sd), minimum (min), maximum (max), root mean square (rms); spectral energy, and the five highest amplitudes of the frequency components in the frequency-domain. Since all features were extracted from each of the 18 IMU signals, this resulted in a final 198-dimensional feature space, as described in table 3.1. Figure 3.4 additionally shows how the selected feature values extracted from accelerometer signals from all participants can vary between different classes. While some features seem to be more discriminative than others, the LDA should optimize the projection of the feature space to maximize the separation between the different classes.

| | Feature | Number of dimensions |
|---------------------------|--------------------|----------------------|
| Time-domain features | mean | 18 |
| | sd | 18 |
| | min | 18 |
| | max | 18 |
| | rms | 18 |
| Frequency-domain features | spectral energy | 18 |
| | highest amplitudes | 90 |
| Total | 7 features | 198 |

TABLE 3.1: Set of features used in classifiers construction

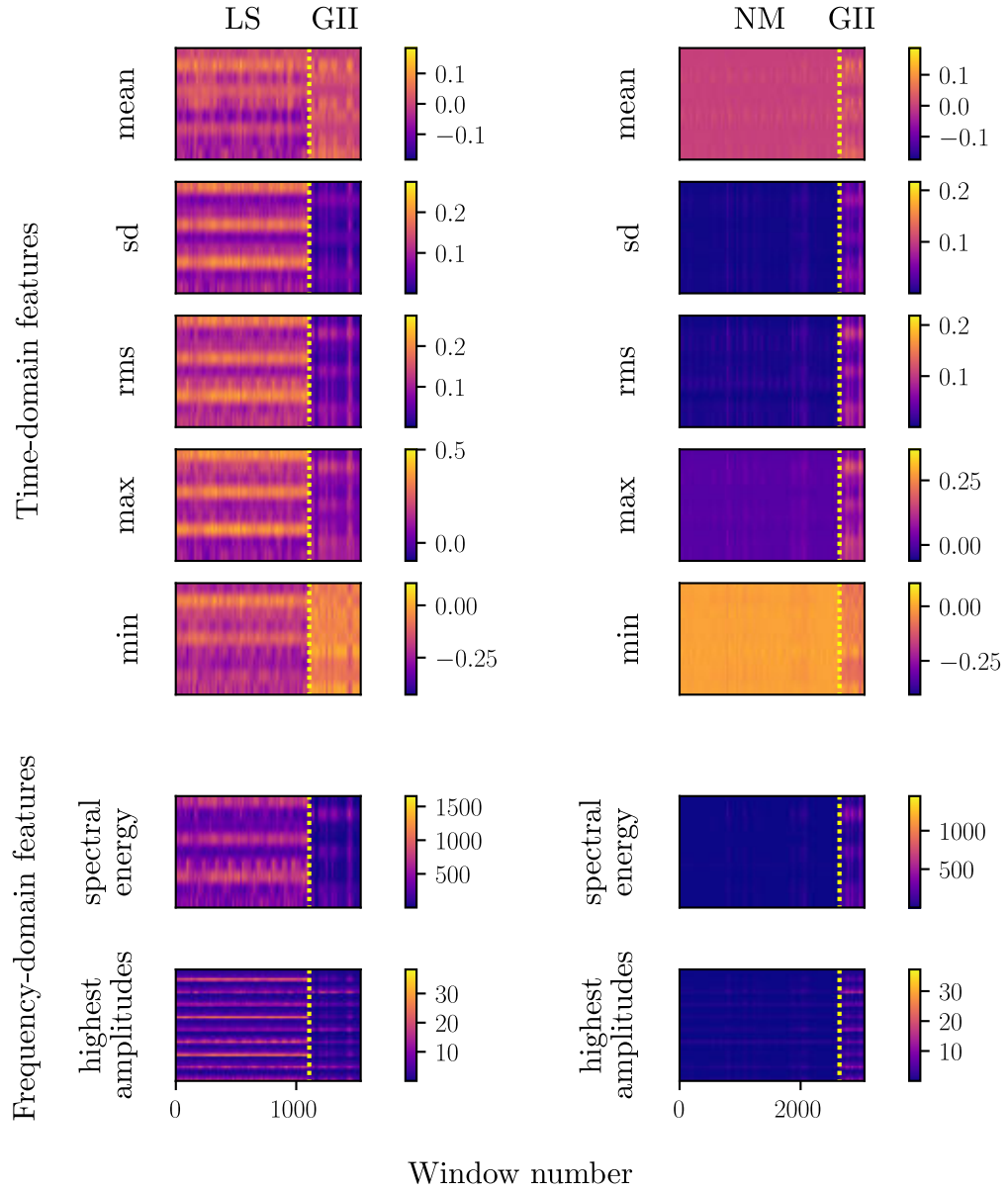


FIGURE 3.4: Values of the selected features extracted from data windows from all participants and all FS condition trials, for the LS and GII classes (left) and the NM and GII classes (right). For each color matrix, lines from top to bottom represent: the right IMU accelerations (x , y , z), the back IMU accelerations (x , y , z), the left IMU accelerations (x , y , z). Classes were concatenated two by two to better see the contrast in feature values. Gyroscope features have been omitted

3.3.3.4 Training and testing the data

Trial-based cross-validation schemes were used to assess offline data classification for the FS condition. In a first setting, participant-specific data were classified according to a leave-one-out rule: training sets were comprised of all but one trial from the same participant, which was then used for testing (intra-participant classification). This was done over all trials, and the overall result was taken as the total average of all classification rates on the testing data. In a second setting, classification was assessed across participants, by leaving one participant's trials out of the training set, and using them as a testing set (inter-participant classification). The overall result was taken as the total average from testing the classifier on each of the left-out participant's trials independently.

Additionally, the Inter-class Distance Nearest Neighbor (IDNN) metric as proposed by Kristoffersen et al. (2019) was used to compute distances in the original 198-dimensional feature space formed by the training data for each participant. Let C be the set of all labeled classes (here, $C = \{1, 2, 3, 4\}$). Then, for $(i, j) \in C^2$, the Mahalanobis distance d_j^i from the cluster of points of class j to the cluster of points of class i is defined as:

$$d_j^i = \frac{1}{2} \sqrt{(\boldsymbol{\mu}_i - \boldsymbol{\mu}_j)^T \mathbf{S}_i^{-1} (\boldsymbol{\mu}_i - \boldsymbol{\mu}_j)} \quad (3.7)$$

where \mathbf{S}_i is the covariance matrix of cluster i , and $\boldsymbol{\mu}_i$ and $\boldsymbol{\mu}_j$ are the centroid coordinates of clusters i and j . Based on the Mahalanobis distance, a distance metric $m_{i,j}$ can be defined as:

$$m_{i,j} = \frac{d_j^i \times d_i^j}{d_j^i + d_i^j} \quad (3.8)$$

The IDNN for a given cluster i is then equal to the lowest distance metric value computed from all other clusters:

$$IDNN_i = \min_{j \in C, j \neq i} m_{i,j} \quad (3.9)$$

In other words, for each cluster i of points, the IDNN measures the product of its Mahalanobis distances with the other clusters in both directions, and normalizes it by their sum: it represents the distance to its nearest neighbor in a variance-normalized space. A low IDNN value for a given class indicates a larger chance of confusion with its nearest neighbor. Equal IDNN values for two different classes indicate that they are necessarily closest to each other in the sense of the Mahalanobis distance.

| | Peak Accelerations [g] | | Peak Angular Velocities [deg/s] | |
|-----------|------------------------|-----------------|---------------------------------|----------------|
| | AP | ML | AP | ML |
| Trunk | 0.05 ± 0.03 | 0.05 ± 0.02 | 21.5 ± 7.1 | 9.5 ± 6.5 |
| Right Arm | 0.05 ± 0.03 | 0.06 ± 0.02 | 23.1 ± 8.8 | 10.3 ± 5.3 |
| Left Arm | 0.10 ± 0.05 | 0.06 ± 0.02 | 18.9 ± 8.3 | 6.2 ± 5.2 |

TABLE 3.2: Peak average (\pm SD) GII accelerations and angular velocities in the ML and AP planes for all IMU placements during the FS experiment.

3.3.4 Results of the study

3.3.4.1 Upper-body kinematics during Gait Initiation in the Free Setting experiment

Figure 3.5 shows the average accelerations and angular velocities for all three IMUs in the medio-lateral (ML) and antero-posterior (AP) planes over all participants from the Free Setting (FS) experiment. Signals are represented from 0.5 s before the movement onset up to the first heel strike event. The green mark indicates the first heel-off event, and the red one indicates the first heel strike event. The shaded areas represent the standard deviations for the different signals. For waveform comparison purposes, and to get rid of amplitude variability effects, individual trial results have been standardized and represented as functions of time advancement (as a percentage value from 0 to 100). The average duration (\pm SD) between the movement onset and the heel-off was 546 ms (\pm 132 ms) for this experiment.

Average peak values for the acceleration phases in the ML and AP planes, as well as the average peak values of gyroscope signals are reported in table 3.2, and they are indicated on figure 3.5. Maximum amplitude during precursor movements for acceleration signals is always reached before the heel-off event, except for the AP acceleration from the left arm, which is slightly delayed and happens after heel-off.

3.3.4.2 Offline classification of the Free Setting signals

Table 3.3 shows the results from the LDA-based offline classification architecture on the FS experiment signals, for both the intra and inter-participant evaluations. In order to assess the classifier's ability to discriminate between all different classes, including LS and RS, it was run over the entire walk for each trial (EW data). Classification accuracy over the first signal windows spanning from the beginning of each trial up to the end of the GII class was also reported in the Table (GII data). Overall, the average classification accuracy for the entire walk was 94.7%, with

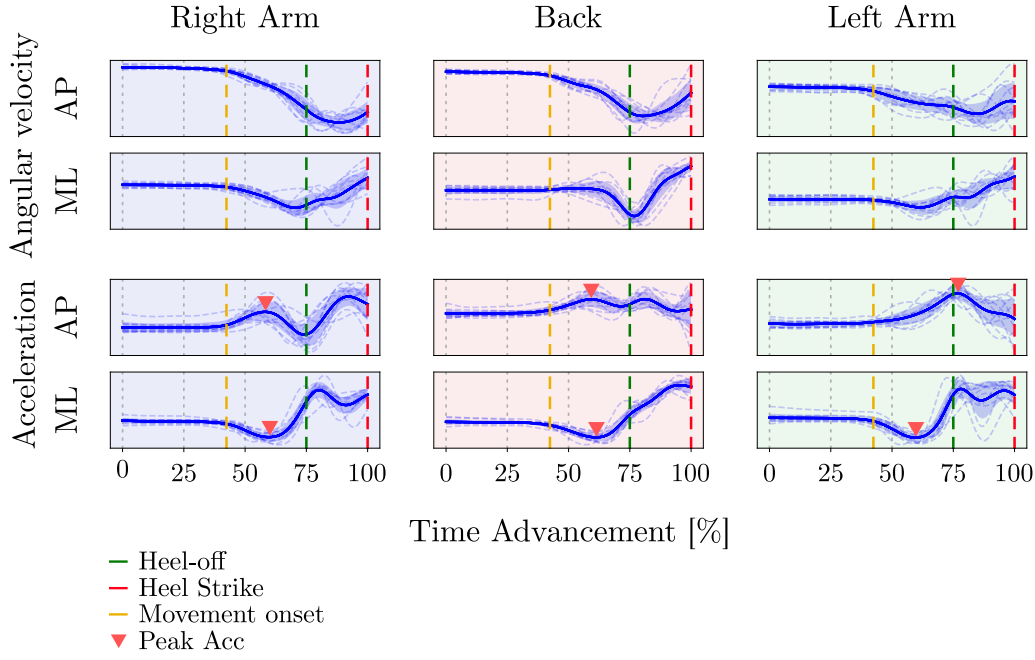


FIGURE 3.5: Average accelerations and angular velocities recorded by all three IMUs during the FS experiment trials in the ML and AP planes. The dashed lines represent the average signals for each participant, and the thick line corresponds to the overall average, with its corresponding standard deviation. Signals are represented from 0.5 s before the movement onset up to the heel-strike. Peak accelerations as defined in Table 3.2 are also indicated in the figure.

a maximum accuracy value reaching 97.9% for the intra-participant setting, and 91.9% with a maximum value of 96.5% for the inter-participant setting. However, for all trials and all participants, gait intention was always correctly detected. Classification rates for the GII data were less than 100% because of time lags, meaning that the GII class was detected a few windows early or late in some cases. The average time lag for intra-participant classification was 0.17 s, and 0.38 s for inter-participant classification, which explains the average loss of 2.5% in the classification rate between both classification schemes for the GII data.

| | Entire Walk | | | Gait Initiation | | |
|----------------------|---------------------|-------|-------|---------------------|-------|-------|
| | average (\pm SD) | max | min | average (\pm SD) | max | min |
| Intra classification | 94.7% (\pm 1.5%) | 97.9% | 92.9% | 97.6% (\pm 1.0%) | 98.7% | 96.4% |
| Inter classification | 91.9% (\pm 2.4%) | 96.5% | 87.8% | 95.1% (\pm 3.5%) | 98.3% | 89.0% |

TABLE 3.3: Classification rates from the offline classification of the FS data.

Additionally, figure 3.6 shows the structure of the individual intra-classifiers constructed from the Free Setting training data as projected on the LDA-computed two-dimensional space. Note that this is essentially a visualization tool. However,

it can still give good insight into the structure of the data, and the effectiveness of the LDA classification: for all participants, the four class clusters seem well separated and organized in the same fashion, with the GII cluster being closer to the NM cluster, and appearing as a transition between the resting state and the two walking states (Left and Right).

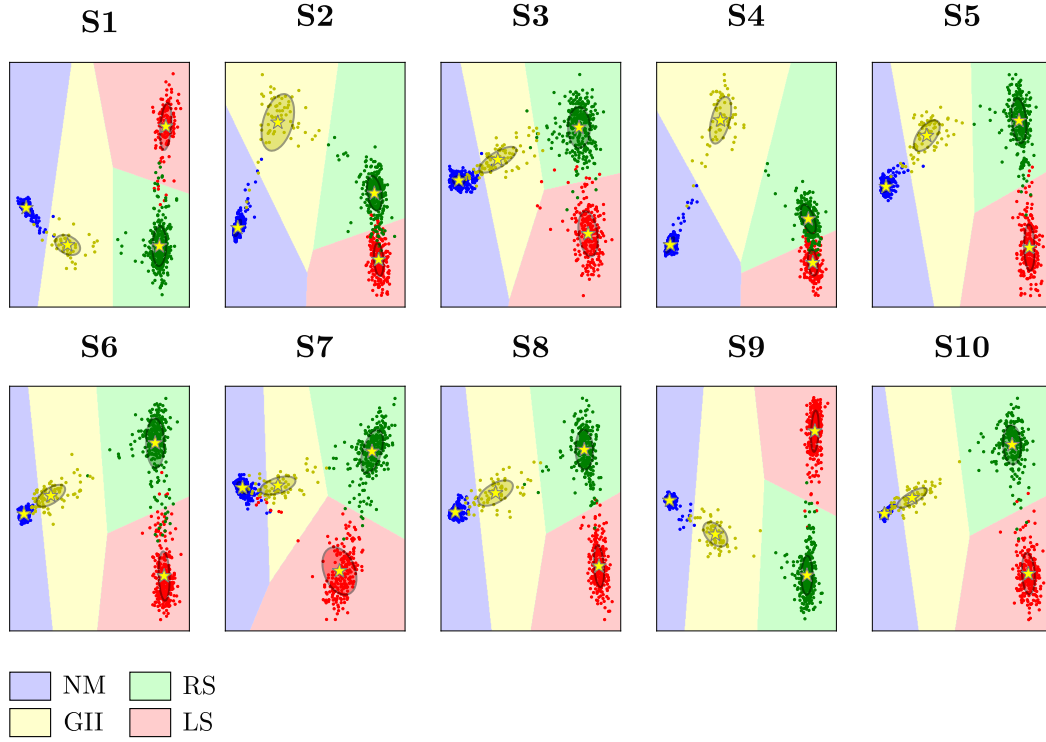


FIGURE 3.6: Representation of the intra classifiers in the two-dimensional LDA-generated projection subspace. The different colored regions represent the classifier decision regions for each of the four labeled classes (NM, RS, LS, GII).

These results are also confirmed by the Inter-class Distance Nearest Neighbor (IDNN) metric computed for each intra classifier in the original 198-dimensional feature space, as shown in figure 3.7. The distance metrics $m_{i,j}$ used for the computation of the IDNN for all labeled classes and all participants have additionally been reported in table 3.4. The table and the figure show that the NM and GII clusters are consistently closest to each other, and that both step classes are closest to each other on average.

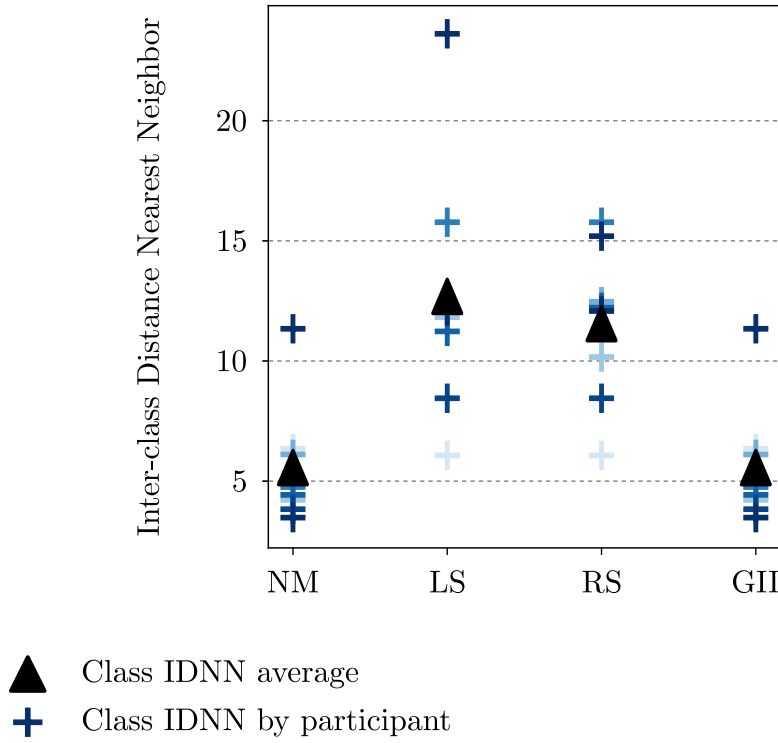


FIGURE 3.7: The Inter-class Distance Nearest Neighbor (IDNN) metric computed in the original 198-dimensional feature space for each class and each participant for the intra classifiers. When the IDNN is the same for two classes, it means they are closest to each other.

3.3.5 Discussion

3.3.5.1 Qualitative analysis of upper-body kinematic signals

Results for the trunk IMU in the FS condition were consistent with previous studies (Brenière et al. 1992; Martinez-Mendez et al. 2011; Martina Mancini et al. 2016), showing that the upper body is accelerated forwards, and towards the standing leg. Therefore, it was possible to validate our method to evaluate kinematic patterns that anticipate gait initiation based on inertial sensors placed on the upper body.

To our knowledge, there is no work investigating arm kinematics during Anticipatory Postural Adjustments (APAs), but shoulder movements have been studied before (Brenière et al. 1992). Our results suggest that both arms follow the same acceleration patterns as the trunk, and that the arms also exhibit repeatable precursor patterns before the heel-off. The overall movement is initiated by the side ipsilateral to the stepping leg (the right side in this study), since the contralateral arm exhibits a delay in its forward acceleration, with a lower peak angular velocity in the Antero-Posterior (AP) plane. The ipsilateral side of the upper body starts

| Class i | Class j | S1 | S2 | S3 | S4 | S5 | S6 | S7 | S8 | S9 | S10 |
|---------|---------|-------------|-------------|--------------|--------------|--------------|--------------|--------------|-------------|--------------|--------------|
| NM | LS | 33.77 | 126.92 | 30.43 | 207.13 | 107.67 | 61.31 | 10.03 | 98.48 | 94.9 | 98.65 |
| | RS | 26.1 | 38.57 | 17.12 | 45.71 | 33.87 | 29.65 | 33.38 | 36.6 | 53.89 | 26.7 |
| | GII | 6.35 | 4.3 | 4.22 | 6.11 | 6.2 | 4.75 | 4.43 | 3.83 | 11.34 | 3.48 |
| LS | NM | 33.77 | 126.92 | 30.43 | 207.13 | 107.67 | 61.31 | 10.03 | 98.48 | 94.9 | 98.65 |
| | RS | 6.91 | 7.23 | 11.81 | 17.29 | 14.79 | 15.85 | 14.22 | 8.41 | 11.92 | 20.12 |
| | GII | 15.96 | 22.3 | 20.58 | 30.39 | 37.58 | 34.77 | 14.15 | 26.87 | 38.87 | 42.1 |
| RS | NM | 26.1 | 38.57 | 17.12 | 45.71 | 33.87 | 29.65 | 33.38 | 36.6 | 53.89 | 26.7 |
| | LS | 6.91 | 7.23 | 11.81 | 17.29 | 14.79 | 15.85 | 14.22 | 8.41 | 11.92 | 20.12 |
| | GII | 9.18 | 13.23 | 10.23 | 17.83 | 14.48 | 14.78 | 13.68 | 12.7 | 17.83 | 15.11 |
| GII | NM | 6.35 | 4.3 | 4.22 | 6.11 | 6.2 | 4.75 | 4.43 | 3.83 | 11.34 | 3.48 |
| | LS | 15.96 | 22.3 | 20.58 | 30.39 | 37.58 | 34.77 | 14.15 | 26.87 | 38.87 | 42.1 |
| | RS | 9.18 | 13.23 | 10.23 | 17.83 | 14.48 | 14.78 | 13.68 | 12.7 | 17.83 | 15.11 |

TABLE 3.4: Distance metric $m_{i,j}$ computed in the feature space for all classes and all participants during the FS experiment. Bold values represent the IDNN for each class and each patient.

to shift forwards and towards the standing leg, and the contralateral arm follows the general forwards movement before the heel leaves the ground. Additionally, standard deviations for average acceleration peak values reported in Table 3.2 confirm that the amplitudes of arms and trunk movements are highly variable between participants.

3.3.5.2 Evaluation of Gait Initiation detection in the Free Setting (FS) based on an offline classification architecture

Intra-participant evaluation Evaluation of the intra-participant classifiers on the Entire Walk data from the FS condition returned accuracy scores higher than 94%, showing that the LDA architecture is capable of correctly discriminating between the different labeled classes in a participant-specific setting. Additionally, loss of accuracy is mainly due to time lags (either positive or negative) during transitions between different classes. Since the Gait Initiation Intention (GII) class is consistently and correctly detected for all trials, this evaluation also confirms that participant-specific kinematic patterns that precede gait initiation are repeatable in the FS condition. Therefore, intra-participant classifiers based on FS data could be used in the exoskeleton to check for similarities in these patterns when the users are constrained by a lower-limb assistive device.

Inter-participant evaluation Evaluation of the inter-participant classifiers on the Entire Walk data from the FS condition returned accuracy scores higher than 91%, showing that the LDA architecture is also capable of correctly discriminating between the different labeled classes based on data acquired from a pool of participants that does not contain the tested participant's trials. However, loss of accuracy is higher on average than the intra-participant evaluation, since time lags can be longer. Again, the GII class is consistently and correctly detected for all trials, which shows that the variability of kinematic patterns that precede gait initiation between participants in the FS condition is low. The inter-participant classifiers based on FS data could therefore also be used in a setting where participants are constrained by the exoskeleton.

This consistency is also supported by figure 3.6, which illustrates the two-dimensional projections of the intra-classifiers, and shows that training data from the different participants seem to lead to similarly structured subspaces as generated by the LDA. The Inter-class Distance Nearest Neighbor (IDNN) metric in figure 3.7 additionally confirms that the No Movement (NM) and GII clusters are consistently closest to each other, and that both step classes are closest to each other on average. This supports the fact that anticipatory patterns preceding gait initiation exhibit low-amplitude dynamics that are separable from walking-related movements.

3.4 Using generic upper-body kinematics data from the Free Setting to detect Gait Initiation Intention in the Atalante exoskeleton.

3.4.1 The experimental setup

3.4.1.1 The Constrained Setting experiment

The same participants who took part in the FS experiment were tested during a validation Constrained Setting (CS) experiment. 20 trials were conducted in which the participants were first equipped with all three NGIMUs as described in chapter 2, then installed in the Atalante exoskeleton. Only two of the participants had never been in the exoskeleton before. The robot was put into its standard standstill position, and participants were instructed to stay motionless with their arms alongside their body, and their heads straight and gazing forwards. Similarly to the FS experiment, the inertial devices were initialized at the beginning of each trial to set the reference frames, and an audio cue was emitted 3 s after the beginning of the recording to indicate the beginning of the walk. Subjects were asked to perform any upper body movements they thought would initiate

the robot's gait, as if they wanted to start walking using their right leg. This is illustrated in figure 3.8. Since two participants did not correctly follow this rule, their results were discarded from the CS experiment analysis, which only included eight participants.

In 15 out of 20 trials, an online classifier based on linear discriminant analysis (LDA, see 3.3.3) was used to detect gait intention using one of three training sets:

- (a) same participant data from the FS experiment (intra-classification);
- (b) other participants data from the FS experiment (inter-classification);
- (c) all participants data from the FS experiment (global classification).

If gait intention was correctly detected, the walking state of the robot was triggered, in which case the participants were asked to stop the robot using its remote control after a few steps. In the remaining 5 trials, (d) the exoskeleton walk was not triggered at all. These four conditions were presented in completely random order across all 20 trials.

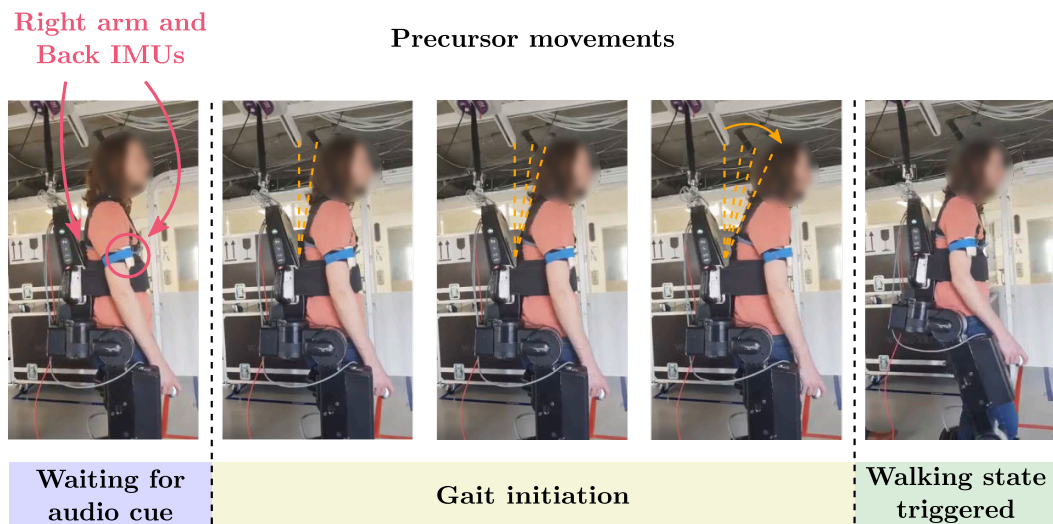


FIGURE 3.8: One participant during the CS experiment. Data from the FS experiment were used to implement online classifiers for the detection of the Gait Initiation Intention in the Atalante exoskeleton.

The software implementation was done in a separate computer that received the IMU inputs and sent a trigger signal to the exoskeleton when the gait initiation intention was detected.

3.4.1.2 The False Positives experiment

In a follow-up False Positives (FP) experiment, eight of the ten participants were equipped with all three IMUs, and installed in the Atalante exoskeleton. The robot was put into its standard standstill position, and similarly to the CS experiment, participants were asked to stay motionless with their arms alongside their body, and their heads straight and gazing forwards. They were then instructed to wait for an audio cue, after which they were asked to perform a set of typical everyday movements: handshakes, covering the mouth while coughing, and reaching an object at different levels (below the waist, at torso level, and over the head). Each movement was alternatively performed with each arm, and repeated for 4 trials. Data recordings from this experiment were analyzed offline.

3.4.2 Data processing

Data filtering and processing as performed during the FS experiment (see section 3.3.2) were also performed on the data from the FP experiment, and implemented online during the CS experiment.

3.4.3 Data analysis and classification

3.4.3.1 Constrained Setting experiment

Classification was implemented online during the CS experiment. Three classifiers were constructed for each participant based on the training data from the FS experiment: (a) one participant-specific classifier based on the participant's trials (intra-classification), (b) one classifier based on the other participants' trials (inter-classification), (c) and an additional global classifier including all participants data, which was common to all participants (global classification).

Additionally, the distance metrics $m_{i,j}$ as defined for the derivation of the IDNN were computed for each participant between the clusters formed by data points from the CS intra trials, and the clusters corresponding to the 4 labeled classes in the corresponding classifier.

3.4.3.2 False Positives experiment

For this experiment, an additional class based on miscellaneous movements (MM) was added to evaluate the classification robustness. The MM class was constructed based on the recordings of typical everyday movements from the FP experiment.

Data sets recorded during the FP experiment were first tested offline using the global classifier to test for the occurrence of false GII positives when performing everyday movements. Half of the data were then included with all the participants data from the FS experiment to construct an enriched 5-class global classifier, which was tested offline:

- on the remaining half of the FP experiment data;
- and on the trials from the CS experiment corresponding to the global classifier.

3.4.4 Results of the study

3.4.4.1 Upper-body kinematics during Gait Initiation in the Constrained Setting experiment

Figure 3.9 shows the average accelerations and angular velocities over the eight participants from the Constrained Setting (CS) experiment for all three IMUs in the ML and AP planes. The signals are represented from 0.5 s before the movement onset, up to the first zero-crossing of the angular velocity around the vertical axis. The shaded areas represent the standard deviations for the different signals. Similarly to the FS experiment, individual trial results have been standardized and represented as functions of time advancement (as a percentage value from 0 to 100).

Signals in figure 3.9 have been further filtered with a low-pass Butterworth (2nd order, cutoff 0.5 Hz) to get rid of extraneous noise, and focus on global signal evolution in time. This was only done to improve readability of the figure, but was not part of the data processing that occurred during the experiment. However, averaging and filtering techniques had a dampening effect on the representation of the signals in figure 3.9. Figure 3.10 shows an example of a typical AP acceleration profile exhibited by one participant on the right arm IMU during the CS experiment without additional processing, as was used by the classifiers. It shows that a short acceleration phase immediately follows the movement onset, before the acceleration direction changes.

Average peak values for the acceleration phases in the ML and AP planes for are reported in table 3.5. Additionally, average peak gyroscope values from the CS signals as represented on figure 3.9 are also reported on Table 3.5.

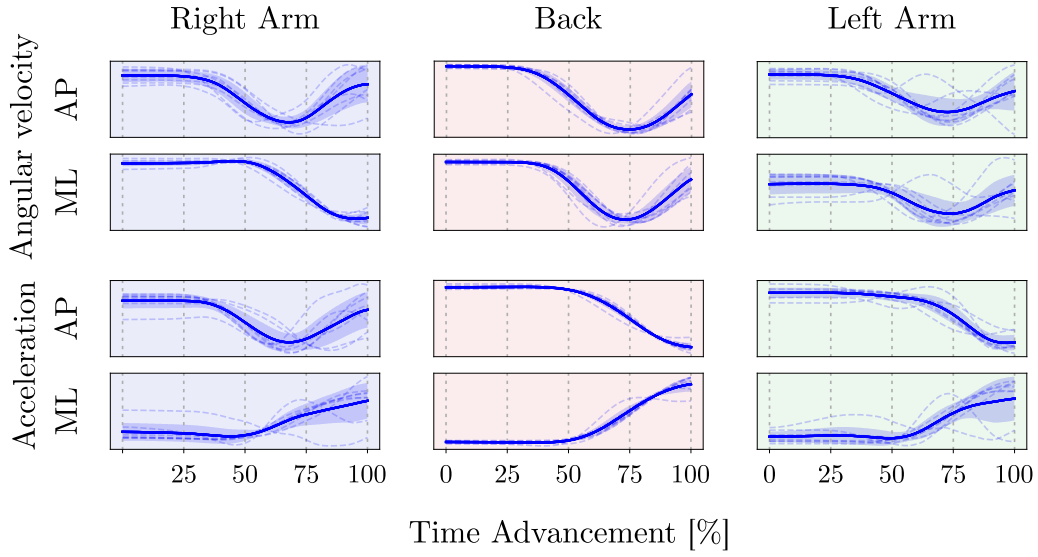


FIGURE 3.9: Average accelerations and angular velocities recorded by all three IMUs during the CS experiment trials in the ML and AP planes. The dashed lines represent the average signals for each participant, and the thick line corresponds to the overall average, with its corresponding standard deviation. Signals are represented from 0.5 s before the movement onset up to the first zero-crossing of the angular velocity around the vertical axis (not shown here).

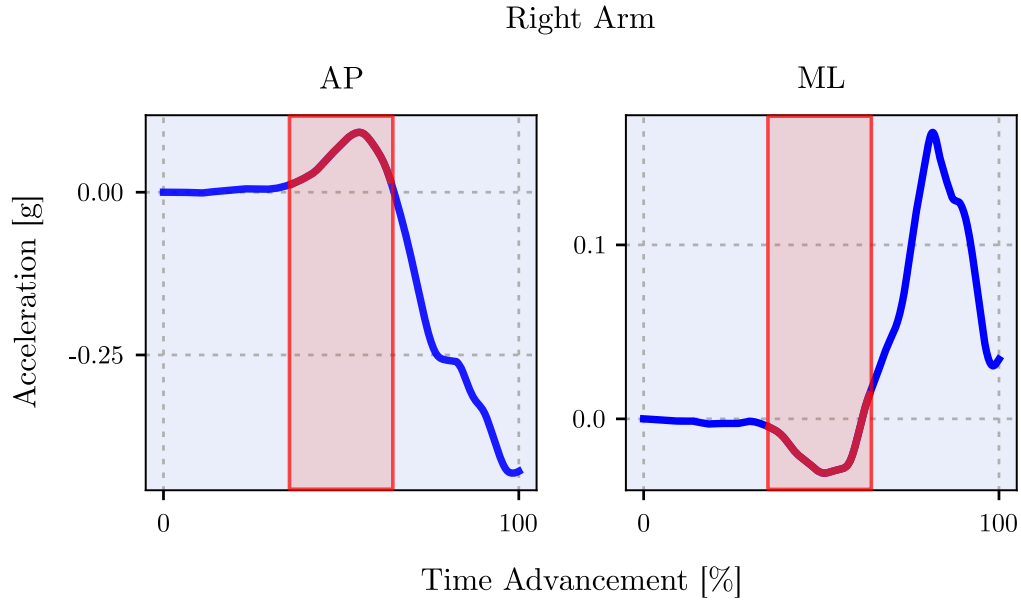


FIGURE 3.10: Typical AP acceleration pattern exhibited by one participant during one trial of the CS experiment on the right arm IMU. The original signal is low-pass filtered by a 2nd order Butterworth filter with a 3 Hz cut-off frequency. The red zone indicates the precursor movements as defined in sec.3.3.4.1. The low-amplitude acceleration phase is distinguishable at the beginning of the movement, and is followed by a strong deceleration phase.

| | Peak Accelerations [g] | | Peak Angular Velocities [deg/s] | |
|-----------|------------------------|-----------------|---------------------------------|----------------|
| | AP | ML | AP | ML |
| Trunk | 0.01 ± 0.01 | 0.01 ± 0.02 | 30.7 ± 12.7 | 19.2 ± 9.6 |
| Right Arm | 0.03 ± 0.03 | 0.04 ± 0.04 | 21.2 ± 13.9 | 15.1 ± 6.8 |
| Left Arm | 0.03 ± 0.03 | 0.04 ± 0.05 | 17.8 ± 11.0 | 15.0 ± 8.7 |

TABLE 3.5: Peak average (\pm SD) GII accelerations and angular velocities in the ML and AP planes for all IMU placements during the CS experiment.

During the CS experiment, participants tilted forwards, and twisted their upper body towards the standing leg (Figure 3.11). They mainly used their right arm to initiate the movement by accelerating it forwards, and rotating it towards the standing leg around the vertical axis. The trunk rotated around the AP and ML axes towards the standing leg, which induced forwards and lateral accelerations in the same direction. The left arm showed less repeatable patterns. Acceleration phases were short and of low amplitude compared to the FS experiment (see Table 3.5), and were followed by a high-amplitude deceleration phase, as shown in figure 3.10. However, participants showed higher angular velocities in both the AP and ML planes for all three IMUs.

3.4.5 Online classification of the CS signals

Figure 3.12 shows the participant-specific and overall results per classifier used from the real-time classification of IMU signals during the CS experiment, for all eight participants included in the CS study. The “Other class detected first” label represents trials for which the Gait Initiation Intention (GII) class was detected after another class was detected first. These trials were considered as false negatives, even if detection of gait intention occurred afterwards. The only false positive detection occurred during one intra trial (S6 in figure 3.12.A). 64.3% of false negatives were due to another class being detected first, and the remaining ones all came from the same participant (S7 in figure 3.12.A). Overall, the robot’s walk was correctly triggered in respectively 72.5% of the intra (a) trials, 95% of the inter (b) trials, and 95% of the global (c) trials.

A Kruskal-Wallis test showed a statistically significant difference between the three classifiers ($H = 6.35, p = 0.042$). An additional post-hoc Dunn test showed that there was no statistical difference in the performance results between the inter and global classifiers ($p = 1.00$). However, performance of both classifiers were statistically different from that of the intra classifier ($p = 0.029$ for both comparisons).

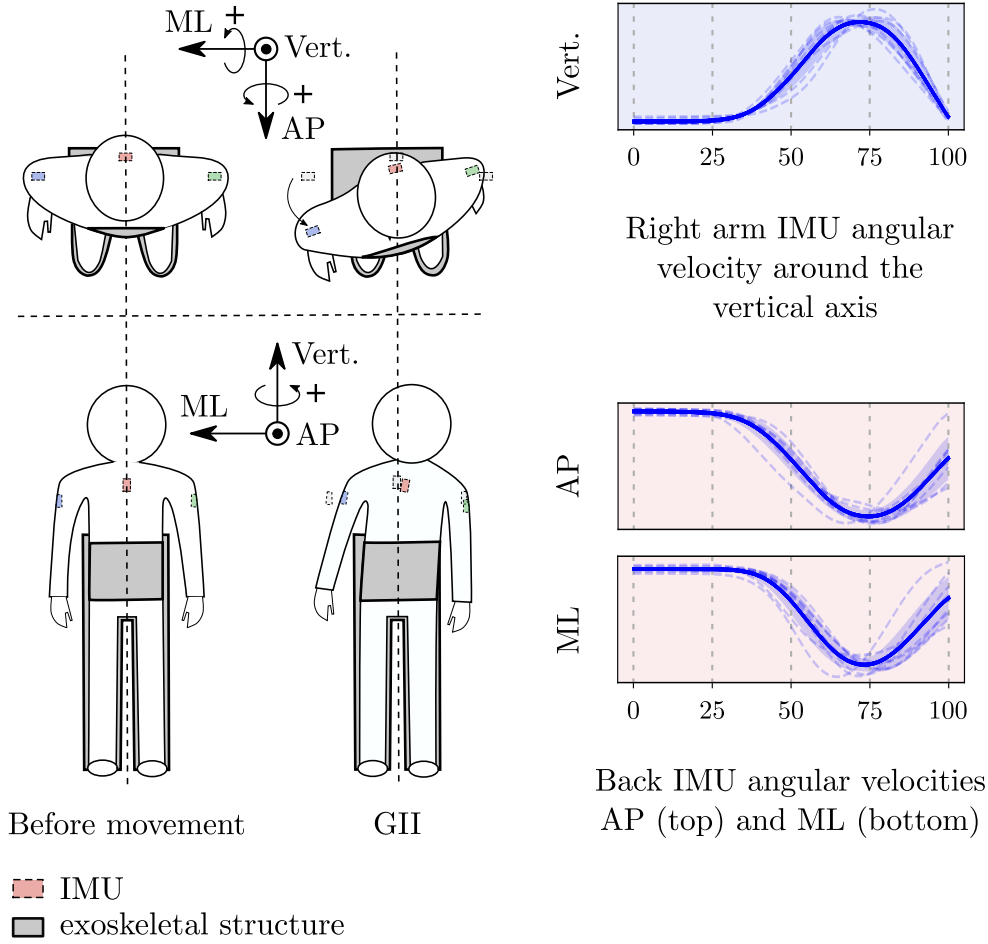


FIGURE 3.11: General strategy exhibited by the participants during the CS experiment to trigger the walking state of the robot.

On average, the GII class was detected 514 ms (± 373 ms SD) after the movement onset, which approximately corresponds to the duration of one buffer window (500 ms), and falls within the range of Anticipatory Postural Adjustments (APAs) duration.

Figure 3.13 shows the two-dimensional LDA projection for the intra classifier from one participant, where data points classified as GII during the CS intra trials were also represented. The figure shows that, in this subspace, the cluster formed by these data points is closer to the step classes than the GII cluster is. This is confirmed in the feature space by the distance metrics between the testing data clusters and the four class clusters reported in table 3.6: in 5 participants out of 8, the closest cluster to the testing points when excluding the GII class is one of the step classes. Interestingly, for two of these participants, the RS class is even closer to the testing data than the GII class.

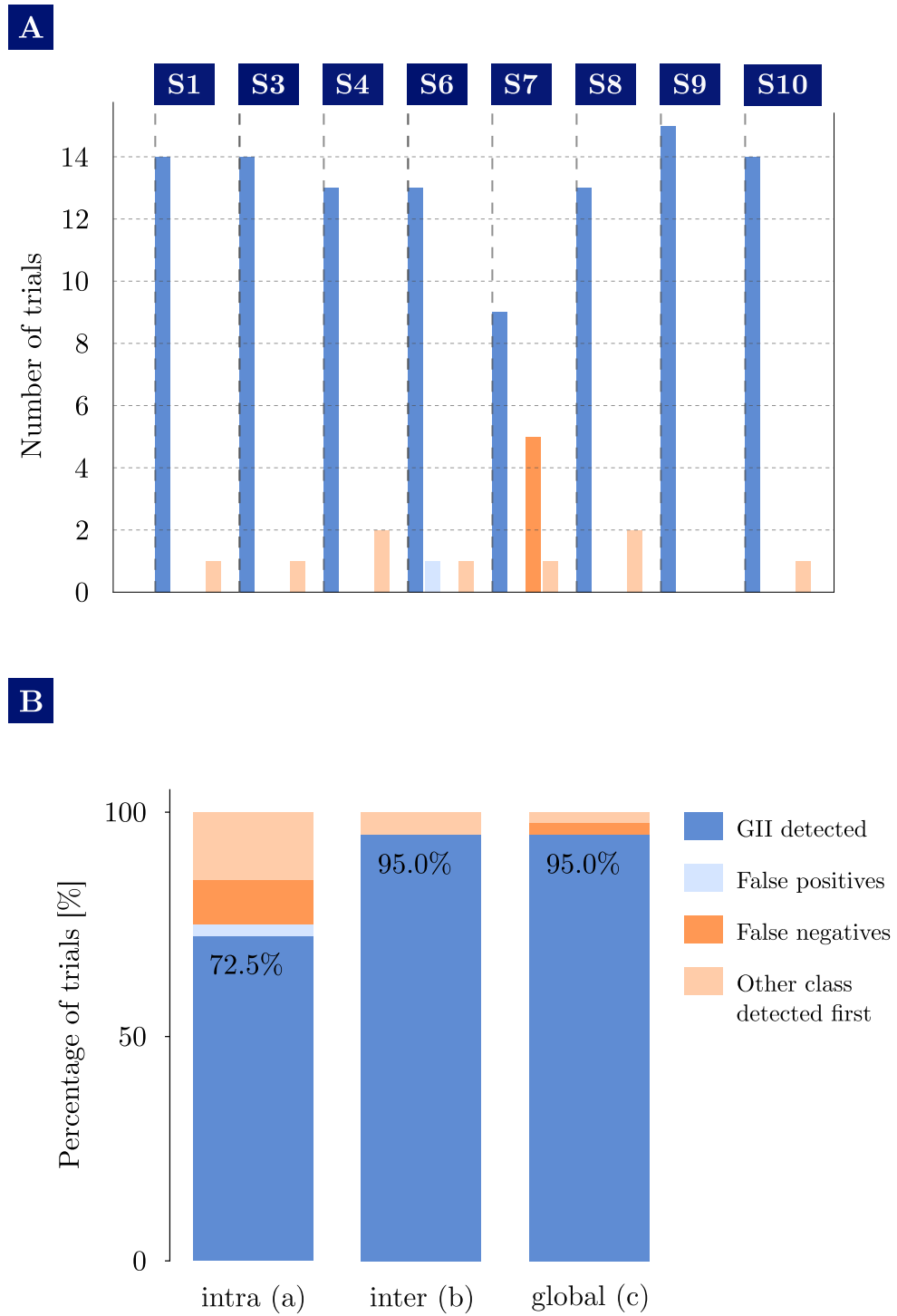


FIGURE 3.12: A. Subject-specific results from the CS experiment. B. Overall results from the real-time classification during the CS experiment per classifier used

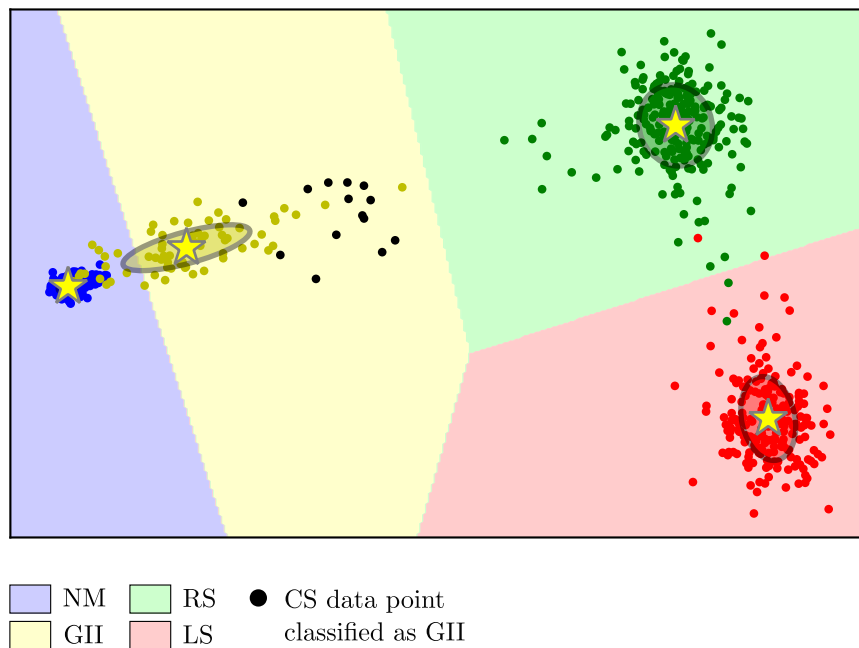


FIGURE 3.13: Representation of the LDA-generated two-dimensional projection subspace based on FS data training from participant S10. The black points represent projected features from data windows which have been classified as GII from CS intra trials from the same participant. These data points, though far from the GII class centroid generated by the training data, are still closer to it than the other classes.

| | S1 | S2 | S3 | S4 | S5 | S6 | S7 | S8 |
|-----|-------------|-------------|-------------|-------------|-------------|------|------|------|
| NM | 4.99 | 3.56 | 2.56 | 2.73 | 4.01 | 3.76 | 3.96 | 4.26 |
| RS | 5.44 | 4.13 | 2.06 | 1.61 | 2.52 | 6.60 | 5.14 | 6.47 |
| LS | 4.94 | 3.18 | 1.80 | 2.09 | 2.80 | 5.06 | 5.58 | 5.00 |
| GII | 3.47 | 2.32 | 1.06 | 2.12 | 3.71 | 0.93 | 3.82 | 2.05 |

TABLE 3.6: Distance metrics $m_{i,j}$ computed in the feature space between the testing data clusters from the intra trials during the CS experiment and the four class clusters. The bold values indicate when one of the step classes is the closest when the GII class is not taken into account.

3.4.6 Testing the classifier for false Gait Initiation Intention (GII) positives induced by everyday movements

Testing the global classifier on the Miscellaneous Movements (MM) recordings showed that on average, 27.6% of the performed movements windows were classified as GII, and only 7.2% as either Left Step (LS) or Right Step (RS). 64.6% of the windows were classified as No Movement (NM), because of transition resting periods, and because the performed movements implied that either one of the arms could be at rest – meaning that data points were likely to fall in the NM region in the LDA features-based subspace.

By adding the MM label to the global classifier training data set using half of the MM recordings, and using the other half as a testing set, there was an average of 98.5% windows classified as either MM or NM, with 1.5% windows falsely classified as GII. Figure 3.14 shows a three-dimensional LDA-generated projection subspace of this 5-class classification problem. As can be seen on the figure, the five classes form highly discriminated clusters of points with little overlap, and the MM and GII class are well separated.

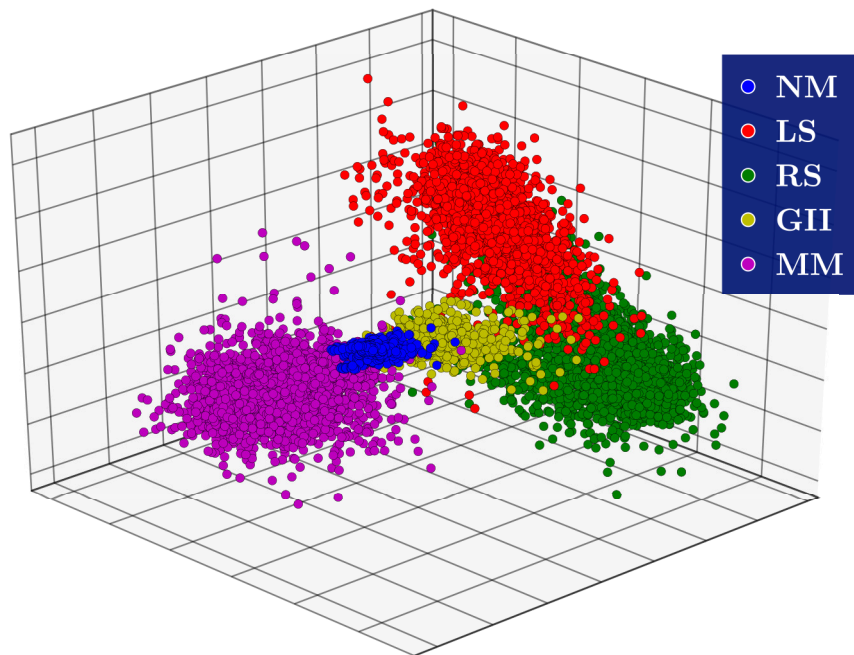


FIGURE 3.14: Representation of the three-dimensional LDA-generated projection subspace based on FS training data from all participants (global classifier), with additional MM data recorded from eight participants.

Additionally, the MM-enriched classifier was tested offline on the trials from the CS experiment corresponding to the global classifier (c) for the eight participants included in the CS study. This showed that the GII class was consistently detected in all trials but one. The remaining trial was a False Negative where the MM class was detected instead.

3.4.7 Discussion

3.4.7.1 Qualitative analysis of upper-body kinematic signals

During the CS experiment, the participants focused on using the side of their upper body ipsilateral to the stepping leg (the right side) to initiate gait. Since their legs were constrained by the exoskeleton, they seemed to focus on upper body movements that they imagined would help lifting the robot's leg, and pushing it forwards. This was achieved by rotating the upper body laterally, and tilting it forwards, while strongly bringing their right shoulder towards the standing leg. Contrary to the FS experiment, where precursor patterns are unconscious, they actively engaged in using the right side of their upper body to initiate gait, and exhibited higher angular velocities in the Medio-Lateral (ML) and Antero-Posterior (AP) planes for the trunk IMU. The phase of forwards acceleration was short and of low amplitude compared to the FS experiment, and was followed by a high amplitude deceleration. This shows that all participants relied on a similar movement strategy that actively focused on using the ipsilateral side of their upper body to bring the robot to start moving, and intuitively used their right arm in a similar way that they naturally did during the FS experiment, with forwards accelerations that lasted for shorter duration. The left arm exhibited less repeatable movements that were mainly due to the dynamics of the right side, and to whether participants controlled their arm or not. Similarly to the FS experiment, standard deviations for average acceleration peak values reported in Table 3.5 confirm that the amplitudes of arms and trunk movements are highly variable between participants in the CS experiment as well.

3.4.7.2 Experimental evaluation of gait initiation detection in the exoskeleton based on a free setting training set

Based on our experimental results, the LDA architecture could be successfully used to detect gait initiation intention for a majority of the CS trials, even though participants exhibited upper body patterns that did not correspond exactly with those of the FS experiment, which provided the training data.

One of the main differences between both experiments lied in the signal amplitudes and duration of the acceleration phases. Additionally, the left arm IMU did not exhibit repeatable patterns. However, it is hypothesized that the amplitude ranges remained closer to what can be exhibited by the trained GII class, meaning that in the feature space, data points extracted from the participants' movements in the CS experiment fell in the GII class region. Additionally, the distance metrics calculated between the clusters formed by the data points classified as GII in the CS experiment and the four labeled classes for the intra trials showed that in 5 participants, the testing points were closer to the step classes than the No Movement class. This supports the fact that the anticipatory patterns preceding gait initiation exhibited stronger dynamics when the participants were equipped

with the exoskeleton. Interestingly, in two participants, the centroid of testing data was even closer to a step class than the GII cluster: this might be due to the fact that the distance metrics rely on the Mahalanobis distance, which introduces a distortion of the feature space through covariance-based normalization. This did not affect the LDA output, which correctly classified the testing points as GII, since the classifier makes the assumption of a common covariance matrix for all classes.

Nevertheless, these results show that the constructed classifier might not be discriminative enough for the GII class to be actually specific to gait initiation precursor patterns, and that similar low-amplitude movements, such as handshakes or reaching movements, could also be detected as GII. Indeed, both the FS and CS experiments were conducted in a controlled setting, where the participants were asked not to move before the audio cue was heard. However, this is not representative of the real-life use of an assistive lower-limb exoskeleton, in which the users would freely move their upper body while the robot is standing still in an upright position. In the classification architecture that was developed for this experimental work, such movements could possibly lead to false GII positives, and a preliminary experiment was conducted in order to assess the robustness of the classifier to such events.

3.4.7.3 Experimental evaluation of the robustness of the global classifier to false Gait Initiation Intention (GII) positives

Testing the global classifier on the recordings from the False Positives (FP) experiment showed that Miscellaneous Movements (MM) were prone to be classified as Gait Initiation Intentions, rather than one of the other movement classes (Left Step or Right Step). This shows that Miscellaneous Movements exhibit features that are similar to the GII class, and can induce false GII positives if not taken into account when training the classifiers. This is not a desired behaviour during the normal use of a lower-limb assistive exoskeleton. However, when adding the FP recordings to the training set of the global classifier, GII false positives were reduced to only 1.5%, most of which happened punctually (meaning that one window was classified as GII in between correctly-classified MM windows). This rate could be further reduced by adding a filter which would not initiate gait of the robot in such cases. Figure 3.14 also shows that the classified movements are differentiable, and confirms the specificity of the patterns used to detect gait initiation intention. Additionally testing the 5-class classifier on the CS experiment confirms that the enriched classification architecture can be used to effectively prevent false GII positives, with limited false negative rates, and no loss of performance compared to the original global classifier.

A preliminary online implementation was tested on one participant who had not taken part to any of the previous experiments, and showed good results in detecting the Gait Initiation Intention, and preventing False Positives by correctly identifying performed Miscellaneous Movements. However, since this was only a preliminary test, no quantitative analysis of the data was performed.

3.5 | Limitations and prospects of the study.

This study shows that anticipatory movements of the upper-body before gait initiation seem to be retrieved in able-bodied participants using a lower-limb exoskeleton. The participants exhibited a similar movement strategy to trigger gait in the robot. However, further experiments need to be conducted with more participants to refine and generalize these results, and strengthen the statistical analysis. For example, by involving more participants who have no previous experience in using the exoskeleton, it would be possible to assess the influence of usage experience on both the movement strategies, and the classification outcome. More trials could also be necessary to assess how strategies can evolve in time, and whether participants are able to adapt to false classification negative occurrences by performing sets of movements that are even more specific, and with less variability.

Additional feature selection steps should also be considered to further reduce the high number of dimensions of the feature space, and properly avoid the overfitting that can occur in more generic settings. This study systematically used all 18 IMU signals to construct the LDA classifiers. However, signal-specific selection can be performed, and the possible redundancies between both arm IMUs due to their symmetrical placement can be exploited.

It is also important to note that lower-limb assistive devices are aimed at being used with SCI patients with different injury levels. Therefore, it is necessary to evaluate how these various experiments can affect the upper-body movements. The Atalante exoskeleton was specifically designed to be used by patients with lower-limb impairments who still have mobility above the waist level. It is hypothesized that such a category of patients could rely on similar movement strategies to express gait initiation intention to those exhibited by the able-bodied participants included in this study. Further experiments with patients need to be conducted to confirm this hypothesis. If it is not confirmed, the classification architecture could still be used by asking the patients to perform any movements they find intuitive to trigger the walking state of the robot. Recording of such movements can then be used as a basis to construct a training data set for a new patient-specific classifier.

3.6 | Conclusion.

This work showed that participants in a non-back drivable exoskeleton actively engaged in a gait initiation strategy similar to the natural precursor patterns exhibited in a free environment, by shifting the right side of their upper body

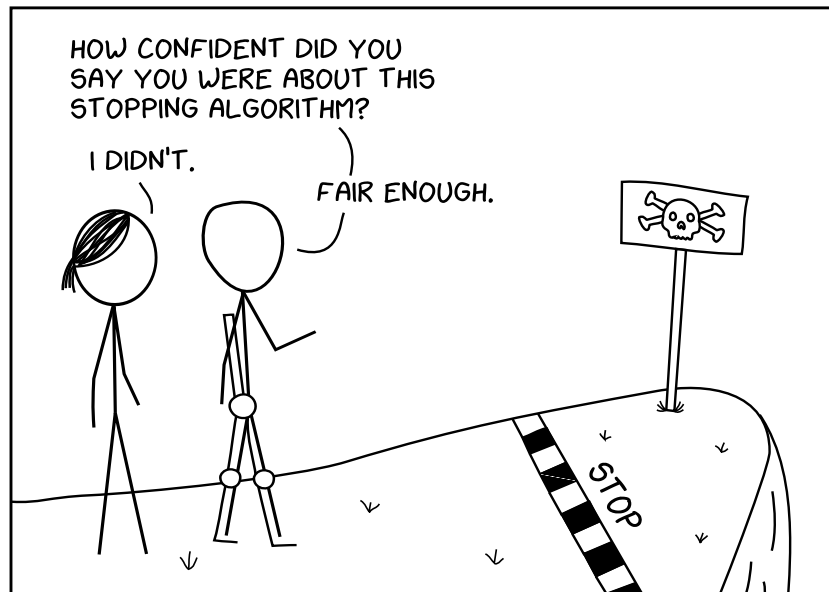
forwards and towards the standing leg. By building a standard classification architecture using free walking data as a training set, gait initiation intention was then successfully detected when starting from an upright standstill position in the lower-limb assistive exoskeleton. Robustness of the classifier against false positives triggered by everyday movements was assessed in a supplementary experiment by adding real life gestures to the training set, which confirmed that the classification architecture could be made more robust to false gait initiation positives.

Further experiments need to be conducted for refinement and generalization of the results. Patients can then be included in more ecological environments to assess the transferability of these methods and the able-based classifiers to more realistic mobility scenarios and real-life use cases. However, this work is encouraging for future developments for machine-learning-based control strategies in lower limb assistive exoskeletons.

Chapter 4

Detecting the Gait Termination Intention

This chapter focuses on gait termination, and investigates how different characteristics of natural arm swing movements can be used to identify and maintain the walking state of the exoskeleton through a dead-man switch approach. Essentially, since the exoskeleton is in a dynamical state during gait, short patterns in the IMU signals specific to gait termination (e.g. a braking movement) can be harder to extract. Therefore, by relying on a threshold-based classifier constructed upon descriptive features of actively maintained arm swing movements, it is possible to build an easier gait termination detection method where the transition between the walking and standstill states occurs whenever arm movements cease, and the corresponding patterns in the IMU signals disappear. First, analysis of arm IMU signals allowed to identify three amplitude and coordination-based features for the classification architecture. Then, an online implementation of this novel gait termination detection interface in the Atalante exoskeleton was tested with 11 unimpaired participants. Lastly, preliminary tests were also conducted with two patients.



Chapter Contents

| | | |
|------------|---|------------|
| 4.1 | Gait termination: definition and characteristics | 80 |
| 4.1.1 | The mechanisms of gait termination | 80 |
| 4.1.2 | Effects of walking speed | 80 |
| 4.1.3 | Upper-body behaviour during gait termination | 82 |
| 4.1.4 | Gait termination in the Atalante exoskeleton | 82 |
| 4.2 | Arm swing movements during gait | 83 |
| 4.2.1 | The mechanisms of arm swing | 83 |
| 4.2.2 | The function of arm swing | 84 |
| 4.2.3 | Arm swing in impaired individuals | 84 |
| 4.2.4 | Walking detection rather than gait termination detection: a dead-man switch approach based on arm swing | 85 |
| 4.3 | Exploring arm swing during walk in the exoskeleton: a preliminary experiment | 85 |
| 4.3.1 | The experimental setup | 86 |
| 4.3.2 | Data analysis | 87 |
| 4.3.3 | The dynamics of arm swing during walk in the exoskeleton | 89 |
| 4.3.4 | Deriving distinctive features of arms swing during walk in the exoskeleton | 92 |
| 4.3.5 | A threshold-based classification architecture as the walking control interface | 102 |
| 4.4 | Using arm swing movements to walk in the exoskeleton: a validation experiment | 105 |
| 4.4.1 | The experimental setup | 105 |
| 4.4.2 | Data and statistical analyses | 105 |
| 4.4.3 | Results of the study | 106 |
| 4.4.4 | Discussion | 112 |
| 4.5 | Preliminary testing with patients | 115 |
| 4.6 | Limitations and prospects of the study | 115 |
| 4.7 | Conclusion | 116 |



4.1

Gait termination: definition and characteristics.

4.1.1 The mechanisms of gait termination

Gait termination, or stopping, is defined as the transition between steady-state walking and upright standing. One of the earliest studies on the subject was conducted by Jaeger et al. (1992), who identified two mechanisms involved in gait termination: a decrease in push-off force during the last step prior to termination, and an increased braking force during the final stance phase (with both feet on the ground). They also found that depending on the timing of a stopping cue during the gait cycle, an additional step might be required to terminate gait (after 18% of the gait cycle for unplanned stopping). However, in some cases, part of the kinetic energy of the body can be converted into potential energy by rising up on the toes, and therefore avoid an extra step (Hase et al. 1998).

Jian et al. (1993) further investigated the relationship between the CoM (Center of Mass) and CoP (Center of Pressure) trajectories during gait termination, and essentially found that they were mirror images of their trajectories during gait initiation: after toe-off of the last swing leg, the CoP is ahead and lateral of the CoM, provoking its fast deceleration in the antero-posterior direction, and bringing it medially between the feet. At heel-strike of the stance leg, the CoP moves laterally and anteriorly to slow down the CoM during a final brake period which extends at about 150% of the gait cycle. Figure 4.1 was adapted from Jian et al. (1993) and summarizes these results.

Different studies have focused on two types of gait termination: planned and unplanned stopping (Sparrow et al. 2005). In planned stopping, the feet usually land parallel to each other after the last stance phase. On the other hand, unplanned stopping is adopted as a reaction to an external cue or an obstacle, and one foot generally stops in front of the other. Planned stopping requires a longer delay of approximately 0.5 s before effective termination, which corresponds to the time needed to bring one foot next to the other (Jaeger et al. 1992).

4.1.2 Effects of walking speed

In a study on the effects of velocity on gait termination strategies, M. Bishop et al. (2004) showed that the soleus muscles of both the stance and swing legs during planned and unplanned stopping trials were active before heel-strike, with a decreasing onset time as the cadence increased. The braking forces required for stopping also increased with the cadence of walking, with more contribution

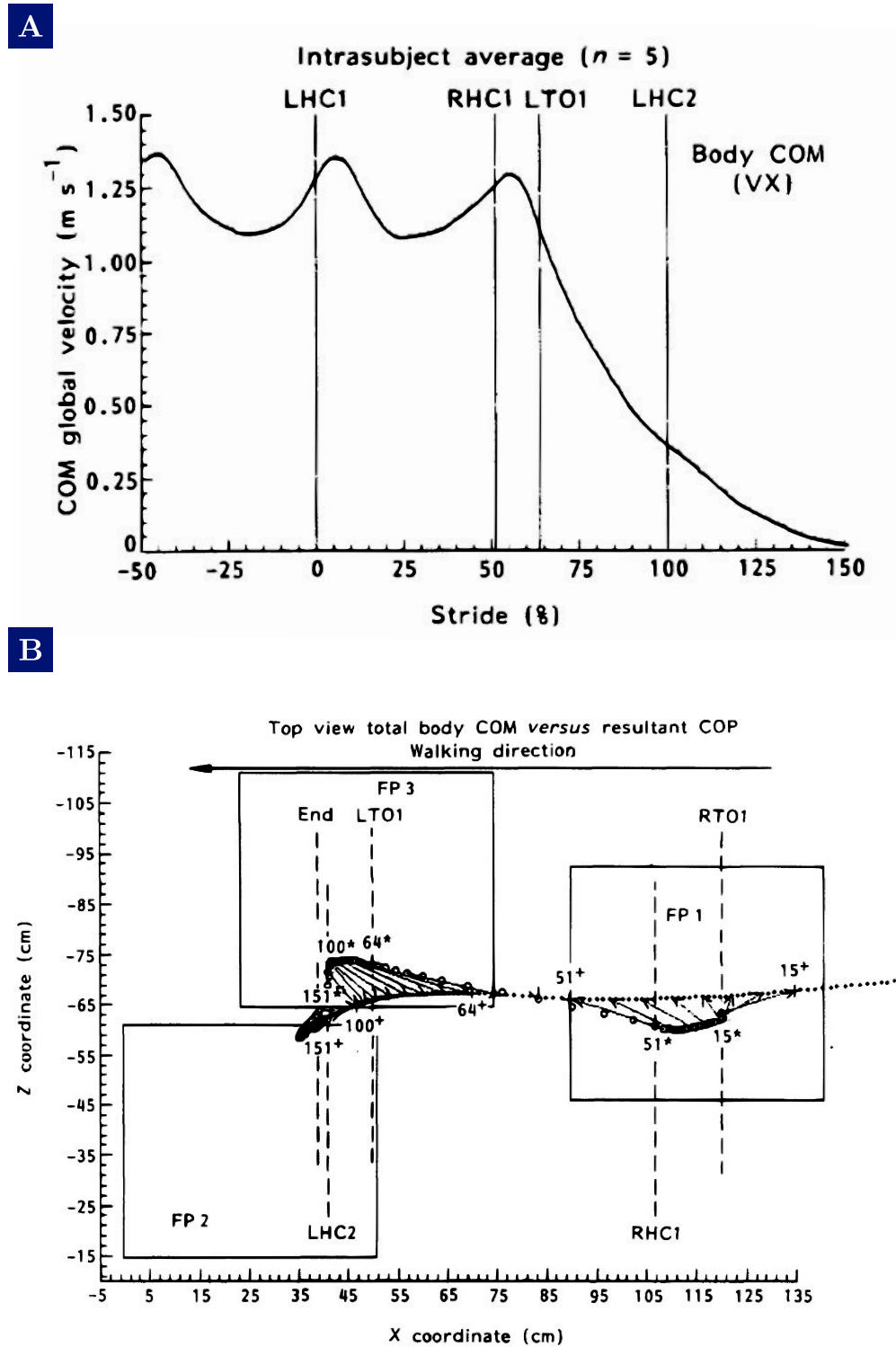


FIGURE 4.1: Adapted from Jian et al. (1993). A. Antero-posterior velocity of the CoM during gait termination. B. Trajectories of the CoM (dots) and CoP (circles) during gait termination. Left leg was the last swing leg. Abbreviations: R/L = Right/Left, HC/TO = Heel-Contact/Toe-Off, FP = Force Plate.

from the last stance leg at higher velocity. Finally, walking speed also affects the probability of adding an extra step to properly terminate gait, as the stopping cue should appear earlier to provide more reaction time for effective stopping: at different speeds, a stopping cue initiated at the same relative time of the gait cycle would provide less total response time when walking at the higher velocity (Tirosh et al. 2004).

4.1.3 Upper-body behaviour during gait termination

The upper-body accounts for two thirds of the total body mass (Winter et al. 1990), and an anticipatory top-down control strategy (from head to pelvis) is used during locomotor tasks for balance, and maintaining a stabilized visual platform for safe ambulation (Prince et al. 1994). During gait termination, the CoP acts on the CoM to bring it into the stability region defined by Pai et al. (1997), and stabilize the body into a halt. This means that the braking forces exerted by the lower limbs act to decelerate the upper-body, and the Head-Arms-Trunk (HAT) segment therefore loses energy in the antero-posterior direction (O’Kane et al. 2003). Comparative studies between young and older women showed an age-related active role of the upper-body in contributing to the gait termination mechanisms (Rum et al. 2017, 2019). Both age groups exhibited slight flexion of the trunk, and backward movements of the head and pelvis during braking. However, young women showed more stable and less variable coordination patterns of the upper body segments, as well as an increased attenuation of accelerations from one segment to the other, and a backward velocity of the trunk during the braking and stabilization phases. Conversely, older women were not able to effectively dampen accelerations across different upper-body levels, and exhibited higher medio-lateral accelerations during the late phase of gait termination, and a tendency to keep flexing the trunk even during stabilization. The medio-lateral accelerations of the upper-body were similarly high in impaired patients suffering from neuropathologies in a different study by O’Kane et al. (2003).

4.1.4 Gait termination in the Atalante exoskeleton

When walking with the Atalante exoskeleton, gait termination can be triggered by pushing on the standstill button on the remote controller. A stop event is sent for the finite state machine to transition between gait and a resting state. The active swing leg finishes its current step, and the other leg is brought forward next to it, so that the robot goes back to its standard standstill position with both feet parallel on the ground.

In the context of this thesis, the possibility of replacing the current button-based method for terminating gait by a more natural and intuitive control interface was evaluated. However, the findings described in 4.1.3 suggest that, contrary to gait initiation, the gait termination mechanisms mainly involve the lower-body

to produce braking forces and decelerate the whole body, while the upper-body patterns can contribute to the overall stabilization and balance, and help bringing back the CoM into the stability region. This poses the problem of identifying an adequate anticipatory behaviour of the upper-body to try and detect the gait termination intention in the Atalante exoskeleton, since no active braking forces can be exerted by the lower limbs in the robot. One possibility would be to predefine a specific anticipatory movement of the upper-body, such as a backward tilt, to express the intention of stopping. However, while a counteracting movement against the forward progression of the exoskeleton might seem intuitive, and on par with the findings of Rum et al. (2019), where the trunk, even though being flexed, showed a backwards velocity towards extension, the dynamics of the robot during walking make it difficult to observe small and punctual transitioning movements in kinematic data recorded by IMUs. The approach taken in this work was to rather rely on a maintained gait-related upper-body movement that would slow down or cease as an anticipation for stopping, and that would be easier to distinguish and extract from kinematics data; namely arm swing.

4.2 | Arm swing movements during gait.

4.2.1 The mechanisms of arm swing

There is an ongoing debate on whether arm swing movements are the result of passive dynamics or active muscle mechanisms, though it seems that both types of phenomena are involved (Collins et al. 2009; Meyns et al. 2013; Goudriaan et al. 2014). However, it is clear that a strong coordination relationship exists between arm and leg movements during gait. A study by Wannier et al. (2001) showed that upper and lower limbs remain coordinated during different human locomotor activities – namely walking, creeping, and swimming – with locked frequencies at a small integer ratio. During gait, this relationship is dependent on walking speed, and shifts from 2:1 at low velocities, with arm swing being locked onto step frequency, to 1:1 at higher velocities, with arm swing being locked onto stride frequency (Van Emmerik et al. 1998). According to results from a study by Wagenaar et al. (2000), the preferred movement frequencies of the arms can be predicted based on their resonant frequencies at low speeds, and those of the legs at higher speeds. Notably, this coordination is preserved even when adding a mass to one of the moving segments: for example, loading an ankle will lead to a general reorganization, where muscle activity and movements of all limbs, including the arms, will be modulated to maintain cadence constancy during gait (Donker et al. 2002). However, while coordination of the upper and lower limbs is preserved, it can also be affected by the walking condition: Carpinella et al. (2010) showed that treadmill and overground walking exhibit significantly different patterns of arm-leg coordination.

Overall, the relationship observed between upper and lower limbs during gait might reflect a task-dependent coupling of neuronal circuits controlling arm and leg movements, through specific pathways that might be gated by the so-called Central Pattern Generator (Dietz 2002a). Further evidence for this hypothesis have been brought by Calancie et al. (1996), who detected interlimb reflex responses at the upper body when stimulating the tibial nerve at the ankle of Spinal Cord Injury (SCI) patients. However, while this might be evidence of a remaining piece of quadrupedal locomotion, arm swing has also shown to be functional during bipedal walking.

4.2.2 The function of arm swing ---

One of the first studies on the function of arms during walking was conducted by Elftman (1939). One of his main findings was that arm swing movements regulate the torsion of the body around the vertical axis through reduction of angular momentum. Additional studies later confirmed his observations (Bruijn et al. 2008; Collins et al. 2009), and also showed reduction in ground reaction moment when arms were involved compared to restricted arm movement conditions (Collins et al. 2009). These findings suggest that arm movements during walking help reducing energy expenditure, which was confirmed in several works where oxygen consumption was measured (Umberger 2008; Collins et al. 2009). However, the contribution of arm swing to gait stability remains unclear (Meyns et al. 2013), although it was shown that excessive arm swing might improve dynamic gait stability in the medio-lateral direction (Punt et al. 2015), and that arm movements provide better resistance to external perturbations, and allow to effectively recover from imbalance and return to normal gait (Bruijn et al. 2010). Deliberate changes in arm swing during walking (such as strapping the arms, or in-phase movements) have also been shown to influence the gait pattern (Eke-Okoro et al. 1997).

4.2.3 Arm swing in impaired individuals ---

In several neurological pathologies, such as Parkinson's Disease (PD), hemiplegia in post-stroke individuals, or SCI, arm swing amplitude during walking can be affected, and is generally decreased (Dietz 2011; Meyns et al. 2013). For example, in people with hemiplegia, the impaired arm shows a reduced movement amplitude compared to the non-involved arm (Ford et al. 2007). Similarly, patients suffering from neurological pathologies can show reduced coordination of the limbs (Meyns et al. 2013). However, for some individuals, synchronization is preserved, but the movement pattern is altered: Tester et al. (2012) showed that incomplete SCI (iSCI) patients kept a high coordination of arm and leg movements during treadmill walking, but with a 1:1 frequency relationship regardless of speed. The altered 1:1 pattern at low speeds might have been indicative of compensatory strategies aiming at enhancing balance. In some other cases, for example with

high-functioning stroke individuals, no differences in coordination were observed compared to unimpaired controls (Stephenson et al. 2008).

Incorporating arm movements during rehabilitation of neurologically impaired individuals might be beneficial, given the growing evidence that upper and lower limbs are strongly coupled during gait-related tasks (Dietz 2011; Meyns et al. 2013). Patients such as hemiplegic individuals have successfully shown their ability at actively responding to instructions and modulating their arm movements (Ford et al. 2007). Furthermore, by involving arm rhythmic movements in rehabilitative settings, lower limb muscle activation might be enhanced (Ferris et al. 2006). This suggests that an arm-swing-based control strategy for a lower-limb exoskeleton might not only be natural, but it would actively engage patients in rehabilitation settings during gait, and therefore prove to be beneficial.

4.2.4 Walking detection rather than gait termination detection: a dead-man switch approach based on arm swing

As already stated above, detecting a punctual transitioning movement from IMU signals to terminate gait in a lower-limb exoskeleton might be difficult to achieve. It was therefore decided to take another approach for building an effective gait termination control interface: rather than detecting the actual gait termination intention, it would be possible to rely on explicitly maintained arm swing movements as an indicator of a walking intention. In such a scheme, the exoskeleton would continue walking as long as arm swing is maintained, and would terminate gait as soon as arm movements cease. This strategy can be related to the dead-man switch approach, where a given mechanism is activated or deactivated when a specific action ceases (for example, in train locomotives, a dead man's switch is mounted on the control handle such that the breaks would engage if the conductor released their grip). A preliminary experiment was therefore conducted to evaluate arm swing possibilities in the Atalante exoskeleton, and build a control interface to be evaluated in a subsequent validation experiment.

4.3 | Exploring arm swing during walk in the exoskeleton: a preliminary experiment.

4.3.1 The experimental setup

This preliminary exploratory experiment (EE) was conducted to determine whether arms dynamics could take over the exoskeleton dynamics during walk, and be easily extracted from IMU signals. A secondary analysis of the signals was then used for the identification of discriminative features of arm swing during gait in the exoskeleton. Four unimpaired participants participated in the EE. They were all men, aged 28 ± 3.9 years old, with an average height of 175.5 ± 3.2 cm and an average weight of 66.8 ± 4.3 kg. They were all used to walking in the exoskeleton. Before the experiment started, they were equipped with 2 NGIMUs: one on each arm, similarly to 3.3.1. Each participant then performed 4 walks in the exoskeleton, over a distance of approximately 5 meters. For each walk, they were asked to exhibit a different amplitude in their arm oscillations: no forced movement (NM), low amplitude (LA), medium amplitude (MA), and high amplitude (HA). At the beginning of each walk, the experimenter triggered the walk starting position, and the participants were asked to start walking by leaning forwards after an audio cue was emitted. At the end of the walk, the exoskeleton was manually stopped by the experimenter using the Atalante remote controls, and the participant could cease oscillating their arms. The experimental setup is described in figure 4.2.

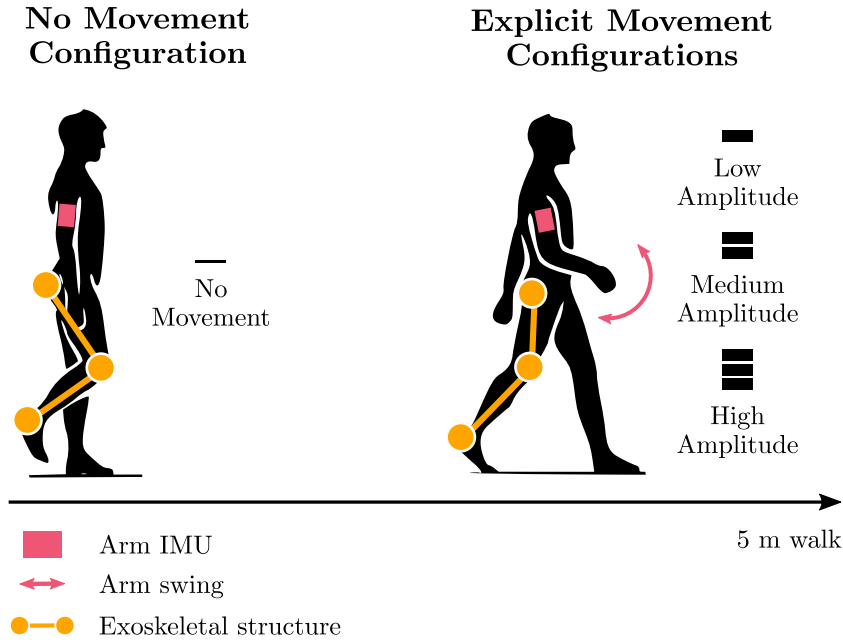


FIGURE 4.2: Setup of the exploratory experiment. Left: no forced arm movements configuration. Right: explicit arm movements configurations with varying amplitudes.

4.3.1.1 No forced arm movements configuration

In a first configuration, the participants were asked to walk in the exoskeleton as they were used to, without any instruction about arm movements (see figure 4.2). This meant that some amount of arm oscillations could be exhibited, either because the involved participant was used to swing their arms while walking in the exoskeleton, or because they were induced by the dynamics of the exoskeleton during the walk.

4.3.1.2 Explicit arm swing configurations with varying amplitudes

In the remaining configurations, the participants were asked to explicitly swing their arms back and forth in the antero-posterior plane, in order to mimic the natural arm oscillations exhibited by unimpaired individuals during walk. For each configuration, they were asked to exhibit a different level of movement amplitude, with no alteration in the frequency of oscillations: low, medium, or high (see figure 4.2). There were no further instructions: this meant that each participant was free to exhibit whatever amplitudes they were comfortable with, as long as the relative differences between the different levels were explicit enough.

4.3.2 Data analysis

4.3.2.1 Signal analysis

Analysis of the IMU data focused on the arm angular velocities in the antero-posterior plane, in which the arm oscillations occur. The signals were low-pass filtered using a second-order Butterworth filter with a 1 Hz cutoff frequency. This frequency was chosen during the post-processing step in order to reduce noise as much as possible, without affecting the oscillatory dynamics of the arms. For all configurations and all participants, the beginning and ending of the walk were respectively defined as the moment after which the participant had leaned forwards and started swinging their arms, and the moment when the arm oscillations had ceased. A preliminary analysis was conducted both in the time domain and in the frequency domain to determine the effects of higher arm oscillation amplitudes on the recorded IMU signals. No statistical analysis was conducted at this point, since the number of samples was too small. However, trends in the data were visually assessed, and used to form base hypotheses for the derivation of arm swing-related features in a secondary analysis.

Time domain In the time domain, amplitude of the movements and coordination of the arms for each participant and each explicit movement configuration were evaluated. The angular velocity signals during walk in these configurations were first divided into half-periods of arm oscillations using a zero-crossing detection algorithm. The output of the algorithm was then checked and manually corrected when necessary. The amplitude of movements for each arm was evaluated based on the average angular range of the integrated angular velocities computed across the full periods of oscillations for each participant and configuration. If x is the integrated IMU signal over one period from a given trial, and x is of length N , the angular range simply writes as:

$$\Delta\theta(x) = \max x[n] - \min x[n] \quad (4.1)$$

Coordination of the arms was evaluated using normalized cross-correlation (NCC) of the arm signals (Ferris et al. 2006; Stephenson et al. 2008). Cross-correlation between two real-valued discrete signals x and y of length N is defined as:

$$(x \star y)[k] = \sum_{n=0}^{N-1} x[n] y[n+k] \quad (4.2)$$

where $k \in \llbracket 0, N-1 \rrbracket$ and $y[n+k] = 0$ if $n+k > N-1$. It measures the similarity between two signals x and y for different time lags or delays k . Similarly, the normalized cross-correlation can be defined as:

$$(x \star y)_{\text{norm}}[k] = \frac{1}{N} \sum_{n=0}^{N-1} \frac{(x[n] - \mu_x)(y[n+k] - \mu_y)}{\sigma_x \sigma_y} \quad (4.3)$$

where μ_x and μ_y are the means of x and y , and σ_x and σ_y are their standard deviations. At lag 0, this is equivalent to the Pearson Correlation Coefficient. Therefore, strongly correlated signals at lag k will have normalized cross-correlation values closer to 1 (for signals in phase) or -1 (for signals in anti-phase), and poorly correlated signals will have values closer to 0.

To evaluate the coordination between the left and right arms, the normalized cross-correlation at lag 0 was calculated for each period of the left arm oscillations (thus using the left arm as a reference), and these values were averaged to get the mean cross-correlation for each participant and each configuration.

For both the angular range and the cross-correlation, outlier values were removed based on the modified z -score approach (Salgado et al. 2016).

Frequency domain For the frequency analysis, the Discrete Fourier Transform (DFT) of the arm angular velocity signals during walk was calculated with a Fast-Fourier Transform (FFT) algorithm scaled by a factor of $1/\sqrt{N}$, where N is the length of the corresponding data array. The scaling choice preserves the equality stated by Parseval's theorem:

$$\sum_{n=0}^{N-1} |x[n]|^2 = \sum_{k=0}^{n-1} |X[k]|^2 \quad (4.4)$$

where $x[n], n \in \llbracket 0, N-1 \rrbracket$ are the time-domain samples of the signals, and $X[k], k \in \llbracket 0, n-1 \rrbracket$ are the DFT components of the signals.

4.3.3 The dynamics of arm swing during walk in the exoskeleton

Figure 4.3 shows the arm angular velocities in the antero-posterior plane for all participants (S1 to S4) and all experimental configurations. The vertical red dashed lines indicate the beginning and ending of the walk. Since the participants kept a similar frequency of arms oscillations across configurations, a change in the amplitude of angular velocities would be positively correlated with a change in movement amplitude. Therefore, looking at the figure, the participants were able to modify the amplitudes of their arm oscillations at relatively different levels, as per the experimenter's instructions. Additionally, the dynamics of the arms seem to take over the dynamics of the robot on the angular velocity signals starting from the medium amplitude, for which there seems to be a stronger oscillatory component for both arms at a fixed frequency with less apparent noise, and where the anti-phase coordination of both arms is more explicit. These aspects are confirmed by the subsequent time-domain and frequency-domain analyses.

4.3.3.1 Time-domain analysis of the arm swing

The successful modulation of amplitudes is confirmed by figure 4.4, which shows the mean angular range of arm movements for the explicit arm movements configurations, both for all participants and averaged across the participants.

The figure shows that, on average, the amplitudes of arm movements could be successfully increased across the configuration levels, even though the relative differences between two configurations do not seem consistent across the participants. In particular, the variability in the average mean angular range seems to increase as the level of amplitude increases. However, the High Amplitude configuration seems to lead to higher values overall when compared to the Low Amplitude configuration.

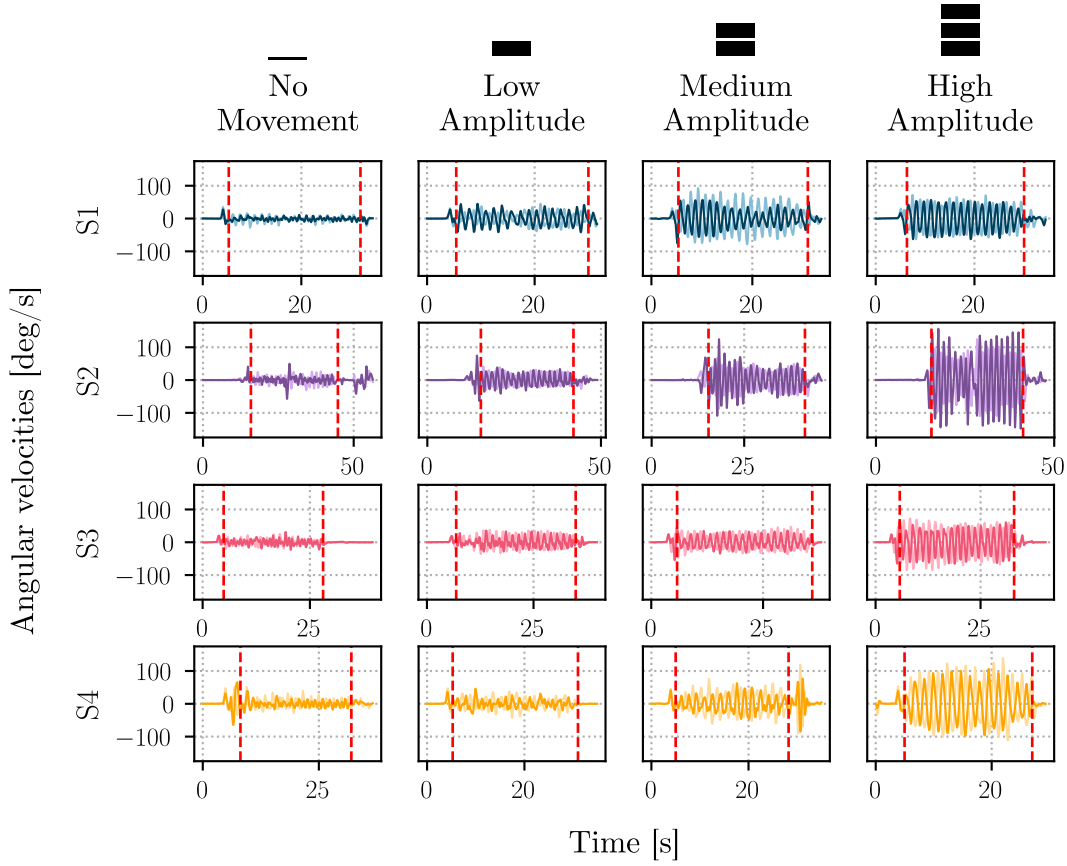


FIGURE 4.3: Left (darker shade) and right (lighter shade) arm angular velocities in the antero-posterior plane for all four subjects and all four experimental configurations during the Exploratory Experiment. The vertical dashed red lines indicate the beginning and end of walking.

For one participant (S3), there does not seem to be a difference between the Low and Medium Amplitude configurations, and for another one (S1) the right arm seems to have a higher mean angular range for the Medium Amplitude configuration than the High Amplitude one. It is also notable that an asymmetry in the mean angular ranges exists between the left and right arms. However, asymmetry in arm swing is documented in the literature, and deemed normal up to a ratio of 2 : 1 – one arm having twice the angular range of the other (Plate et al. 2015; Killeen et al. 2018).

Additionally, the values of arm swing angular ranges reported in the literature for natural-speed gait are around 20° (Carpinella et al. 2010; Plate et al. 2015; Punt et al. 2015). This means that the movements exhibited by the participants in the Medium Amplitude configurations fall in the normal range of amplitudes for arm swing. In the High Amplitude configuration, two participants (S2 and S3) exhibited movements within a similar range, but the other two exhibited values usually linked to high-speed gait or exaggerated swing. Similarly, values for the Low Amplitude configuration seem closer to those of low-speed gait.

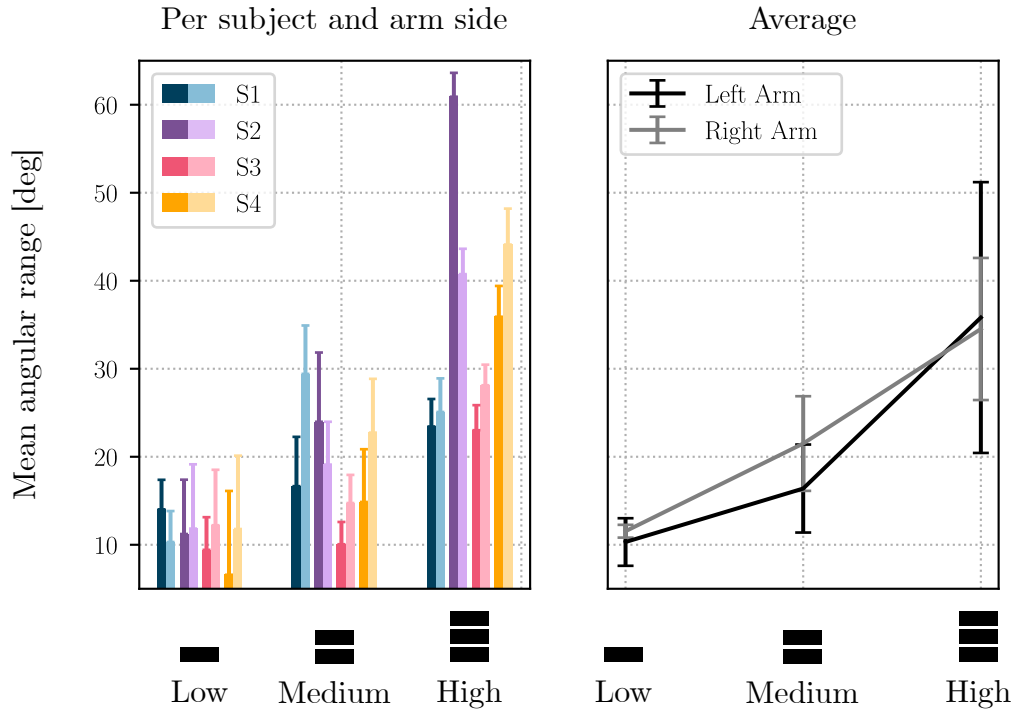


FIGURE 4.4: Mean angular range of left (darker shade) and right (lighter shade) arm movements in the antero-posterior plane during the Exploratory Experiment for all participants and all explicit movement configurations. *Left*: mean angular range (+ SD) for all participants and configurations. *Right*: Mean angular range values (pm SD) averaged across all participants for each configuration.

Figure 4.5.A shows the mean normalized cross-correlation values at lag 0 between the angular velocity signals of both arms for all subjects and all explicit oscillation configurations. The normalized cross-correlations between the left and right arm angular velocities were calculated with the left arm as a reference for the oscillation periods, and indicate how the inter-arms coordination evolves as the amplitude increases.

The figure shows that the mean cross-correlation values are closer to -1 for the higher amplitude configurations, with lower standard deviations. This means that the arms coordination, corresponding to back and forth oscillations of the arms in anti-phase, can be better detected when the arms swing at higher amplitudes. This was expected, since the signals at higher amplitudes seem less affected by the exoskeleton's dynamics.

Figure 4.5.B shows one example of inter-arms coordination during the High Amplitude configuration of participant S2. On the left side of the figure, the normalized left and right angular velocities in the antero-posterior plane have been represented as a function of cycle advancement for all periods of arm oscillations, using the left arm as a reference. Normalized angular velocities have also been plotted on the left arm - right arm plane on the right side of the figure, after the data have been subsampled at 80 Hz for better visualization. On this plot, the

data points mainly lie on the -45° -oriented diagonal, confirming that there is a strong anti-phase coordination between the arms.

4.3.3.2 Frequency-domain analysis of the arm swing

Figure 4.6.A represents the Discrete Fourier Transform (DFT) of the arm angular velocity signals during walk for all participants and all configurations up to 10 Hz.

Figure 4.6.B shows the frequencies with the highest coefficient magnitudes for all participants and all configurations.

Together, both figures show how a frequency component in the range of $[0.6, 0.7]$ Hz is more present as the amplitude increases, which therefore corresponds to the arm swing frequency. Knowing that the exoskeleton walks at a stride frequency of approximately 1.3 to 1.4 Hz, this seems to show a natural tendency of the participants to try and lock their arm oscillations onto the steps pace of the robot, without being explicitly told to do so. These observations confirm that the oscillatory dynamics of the arms are more visible in the IMU signals as the amplitude increases.

4.3.4 Deriving distinctive features of arms swing during walk in the exoskeleton

The previous section shows that medium to high amplitude oscillatory movements of the arms during walk in the exoskeleton can be extracted from gyroscopic signals in spite of the dynamics of the robot and the disturbances they induce. In particular, it seems possible to build a walking control interface based on the dead-man switch approach by relying on such arm movements and extracting relevant features that can discriminate between the walking and resting states of arm oscillations. These features can be derived based on the observations made in the previous section:

- The possibility of modulating the amplitude of arm swing, and preserving medium to high amplitude movements while walking in the exoskeleton;
- The coordination between the left and right arm as they oscillate in an anti-phase fashion in the antero-posterior plane;
- The rhythmic movements of the arms at a given frequency around 0.6 to 0.7 Hz.

A secondary analysis of data signals obtained from the EE allowed to derive a set of such distinctive features, for which a threshold-based classification architecture can be implemented to correctly detect the walking intention of an

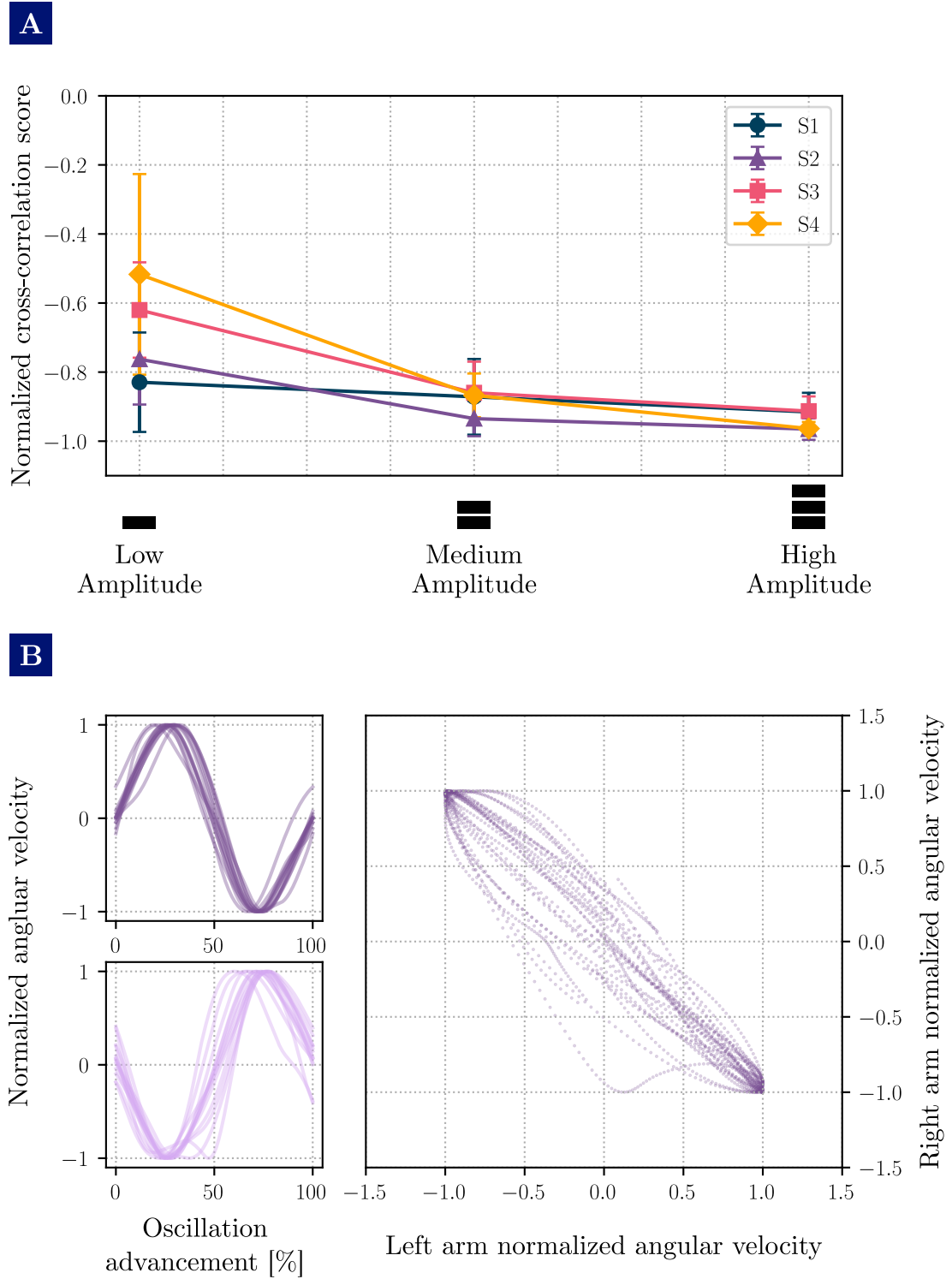


FIGURE 4.5: A. Mean cross-correlation (\pm SD) at lag 0 between angular velocity signals of both arms during the Exploratory Experiment for all participants and all explicit movement configurations. B. Example of inter-arms coordination for participant S3 during the High Amplitude configuration. *Left*: Normalized angular velocities in the antero-posterior plane of the left (dark shade, top) and right (light shade, bottom) arms for all periods of arm oscillations, using the left arm as a reference. *Right*: Normalized angular velocities represented in the left arm - right arm plane.

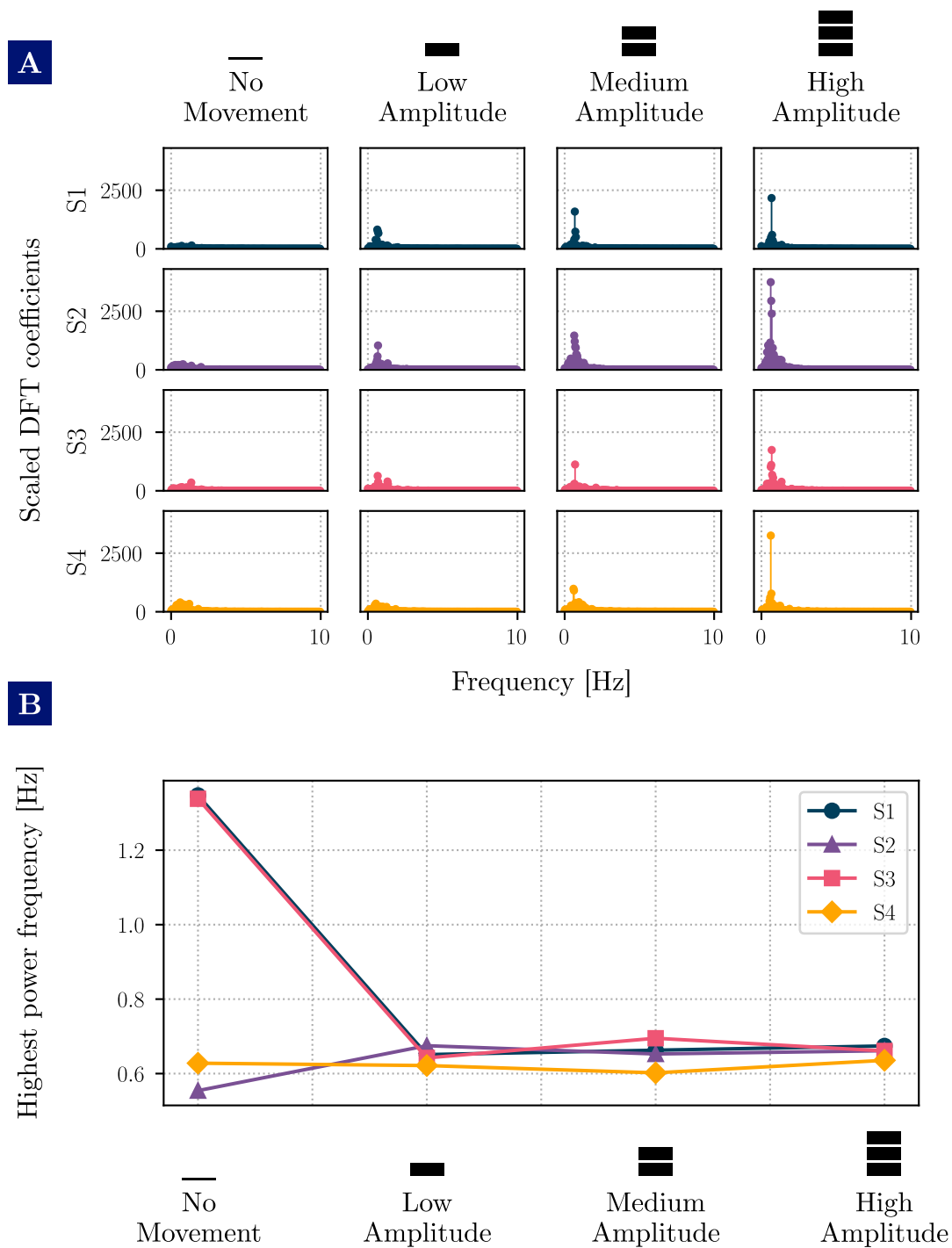


FIGURE 4.6: A. Frequency-domain representations of the left arm angular velocity signals in the antero-posterior plane for all four subjects and all four configurations. B. Frequencies with the highest power in the frequency-domain for all four subjects, and all four configurations.

exoskeleton user. All these features were chosen to be scalar, and derived from a 1 s sliding window with a 50% increment on the left and right arm angular velocities in the antero-posterior plane during walk. The window size was chosen to be greater than a half-period of arms oscillations.

Since only a small number of participants took part in the EE, no statistical analysis could be performed to assess the differences in the feature values across the different configurations other than visually. Thus, it is important to note that the chosen features can only be hypothesized to be good candidates for a threshold-based classification architecture, by relying on the observations made from the available data.

4.3.4.1 Amplitude-based features

Amplitude-based features aim at correctly detecting the presence of arm oscillations explicitly maintained by the exoskeleton user, rather than them being an effect of the robot dynamics. For example, the Maximum Absolute Value (MAV) of a data window can be one such feature. However, it is a spatial feature that does not take into account the temporal evolution of a signal – which can introduce time delays in a detection architecture. Therefore, the Root Mean Square (RMS) value of the window was used instead. The RMS of a discrete signal x of length N is defined as:

$$RMS(x) = \sqrt{\frac{1}{N} \sum_{n=0}^{N-1} |x[n]|^2} \quad (4.5)$$

It is a more descriptive feature that can encompass temporal aspects of the signal while giving out information about its amplitude. It is common to use it on acceleration signals when conducting gait analyses (Sekine et al. 2013). Physically, it can be seen as a measure of “energy”.

Figure 4.7.A shows the mean RMS values of the angular velocities computed across the sliding window during walk, for each participant and each configuration, and averaged across all participants for each configuration. Looking at the figure, it seems that the RMS of the signals increases when higher amplitude oscillations are maintained, as expected. More importantly, it seems that the RMS for the High and Medium Amplitude configurations can be distinguished from the lower values of the No Forced Movement configuration by relying on a common threshold for all participants. Thus, it can be hypothesized that the RMS is a good candidate for a threshold-based classification architecture. Note however that there are more variations in the RMS values between participants for the High Amplitude configuration: in particular, participant S2 exhibited higher amplitude movements, with RMS values twice as high as participants S1 and S3 for the left arm.

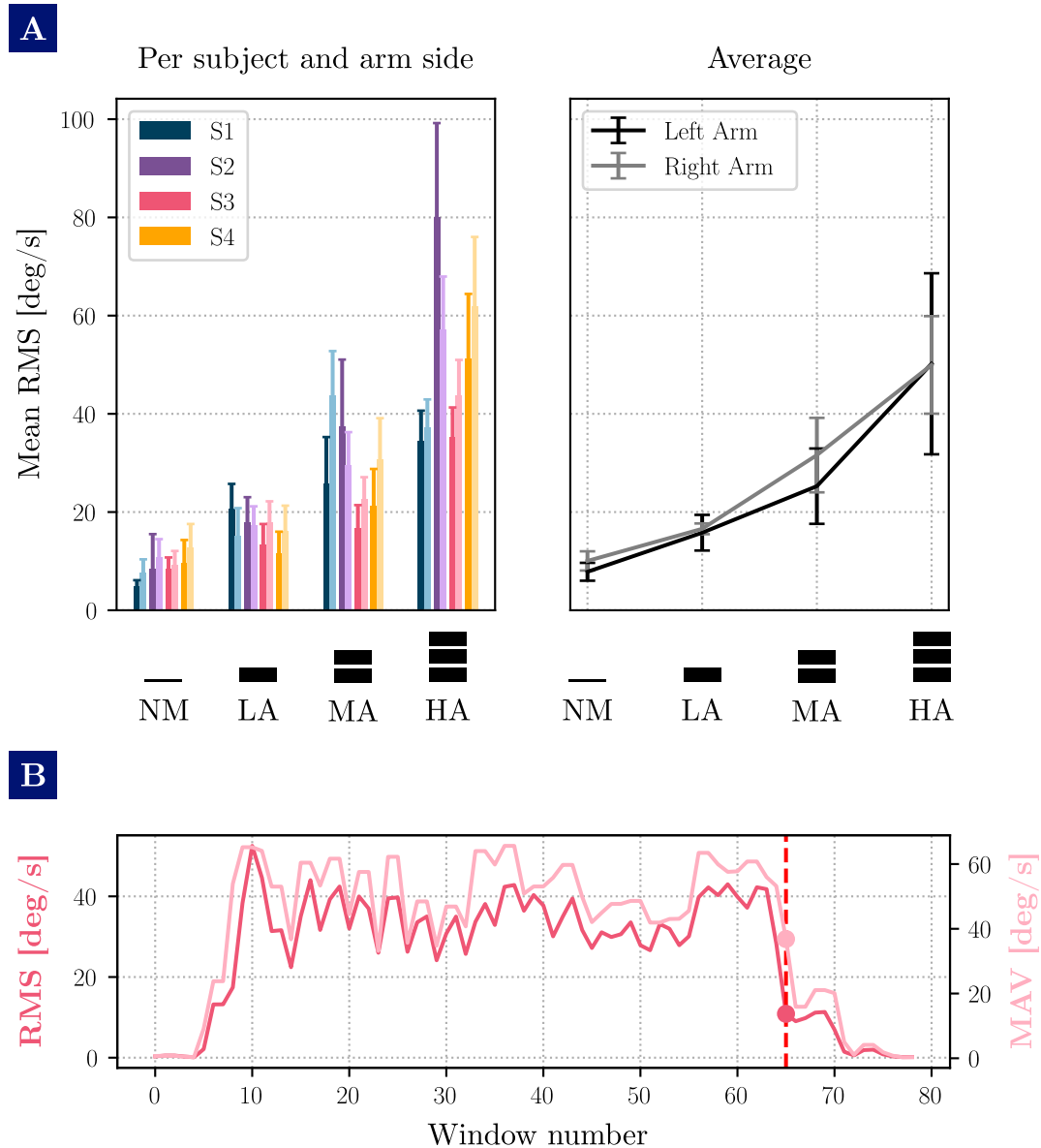


FIGURE 4.7: A. Mean RMS values of the angular velocity signals in the antero-posterior plane during walk in the Exploratory Experiment. *Left*: Left arm (darker shade) and right arm (lighter shade) mean RMS (+ SD) for all participants and configurations. *Right*: Mean RMS values (\pm SD) averaged across all participants for each configuration. B. Comparison between the RMS (dark pink) and MAV (light pink) of the left arm angular velocity of participant S3 during the High Amplitude configuration, computed across the sliding window.

Figure 4.7.B additionally shows one example of how the RMS value drops earlier than the Maximum Absolute Value (MAV), thus making it more suitable for the detection of gait termination when the arms cease to swing. The example is taken from the High Amplitude data of the left arm from participant S3. The window indicated by the dashed red line presents a high value of angular velocity in its early samples (as seen on the bottom plot), which is captured by the MAV, but nuanced through the RMS.

4.3.4.2 Coordination-based features

As seen in 4.3.3, coordination of the arms during walk can be assessed using the normalized cross-correlation of the angular velocity signals at lag 0 (Eq.4.3). Figure 4.8 shows the mean normalized cross-correlation values at lag 0 between the left and right arm signals computed across the sliding window during walk, for each participant and each configuration, and averaged across all participants. It can be seen that the normalized cross-correlation is closer to -1 for the Medium and High Amplitude configurations, with little variance. It therefore seems that the normalized cross-correlation can be used as an indicator of explicitly maintained arm swing in a threshold-based classification architecture.

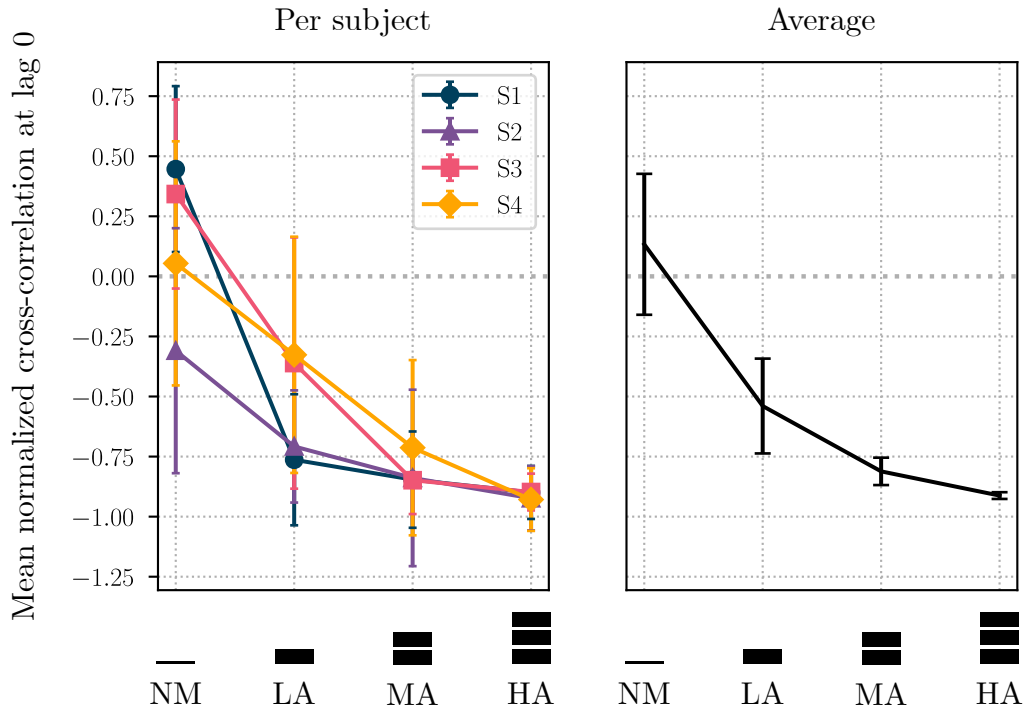


FIGURE 4.8: Mean normalized cross-correlation (\pm SD) at lag 0 computed between the left and right arm angular velocities in the antero-posterior plane during the Exploratory Experiment. *Left*: Mean values for all participants and configurations. *Right*: Mean values averaged across all participants for each configuration.

Figure 4.5.B showed how the anti-phase coordination between the arms can be visualized in the left arm - right arm plane, where the normalized data points mainly lie on the -45° diagonal when the movements are coordinated (normalization is important to erase the effects of arm swing asymmetry). Therefore, for each window of data, it would be possible to evaluate arm coordination through the angle of the principal direction along which the data points vary. This can be achieved through Principal Component Analysis (PCA). PCA is a dimensionality reduction technique that consists in orthogonally projecting a data set onto a linear subspace that maximizes its variance (C. Bishop 2006). For a data set of dimension N , it can be proven that the optimal subspace of dimension $M < N$ for which the variance of the linear projection of the data is maximized is defined by the M eigenvectors corresponding to the M largest eigenvalues of the data covariance matrix. Each eigenvalue is then equal to the variance of the data along the corresponding eigenvector, and the eigenvectors are known as the principal components of the data.

PCA has been previously used to evaluate the coordination between different parts of the body during movement (St-Onge et al. 2003). In the case of anti-phase movements of the arms during walking, the first principal component of the data formed by the left and right arm angular velocities was hypothesized to be the -45° diagonal. This is confirmed in figure 4.9.A, where the direction of the first principal component has been reported for each participant and each configuration for the normalized angular velocity data during walk. It can be seen that for all the explicit movement configurations, the first principal component computed for the data during walk seems oriented along a similar direction, that gets closer to -45° as the amplitude increases. Additionally, the variance of the data along the direction orthogonal to the principal component seems to decrease as the amplitude increases.

Figure 4.9.B shows the mean angle values of the first principal component computed across the sliding window during walk, for each participant and each configuration, and averaged across all participants for each configuration. It confirms that the angle of the first principal component tends to be closer to -45° for the higher amplitude configurations, even when the PCA is computed over fewer data points than the entire walk. It might therefore be a good candidate as a feature for a threshold-based classification architecture, by setting both a high and low threshold that would delimit an interval containing the -45° value.

4.3.4.3 Frequency-based features

Most frequency-related metrics that can be derived from a stream of data rely on the spectral analysis of the signals, which is possible through DFT via a FFT algorithm. However, the frequency resolution for the FFT of a signal x of length N and sampling frequency f_s is given by:

$$\Delta f = \frac{f_s}{N} \quad (4.6)$$

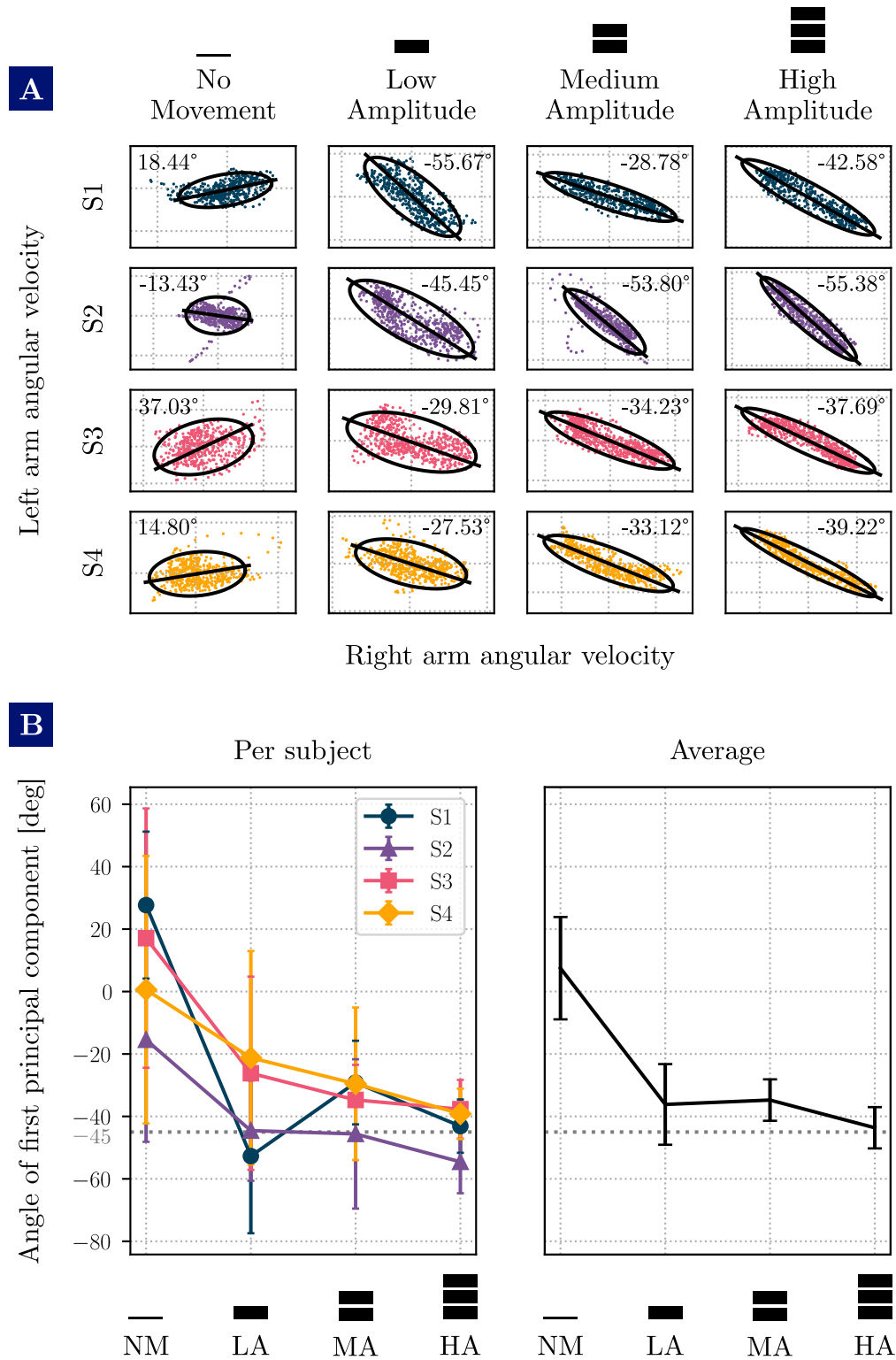


FIGURE 4.9: A. Angular velocity data in the left arm - right arm plane for each participant and each configuration during walk for the Exploratory Experiment. The black solid lines represent the direction of the first principal component, which angle is mentioned on each individual plot, and the ellipses represent 90% of the variance of the data along the directions of the two principal components of the data. Axis values have been omitted for clarity. B. Mean angle of the first principal component of the arms velocity data (\pm SD). *Left*: Mean values for all participants and configurations. *Right*: Mean values averaged across all participants for each configuration.

In the case of the 1 s windowed angular velocity signals, $\Delta f = 1$ Hz, which is a poor resolution for the frequency range described in 4.3.3.2.

Therefore, no frequency-related feature were derived. However, the frequency analysis in 4.3.3.2 confirms that the 1 Hz cutoff frequency for the Butterworth filter can be retained in an online implementation of a threshold-based classification architecture, since arm swing movements operate in the frequency range of $[0.6, 0.7]$ Hz.

4.3.4.4 Choosing adequate threshold values

The features described in the previous paragraphs have also been chosen so that the retained threshold values could be expected to be good approximations in a first implementation of the classification architecture, despite the small number of samples. This could lead to some amount of overfitting when choosing the threshold values, but adjustments and more fine-tuning can be easily made if required.

Overall, the base rule for choosing a threshold value was that for all participants in the Medium and High Amplitude configurations, the mean feature values \pm one standard deviation would be recognized as walking values.

Figure 4.10 shows the feature space obtained by computing the different features over the sliding window during walk for all participants, for the Medium and High Amplitude configurations (in red) and the No Forced Movement configuration (in blue). For the RMS feature, only the RMS of the left arm was taken into account for the visualization. The figure also shows the projections of the data points on the planes formed by the different pairs of features, with the threshold values represented as dashed red lines.

The RMS feature The threshold for the RMS feature was chosen to be $11^\circ/\text{s}$.

One note of importance is that the classification architecture would require the exoskeleton users to actively stop their arm swing movements in order to express their gait termination intention and make the robot stop. Such a behaviour is different from what was displayed during the No Forced Movement configuration, where some amount of oscillations could still be expressed, as an effect of the dynamics of the robot for example. However, it can be hypothesized that actively stopping the arm movements would make the upper body behave as a damping system, leading to even smaller RMS values than the No Forced Movement configuration, and an even lower threshold.

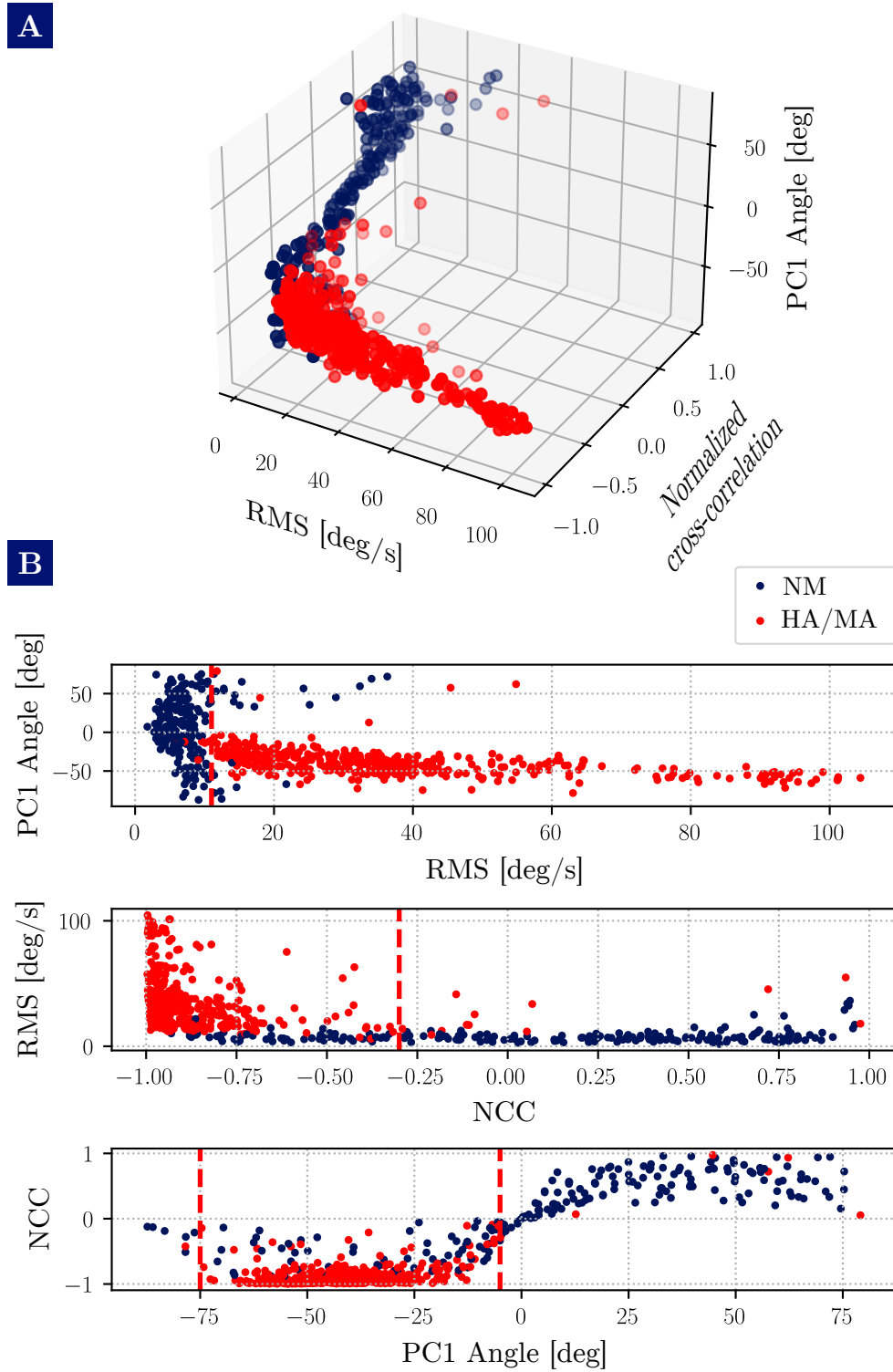


FIGURE 4.10: A. Representation of the data from the Exploratory Experiment during walk in the feature space formed by the (left arm) RMS, first PC angle, and normalized cross-correlation. B. Projections of the data in the three planes formed by the feature pairs.

The normalized cross-correlation feature The threshold for the normalized cross-correlation was chosen to be -0.3 .

The angle of the first principal component feature For the angle of the first principal component, there were both a high and a low threshold. The interval was chosen to be $[-5^\circ, -75^\circ]$.

4.3.5 A threshold-based classification architecture as the walking control interface

The three features derived in 4.3.4 can be used in a simple threshold-based classification architecture that would distinguish between two possible states:

- The exoskeleton user is currently walking;
- The exoskeleton user wishes the robot to stop.

The first state should be maintained as long as the user actively swings their arms with a medium to high amplitude, and gait termination should occur when the oscillations of the arms cease. Therefore, the three features can be derived from a sliding buffer window of data recorded in real-time by the arm IMUs, and serve as an input for the classification architecture. The classifier would implement three rules based on the derived thresholds for each feature, and could then rely on a majority-vote scheme to decide between the two possible states – meaning that the global output of the classifier is taken as the output given by at least two out of the three threshold-based rules (Preece et al. 2009b).

For a window of data containing the angular velocity signals x_l and x_r , the three threshold-based rules can be summarized as follows:

$$\begin{aligned} \mathbf{r}_{\text{RMS}}(x_l, x_r) &= \begin{cases} 1 & \text{if } \text{RMS}(x_l) > 11 \text{ and } \text{RMS}(x_r) > 11, \\ 0 & \text{if } \text{RMS}(x_l) \leq 11 \text{ or } \text{RMS}(x_r) \leq 11 \end{cases} \\ \mathbf{r}_{\text{angle}}(x_l, x_r) &= \begin{cases} 1 & \text{if } \text{angle}(x_l, x_r) \in [-5, -75], \\ 0 & \text{if } \text{angle}(x_l, x_r) \notin [-5, -75] \end{cases} \\ \mathbf{r}_{\text{NCC}}(x_l, x_r) &= \begin{cases} 1 & \text{if } (x_l \star x_r)_{\text{norm}}[0] < 0.3, \\ 0 & \text{if } (x_l \star x_r)_{\text{norm}}[0] \geq 0.3 \end{cases} \end{aligned} \quad (4.7)$$

where, for two signals x and y , $\text{angle}(x, y)$ is the angle of the first principal component of the data formed by x and y . Therefore, the final output of the classifier is given by:

$$\mathbf{r}_{\text{total}}(x_l, x_r) = \begin{cases} 1 & \text{if } r_{RMS}(x_l, x_r) + r_{\text{angle}}(x_l, x_r) + r_{NCC}(x_l, x_r) \geq 2, \\ 0 & \text{if } r_{RMS}(x_l, x_r) + r_{\text{angle}}(x_l, x_r) + r_{NCC}(x_l, x_r) < 2 \end{cases} \quad (4.8)$$

Figure 4.11 shows the output results when the classification architecture is implemented offline on the data from the EE, for all participants and all configurations. As expected, the classifier seems to perform well on the data from the Medium and High Amplitude configurations, with the walking state being correctly detected compared to the No Movement and the Low Amplitude configurations: for the High Amplitude configuration, all windows corresponding to the walking state were correctly classified; for the Medium Amplitude configuration, one window was misclassified during the walk for participants S1 and S4. However, it is possible to make the classifier more robust to such misclassifications by requiring that a certain number of subsequent windows should output the gait termination state before the robot can be effectively stopped. Note that the delay in detecting gait termination for participant S4 during the Medium Amplitude configuration is due to them not having correctly stopped swinging their arms after the exoskeleton has come to a halt (see figure 4.2). This classification architecture was more thoroughly tested during a validation experiment.

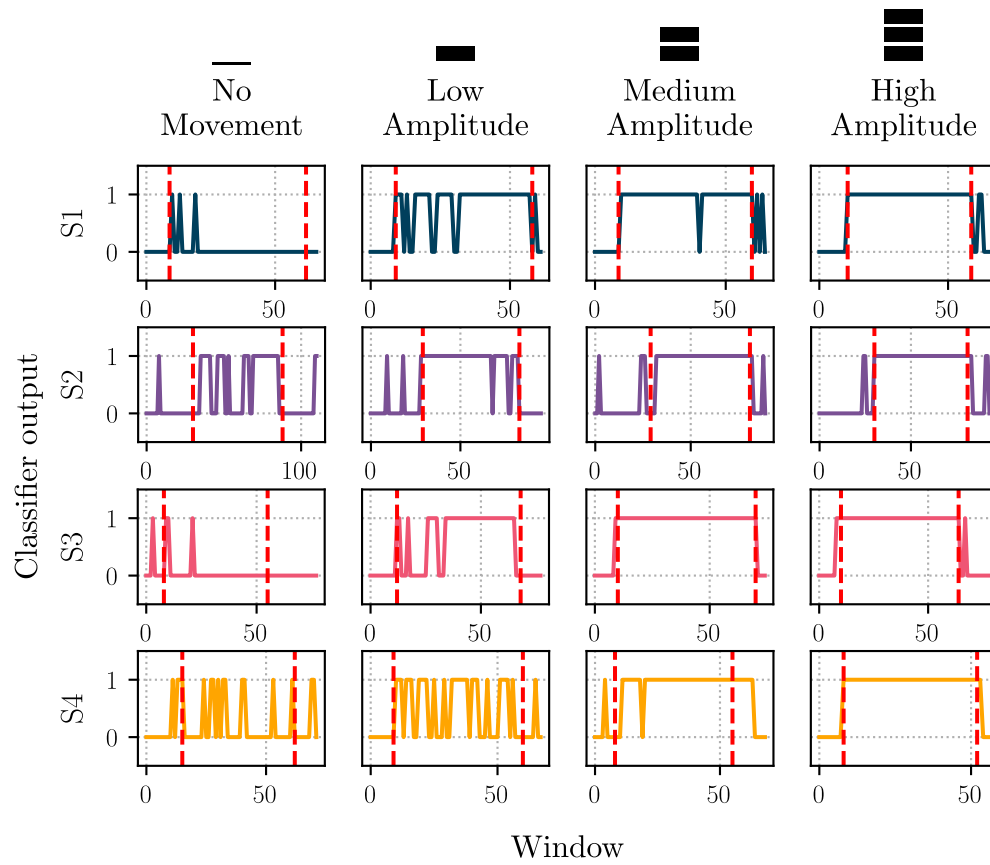


FIGURE 4.11: Output of the threshold-based classifier on the data from the Exploratory Experiment, for all participants and all configurations. The dashed red lines indicate the start and end times of walking.

4.4 | Using arm swing movements to walk in the exoskeleton: a validation experiment.

4.4.1 The experimental setup

A two-configurations Validation Experiment (VE) was conducted to evaluate the threshold-based classification architecture as an effective control interface for terminating gait in the walking exoskeleton. 11 unimpaired participants (7 men and 4 women) used to walking with the exoskeleton took part in the experiment. They were aged 27.5 ± 4.0 years old, with an average height of 176.6 ± 8.8 cm and an average weight of 68.0 ± 8.4 kg. They were equipped with the IMU-embedded jacket described in chapter 2. In both configurations, the classification architecture built on the features derived from the Exploratory Experiment was used to determine the state of the robot (walking or not). During the first configuration, the participants were asked to perform 10 5m-long walks in the exoskeleton while exhibiting high-amplitude arm movements to express their walking intention (High Amplitude configuration, HA). The starting and ending points of the walks were marked on the ground with visible tape. During the second configuration, the participants were asked to perform 5 5m-long walks while exhibiting medium-amplitude arm swing movements (Medium Amplitude configuration, MA). During both configurations, if the exoskeleton stopped before the end of a walk, the participants were asked to resume walking to complete the 5 m distance. The failed runs were marked as unwanted stops, and the successful resumed walk was marked as a re-run. Therefore, the total number of trials in each configuration corresponded to the total number of successful runs (including reruns), plus the total number of unwanted stops.

Additionally, in order to make the classification more robust to unwanted stops during the walk, it was required that two consecutive windows be classified as a gait termination intent before effectively stopping the robot.

4.4.2 Data and statistical analyses

In this experiment, False Negatives (FNs) corresponded to the occurrences where the exoskeleton stopped walking despite the participant still swinging their arms. Accuracy of the threshold-based architecture was therefore evaluated based on the rate of FNs among the total number of trials.

Signal data from all successful trials (excluding unwanted stops) were used to assess the amplitude of arm swing, as well as evaluate the time delays for correctly detecting gait termination after the arms have stopped swinging. A comparison

of movement amplitudes between both configurations was also conducted, and the trends for the coordination and amplitude-based features were derived.

For comparing time delays and arm swing amplitudes between both configurations, repeated measures ANOVA tests were conducted based on the participant values averaged across trials, with the configurations as the within variable. Normality of the data was assessed using the Shapiro-Wilk test, and the repeated measures ANOVA was replaced by the non-parametric Friedman test when the normality assumption failed. Sphericity of the data was also confirmed using Mauchly's test. The same tests were used for the analysis of the individual features.

4.4.3 Results of the study

4.4.3.1 Accuracy of the classification architecture

A total of 109 trials were retained for the analysis of the HA configuration. 3 trials from 2 different participants were discarded because the data revealed that the exoskeleton stopped due to a robot balance error, and not because of the classification architecture, and only 2 occurrences of FNs appeared, corresponding to a FN rate of 1.83%. In one case, the FN was due to one arm not swinging at a high enough amplitude, which affected all features. In the other, the FN was due to a loss of synchronization between both arms, which affected the coordination-based features.

Figure 4.12.A is an illustration of the latter. In the figure, the result from each feature is 1 when the walking state is detected, and 0 when gait termination intention is detected, as described in 4.3.5. For this particular trial, it can be seen that both coordination-based features output a result of 0 for at least 2 consecutive windows when a loss of synchronization in arms swing appears. Therefore, the classifier detects a gait termination intention, even though the RMS feature still outputs 1. The dashed blue line indicates when the stopping event is sent to the exoskeleton and the classifier stops running. For comparison purposes, a typical successful trial from the same participant can be seen in figure 4.12.B: when the arms stop swinging (indicated by the light blue dashed line), all three features output 0. It is important to note that since the output results in the figure are time-indexed, the light blue dashed line does not correspond to a 0 in the results plots. However, the overlapping shaded areas on the IMU data plot represent the two consecutive windows for which the classifier has detected a gait termination intention, and it can be seen that they are comprised of the data immediately following the arms stop.

For the MA configuration, no trial was discarded. There were 8 FN occurrences: 1 in one trial from participant S2, 4 in two trials from participant S6, and 3 in two trials from participant S8. These corresponded to 5 reruns, for a total number of successful trials of 55, and a FN rate of 14.55%.

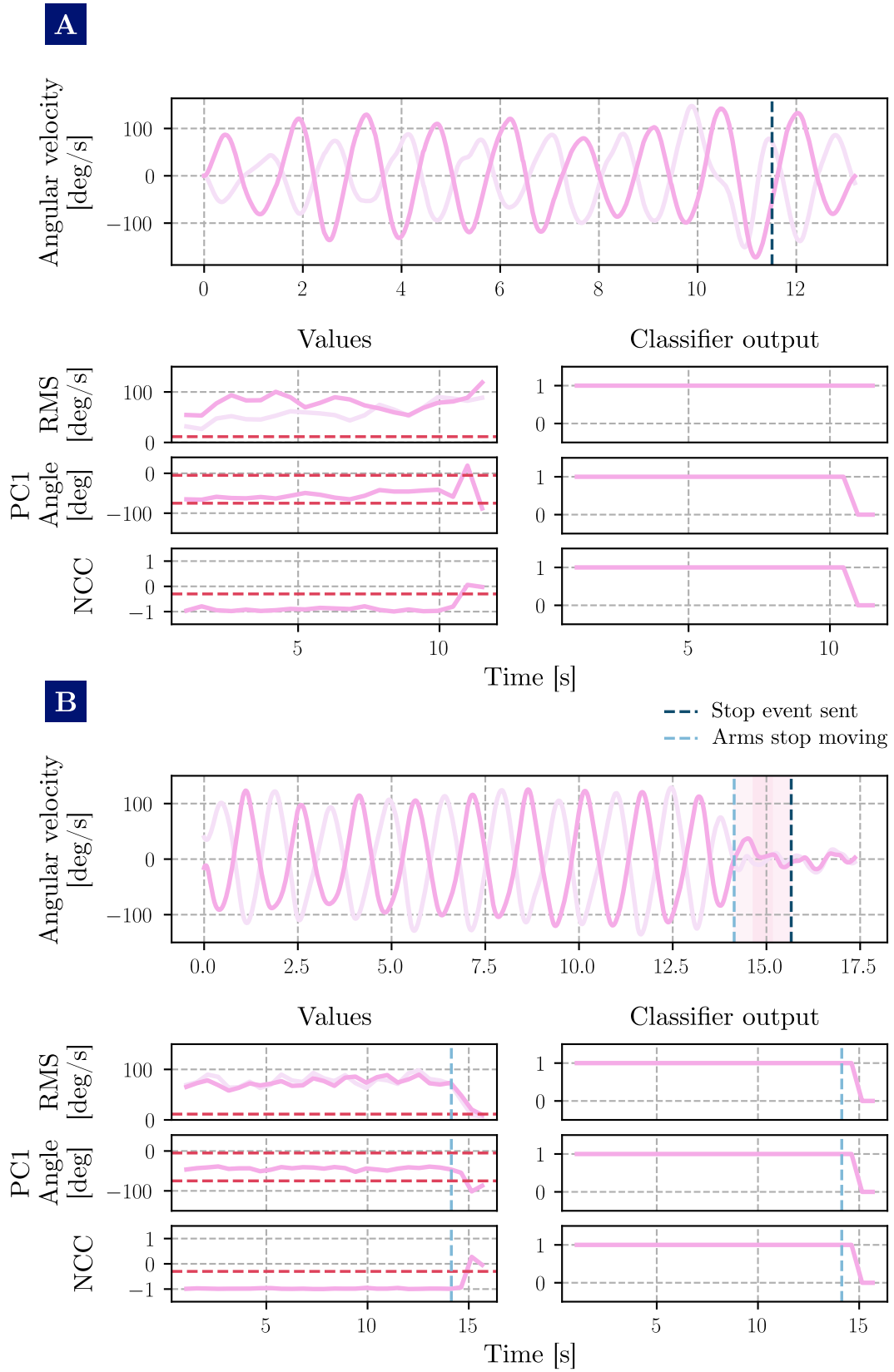


FIGURE 4.12: Left (darker shade) and right (lighter shade) arm angular velocities for one FN trial (A) and one successful trial (B), and the corresponding feature values and output results. In (B), the shaded areas on the top plot represent two consecutive windows of data after the arms stop.

4.4.3.2 Analysis of gait termination detection time delays

To evaluate gait termination detection delays, each trial was manually labeled to determine the time at which both arms have stopped swinging, based on the amplitude of the angular velocity IMU signals (see the light blue dashed line in figure 4.12.B). The delay for a single trial was then derived as the time duration elapsed between this labeled point and the time at which the stop event was effectively sent to the exoskeleton. Figure 4.13 shows the average delays for each participant and each configuration, as well as the overall average per configuration, which was evaluated at 1.55 s for the HA configuration and 1.23 s for the MA configuration. The difference in delays was statistically significant ($p < 10^{-2}$).

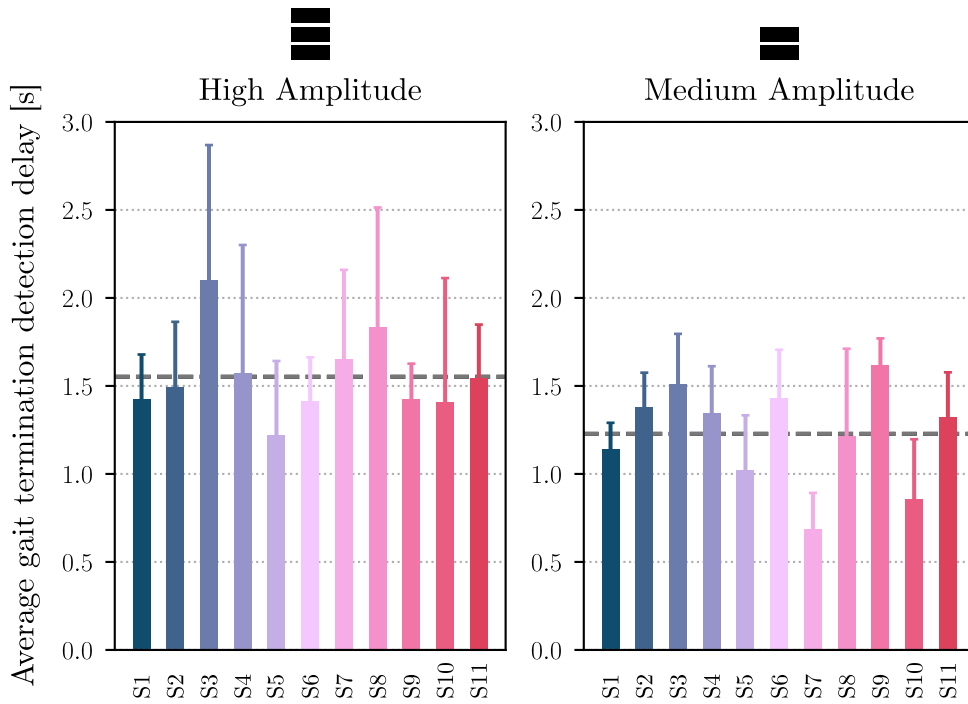


FIGURE 4.13: Average gait termination intention detection delays during the Validation Experiment for all participants and both configurations. The dashed lines represent the averaged values across all participants

4.4.3.3 Analysis of arm swing amplitude

Arm swing amplitude was evaluated by deriving the mean angular ranges for each participant, as described in 4.3.2.1. Figure 4.14 shows the resulting values for both configurations HA and MA.

The average values across all participants were reported on the figure as dashed lines. For the left arm, they were $41.3^\circ \pm 10.9^\circ$ for the HA configuration and $20.6^\circ \pm 9.2^\circ$ for the MA configuration, and for the right arm, they were $40.2^\circ \pm 9.6^\circ$ for the HA configuration and $20.7^\circ \pm 9.2^\circ$ for the MA configuration. For both arms,

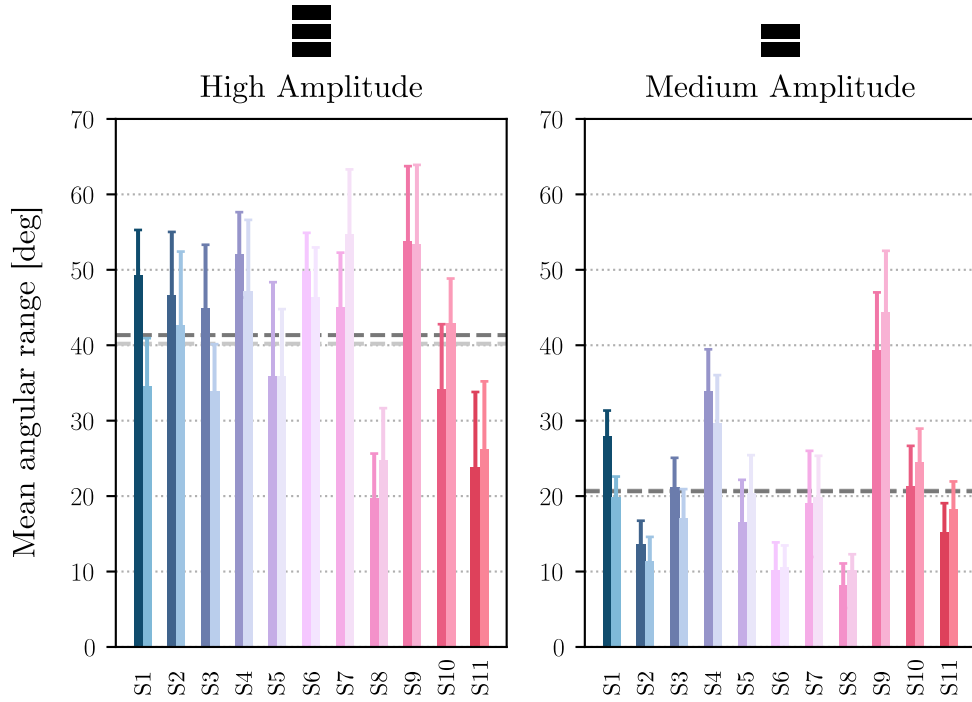


FIGURE 4.14: Mean angular range of left (darker shade) and right (lighter shade) arm swing movements during the Validation Experiment for all participants and both configurations. The dashed lines represent the averaged values across all participants (darker shade for the left arm, lighter shade for the right arm).

the difference in mean angular ranges between both configurations was statistically significant ($p < 10^{-4}$).

4.4.3.4 Analysis of the classifier features

To analyze the different classifier features, their mean values for each trial were computed during walking (up to the manually labeled arms stop). Average values across all trials for each participant were then derived. The same methods were applied for the mean standard deviations, in order to evaluate the mean variations in the feature values during the participants' trials. The results are presented in figure 4.15, which shows the average values during walking for each of the three features for all participants, and both configurations. The vertical bars and shaded areas represent the average standard deviations, and the dashed red lines represent the threshold values for the different features.

The differences in average means between both configurations were statistically significant for both arms RMS values ($p < 10^{-4}$) and the normalized cross-correlation feature ($p < 10^{-2}$), but not for the angle of the first principal component. The differences in average standard deviations were statistically significant for all features: for both arms RMS values, the standard deviations were higher

for the HA configuration ($p < 10^{-4}$), and for the normalized cross-correlation and angle features, the standard deviations were higher for the MA configuration ($p < 0.05$).

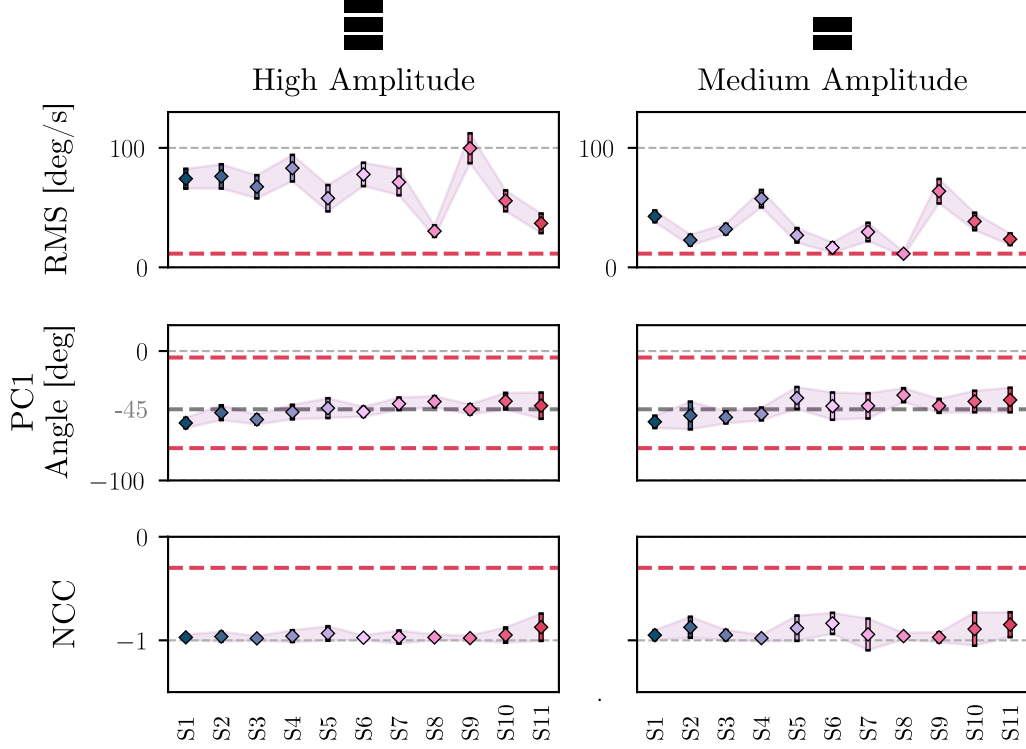


FIGURE 4.15: Mean average values of the three features for each participant and for both configurations. For the RMS feature, only the left arm is shown. The vertical bars and shaded areas represent the average standard deviations of the corresponding features for each participant. The dashed red lines represent the threshold values for the different features.

The rates of wrong outputs (0 instead of 1) for each feature during walking in the successful trials were also derived, and can be seen in table 4.1. In the HA configuration, the output from the angle feature was wrong in 0.27% of the data windows across all participants and all trials, in 0.18% from the normalized cross-correlation feature, and in 0.06% from the RMS feature. In the MA configuration, the rates were 0.18% for the angle feature, 0.30% for the normalized cross-correlation feature, and 4.7% for the RMS feature. The distribution of wrong outputs between all participants are shown for both configurations in figure 4.16: in the HA configuration, wrong outputs in at least one feature were exhibited by only four different participants, and most came from participant S11. In the MA configuration, wrong outputs were exhibited by seven different participants. Three participants never showed any wrong output.

| | High Amplitude | Medium Amplitude |
|-----------|----------------|------------------|
| RMS | 0.06% | 4.7% |
| PC1 angle | 0.27% | 0.18% |
| NCC | 0.18% | 0.30% |

TABLE 4.1: Rates of wrong outputs during the Validation Experiment for both configurations and all features.

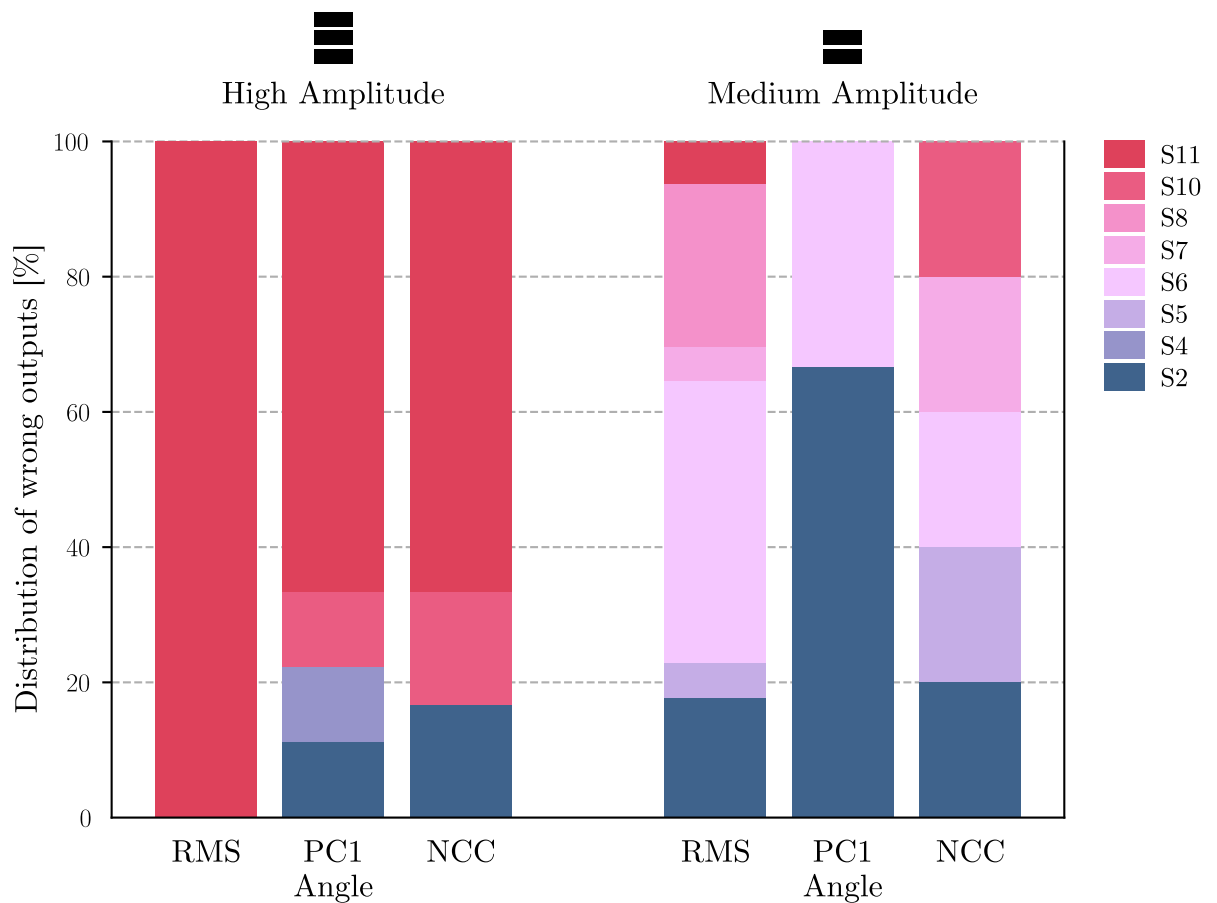


FIGURE 4.16: Distribution of wrong output windows during walking among the participants for each feature and both configurations, in all successful trials during the Validation Experiment.

4.4.4 Discussion

4.4.4.1 Effectiveness of the threshold-based classifier architecture

Overall, the previous results suggest that the threshold-based classifier architecture was effective at detecting the gait termination intention with low occurrences of False Negatives in both amplitude configurations – and a lower rate of FNs for the HA configuration. The participants were successfully able at lowering their arm swing amplitude for the MA configuration, which was on average divided by two between both configurations: the average value for the mean arm angular range was 20° , which corresponds to the values reported in the literature for natural-speed gait (Carpinella et al. 2010; Plate et al. 2015; Punt et al. 2015). This shows that the proposed control interface can be effective when exhibiting natural arm swing movements, and can therefore be intuitive for exoskeleton users while requiring minimal cognitive burden.

Additionally, analysis of the three different features showed that arms coordination is better when the movements amplitude is high, with less variance in the feature values, and normalized cross-correlation coefficients closer to -1 on average. However, in both configurations, the average values for the coordination-based features were far from the thresholds used during the experiment, and could therefore be modified. On the contrary, the RMS feature showed higher variance at a high amplitude, but values closer to the threshold in the MA configuration. Exaggerated movements therefore seem to express a tighter coupling of the upper limbs, but give less control on the amplitude of arm swing.

Overall, the three features were individually effective at detecting the walking intention, with very low rates of wrong outputs: $1\% <$ for all features when arm swing amplitude was high, $1\% <$ for the first principal component angle and the normalized cross-correlation features when arm swing amplitude was medium, and a 4.7% rate for the RMS feature when arm swing amplitude was medium. The higher number of FNs in the MA configuration was mostly due to low amplitudes of the arms movements, which seems to correlate with the higher rate of wrong outputs from the RMS feature: 5 of the 6 FNs in this configuration came from participants S6 and S8, who had the lowest average RMS values, and average angular ranges of motion around 10° . More generally, wrong outputs are not evenly distributed among participants, which shows that subject-dependant parameters could be selected for an increased effectiveness of the control interface, or that additional training could improve its accuracy.

4.4.4.2 Lowering the time delay for gait termination

The previous results seem to confirm that the choice of features to build the threshold-based classifier architecture was appropriate. However, the time delays for the detection of gait termination intention can seem relatively high compared to the 0.5 s delay for planned stopping in the literature (Jaeger et al. 1992), with average delays higher than 1 s for both configurations. It is important to note that this duration cannot be lower than 0.5 s, since the design of the classification algorithm requires two successive windows to output the gait termination state before effectively sending a stop signal to the exoskeleton. In many cases, when the arms stop moving, the current window can still be classified as a walking state, since it can contain data points that were recorded before the arms stopped swinging (see figure 4.12.B for example). This virtually causes a higher latency, with delays higher than 1 s (corresponding to two windows). Additionally, the inertia from the exoskeleton dynamics can cause the arms to continue swinging for a short time after the participant has ceased any explicit movements, which may introduce additional delay. This might explain why the average delay was lower for the MA configuration.

Importantly, the Atalante exoskeleton executes one step in approximately 700 ms, with a step length between 14 and 16 cm. Since the device completes its current step when the stop event is sent, this means that the time delay results correspond to stopping it within 2 or 3 steps on average, or approximately 28 to 48 cm. This can be acceptable in settings where precise stopping is not required, such as in rehabilitation centers where exoskeletons are usually used in long walkways.

To lower the time delays before the stop event is effectively sent to the exoskeleton, possible solutions include lowering the time increment of the data windows, and fine-tuning the feature thresholds for earlier detections. This was evaluated offline using the data from the Validation Experiment, by applying different values of the window increment and threshold parameters. For different parameter combinations, the gain in time delays compared to an offline simulation with the experiment parameters was computed for each trial in both configurations. The mean and standard deviation values were derived for each participant, and then averaged across all participants. The window increment was set every 50 ms between 50 ms and 500 ms. The threshold values were set based on figure 4.15, which shows that the experiment thresholds for the angle of the first principal component feature can be set closer to -45° , and that the threshold for the normalized cross-correlation can be lowered. The threshold value for the RMS was not modified. A total of three different combinations of the threshold parameters were tested: (1) same thresholds as the experiment; (2) -0.5 for the normalized cross-correlation and $[-70^\circ, -15^\circ]$ for the first principal component angle; and (3) -0.7 for the normalized cross-correlation and $[-60^\circ, -25^\circ]$ for the first principal component angle.

Results from this offline evaluation are shown in figure 4.17, where the rate of potential FNs for each combination was also reported.

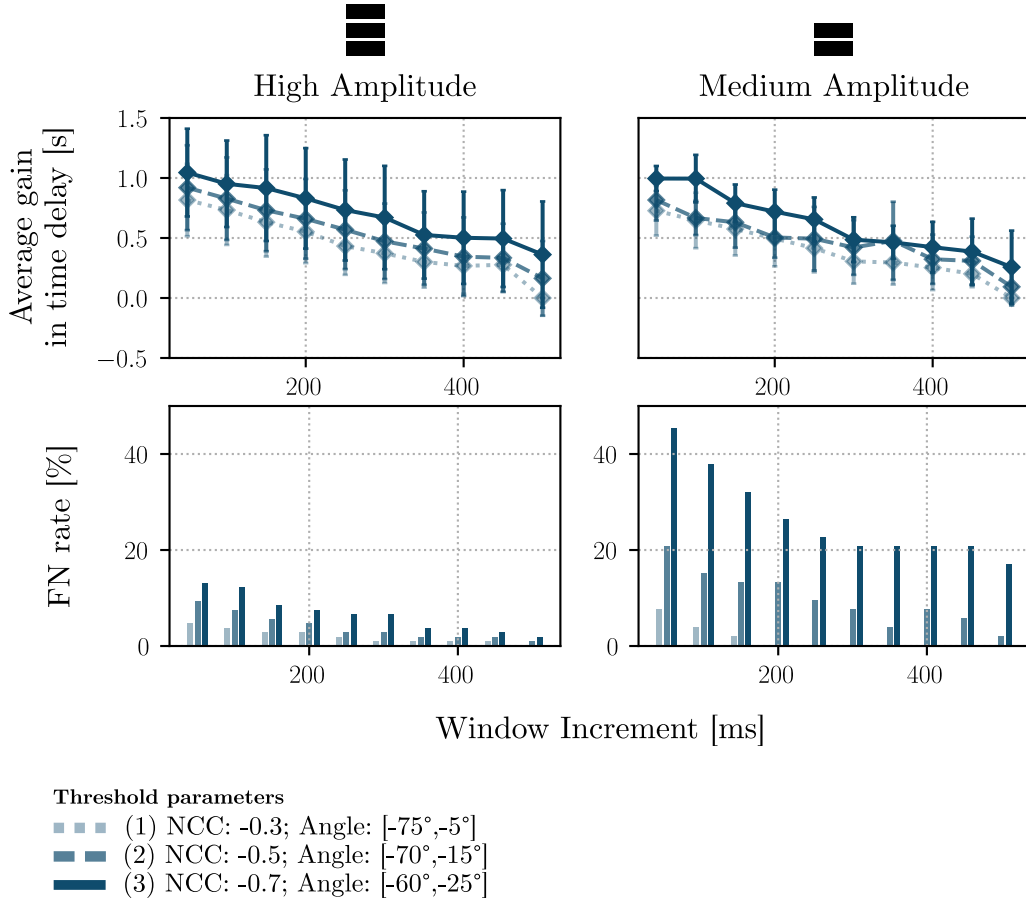


FIGURE 4.17: *Top*: Average gain in time delays for both configurations for different combinations of the window increment and feature threshold parameters. *Bottom*: Number of FNs detected for the different combinations of parameters.

From the figure, it is clear that time delays can be successfully lowered in both configurations when the window increment is made shorter, and when the threshold values for the coordination-based features are modified. However, this induces higher occurrences of FNs as the window increment gets shorter, and as the thresholds allow for less variability of the feature values. In particular, combination (3) of the threshold parameters seems to highly increase the rate of FNs, even at high window increments in the MA configuration. Setting the window increment between 250 and 400 ms with combination (1) of the threshold parameters might offer a good trade-off between the gain in detection delays (around 0.5 s) and occurrences of FNs (up to 10% in the MA configuration). Additionally, it can be reasonably hypothesized that some amount of training with the control interface might reduce the number of FNs (for example, by getting used to the right arm swing amplitude, and avoiding loss of coordination between the arms).

4.5 | Preliminary testing with patients.

Two preliminary qualitative tests of the gait termination control interface evaluated in the previous section were conducted with two different patients: one paraplegic patient, and one patient suffering from post-cancer body impairments. They were both regular users of the Atalante exoskeleton, and used to its original control interface. They were asked to perform at least 2 walks in a 10-m walkway, using high-amplitude arm swing movements to control the gait after the robot has started walking.

No quantitative analyses were conducted on the data from these tests, as they were only conducted as a preliminary investigation to assess whether patients could successfully use their arm swing movements to control walking and gait termination in the Atalante exoskeleton. Indeed, both patients were able to perform the necessary arm movements to successfully maintain the walk, and stop the exoskeleton by ceasing to move, showing that such an interface is a promising method for the detection of gait termination intention in assistive lower-limb devices.

4.6 | Limitations and prospects of the study.

This study shows promising results for the implementation of a gait termination interface based on the identification of a maintained walking state through natural arm swing movements. Participants of the Validation Experiment were able to successfully control walking and stopping in the exoskeleton with minimal unwanted stops from False Negatives, and preliminary tests on patients showed similarly good results. However, larger cohorts of patients with different pathology levels should be enrolled in order to assess whether the empirically derived thresholds for the three amplitude and coordination-based features can be generalized to all exoskeleton users.

Another idea would be to provide a parametrizable user-friendly interface, where individual patients could select different threshold values to adjust to their own capabilities and training levels. The window size and increment could also be editable, which would allow finer control over the time delays for proper gait termination. Such an interface could be an integral part of rehabilitation sessions with an exoskeleton, where patients could select, for example, the required arm swing amplitude to keep the exoskeleton going. Additional improvements could also be made to force proper coordination of the arms and legs during rehabilitation, for example by requiring that each arm should move in phase with the opposite leg,

as is the case in natural gait patterns. Overall, as there is growing evidence that actively including the upper-body into lower-limb rehabilitative settings might be beneficial to impaired individuals (Ferris et al. 2006; Meyns et al. 2013), an arm-swing based interface could help patients train more efficiently by involving their arms during walking. In particular, one of the patients who preliminarily tested the interface appreciated that she could actively move her arms to walk with the exoskeleton, rather than needing the remote to stop the gait.

However, while such an interface seems promising for rehabilitation settings, it might be inadequate for certain real-world situations. In particular, the other patient noted that while the remote control is no longer necessary to stop the exoskeleton, requiring active movements of the arms might make it difficult to achieve certain tasks while walking (e.g. holding a kitchen tray or similar objects with both hands). This difficulty could be overcome by making it possible to switch between different gait termination methods, and implement less natural IMU-based gestured inputs to stop the exoskeleton in particular situations (e.g. lifting the arms sideways in the frontal plane while holding the tray).

4.7 | Conclusion.

In this chapter, a control interface for the detection of gait termination was built. Instead of focusing on a specific movement as a transition between walking and stopping – similarly to what was done for gait initiation in chapter 3 – the classical paradigm consisting in detecting punctual inputs for the transition between different activity modes was reverted to rather focus on maintained arm swing movements as an identifier of the walking state. A dead-man switch approach was then used to detect gait termination when arm movements ceased. This was done by building a threshold-based classification architecture, and relying on a set of three features: the RMS feature to evaluate the amplitude of arm movements, and the normalized cross-correlation and angle of the first principal component features to evaluate arm coordination. Thresholds for these features were set based on the data from a preliminary Exploratory Experiment.

Results from a Validation Experiment confirmed the effectiveness of such a classification architecture, which was successful at detecting the walking and gait termination intentions, with minimal False Negatives. However, time delays higher than for unimpaired planned stopping could exist after the arms had stopped moving, and before the stop event was sent to the exoskeleton, corresponding to stopping the exoskeleton within 0.5 m. This problem can be solved by adjusting the time increment of the sliding window, and the threshold values used for the three features in the classifier. Training with the control interface might help avoiding additional False Negatives with this new set of parameters.

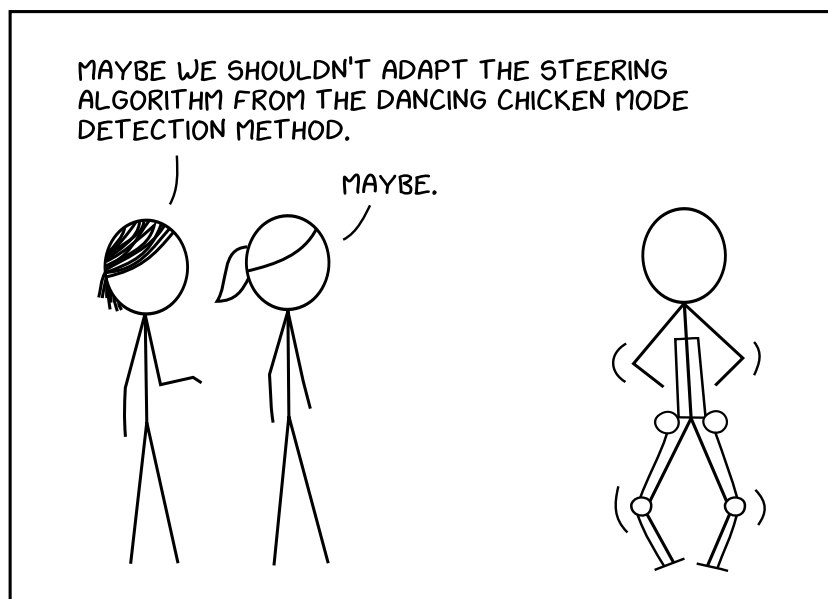
Preliminary tests with patients additionally showed that this control interface could be effectively implemented in a real-usage setting.

Overall, this control interface seems to be both intuitive and effective, and would require minimal learning and training. It allows to actively control the gait when walking with the exoskeleton, without requiring additional inputs from a remote controller.

Chapter 5

Detecting the Steering Intention

This chapter proposes a preliminary exploratory study that focuses on the steering or turning intention while walking with a medical lower-limb exoskeleton. In particular, it investigates the possibility of building a new detection layer on top of the gait termination interface described in the previous chapter. Such a layer would be able to capture predictive movements of the steering intention while swinging both arms to keep the exoskeleton walking. Two strategies, based on either a specific trunk motion, or an asymmetric alteration of the arm swing movements, were proposed. They were evaluated offline based on IMU signals recorded from five unimpaired participants. A preliminary test with one unimpaired participant was also conducted to evaluate an online implementation of the asymmetric arm swing strategy, which was shown to be the more robust and effective at detecting the intention and direction of turning, with no false negatives.



Chapter Contents

| | | |
|------------|--|------------|
| 5.1 | Steering during gait: definition and characteristics | 120 |
| 5.1.1 | The different steering strategies | 120 |
| 5.1.2 | The mechanisms of turning | 122 |
| 5.1.3 | Upper-body movements and the anticipation of steering | 123 |
| 5.1.4 | Steering in the Atalante exoskeleton: detection and implementation . . | 123 |
| 5.2 | The detection of the steering intention | 124 |
| 5.2.1 | Steering detection: existing solutions | 124 |
| 5.2.2 | A steering detection method compatible with arm swing controlled walking | 125 |
| 5.3 | Exploring upper-body-based steering strategies in the exoskeleton . | 127 |
| 5.3.1 | The experimental setup | 127 |
| 5.3.2 | Data analysis | 127 |
| 5.3.3 | Results of the study | 132 |
| 5.3.4 | Discussion on the asymmetric arm swing strategy | 138 |
| 5.4 | Preliminary online validation with one participant | 142 |
| 5.4.1 | Experimental setup | 142 |
| 5.4.2 | Results and Discussion | 143 |
| 5.5 | Limitations and prospects of the study | 144 |
| 5.6 | Conclusion | 145 |



5.1 | Steering during gait: definition and characteristics.

5.1.1 The different steering strategies

Steering (or turning) during gait can be defined as an alteration of the walking direction without stopping. During their investigation of 180° turns, Hase et al. (1999) identified two main strategies for turning: spin turns, which involve spinning the body towards the side of the stance leg, and step turns, where the swing leg operates the directional change towards the side opposite to the stance

limb. By conducting 3D analyses of 90° turns, Taylor et al. (2005) further identified two subcategories for the spin turn: the ipsilateral pivot, where the stance leg spins at mid-stance, and the crossover, where the swing leg comes across and over the stance leg. Diagrams of the different strategies are shown in figure 5.1, adapted from Taylor et al. (2005).

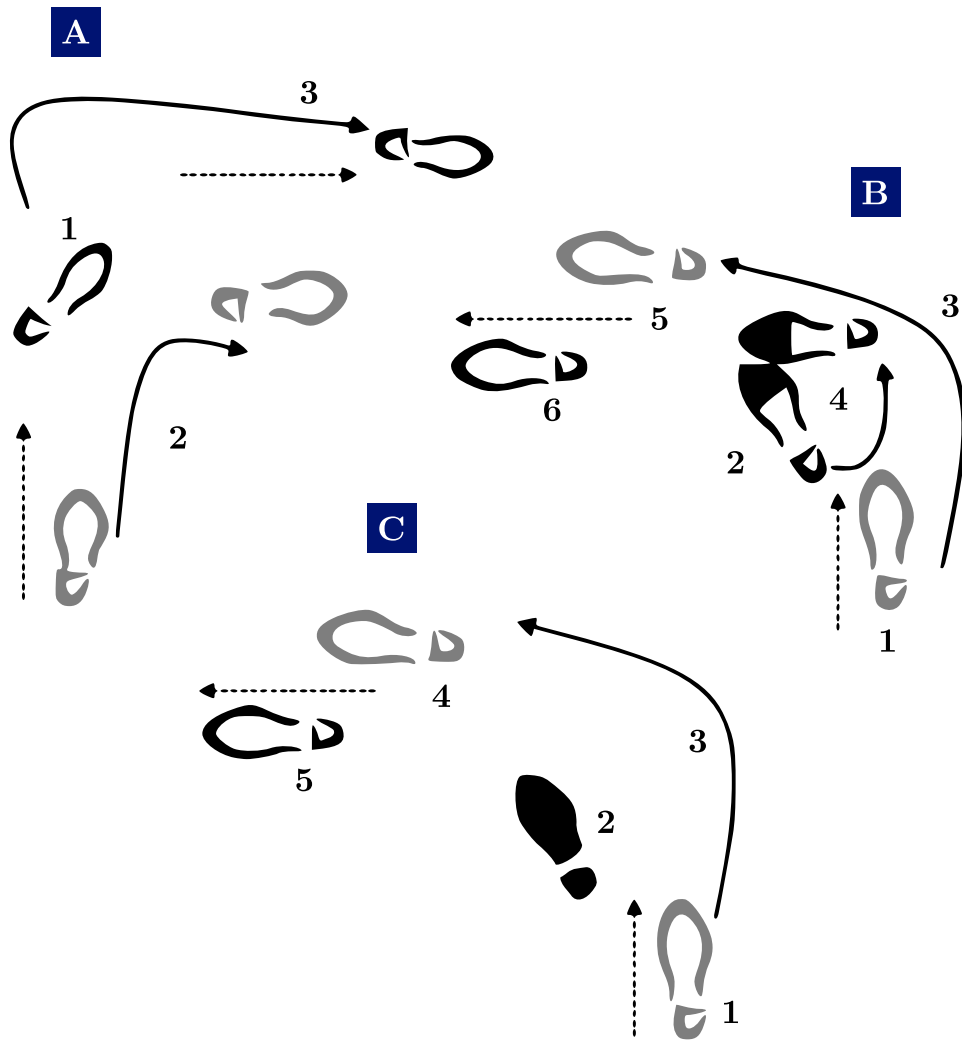


FIGURE 5.1: The different steering strategies, adapted from Taylor et al. (2005). Dashed arrows indicate the direction of walking. Solid arrows indicate swing. Right foot is represented in grey, left foot is represented in black. Black filled foot traces represent the part of foot touching the ground. A. 90° step turn towards the right. B. 90° ipsilateral pivot towards the right. C. 90° ipsilateral crossover towards the right. Please refer to the original paper for more indications on the successive steps of each strategy.

While instability in the lower-limb joints has been shown to be higher during turning compared to straight walking (Segal et al. 2008), the step turn strategy offers more stability than the spin turn, by providing a large base of support, and keeping the Center of Gravity (CoG) between the feet (Hase et al. 1999; Taylor

et al. 2005). Conversely, during the spin strategies, the CoG is displaced outside of the stance limb, which facilitates the turn, but generates higher instability.

Importantly, in a study of turning and steering during activities of daily living, Glaister et al. (2007) only observed step turns, and hypothesized that spin turns might be restricted to specific activities. They further showed that most turns relied on a multi-step strategy, and that the prevalence of turning steps depended on architectural constraints, with a range of 35 to 45% in areas such as a cafeteria, an office, a store, or to reach a parked car.

5.1.2 The mechanisms of turning

During steering at different angles, the Center of Mass (CoM) is laterally translated towards the direction of turn through different mechanisms, mainly foot placement and the so-called hip strategy (Patla et al. 1999; Hollands et al. 2001). The first consists in altering the placement of the feet by increasing the step width, and effectively accelerating the CoM towards the new direction of travel. The second involves specific action of the hips and trunk muscles to control the body as a double pendulum, with upper and lower limbs moving in opposite directions in the frontal plane. Increased medio-lateral ground reaction forces at the outside limb have also been observed during turns, which might help modulating the acceleration of the CoM by increasing the braking impulse, and the lateral propulsion of the stance leg (Orendurff et al. 2006; Strike et al. 2009). These mechanisms are diminished in patients suffering from Parkinson's Disease (PD), who exhibit a shorter CoP-CoM distance during turning, and therefore altered postural control while steering (Song et al. 2012).

Lower-body joint angular displacements and moments are generally similar in the sagittal and frontal planes between the turning strategies described above (Taylor et al. 2005). However, transverse plane moments are strategy-dependent. In particular, the spin turns strategy requires higher muscular activity due to higher moments in the transverse plane, as well as higher ranges of motion at the joints, making it a more demanding strategy. Fukuda et al. (2020) further showed that the kinematics of lower-body joints during steering exhibits age-related changes, with a higher reliance on the hip joint in all planes in older adults.

Walking velocity is also affected during steering, with speed decreasing at higher turn angles, probably as a stabilizing effect (Sreenivasa et al. 2008; Strike et al. 2009). More generally, temporal-spatial variables, such as stride length, and stride velocity, are significantly different for turning gait (Strike et al. 2009). In particular, some of these variables are also affected during the approach phase, showing a possible feed-forward mechanism when aware of an incoming turn. Patla et al. (1991) had already shown that a change in direction cannot happen when cued during the ongoing step, and must be preplanned in the previous step.

Lastly, Courtine et al. (2004) analyzed body coordination patterns between straight and turning gait using Principal Component Analysis. They concluded

that similar neural pathways might govern both types of gait by relying on basic coordination patterns, and that limb and turn dependent adaptations allow for further fine-tuning.

5.1.3 Upper-body movements and the anticipation of steering

Multiple studies have shown that the upper-body exhibits a synergic anticipatory behaviour before turn onset. In particular, the eyes, head, and trunk present an anticipatory coordinated pattern, and predictively rotate towards the direction of turn (Grasso et al. 1998; Hollands et al. 2001; Hicheur et al. 2005; Sreenivasa et al. 2008; Fourati et al. 2013). This reorientation follows a cranial to caudal temporal sequence, where the head starts turning before the rest of the body. However, PD patients exhibit an axial rotation rigidity, and simultaneously rotate the head, thorax and pelvis. This effectively increases their lateral instability, and requires them to take extra turning steps (Spildooren et al. 2013; Yang et al. 2016).

Hollands et al. (2001) showed that significant changes in upper-body behaviour occur when immobilizing the head during steering, supporting the hypothesis that the alignment of the head with the direction of walking is a gaze-independent prerequisite that provides a frame of reorientation for the rest of the body. While they observed that the rotation of the head occurred approximately 250 ms on average before the turn onset, Sreenivasa et al. (2008) found that for angles up to 135°, the head rather turns at a constant distance before the change of direction. During their investigations, they also found higher maximum relative yaw between the head and the trunk at larger turns.

Fourati et al. (2013) further studied the coordination patterns between the shoulders and hips during turns, and found that they were coupled by a linear relationship that becomes tighter as the angle of steering increases.

5.1.4 Steering in the Atalante exoskeleton: detection and implementation

Steering in the Atalante exoskeleton is implemented through a step turn strategy. While walking, the patient can push on one of two remote buttons to choose the turning direction. During the swing phase of the leg on the side of the chosen direction, the angular displacement of the transverse hip joint is incremented so that the robot starts shifting towards its new walking direction. Once the directional change is initiated, additional pushes on the button further increment the angular displacement of the hip, while the button for the opposite direction allows to reduce it. The button normally used to initiate gait from the standstill state can be pushed to resume straight walking.

Importantly, this implementation only allows small directional changes aiming at correcting deviations from the straight walking trajectory, with steering angles not exceeding 5° . Therefore, the increments at the transverse hip joint result in small angular changes, requiring multiple steps to actually perform a high-angle turn.

5.2 | The detection of the steering intention.

5.2.1 Steering detection: existing solutions

A few studies have worked on the detection of steering or turning during walking based on various inputs. Tunca et al. (2017) used a foot-worn inertial sensor for the analysis of gait in a non-hospital setting, and derived the foot orientation from the collected data using a particle filter. They then detected 180° turns as consecutive turning steps, where the angle change from the beginning to the end of the step exceeded a given threshold. Similarly, Mariani et al. (2010, 2013) used data from a foot-worn IMU to identify turning periods based on the relative change in foot orientation between the beginning and end of a gait cycle.

However, since the upper-body exhibits an anticipatory behaviour before a change in the direction of gait, the analysis of its movements can provide a more suitable method for an early detection of the steering intention. This would additionally be compatible for use with lower-limb assistive devices. Some research teams have worked on the implementation of such a strategy: Rehman et al. (2020) used an angle threshold to detect turns based on the integrated gyroscope signal around the vertical axis from an IMU placed on the lower-back of participants, while El-Gohary et al. (2014) directly relied on the angular velocity value from a similarly placed sensor. Novak et al. (2014) employed a hybrid strategy, where thresholds on both the angle and angular velocity values were used online to detect the onset of steering. Threshold values were first derived from a training database using a specific cost function. When a turn was detected, an additional Linear Discriminant Analysis classifier was used to determine its direction. This hybrid approach showed better results than the single threshold ones, with better accuracy when IMUs were placed on the upper or lower back than on the head or legs. Lastly, Farkhatdinov et al. (2017) demonstrated the efficacy of a head-based method for the anticipatory detection of 90° turns compared to a pelvis-based threshold solution. They used k -means clustering on training data comprised of head and pelvis yaw angles to distinguish between straight walking (including when the head is turning to one or the other side without actual steering) and turning to the left or right. A k -nearest neighbours algorithm was then used to

classify the testing data. This method also proved efficient in classifying multiple turns, and turns with different angles, as well as the control of steering in a simulated human-exoskeleton model.

5.2.2 A steering detection method compatible with arm swing controlled walking

Chapter 4 describes a gait termination high-level control interface where the walk is maintained based on arm swing movements. Therefore, the exploration of new steering detection methods in the Atalante exoskeleton should be compatible with such an interface. Two strategies were explored, both of which were based on upper-body kinematic patterns extracted from the previously described arm and back IMUs:

Trunk motion Similarly to the existing methods described in 5.2.1, one strategy can be based on the motion of the trunk around the vertical axis, which is displayed as a natural anticipatory behaviour before steering in unimpaired individuals. However, as explained in chapter 2, since the yaw value cannot be obtained from the IMU measurements, such a strategy can only rely on the raw gyroscope signal as an input. Additionally, since the implementation of steering in the exoskeleton only allows small angular changes per step, there might be a discrepancy between the required magnitude of trunk motion and the actual change of direction in the walking trajectory. One solution would be to maintain the rotation of the trunk until the desired angle has been reached. This could be achieved by defining adequate positive and negative thresholds on the gyroscope signal to detect the onset and direction of turn, as well as the end of the movement when the trunk rotates back to its straight position. However, a maintained trunk rotation with slow exoskeletal movements might seem unnatural to users, and the resulting continuous shift in body weight towards one side of the exoskeleton might impede its stability during walking. Instead, another solution was explored: it consists in repeatedly rotating the trunk towards the new direction of walking in coordination with the arm swing movements (rotating the trunk when the arm on the side of the new direction is swung backwards).

Adapted arm swing movements A different strategy would be to take advantage of the existing arm swing movements required for the walking and gait termination interface, and explore how a simple alteration of these movements can be used as a detection method for the steering intention. In particular, an asymmetric arm swing amplitude could be indicative of both the intention and direction of turning. While a slight asymmetry in the amplitude of arm movements already exists as discussed in the previous chapter, explicitly increasing one arm's amplitude compared to the other should be more distinguishable. Furthermore, it was hypothesized that such a method might feel intuitive, even though

not specifically representative of a natural behaviour: an asymmetric swing can be imagined to increase the torsional moment of the body around the vertical axis in the direction opposite to the arm with the highest amplitude.

Both described strategies were subsequently investigated during an exploratory experiment.

5.3 | Exploring upper-body-based steering strategies in the exoskeleton.

5.3.1 The experimental setup

This exploratory experiment was conducted to assess the feasibility of one of the two steering detection strategies described in the previous section, and investigate whether the repeated trunk motions or asymmetric arm swing movements can yield characteristic IMU signals during walking in the Atalante exoskeleton, and therefore be used as an input for a high-level steering control interface. Similarly to the previous chapter, recordings from the sensors were analyzed to identify indicative features for each strategy. Five unimpaired male participants took part in the experiment. They were aged 29.6 ± 4.2 years old, with an average weight of 66.8 ± 3.6 kg and an average height of 179.8 ± 3.0 cm. They were used to using the exoskeleton. Each participant performed four trials, consisting in walking along a 5-m path with the exoskeleton using the arm-swing based gait termination interface described in chapter 4, while exhibiting one of the movements corresponding to the selected strategies: repeated trunk motion towards the left (RTML) or the right (RTMR), and asymmetric arm swing with a higher amplitude at the left (AASL) or right arm (AASR). For each trial, the participant was first told which movement to exhibit. The experimenter then gave the explicit instruction during the walk as to when to start and stop performing the movement. This experimental setup is described in figure 5.2.

5.3.2 Data analysis

Similarly to the previous chapter, the main objective of this preliminary experiment was to test whether any specific features could be effectively used to detect the steering or turning intention with a threshold-based classifier. However, it is important to note that this experimental setup was exploratory, and involved a small number of participants, who performed only one repetition for each movement. Therefore, no meaningful statistical analysis can be conducted, and any comparison results between different features or threshold choices can only be taken as hypotheses that should be verified on larger cohorts to avoid any form of overfitting.

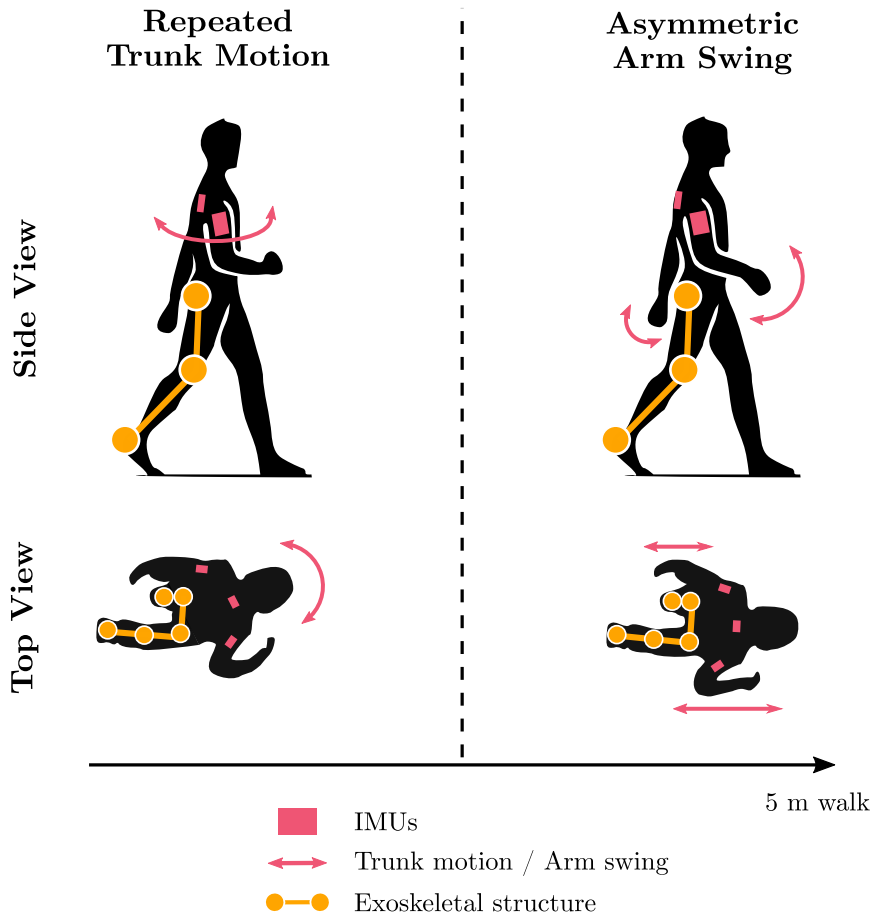


FIGURE 5.2: Experimental setup for the exploration of upper-body-based steering strategies: repeated trunk motion, and asymmetric arm swing. The figure illustrates a turn toward the left for both strategies.

5.3.2.1 Asymmetric arm swing

For all trials, the onset and end of steering were manually labelled based on the gyroscope data from all participants: significant changes in the angular velocity amplitude after a zero-crossing were used to distinguish between walking and steering.

To determine whether the participants were able to successfully modulate their arm swing for steering, the amplitudes of the arm movements in the sagittal plane during steering and walking were evaluated based on the angular ranges of both arms, computed as explained in 4.3.2.1.

Furthermore, since the arms move at a fixed frequency, a change in the amplitude of swing would also induce a change in its angular velocity. Therefore, signal features could also be computed directly from the gyroscope recordings from the

arm IMUs in the sagittal plane. Three heuristic parametrized features were hypothesized to be good indicators of the asymmetry in arm swing, and therefore effective for the implementation of a threshold-based classifier. They were derived from a 1 s sliding window, with a 500 ms increment. Let x be the sampled data of length N , and $\alpha = 2p, p \in \mathbb{N}$. The three features were defined as follows:

Modified RMS feature This is similar to the RMS feature used in chapter 4, taken to the power α .

$$f_{RMS}(x, \alpha) = \left(\frac{1}{N} \sum_{k=0}^{N-1} x[k]^2 \right)^{\alpha/2} \quad (5.1)$$

Modified MAV feature For a given signal x , it represents the Maximum Absolute Value, taken to the power α .

$$f_{MAV}(x, \alpha) = \max_{k \in \llbracket 0, N-1 \rrbracket} |x[k]|^\alpha \quad (5.2)$$

Scaled Moment feature Let σ_x be the standard deviation of the sampled data x . Then, the scaled moment was defined as:

$$f_{moment}(x, \alpha) = \frac{\left| \frac{1}{N} \sum_{k=0}^{N-1} x[k]^\alpha \right|}{\sigma_x} \quad (5.3)$$

The scaling factor σ_x was chosen empirically.

For all three features, five values for α were tested: 2, 4, 6, 8 and 10. The expected effect of the α parameter was to increase the separability between the class feature means at higher values, while lowering the standard deviation for the walking state (relative to the difference in means). However, higher values for α would also increase the relative standard deviation of the feature for the steering state.

The feature values for each of the left and right arm signals x_L and x_R were combined into a single quantity $C_{f,\alpha}$, defined as:

$$C_{f,\alpha}(x_R, x_L) = \max[f(x_R, \alpha), f(x_L, \alpha)] \times s[f(x_R, \alpha) - f(x_L, \alpha)] \quad (5.4)$$

where f is one of the three features, and s is the sign function. This combined feature was chosen to indicate which arm swings with the highest amplitude, and therefore determine the direction of steering.

5.3.2.2 Repeated trunk motion

Similarly to the arm swing movements, the amplitude of the trunk rotation was evaluated based on the calculated angular ranges around the vertical axis. However, different participants might exhibit different velocity profiles during straight walking: for some, the dynamics of the exoskeleton and the arm swing movements might result in trunk oscillations around the vertical axis, as in figure 5.3. For others, the core muscles might act as a dampening system, and little oscillations might appear. Therefore, angular ranges of the trunk rotation were only calculated during the steering state.

Additionally, since all previously described features were chosen to be indicative of changes in the amplitude of a signal, they could also be used for the analysis of the repeated trunk motion, based on the back IMU gyroscope signal x_B around the vertical axis. However, while such features would be appropriate for the detection of the steering intention, they cannot be indicative of the direction of turning. Since the IMU orientation is not available, one solution would be to directly rely on the gyroscope data and a signed threshold, as explained in figure 5.3. Such a method can only be implemented if a common threshold can be set for all participants: this was evaluated through a comparison of the trunk movements between the walking and steering states, based on the maximal deviation of the angular velocity before and during turning.

5.3.2.3 Comparing the feature performances

Since 15 different feature values can be computed for each window (3 features, and 5 values for the parameter α), a method for feature comparison is proposed. For a threshold classifier to be effective, the feature values for the different states should be separable, with distinguishable average values, and low within-state variance. Similarly to Fisher's linear discriminant introduced in chapter 3, the ratio $F_{f,\alpha}$ between the difference in class means to the sum of standard deviations can be introduced:

$$F_{f,\alpha} = \frac{|\mu_{w,f,\alpha} - \mu_{s,f,\alpha}|}{\sigma_{w,f,\alpha} + \sigma_{s,f,\alpha}} \quad (5.5)$$

where $\mu_{w,f,\alpha}$ and $\sigma_{w,f,\alpha}$ (resp. $\mu_{s,f,\alpha}$ and $\sigma_{s,f,\alpha}$) are the mean and standard deviation during walk (resp. steering) of either the combined feature $C_{f,\alpha}$ for arm signals x_R and x_L (AASL and AASR trials), or the feature f for the back gyroscope signal x_B (RTML and RTMR trials).

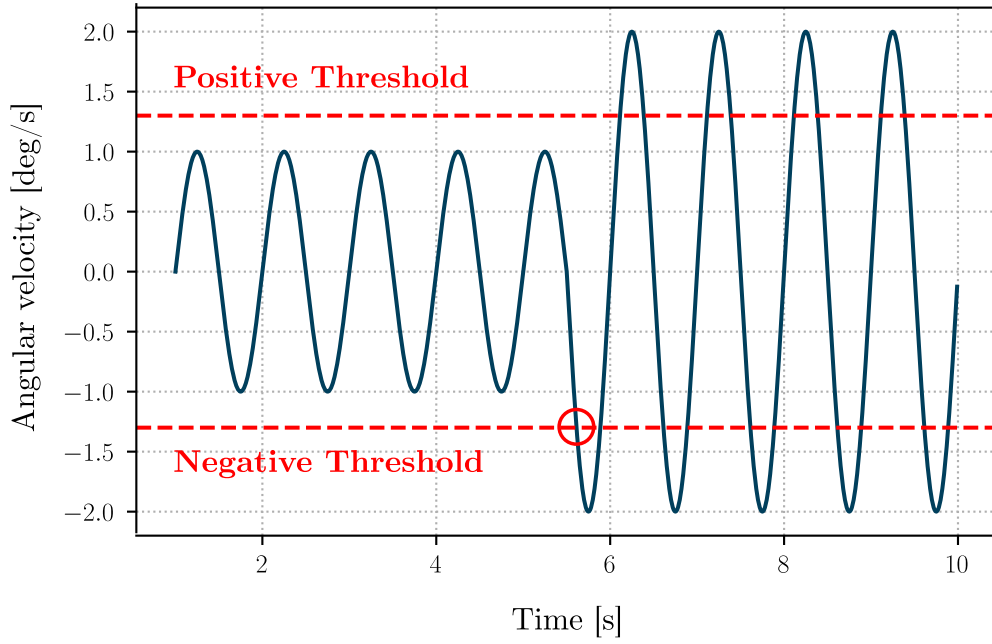


FIGURE 5.3: Possible solution for the detection of the steering direction with the repeated trunk motion strategy. The plot shows the expected waveform from the repeated trunk motion trials: in this example, the trunk movements during straight walking were modelled as small-amplitude oscillations. During the steering state, the repeated trunk motion is expected to result in a higher amplitude angular velocity profile. Therefore, if the steering intention is properly detected from one of the described features, the direction of turning can be derived from the first threshold to be reached (circle in the figure): in this mock example, the negative threshold would indicate a turn towards the left.

For the computation of $F_{f,\alpha}$, a data window was given the label corresponding to at least half of its content, and $C_{f,\alpha}$ or f values that were more than 3 standard deviations away from the labelled state mean were considered outliers and discarded (these usually correspond to transition windows between both states).

An example of the relevant values for computing the $F_{f,\alpha}$ ratio from a single AASL trial can be seen in figure 5.4. In practice, after discarding outliers, walking and steering data from all participants were concatenated to compute a single $F_{f,\alpha}$ per (f, α) pair. For the asymmetric arm swing strategy, the AASL and AASR data were merged after taking the absolute value of $C_{f,\alpha}$, under the hypothesis that a single threshold value with opposite signs could be used to detect the direction of turning.

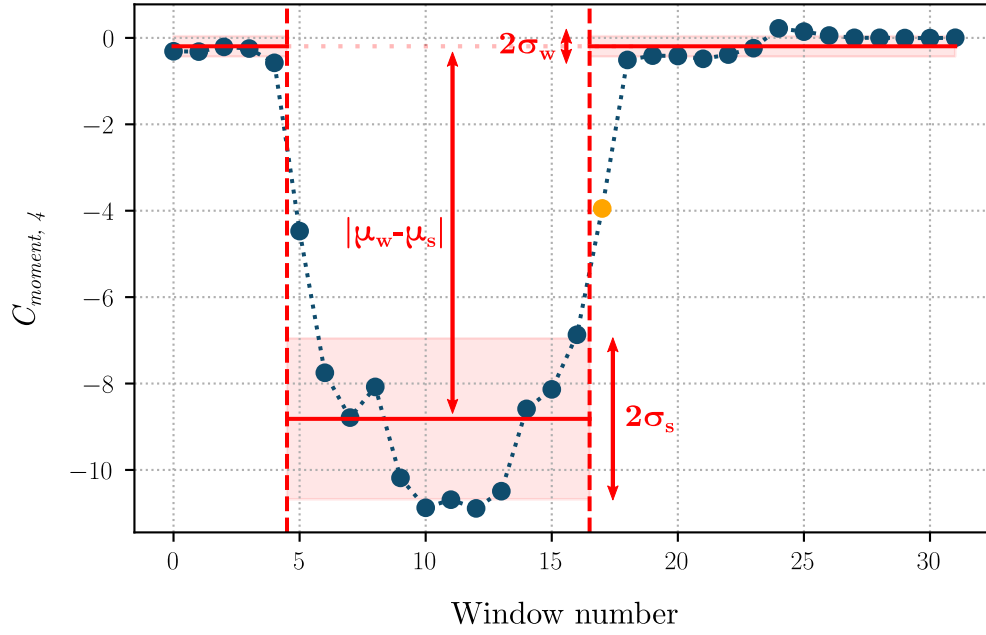


FIGURE 5.4: Relevant values for the computation of the $F_{f,\alpha}$ ratio for an AASL trial, with $f = f_{moment}$ and $\alpha = 4$. The red dashed lines differentiate between the walking and steering data windows, as derived from the manual labels on the gyroscope data. The state means, the difference in means, and the standard deviations are reported on the figure. The transition window between steering and walking (in yellow) was discarded, because it was associated with the walking state (more than half of its content labelled as walking), but was more than 3 SDs from the state mean. The transition window between walking and steering was not discarded, because it was associated with steering, and was less than 3 SDs from the state mean.

5.3.3 Results of the study

5.3.3.1 Repeated Trunk Motion

Amplitude of trunk rotation Figure 5.5 shows typical results from two participants during the RTML trials. Figure 5.5.A specifically shows the angular velocity signals around the vertical axis. For both participants, during the steering state, the trunk exhibited an oscillatory signal at around 0.6 – 0.7 Hz at a higher amplitude than during straight walking. This result was similar across all participants, and both directions of steering: it corresponded to a rotational movement at an average angular range of $28.00^\circ \pm 4.26^\circ$ for the RTML trials, and $25.72^\circ \pm 8.96^\circ$ for the RTMR trials. Individual values from each participant are shown in figure 5.6.

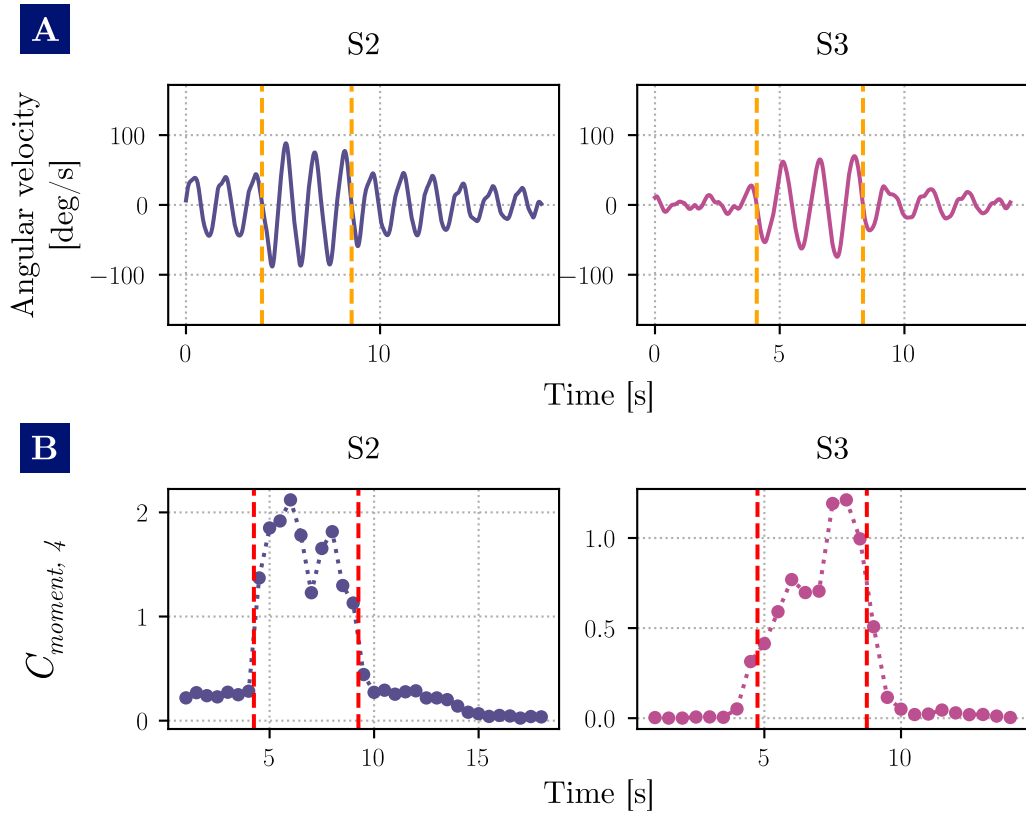


FIGURE 5.5: Results from participants S2 and S3 during the RTML trials. A. Angular velocity signals around the vertical axis; the orange dashed lines represent the onset and end of the explicit trunk repeated rotation. B. Corresponding $C_{moment,4}$ values; the red dashed lines distinguish between the walking-labelled and steering-labelled windows.

Comparison of the signals before and during steering Figure 5.5.B shows the $C_{moment,4}$ values corresponding to the RTML trials from participants S2 and S3. For this (f, α) pair, the combined feature values for the walking and steering states seem to be distinguishable for each participant. However, the direction of turning cannot be derived from these values alone. Angular velocity signals were therefore further analyzed to evaluate whether a method as described in figure 5.3 can be implemented. As expected, figure 5.5.A shows that trunk movements during straight walking can be different between participants: for participant S3, the signal before steering is noisy, with a low amplitude compared to the oscillations from participant S2 (which are similar to the model proposed in figure 5.3). After the end of the explicit trunk movements, a small rotation seems to persist in participant S3. Figure 5.7 additionally compares the maximum angular velocities around the vertical axis for each participant before starting and during the explicit trunk motion, as well as the angular velocity reached during the first explicit rotation of the trunk. From the figure, it seems that for all participants, a relative increase in the amplitude of the angular velocity signal around the vertical axis effectively appears as soon as the explicit trunk movements start. However, the participants exhibit different levels of angular velocity amplitudes: for example,

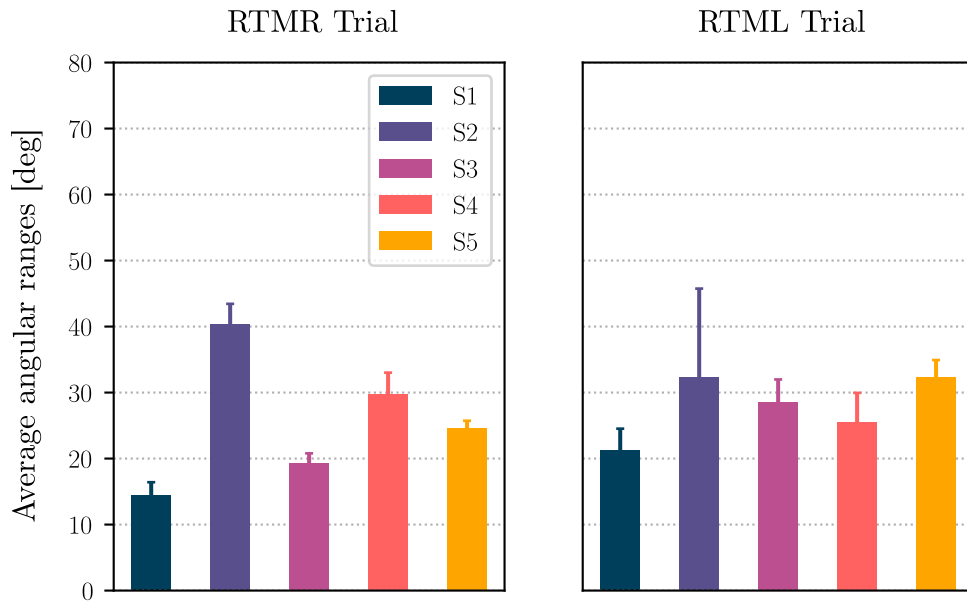


FIGURE 5.6: Average angular ranges of the trunk rotation for each participant during steering in the repeated trunk motion trials. Vertical bars represent one standard deviation.

in the RTMR trial, the maximum value for participant S2 before steering is higher than the maximum values reached by participants S1 and S3 during steering. Since such an overlap can exist between participants, it seems difficult to define a common threshold for the detection of the turning direction. Therefore, results from the repeated trunk motion trials were not further analyzed.

5.3.3.2 Abandoning the repeated trunk motion strategy

During the repeated trunk motion trials, the participants exhibited high amplitude trunk movements during steering, with variable angular ranges. However, while this repeated pattern could be distinguished by one of the proposed features, it seems more difficult to properly derive the new direction of walking, because of the inter-participant variability in movements exhibited by the trunk during straight walking. If such a variability exists in a small cohort of five participants, it can be expected that it would also appear in larger groups of exoskeleton users, especially in patients with different levels of pathology and core muscles affections. Therefore, the repeated trunk motion strategy doesn't seem to offer an immediate robustness for the detection of the steering direction inside a moving exoskeleton, unless adaptive thresholds curated to each individual are implemented. Moreover, during the RTM trials, since the participants needed to be constantly turning towards one side of the robot to express the steering intention, their head (and therefore the direction of their gaze) was constantly moving: this can be considered unnatural, and could rapidly prove unpleasant for an exoskeleton user. Overall,

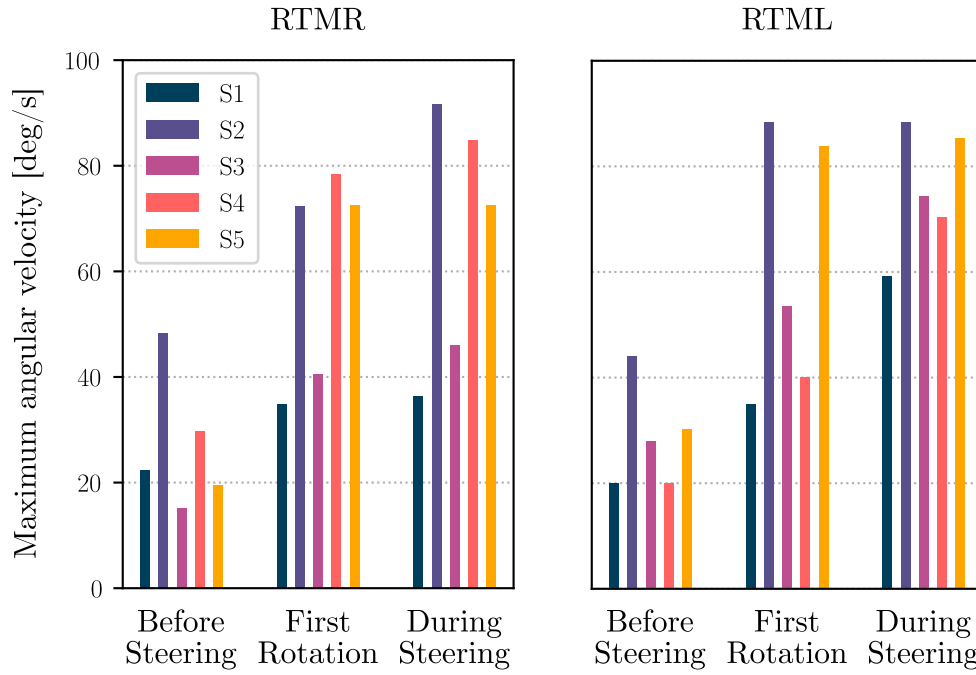


FIGURE 5.7: Maximum angular velocities around the vertical axis during the RTML and RTLR trials for each participant: (1) before the onset of the steering state; (2) for the first explicit rotation of the trunk; (3) during the steering state.

these conclusions don't plead in favor of implementing the repeated trunk strategy, which will not be discussed further.

5.3.3.3 Asymmetric arm swing

Amplitude of arm movements Figure 5.8 shows typical results from an AASL trial: the top row shows the sagittal angular velocities from both arms, the middle row shows the corresponding angular ranges, and the bottom row shows the $C_{f,\alpha}$ values for all features and $\alpha = 4$. The plots on the first two rows indicate that the amplitude of the right arm movements were effectively higher than those of the left arm during the asymmetric motion. Importantly, there were no False Negatives from the gait termination interface.

Figure 5.9 confirms this result for all participants, and both left and right trials. It shows the average angular ranges for each participant during the AASL and AASR trials, for the walking and steering states. Table 5.1 additionally shows the averaged values across all participants. Overall, the angular ranges from the arm swing movements of the arm opposite to the new direction of walking (contralateral arm) were higher than those of the arm on the side of the turning direction (ipsilateral arm). On average, the increase between the walking and steering states for the contralateral arm was more than two-fold. Its amplitude was 1.5 (AASL trial) to 1.8 (AASR trial) higher than that of the ipsilateral arm.

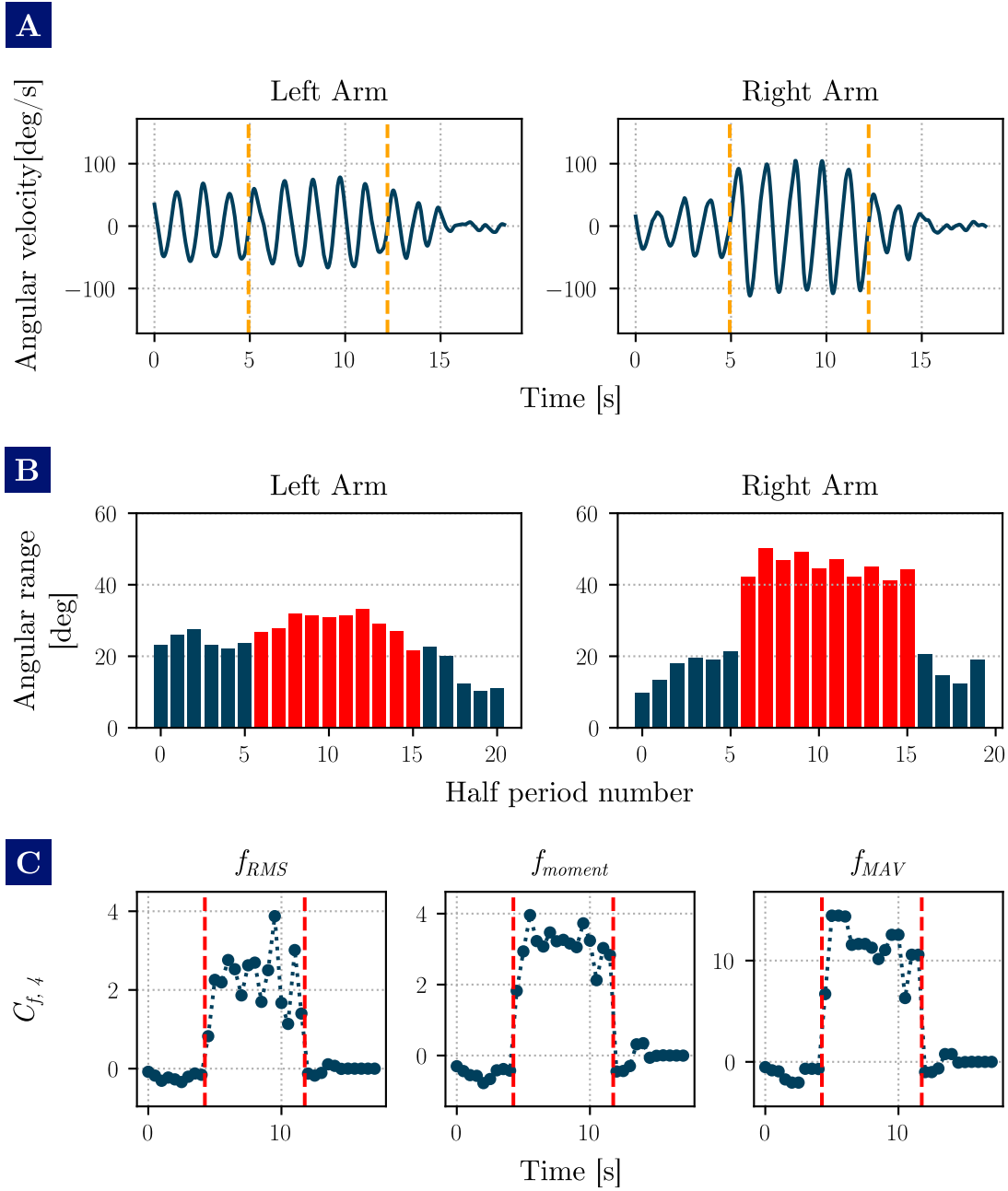


FIGURE 5.8: Example results from an AASL trial from participant S1. A. Angular velocities in the sagittal plane for each arm; the orange red lines indicate the manually labelled start and end times of the steering state. B. Angular ranges for each arm and each half-period of arm-swing; the blue bars indicate the walking state, and the red bars indicate the steering state. C. $C_{f,4}$ values for all features; the red dashed lines distinguish between the walking-labelled and steering-labelled windows.

Interestingly, except for participant S5 in the AASR trial, the amplitude of the ipsilateral arm movements also seemed to increase slightly between the walking and steering states, with an average increase of approximately 50%.

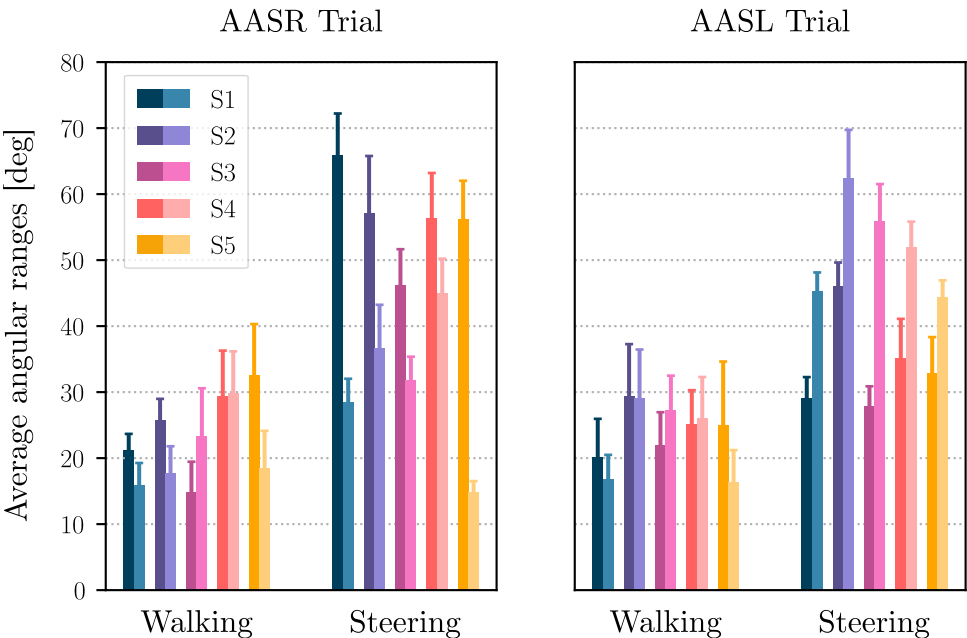


FIGURE 5.9: Average angular ranges for each participant during the asymmetric arm swing trials, for the left (darker shade) and right (lighter shade) arms, and both the walking and steering states. Vertical bars represent one standard deviation.

| | AASR | | AASL | |
|-----------|--------------|--------------|--------------|--------------|
| | Walking | Steering | Walking | Steering |
| Left Arm | 24.73 ± 6.20 | 56.34 ± 6.22 | 24.35 ± 3.16 | 34.17 ± 6.46 |
| Right Arm | 21.04 ± 5.05 | 31.33 ± 9.93 | 23.08 ± 5.42 | 51.93 ± 6.71 |

TABLE 5.1: Average ± SD values for the left and right arm angular ranges (in deg) during the AASL and AASR trials, for both the steering and walking states.

Features analysis The last row from figure 5.8 shows that in this specific example, all features seem to exhibit distinctive values for the walking and steering state for $\alpha = 4$. However, it is important that this could be generalized to all participants and trials, and the comparison method described in 5.3.2.3 was used to determine whether a specific choice for α and f could serve as a basis for a threshold-based classifier.

Figure 5.10.A shows the $F_{f,\alpha}$ ratio for all features and values of α during the asymmetric arm swing trials. The figure shows that higher values of the α parameter induce a decreased ratio. For a given α value, the f_{moment} feature seems to have the highest ratio. Figure 5.10.B additionally shows the standard deviations σ_w and σ_t for the walking and steering states for each (f, α) pair, normalized by the difference in means. Overall, higher α values induce a higher standard deviation for the turning state, as was expected. For all features, $\alpha = 2$ results in the highest walking state standard deviations. For the f_{moment} and f_{MAV} features, the walking standard deviation slightly increases with higher α values, starting from $\alpha = 4$. For the f_{RMS} feature, the walking standard deviation is lower as α increases.

Lastly, for all participants, the combined feature values during the steering state were effectively positive for the AASL trials, and negative for the AASR trials.

5.3.4 Discussion on the asymmetric arm swing strategy

5.3.4.1 Amplitude of movements

Results from the amplitude analysis show that the participants were able to successfully modulate their arm swing movements so that the contralateral arm would swing at a higher amplitude than the ipsilateral arm. On average, the amplitude of the ipsilateral arm also increased during the steering state. This might be indicative of a coupling effect, where a relative increase is observed in both arms, since no specific instructions were given for the ipsilateral arm. Additionally, since there were no False Negatives from the gait termination interface, the asymmetry in arm swing movements can be considered compatible with the method for the detection of maintained walking. Therefore, if a feature is capable of robustly capturing this asymmetry, such a strategy might prove a good candidate for detecting the steering intention.

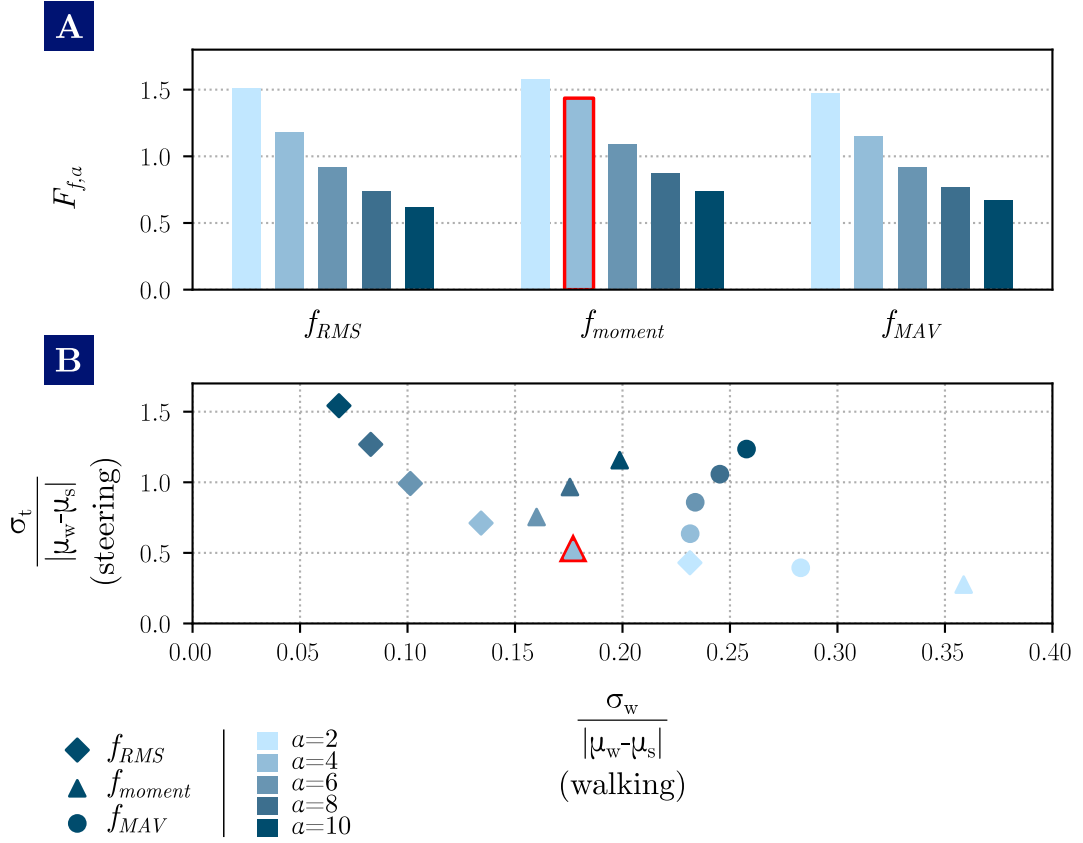


FIGURE 5.10: Evaluation of the performance of the different features during the asymmetric arm swing trials. The red stroke indicates the chosen (f, α) pair. A. $F_{f,\alpha}$ ratio for all features and possible values of α , obtained from the merged data from all participants and trials. B. Associated standard deviations for the walking and steering states, normalized by the difference in means. Note that the scales on the axes are different.

5.3.4.2 Features analysis

The better candidate features for a threshold-based classifier seem to be the ones with a low α parameter value. In particular, all features with $\alpha = 2$, as well as the f_{moment} feature with $\alpha = 4$ show the highest $F_{f,\alpha}$ values, meaning that they allow for a good separation of the data corresponding to the walking and steering states, with low intra-state variation. However, it can be expected that higher variance would be observed when one arm is swung at a higher amplitude, as was the case for the RMS feature in 4.4.4.1. Therefore, a threshold value closer to the walking state mean seems more appropriate to build a robust classifier, based on a feature with low deviation during walking. Based on these conclusions, the f_{moment} feature with $\alpha = 4$ was chosen and tested offline, with a threshold value t chosen such that:

$$t = (\mu_w + \sigma_w) + \frac{(\mu_s - \sigma_s) - (\mu_w + \sigma_w)}{4} \quad (5.6)$$

where the indices *moment* and 4 were omitted for clarity. This results in $t = 1.85$. Therefore, for a window $k \in \mathbb{N}$ of data containing the sagittal angular velocity signals $x_{l,k}$ and $x_{r,k}$ from the left and right arm, a steering rule can be summarized as follows:

$$\mathbf{r}_{\text{steering}}(x_{r,k}, x_{l,k}) = \begin{cases} 0 & \text{if } -t \leq C_{\text{moment},4}(x_{r,k}, x_{l,k}) \leq t \\ 1 & \text{if } C_{\text{moment},4}(x_{r,k}, x_{l,k}) > t \\ 2 & \text{if } C_{\text{moment},4}(x_{r,k}, x_{l,k}) < -t \end{cases} \quad (5.7)$$

Similarly to the walking and termination interface described in chapter 4, the implementation of the steering intention detection can require that a transition between two states (walking straight, steering towards the left, steering towards the right) only occurs if two consecutive windows $k-1$ and k are classified into the new state. If $C_k = C_{\text{moment},4}(x_{r,k}, x_{l,k})$, then a pseudo-code implementation of the rule above writes as:

```

while walking do
  if  $C_{k-1} > t$  and  $C_k > t$  then
    | steer left;
  else if  $C_{k-1} < -t$  and  $C_k < -t$  then
    | steer right;
  else if  $t \leq C_{k-1} \leq t$  and  $t \leq C_k \leq t$  then
    | walk straight;
  end
end

```

Algorithm 1: Pseudo-code for the implementation of a steering intention detection method

Figure 5.11 and table 5.2 show results from an offline implementation of the algorithm described above on the AASL and AASR trials from all participants. The method accurately captures both the steering intention and the direction of turning, with maximum delays of 2 windows (corresponding to at least 1 s) compared to the manual labels. These delays are mainly due to falsely classified windows during transitions between the walking straight and steering states, corresponding to the low False Positive and False Negative classification rates. However, since these misclassifications only appeared at transitions, it can be considered that no false positive or negative triggers have occurred, and that the steering method detection was effective at detecting both the intention and direction of turning in this offline setting. Moreover, since two consecutive windows should be classified into the same state for a transition to occur, minimal delays were expected. An online implementation of this method was preliminarily tested in one participant, as described in the following section.

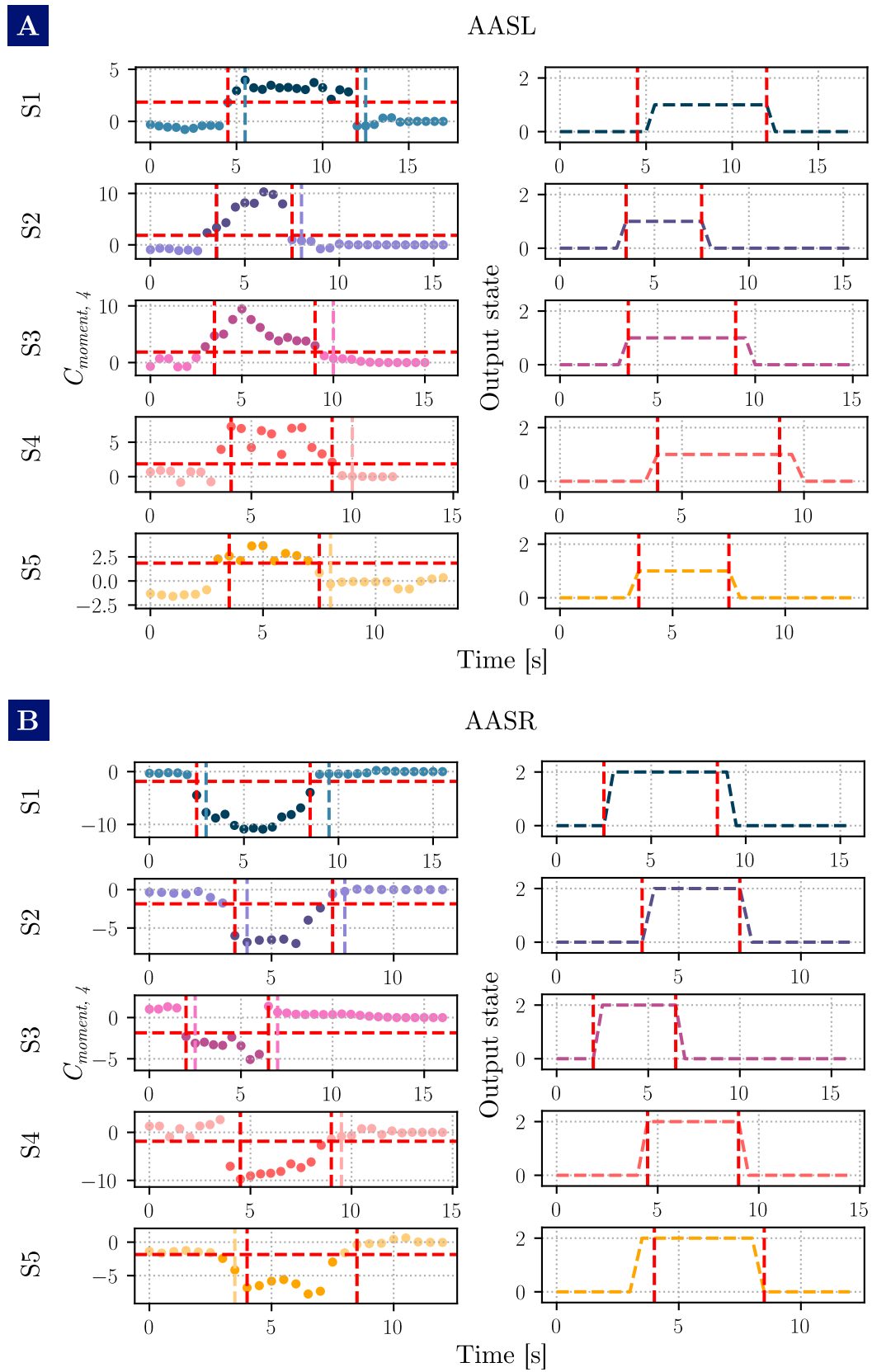


FIGURE 5.11: Results from an offline implementation of a steering detection method based on the asymmetric arm swing strategy, with $f = f_{moment}$ and $\alpha = 4$: A. AASL trials, B. AASR trials. Light and dark colors are used to distinguish between data points above or below a threshold. Dashed lines indicate the first window to be classified into a given state: (1) in red for the manual labels, (2) in light participant color for the implementation output (after two windows have been assigned the same class). When an implementation output corresponds to a manual label, only the latter is indicated.

| | AASL | | | | | | AASR | | | | | |
|---------|-------|-------|-------|------|-------------|-----------|-------|------|-------|-------|-------------|-----------|
| | TP | FP | TN | FN | Start delay | End delay | TP | FP | TN | FN | Start delay | End delay |
| S1 | 93.33 | 0 | 100 | 6.67 | 2 | 1 | 100 | 5 | 95 | 0 | 1 | 2 |
| S2 | 100 | 4.35 | 95.65 | 0 | 0 | 1 | 100 | 0 | 100 | 0 | 1 | 1 |
| S3 | 100 | 10 | 90 | 0 | 0 | 2 | 100 | 0 | 100 | 0 | 1 | 1 |
| S4 | 100 | 13.33 | 86.67 | 0 | 0 | 2 | 100 | 4.76 | 95.24 | 0 | 0 | 1 |
| S5 | 100 | 5.26 | 94.74 | 0 | 0 | 1 | 88.89 | 12.5 | 87.5 | 11.11 | 1 | 0 |
| Average | 98.67 | 6.69 | 93.41 | 1.33 | / | / | 97.78 | 4.45 | 93.55 | 2.22 | / | / |

TABLE 5.2: Window classification rates and delays for the offline implementation of the steering detection method for each participant, and both AASR and AASL trials. Average rate values are also mentioned. Delays are in number of windows, rates are in %. TP: True Positive rate (windows correctly classified as steering); FP: False positive rate (windows incorrectly classified as steering); TN: True Negative rate (windows correctly classified as straight walking); FN: False Negative rate (windows incorrectly classified as straight walking)

5.4 Preliminary online validation with one participant.

5.4.1 Experimental setup

The steering detection method described above was preliminarily tested in one unimpaired male participant aged 27, who was used to walking with the exoskeleton. He was asked to perform 10 5-m walks, where gait termination was controlled based on the arm swing method described in chapter 4. In 5 of the trials (left trials), after having started to walk, the participant was asked to wait for the experimenter's signal to start steering towards the left using the asymmetric arm swing strategy, and resume straight walking on another cue from the experimenter. Similarly, 5 trials (right trials) were conducted with steering towards the right. Before starting the experiment, the participant trained with the steering interface for 4 walks.

Since this was only a preliminary test aiming at evaluating whether the proposed steering detection interface could be effectively implemented online, there were no quantitative analyses of the data, and only false trigger occurrences (falsely detecting one of the walking straight, steering left, or steering right classes when the intention was not expressed) were assessed.

5.4.2 Results and Discussion

Figure 5.12 shows $C_{moment,4}$ values for the left and right trials, and the corresponding output results from the steering detection interface. Note that data recordings stop when the exoskeleton stops walking, which is why individual trials are linked with straight lines. The results show that the participant was able to correctly steer towards the left or right, with no false triggers from the steering interface. However, there was a FN from the gait termination interface during the fourth left trial, and the trial was rerun.

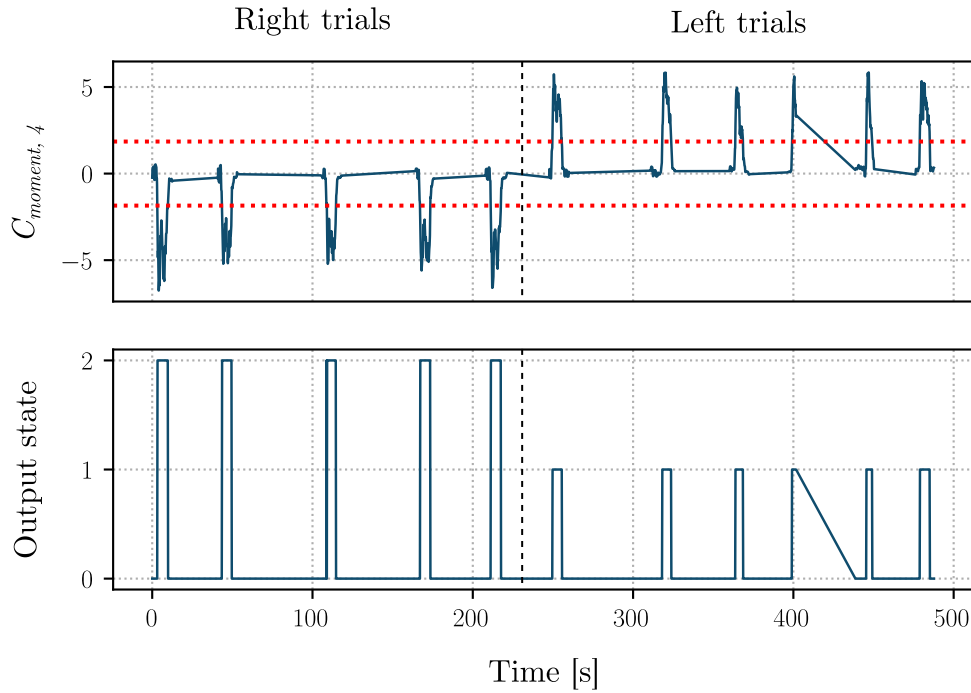


FIGURE 5.12: Results from a preliminary online test of the steering detection interface. The top plot represents the $C_{moment,4}$ values for the individual trials, and the bottom plot shows the corresponding output results. Note that data from the individual trials are linked with straight lines, since recording stop when the exoskeleton is stopped.

Overall, this preliminary test shows promising results that an online implementation of the proposed steering detection interface could be effective at detecting the turning intention in the Atalante exoskeleton.

5.5 | Limitations and prospects of the study.

While the previous section showed promising results for an online implementation of the asymmetric arm swing steering detection method, more experiments need to be conducted on larger cohorts of participants to confirm that the selected feature and threshold value can be generalized to more users, and are not overfit results from the small sample who participated to the exploratory experiment. In this sense, this chapter mainly comes as preliminary work that needs to be further extended to draw general conclusions on the effectiveness of the proposed interface.

Similarly, patients should be involved in any future experiments: while it can be hypothesized that users with good upper-body capabilities could correctly alter their arm swing movements to control steering in the exoskeleton, it might prove more difficult for patients with neurological impairments that also affects the upper limbs. In particular, it can be expected that an active alteration of the arm swing movements could be tiring, and perceived as extra cognitive burden in untrained patients, and that the asymmetry method would be learnt throughout rehabilitation sessions. As was already stated at the end of the previous chapter, a parametrized interface could be implemented to switch between different features or threshold values, which would be adapted as patients progress.

Lastly, the implementation of an effective steering intention detection method is also strongly dependent on how the actual turning movements are implemented in the exoskeleton. Since the Atalante device can only slightly turn by 5° in one step, it highly impacts the way that an effective steering control interface can be developed. In particular, an ideal solution that would solely be based on the trunk being directed towards the new walking direction (without repeated movements) cannot be implemented, since it would affect the balance of the robot, and would provoke a discrepancy between the rotation of the user in the exoskeleton, and the direction towards which the latter is walking. Therefore, while the proposed solution is not based on a natural motion (contrary to the gait initiation and termination solutions evaluated in the previous chapters), it can be easily added to the arm swing-based termination interface, and doesn't need the use of a remote button. Furthermore, it can be hypothesized that the proposed steering detection method could be rapidly learnt by patients with high upper-limb motor capabilities, and become intuitive.

5.6 | Conclusion.

In this chapter, the possibility of implementing a steering detection method on top of the arm-swing-based gait termination interface was investigated through a preliminary exploratory experiment. Two possible solutions were presented: one consisting in continuously rotating the trunk towards the new direction of walk while keeping the arm swing movements going, and the other consisting in altering the arm swing by introducing an asymmetry in the amplitude of movements between the arms. Different parametrized features were derived for each strategy to evaluate the possibility of robustly detecting both the intention and direction of turning based on a single amplitude-based metric. The trunk method wasn't effective at robustly detecting the direction of turn due to individual differences in the IMU signals during straight walking. Conversely, the asymmetric arm swing strategy could be used to predict both the intention and direction of turn, with no false class triggers for both an offline implementation, and a preliminary online test with one participant.

However, further investigations should be conducted to more thoroughly analyze the detection capabilities of the retained method in an online setting, while including patients with different levels of disabilities to ensure that this strategy can be effectively and easily learnt and used in a lower-limb exoskeleton.

Conclusion

| Summary of the thesis.

This thesis work revolved around the development of a high-level controller interface for the detection of motion intentions in a medical lower-limb exoskeleton. It was based on the Atalante device, from the French company Wandercraft, and primarily targeted three possible state transitions or alterations:

- The transition going from the standstill position to walking, namely gait initiation;
- the transition going from walking to the standstill position, namely gait termination;
- and the alteration of the gait pattern to change the direction of walking, namely steering.

One of the main purposes of this work was to develop a novel human-machine interface for the detection intentions related to these states, by providing natural and intuitive means to control the self-balanced lower-limb exoskeleton. In particular, it aimed at detecting transitions between the activity modes of the exoskeleton without having to go through transitioning states, or requiring the use of remote controls. In this context, the control interface was movement-driven, and implemented based on inputs from three Inertial Motion Units (IMUs) worn on the back and the arms of the users. These sensors send acceleration and angular velocity signals that can be analyzed through a classification architecture to indicate whether a specific transition should occur. Therefore, the general paradigm adopted throughout this thesis was to first analyze how some categories of movements could serve as predictive patterns for the detection of given motion intentions, and then build classifiers based on such experimental observations.

Gait Initiation

For the detection of gait initiation, it was shown that anticipatory postural adjustments that occur before heel-off of the swing leg could possibly be preserved in the constrained setting of wearing a lower-limb exoskeleton. In particular, training data gathered from a free walking setting were used to train a supervised learning classifier, that was able to robustly detect the gait initiation intention, while avoiding to trigger the walking state when typical everyday movements were exhibited. This interface could only be tested online with unimpaired participants.

Gait Termination

Instead of focusing on a punctual movement pattern in the IMU data – which could be complex to extract due to the dynamical state of the robot – the gait termination interface was instead implemented through a dead-man switch approach: the walking state is maintained as long as coordinated arm swing movements are exhibited. This strategy was successfully implemented online, with low false negative occurrences, and preliminarily tested with two patients. While these experiments showed that a delay in the termination of gait could be present when relying on this strategy, it is expected that training and the possibility of adapting the parameter values of the control interface could reduce the time necessary to stop the exoskeleton.

Steering

The detection of the steering intention was only preliminarily explored. It was implemented as an additional layer to the gait termination interface, where an asymmetric swing amplitude between the arms was used to indicate both the intention and the direction of walking. It is the only solution that doesn't necessarily rely on natural or intuitive movements, which is mainly due to the way that the Atalante exoskeleton is able to turn. However, offline analysis of IMU signals showed that such a strategy could be effectively used, with no false class trigger occurrences, and a preliminary online test conducted with one participant showed similarly promising results. Nevertheless, this solution needs to be more thoroughly tested, and future experiments should involve patients instead of unimpaired participants.

| Future work.

Ultimately, the methods described above could be implemented together to form a unified high-level control interface for the Atalante exoskeleton, and provide users with seamless means to transition between different states without having to use a remote controller. However, more experiments involving patients need to be conducted to evaluate each of the intention detection methods more thoroughly, and in more ecological settings.

The gait initiation interface could evolve to become more adaptive, and benefit from real usage data to enrich the training base and become even more robust and accurate. For example, it would be possible to provide an implementation where individual users could annotate their own data, and mark occurrences of false positives or negatives so that the classifier continues learning, and becomes more individually curated. Similarly, a user-friendly interface could be provided to allow control of the parameters for the gait termination and steering detection methods, and adapt them as the user gets more training with using their arm swing movements or altering them. However, it is also important to check whether these arm swing-based methods could be sustainable in the long term in terms of physical and cognitive burden, since actively maintained movements are necessary and can be tiring. Note that these methods could also be used in settings other than exoskeleton usage, where human activities such as running or walking at different speeds could be monitored through upper-body movements and arm swing behaviour.

On a separate note, as the Atalante exoskeleton continues evolving, additional movements could be added to its repertoire, and the detection of the corresponding motion intentions could benefit from this work. Recently, the exoskeleton was part of the Cybathlon competition, which required the implementation of additional capabilities, such as walking sideways or backwards. The gait initiation method, based on the detection of precursor movement patterns, could be extended to also predict the future direction of walking. Similarly, a novel method that allows wider turns performed in single steps was implemented. This could provide for a better basis for the study of more natural and intuitive ways to detect the intention of steering.

Lastly, all the intention detection solutions that were developed as part of this thesis solely rely on inputs from three IMUs. However, it might be possible to benefit from other types of sensors which would also be descriptive of upper-body movements. For example, force sensors underneath the feet could be used to get measurements of body weight shifts, which would indirectly be a measure of how the trunk and arms move in the robot. Similarly, pressure sensors around the waist could give precious information about the direction towards which the body might be leaning.

Overall, the proposed high-level control interface shows that it is possible to provide exoskeleton users with more natural and intuitive means to express their

motion intentions. This ultimately paves the road towards a better integration of intention detection methods with the sensory-motor capabilities of patients, and the possibility of making exoskeletal devices true extensions of their bodies.

Bibliography

- Aliman, Norazam, Rizauddin Ramli, and Sallehuddin Mohamed M. Haris (2017). “Design and development of lower limb exoskeletons: A survey”. In: *Robotics and Autonomous Systems* 95, pp. 102–116.
- Anand, Manish, Justin Seipel, and Shirley Rietdyk (2017). “A modelling approach to the dynamics of gait initiation”. In.
- Army Technology (2021a). *Human Universal Load Carrier (HULC)*. URL: <https://www.army-technology.com/projects/human-universal-load-carrier-hulc/> (visited on 03/26/2021).
- (2021b). *Raytheon XOS 2 Exoskeleton, Second-Generation Robotics Suit*. URL: <https://www.army-technology.com/projects/raytheon-xos-2-exoskeleton-us/> (visited on 03/26/2021).
- B-TEMIA (2021). *Keeogo website*. URL: <https://keeogo.com/> (visited on 03/31/2021).
- Banala, Sai K. et al. (2008). “Robot assisted gait training with active leg exoskeleton (ALEX)”. In: *Proceedings of the 2nd Biennial IEEE/RAS-EMBS International Conference on Biomedical Robotics and Biomechatronics, BioRob 2008* 17.1, pp. 653–658.
- Bao, Ling and Stephen S Intille (2004). “Activity Recognition from User-Annotated Acceleration Data”. In: *Pervasive*, pp. 1–17.
- Barbareschi, Giulia et al. (2015). “Statically vs dynamically balanced gait: Analysis of a robotic exoskeleton compared with a human”. In: *Proceedings of the Annual International Conference of the IEEE Engineering in Medicine and Biology Society, EMBS 2015-Novem*, pp. 6728–6731.
- Bartlett, Harrison L. and Michael Goldfarb (2017). “A Phase Variable Approach for IMU-Based Locomotion Activity Recognition”. In: *IEEE Transactions on Biomedical Engineering* 65.6, pp. 1–1.
- Benabid, Alim Louis et al. (2019). “Articles An exoskeleton controlled by an epidural wireless brain – machine interface in a tetraplegic patient : a proof-of-concept demonstration”. In: 4422.19, pp. 1–11.
- Bionik Laboratories Corp. (Aug. 8, 2017). *Bionik Laboratories Corp. Completes Integration of Amazon Echo into its ARKE™ Exoskeleton*. URL: <https://www.prnewswire.com/news-releases/bionik-laboratories-corp-completes-integration-of-amazon-echo-into-its-arke-exoskeleton-300501030.html> (visited on 03/05/2021).
- Bishop, Christopher (2006). “Continuous Latent Variables”. In: *Pattern Recognition and Machine Learning*. 1st ed. New York: Springer-Verlag. Chap. 12, pp. 559–603.

- Bishop, Mark et al. (2004). "The effect of velocity on the strategies used during gait termination". In: *Gait and Posture* 20.2, pp. 134–139.
- Bodenheimer, Bobby et al. (1997). "The Process of Motion Capture: Dealing with the Data". In: *Computer Animation and Simulation '97*. Ed. by Daniel Thalmann and Michiel van de Panne. Vienna: Springer Vienna, pp. 3–18.
- Bouisset, S. and M. Zattara (1987). "Biomechanical study of the programming of anticipatory postural adjustments associated with voluntary movement". In: *J. Biomech.* 20.8, pp. 735–742.
- Bouyer, Laurent J et al. (2014). "Dermoskeletal technology as a means to improve mobility in individuals with multiple sclerosis: a pilot study". In: *Resna*, p. 5.
- Breniere, Y and M C Do (1986). "Technical Note When and How Does Steady State Gait Movement From Upright Posture Begin ?" In: *journal of Biomechanics* 19.12, pp. 1035–1040.
- Brenière, Y and G Dietrich (Feb. 1992). "Heel-off perturbation during gait initiation: biomechanical analysis using triaxial accelerometry and a force plate." In: *Journal of biomechanics* 25.2, pp. 121–7.
- Brenière, Yvon, Manh Cuong Do, and Simon Bouisset (1987). "Are dynamic phenomena prior to stepping essential to walking?" In: *Journal of Motor Behavior* 19.1, pp. 62–76.
- Brenière, Yvon and Manh Cuong Do (1991). "Control of gait initiation". In: *Journal of Motor Behavior* 23.4, pp. 235–240.
- Brigante, Carmen M N et al. (2011). "Towards Miniaturization of a MEMS-Based Wearable Motion Capture System". In: *IEEE Transactions on Industrial Electronics* 58.8.
- Bruijn, Sjoerd M. et al. (2008). "Coordination of leg swing, thorax rotations, and pelvis rotations during gait: The organisation of total body angular momentum". In: *Gait Posture* 27, pp. 455–462.
- Bruijn, Sjoerd M. et al. (2010). "The effects of arm swing on human gait stability". In: *Journal of Experimental Biology* 213.23, pp. 3945–3952.
- Brunt, Denis et al. (Oct. 1999). "Principles underlying the organization of movement initiation from quiet stance". In: *Gait Posture* 10.2, pp. 121–128.
- Calancie, Blair, Stephanie Lutton, and James G. Broton (1996). "Central nervous system plasticity after spinal cord injury in man: Interlimb reflexes and the influence of cutaneous stimulation". In: *Electroencephalography and Clinical Neurophysiology - Electromyography and Motor Control* 101.4, pp. 304–315.
- Carpinella, Ilaria et al. (2010). "Coordination between upper-and lower-limb movements is different during overground and treadmill walking". In: *Eur J Appl Physiol* 108, pp. 71–82.
- Casadio, Maura, Rajiv Ranganathan, and Ferdinando A Mussa-Ivaldi (2012). "The Body-Machine Interface: A new perspective on an old theme". In: *Journal of Motor Behaviour* 44.6, pp. 419–433.
- Castellini, Claudio et al. (2014). "Proceedings of the first workshop on Peripheral Machine Interfaces: going beyond traditional surface electromyography". In: *Comparison of Trunk Activity during Gait Initiation and Walking in Humans*. In: *PLoS ONE* 4.12. Ed. by Jonatan R. Ruiz, e8193.

- Chen, Bing et al. (2016). “Recent developments and challenges of lower extremity exoskeletons”. In: *Journal of Orthopaedic Translation* 5, pp. 26–37.
- Cobb, George L (Aug. 6, 1935). *Walking Motion*. U.S. pat. United States Patent Office.
- Collins, Steven H., Peter G. Adamczyk, and Arthur D. Kuo (2009). “Dynamic arm swinging in human walking”. In: *Proceedings of the Royal Society B: Biological Sciences* 276.1673, pp. 3679–3688.
- Colombo, Gery et al. (2000). “Treadmill training of paraplegic patients using a robotic orthosis”. In: *Journal of Rehabilitation Research and Development* 37.6, pp. 693–700.
- Courtine, Grégoire and Marco Schieppati (2004). “Tuning of a Basic Coordination Pattern Constructs Straight-Ahead and Curved Walking in Humans”. In: *Journal of Neurophysiology* 91.4, pp. 1524–1535.
- Cramer, Steven C. and Jeff D. Riley (2008). “Neuroplasticity and brain repair after stroke”. In: *Current Opinion in Neurology* 21.1, pp. 76–82.
- Cyberdyne (2021a). *Cyberdyne website*. URL: <https://www.cyberdyne.jp/english/> (visited on 03/26/2021).
- (2021b). *HAL for Medical Use*. URL: https://www.cyberdyne.jp/english/products/LowerLimb_medical.html (visited on 03/31/2021).
- Dietz, Volker (1997). “Neurophysiology of gait disorders: Present and future applications”. In: *Electroencephalography and Clinical Neurophysiology* 103.3, pp. 333–355.
- (2002a). “Do human bipeds use quadrupedal coordination?” In: *TRENDS in Neurosciences* 25.9.
- (2002b). “Proprioception and locomotor disorders”. In: *Nature Reviews Neuroscience* 3.10, pp. 781–790.
- (Aug. 2011). “Quadrupedal coordination of bipedal gait: Implications for movement disorders”. In: *Journal of Neurology* 258.8, pp. 1406–1412.
- Dietz, Volker and Susan J Harkema (2013). “Locomotor activity in spinal cord-injured persons Neural Control of Movement Locomotor activity in spinal cord-injured persons”. In: *Journal of applied physiology* 96, pp. 1954–1960.
- Dollar, Aaron M. and Hugh Herr (2008). “Lower extremity exoskeletons and active orthoses: Challenges and state-of-the-art”. In: *IEEE Transactions on Robotics* 24.1, pp. 144–158.
- Donker, S. et al. (2002). “Adaptations in arm movements for added mass to wrist or ankle during walking”. In: *Experimental Brain Research* 146.1, pp. 26–31.
- Duschau-Wicke, Alexander et al. (2010). “Path control: A method for patient-cooperative robot-aided gait rehabilitation”. In: *IEEE Transactions on Neural Systems and Rehabilitation Engineering* 18.1, pp. 38–48.
- Duysens, J and H W A A Van de Crommert (1998). “Neural control of locomotion; Part 1: The central pattern generator from cats to humans”. In: *Gait and Posture* 7.2, pp. 131–141.
- Eke-Okoro, S. T., M. Gregoric, and L. E. Larsson (1997). “Alterations in gait resulting from deliberate changes of arm-swing amplitude and phase”. In: *Clinical Biomechanics* 12.7-8, pp. 516–521.
- Ekso Bionics (2021). *Ekso Bionics website*. URL: <https://eksobionics.com/> (visited on 03/26/2021).

- Elble, Rodger J. et al. (Oct. 2004). "The initiation of normal walking". In: *Movement Disorders* 9.2, pp. 139–146.
- Elftman, Herbert (1939). "The function of the arms in walking". In: *Human biology* 11.4, p. 529.
- Esquenazi, Alberto et al. (2012). "The Rewalk powered exoskeleton to restore ambulatory function to individuals with thoracic-level motor-complete spinal cord injury". In: *American Journal of Physical Medicine and Rehabilitation* 91.11, pp. 911–921.
- Farkhatdinov, Ildar, Nicolas Roehri, and Etienne Burdet (2017). "Anticipatory detection of turning in humans for intuitive control of robotic mobility assistance". In: *Bioinspiration & Biomimetics* 12.5.
- Farris, Ryan J., Hugo A. Quintero, and Michael Goldfarb (Dec. 2011). "Preliminary evaluation of a powered lower limb orthosis to aid walking in paraplegic individuals". In: *IEEE Transactions on Neural Systems and Rehabilitation Engineering* 19.6, pp. 652–659.
- Ferris, Daniel P., Helen J. Huang, and Pei Chun Kao (2006). "Moving the arms to activate the legs". In: *Exercise and Sport Sciences Reviews* 34.3, pp. 113–120.
- Fick, Bruce R. and John B. Makinson (1971). *Final Report on Hardiman I Prototype for Machine Augmentation of Human Strength and Endurance*. Tech. rep. Work Unit Number NR 196-049. General Electric Company, p. 18.
- Filippi, Pietro (Dec. 15, 1942). "Device for the automatic control of the articulation of the knee applicable to a prosthesis of the thigh". U.S. pat. 2,305,291. United States Patent Office.
- Fisher, R A (1936). "The use of multiple measurements in taxonomic problems". In: *Annals of Eugenics* 7.2, pp. 179–188.
- Ford, Matthew P., Robert C. Wagenaar, and Karl M. Newell (2007). "Phase manipulation and walking in stroke". In: *Journal of Neurologic Physical Therapy* 31.2, pp. 85–91.
- Fourati, Nesrine and Catherine Pelachaud (2013). "Head, Shoulders and Hips Behaviors during Turning". In: *Lecture Notes in Computer Science*. Vol. 8212. January 2014.
- Fukuda, Yuto, Kei Masani, and Takeshi Yamaguchi (2020). "Comparison of lower limb joint moment and power during turning gait between young and old adults using hierarchical Bayesian inference". In: *Journal of Biomechanics* 103, p. 109702.
- Gancet, Jeremi et al. (2012). "MINDWALKER: Going one step further with assistive lower limbs exoskeleton for SCI condition subjects". In: *Proceedings of the IEEE RAS and EMBS International Conference on Biomedical Robotics and Biomechatronics* 2010, pp. 1794–1800.
- Gardner, Amy D., Johan Potgieter, and Frazer K. Noble (2017). "A review of commercially available exoskeletons' capabilities". In: *2017 24th International Conference on Mechatronics and Machine Vision in Practice, M2VIP 2017* 2017-Decem, pp. 1–5.
- Glaister, Brian C. et al. (2007). "Video task analysis of turning during activities of daily living". In: *Gait and Posture* 25.2, pp. 289–294.
- El-Gohary, Mahmoud et al. (2014). "Continuous monitoring of turning in patients with movement disability". In: *Sensors (Switzerland)* 14.1, pp. 356–369.

- Goudriaan, Marije et al. (2014). *Arm swing in human walking: What is their drive?*
- Grasso, Renato et al. (1998). “Eye-head coordination for the steering of locomotion in humans: an anticipatory synergy”. In: *Neuroscience Letters* 253.2, pp. 115–118.
- Griffin, Robert et al. (2017). “Stepping Forward with Exoskeletons”. In: Gurriet, Thomas et al. (May 2018). “Towards Restoring Locomotion for Paraplegics: Realizing Dynamically Stable Walking on Exoskeletons”. In: *2018 IEEE International Conference on Robotics and Automation (ICRA)*. IEEE, pp. 2804–2811.
- Halliday, Suzanne E et al. (Aug. 1998). “The initiation of gait in young, elderly, and Parkinson’s disease subjects”. In: *Gait Posture* 8.1, pp. 8–14.
- Harib, Omar et al. (Dec. 2018). “Feedback Control of an Exoskeleton for Paraplegics: Toward Robustly Stable, Hands-Free Dynamic Walking”. In: *IEEE Control Systems* 38.6, pp. 61–87.
- Hariharan, G (2019). “Wavelet Analysis—An Overview”. In: *Wavelet Solutions for Reaction–Diffusion Problems in Science and Engineering*. Singapore: Springer Singapore, pp. 15–31.
- Harper, Douglas (2021). *Exoskeleton*. In: *Online Etymology Dictionary*. URL: <https://www.etymonline.com/word/exoskeleton> (visited on 03/10/2021).
- Hase, K. and R. B. Stein (1998). “Analysis of rapid stopping during human walking”. In: *Journal of Neurophysiology* 80.1, pp. 255–261.
- (1999). “Turning strategies during human walking”. In: *Journal of Neurophysiology* 81.6, pp. 2914–2922.
- Hastie, Trevor, Robert Tibshirani, and Jerome Friedman (2001). *The Elements of Statistical Learning*. Springer Series in Statistics. New York, NY, USA: Springer New York Inc.
- He, Yong et al. (2019). “Development of a novel autonomous lower extremity exoskeleton robot for walking assistance”. In: *Frontiers of Information Technology and Electronic Engineering* 20.3, pp. 318–329.
- Herr, Hugh (2009). “Exoskeletons and orthoses: Classification, design challenges and future directions”. In: *Journal of NeuroEngineering and Rehabilitation* 6.1.
- Hicheur, Halim and Alain Berthoz (2005). “How do humans turn? Head and body movements for the steering of locomotion”. In: *Proceedings of 2005 5th IEEE-RAS International Conference on Humanoid Robots 2005*, pp. 265–270.
- Hollands, M., K. Sorensen, and A. Patla (2001). “Effects of head immobilization on the coordination and control of head and body reorientation and translation during steering”. In: *Experimental Brain Research* 140.2, pp. 223–233.
- Huo, Weiguang et al. (2016). “Lower Limb Wearable Robots for Assistance and Rehabilitation: A State of the Art”. In: *IEEE Systems Journal* 10.3, pp. 1068–1081.
- Jaeger, R. J. and Vanitchachavan P. (1992). “Ground reaction forces during termination of human gait”. In: *J. Biomech.* 25.10, pp. 1233–1236.
- Jian, Yuancheng et al. (1993). “Trajectory of the body COG and COP during initiation and termination of gait”. In: *Gait Posture* 1.1, pp. 9–22.
- Kagawa, Takahiro and Yoji Uno (2009). “A human interface for stride control on a wearable robot”. In: *2009 IEEE/RSJ International Conference on Intelligent Robots and Systems, IROS 2009* 1, pp. 4067–4072.

- Kang, Yi et al. (2017). “Epidemiology of worldwide spinal cord injury: a literature review”. In: *Journal of Neurorestoratology* Volume 6, pp. 1–9.
- Karantonis, Dean M. et al. (2006). “Implementation of a real-time human movement classifier using a triaxial accelerometer for ambulatory monitoring”. In: *IEEE Transactions on Information Technology in Biomedicine* 10.1, pp. 156–167.
- Kawamoto, Hiroaki et al. (2003). “Power assist method for HAL-3 using EMG-based feedback controller”. In: *Proceedings of the IEEE International Conference on Systems, Man and Cybernetics* 2, pp. 1648–1653.
- Kazerooni, H. (2021). *Berkeley Robotics & Human Engineering Laboratory website*. URL: <https://bleex.me.berkeley.edu/research/exoskeleton> (visited on 03/26/2021).
- Kazerooni, H. et al. (2005). “On the control of the Berkeley Lower Extremity Exoskeleton (BLEEX)”. In: *Proceedings - IEEE International Conference on Robotics and Automation*. Vol. 2005, pp. 4353–4360.
- Kelley, Leslie C. (July 1, 1919). “Pedomotor”. U.S. pat. 1,308,675. United States Patent Office.
- Kilicarslan, Atilla et al. (2013). “High accuracy decoding of user intentions using EEG to control a lower-body exoskeleton”. In: *Proceedings of the Annual International Conference of the IEEE Engineering in Medicine and Biology Society, EMBS*, pp. 5606–5609.
- Killeen, Tim et al. (2018). “Arm swing asymmetry in overground walking”. In: *Scientific Reports* 8.1, pp. 1–10.
- Kolakowsky-Hayner, Stephanie A (2013). “Safety and Feasibility of using the EksoTM Bionic Exoskeleton to Aid Ambulation after Spinal Cord Injury”. In: *Journal of Spine*.
- Kong, Kyoungchul and Doyoung Jeon (2006). “Design and control of an exoskeleton for the elderly and patients”. In: *IEEE/ASME Transactions on Mechatronics* 11.4, pp. 428–432.
- Kristoffersen, Morten B. et al. (Oct. 2019). “The Effect of Feedback During Training Sessions on Learning Pattern-Recognition-Based Prosthesis Control”. In: *IEEE Transactions on Neural Systems and Rehabilitation Engineering* 27.10, pp. 2087–2096.
- Kumar, Ramesh et al. (2018). “Traumatic Spinal Injury: Global Epidemiology and Worldwide Volume”. In: *World Neurosurgery* 113, e345–e363.
- Kwa, Hian Kai et al. (2009). “Development of the IHMC mobility assist exoskeleton”. In: *Proceedings - IEEE International Conference on Robotics and Automation*, pp. 2556–2562.
- Lee, Hao, Peter Walker Ferguson, and Jacob Rosen (2020). *Lower Limb Exoskeleton Systems—Overview*. INC, pp. 207–229.
- Lemaire, Edward D. et al. (2017). “Lower extremity robotic exoskeleton training: Case studies for complete spinal cord injury walking”. In: *NeuroRehabilitation* 41.1, pp. 97–103.
- Lepers, R. and Y. Brenière (Nov. 1995). “The role of anticipatory postural adjustments and gravity in gait initiation”. In: *Experimental Brain Research* 107.1, pp. 118–124.

- Lewek, Michael D. et al. (Aug. 2009). “Allowing intralimb kinematic variability during locomotor training poststroke improves kinematic consistency: A subgroup analysis from a randomized clinical trial”. In: *Physical Therapy* 89.8, pp. 829–839.
- Li, Tao, Shenghuo Zhu, and Mitsunori Ogihara (Oct. 2006). “Using discriminant analysis for multi-class classification: an experimental investigation”. In: *Knowledge and Information Systems* 10.4, pp. 453–472.
- Lobo-Prat, Joan et al. (2014). “Evaluation of EMG, force and joystick as control interfaces for active arm supports”. In: *Journal of NeuroEngineering and Rehabilitation* 11.1.
- Lünenburger, Lars et al. (2007). “Combining immersive virtual environments with robot-aided gait training”. In: *2007 IEEE 10th International Conference on Rehabilitation Robotics, ICORR’07* 00.c, pp. 421–424.
- Mahony, Robert, Tarek Hamel, and Jean Michel Pflimlin (2008). “Nonlinear complementary filters on the special orthogonal group”. In: *IEEE Transactions on Automatic Control* 53.5, pp. 1203–1218.
- Makinson, John B. (1971). *Research and Development Prototype for Machine Augmentation of Human Strength and Endurance - Hardiman I Project*. Tech. rep. Work Unit Number NR 196-049. General Electric Company, p. 25.
- Mancini, M. et al. (2009). “Anticipatory postural adjustments prior to step initiation are hypometric in untreated Parkinson’s disease: An accelerometer-based approach”. In: *European Journal of Neurology* 16.9, pp. 1028–1034.
- Mancini, Martina et al. (2016). “Validity and reliability of an IMU-based method to detect APAs prior to gait initiation”. In: *Gait and Posture* 43, pp. 125–131. eprint: [15334406](#).
- Mariani, Benoit et al. (2010). “3D gait assessment in young and elderly subjects using foot-worn inertial sensors”. In: *Journal of Biomechanics* 43.15, pp. 2999–3006.
- Mariani, Benoit et al. (2013). “On-shoe wearable sensors for gait and turning assessment of patients with parkinson’s disease”. In: *IEEE Transactions on Biomedical Engineering* 60.1, pp. 155–158.
- Martinez-Mendez, Rigoberto, Masaki Sekine, and Toshiyo Tamura (Apr. 2011). “Detection of anticipatory postural adjustments prior to gait initiation using inertial wearable sensors”. In: *Journal of NeuroEngineering and Rehabilitation* 8.1, p. 17.
- McLeod, Jonathan C., Susie J.M. Ward, and Audrey L. Hicks (2019). “Evaluation of the Keeogo™ Dermoskeleton”. In: *Disability and Rehabilitation: Assistive Technology* 14.5, pp. 503–512.
- Meyns, Pieter, Sjoerd M. Bruijn, and Jacques Duysens (2013). “The how and why of arm swing during human walking”. In: *Gait and Posture* 38.4, pp. 555–562.
- Millán, J. D.R. et al. (2010). “Combining brain-computer interfaces and assistive technologies: State-of-the-art and challenges”. In: *Frontiers in Neuroscience* 4.SEP, pp. 1–15.
- Mizen, Neil J. (1963). *Preliminary Design of a Full-scale, Wearable, Exoskeletal Structure*. Tech. rep. VO-1692-V-2. Buffalo, NY, USA: Cornell Aeronautic Laboratory.

- Mizen, Neil J. (1964). *Design and test of a full-scale, wearable, exoskeletal structure*. Tech. rep. VO-1692-V-3. Buffalo, NY, USA: Cornell Aeronautic Laboratory, pp. 1–65.
- (June 17, 1969). “Powered Exoskeleton Apparatus for Amplifying Human Strength in Response To Normal Body Movements”. U.S. pat. 3,499,769. United States Patent Office.
- Molteni, Franco et al. (2017). “Wearable robotic exoskeleton for overground gait training in sub-acute and chronic hemiparetic stroke patients: preliminary results”. In: *European journal of physical and rehabilitation medicine* 53.5, pp. 676–684.
- Mosher, Ralph S. (1967). “Handyman to Hardiman”. In: *SAE Technical Papers*.
- Murphy, John H (Nov. 6, 1951). “Leg Brace”. U.S. pat. 2,573,866. United States Patent Office.
- Novak, Domen and Robert Riener (2015). “A survey of sensor fusion methods in wearable robotics”. In: *Robotics and Autonomous Systems* 73, pp. 155–170.
- Novak, Domen et al. (Dec. 2013). “Automated detection of gait initiation and termination using wearable sensors”. In: *Medical Engineering & Physics* 35.12, pp. 1713–1720.
- Novak, Domen et al. (Oct. 2014). “Toward Real-Time Automated Detection of Turns during Gait Using Wearable Inertial Measurement Units”. In: *Sensors* 14.10, pp. 18800–18822.
- O’Kane, Francis W., Chris A. McGibbon, and David E. Krebs (2003). “Kinetic analysis of planned gait termination in healthy subjects and patients with balance disorders”. In: *Gait and Posture* 17.2, pp. 170–179.
- St-Onge, Nancy and Anatol G. Feldman (2003). “Interjoint coordination in lower limbs during different movements in humans”. In: *Experimental Brain Research* 148.2, pp. 139–149.
- Orendurff, Michael S. et al. (2006). “The kinematics and kinetics of turning: Limb asymmetries associated with walking a circular path”. In: *Gait and Posture* 23.1, pp. 106–111.
- Oxford University Press (2021). *Exoskeleton*. In: *Oxford Advanced Learner’s Dictionary*. URL: <https://www.oxfordlearnersdictionaries.com/definition/english/exoskeleton> (visited on 03/10/2021).
- Pai, Yi Chung and James Patton (1997). “Center of mass velocity-position predictions for balance control”. In: *Journal of Biomechanics* 30.4, pp. 347–354.
- Palermo, E. et al. (2014). “Experimental evaluation of indoor magnetic distortion effects on gait analysis performed with wearable inertial sensors”. In: *Physiological Measurement* 35.3, pp. 399–415.
- Parker Hanifin Corporation (2021). *Indego*. URL: <http://www.indego.com/indego/us/en/home> (visited on 03/31/2021).
- Patchay, Sandhiran, Yves Gahéry, and Georges Serratrice (Mar. 2002). “Early postural adjustments associated with gait initiation and age-related walking difficulties”. In: *Movement Disorders* 17.2, pp. 317–326.
- Patla, Aftab E., Allan Adkin, and Tonya Ballard (1999). “Online steering: Coordination and control of body center of mass, head and body reorientation”. In: *Experimental Brain Research* 129.4, pp. 629–634.

- Patla, Aftab E. et al. (1991). “Visual control of locomotion: strategies for changing direction and for gait”. In: *Journal of Experimental Psychology: Human perception and performance* 17.3, pp. 603–634.
- Patla, A. et al. (2015). “Normative data for arm swing asymmetry: How (a)symmetrical are we?” In: *Gait and Posture* 41.1, pp. 13–18.
- Pons, José L. (2008). “Human-robot cognitive interaction”. In: *Wearable Robots: Biomechatronic Exoskeletons*. John Wiley & Sons. Chap. 4, pp. 87–125.
- Pons, José L. et al. (2013). “Principles of human locomotion: A review”. In: *Proceedings of the Annual International Conference of the IEEE Engineering in Medicine and Biology Society, EMBS*, pp. 6941–6944.
- Preece, Stephen J et al. (2009a). “A comparison of feature extraction methods for the classification of dynamic activities from accelerometer data”. In: *IEEE Trans Biomed Eng* 56.3, pp. 871–879.
- Preece, Stephen J et al. (2009b). “Activity identification using body-mounted sensors—a review of classification techniques”. In: *Physiol. Meas* 30, pp. 1–33.
- Prince, F. et al. (1994). “Anticipatory control of upper body balance during human locomotion”. In: *Gait and Posture* 2.1, pp. 19–25.
- Punt, Michiel et al. (2015). “Effect of arm swing strategy on local dynamic stability of human gait”. In: *Gait and Posture* 41.2, pp. 504–509.
- Quintero, Hugo A., Ryan J. Farris, and Michael Goldfarb (2011). “Control and Implementation of a powered lower limb orthosis to aid walking in paraplegic individuals”. In: *2011 IEEE International Conference on Rehabilitation Robotics*, pp. 1–6.
- Reberšek, Peter et al. (2011). “Intention detection during gait initiation using supervised learning”. In: *IEEE-RAS International Conference on Humanoid Robots*, pp. 34–39.
- Rehman, Rana Zia Ur et al. (2020). “Turning detection during gait: Algorithm validation and influence of sensor location and turning characteristics in the classification of parkinson’s disease”. In: *Sensors (Switzerland)* 20.18, pp. 1–24.
- Reswick, James B. (1972). “Development of Feedback Control Prosthetic and Orthotic Devices”. In: *Advances in Biomedical Engineering*, pp. 139–217.
- Reswick, James B. and L. Vodovnik (1967). “External power in prosthetics and orthotics, an overview.” In: *Artificial limbs* 11.2, pp. 5–21.
- ReWalk Robotics Ltd. (2021). *Rewalk website*. URL: <https://rewalk.com/> (visited on 03/31/2021).
- REX Bionics (2021). *REX Bionics website*. URL: <https://www.rexbionics.com/> (visited on 03/31/2021).
- Riener, Robert et al. (2010). “Locomotor training in subjects with sensori-motor deficits: An overview of the robotic gait orthosis Lokomat”. In: *Journal of Healthcare Engineering* 1.2, pp. 197–216.
- Rocchi, Laura et al. (2006). “Dependence of anticipatory postural adjustments for step initiation on task movement features: A study based on dynamometric and accelerometric data”. In: *Annual International Conference of the IEEE Engineering in Medicine and Biology - Proceedings*, pp. 1489–1492.

- Rum, Lorenzo et al. (2017). “Upper body accelerations during planned gait termination in young and older women”. In: *Journal of Biomechanics* 65, pp. 138–144.
- Rum, Lorenzo et al. (2019). “Age-related changes in upper body contribution to braking forward locomotion in women”. In: *Gait and Posture* 68.November 2018, pp. 81–87.
- Salgado, Cátia M et al. (2016). “Noise Versus Outliers”. In: *Secondary Analysis of Electronic Health Records*. Cham: Springer International Publishing, pp. 163–183.
- Sankai, Yoshiyuki (2010). “HAL: Hybrid assistive limb based on cybernics”. In: *Springer Tracts in Advanced Robotics* 66.STAR, pp. 25–34.
- Schönauer, Christian, Thomas Pintaric, and Hannes Kaufmann (2012). “Full Body Motion Capture - A Flexible Marker Based Solution”. In: *Proceedings of Workshop on Accessibility Engineering with user models, simulation and VR*. Talk: Joint Virtual Reality Conference (JVRC 2011), Nottingham, UK; 2011-09-20 – 2011-09-21.
- Schütz, Anja (2012). *Robotic exoskeleton: For a better quality of life*. URL: https://www.maxongroup.com/medias/sys_master/8808028438558.pdf (visited on 03/05/2021).
- Segal, Ava D. et al. (2008). “Local dynamic stability in turning and straight-line gait”. In: *Journal of Biomechanics* 41.7, pp. 1486–1493.
- Sekine, Masaki et al. (2013). “A gait abnormality measure based on root mean square of trunk acceleration”. In: *Journal of NeuroEngineering and Rehabilitation* 10.1, pp. 4–8.
- Seymour, Wendy (Feb. 1998). *Remaking the Body*. Routledge.
- Skorzewski, Comte Vladimir (July 28, 1904). “Apparatus for facilitating walking or running”. British pat. 190414477A (GB).
- Šljapah, S., R. Kamnik, and M. Munih (2014). “Kinematics based sensory fusion for wearable motion assessment in human walking”. In: *Computer Methods and Programs in Biomedicine* 116.2, pp. 131–144.
- Song, Joeeun et al. (2012). “Altered dynamic postural control during step turning in persons with early-stage Parkinson’s disease”. In: *Parkinson’s Disease* 2012.
- Sparrow, W. A. and Oren Tirosh (2005). “Gait termination: A review of experimental methods and the effects of ageing and gait pathologies”. In: *Gait and Posture* 22.4, pp. 362–371.
- Spildooren, Joke et al. (2013). “Head-pelvis coupling is increased during turning in patients with Parkinson’s disease and freezing of gait”. In: *Movement Disorders* 28.5, pp. 619–625.
- Sreenivasa, Manish N. et al. (2008). “Walking along curved paths of different angles: The relationship between head and trunk turning”. In: *Experimental Brain Research* 191.3, pp. 313–320.
- St. Paul Daily Globe (Dec. 10, 1889). “A Walking Machine”. In: *St. Paul Daily Globe*.
- Stephenson, Jennifer L, Anouk Lamontagne, and Sophie J De Serres (2008). “The coordination of upper and lower limb movements during gait in healthy and stroke individuals”. In: *Gait & Posture* 29.1.

- Strausser, Katherine A. and H. Kazerooni (2011). "The development and testing of a human machine interface for a mobile medical exoskeleton". In: *IEEE International Conference on Intelligent Robots and Systems*, pp. 4911–4916.
- Strike, Siobhan C. and Matthew J.D. Taylor (2009). "The temporal-spatial and ground reaction impulses of turning gait: Is turning symmetrical?" In: *Gait and Posture* 29.4, pp. 597–602.
- Suzuki, K. et al. (2005). "Intention-based walking support for paraplegia patient". In: *Conference Proceedings - IEEE International Conference on Systems, Man and Cybernetics* 3, pp. 2707–2713.
- Tadano, Shigeru, Ryo Takeda, and Hiroaki Miyagawa (July 2013). "Three Dimensional Gait Analysis Using Wearable Acceleration and Gyro Sensors Based on Quaternion Calculations". In: *Sensors* 13.7, pp. 9321–9343.
- Tao, Weijun et al. (Feb. 2012). "Gait Analysis Using Wearable Sensors". In: *Sensors* 12.2, pp. 2255–2283.
- Tariq, Madiha, Pavel M. Trivailo, and Milan Simic (Aug. 2018). "EEG-Based BCI Control Schemes for Lower-Limb Assistive-Robots". In: *Frontiers in Human Neuroscience* 12, p. 312.
- Taylor, M. J.D., P. Dabnichki, and S. C. Strike (2005). "A three-dimensional biomechanical comparison between turning strategies during the stance phase of walking". In: *Human Movement Science* 24.4, pp. 558–573.
- Tester, Nicole J et al. (2012). "Arm and leg coordination during treadmill walking in individuals with motor incomplete spinal cord injury: A preliminary study". In: *Gait Posture* 36, pp. 49–55.
- Tirosh, Oren and W. A. Sparrow (2004). "Gait termination in young and older adults: Effects of stopping stimulus probability and stimulus delay". In: *Gait and Posture* 19.3, pp. 243–251.
- Torres-Oviedo, Gelsy and Lena H. Ting (2010). "Subject-specific muscle synergies in human balance control are consistent across different biomechanical contexts". In: *Journal of Neurophysiology* 103.6, pp. 3084–3098.
- Tsukahara, Atsushi et al. (2010). "Sit-to-stand and stand-to-sit transfer support for complete paraplegic patients with robot suit HAL". In: *Advanced Robotics* 24.11, pp. 1615–1638.
- Tucker, Michael R. et al. (2015). "Control strategies for active lower extremity prosthetics and orthotics: A review". In: *Journal of NeuroEngineering and Rehabilitation* 12.1.
- Tunca, Can et al. (2017). "Inertial sensor-based robust gait analysis in non-hospital settings for neurological disorders". In: *Sensors (Switzerland)* 17.4, pp. 1–29.
- Umberger, Brian R. (2008). "Effects of suppressing arm swing on kinematics, kinetics, and energetics of human walking". In: *Journal of Biomechanics* 41.11, pp. 2575–2580.
- Van Emmerik, Richard E. A., Robert C. Wagenaar, and Erwin E. H. Van Wegen (Nov. 1998). "Interlimb Coupling Patterns in Human Locomotion: Are We Bipedes or Quadrupeds?" In: *Annals of the New York Academy of Sciences* 860.1 NEURONAL MECH, pp. 539–542.
- Veneman, Jan F. et al. (Sept. 2007). "Design and evaluation of the LOPES exoskeleton robot for interactive gait rehabilitation". In: *IEEE Transactions on Neural Systems and Rehabilitation Engineering* 15.3, pp. 379–386.

- Viteckova, Slavka, Patrik Kutilek, and Marcel Jirina (2013). “Wearable lower limb robotics: A review”. In: *Integrative Medicine Research* 33, pp. 96–105.
- Vouga, Tristan et al. (2017). “TWIICE - A lightweight lower-limb exoskeleton for complete paraplegics”. In: *IEEE International Conference on Rehabilitation Robotics*, pp. 1639–1645.
- Vukobratović, Miomir et al. (1990). “Realization of Anthropomorphic Mechanisms”. In: *Biped Locomotion*. Ed. by Springer-Verlag. Vol. 7. Scientific Fundamentals of Robotics. Berlin. Chap. 4, pp. 316–345.
- Wagenaar, R C and R E A Van Emmerik (2000). “Resonant frequencies of arms and legs identify different walking patterns”. In: *Journal of Biomechanics* 33, pp. 853–861.
- Wandercraft (2021). *Wandercraft website*. URL: <https://www.wandercraft.eu/> (visited on 05/05/2021).
- Wang, Jiacun et al. (July 2019). “Finite State Machine”. In: *Formal Methods in Computer Science*. Chapman and Hall/CRC, pp. 33–54.
- Wang, Shiqian et al. (2015). “Design and Control of the MINDWALKER Exoskeleton”. In: *IEEE Transactions on Neural Systems and Rehabilitation Engineering* 23.2, pp. 277–286.
- Wannier, Thierry et al. (2001). “Arm to leg coordination in humans during walking, creeping and swimming activities”. In: *Experimental Brain Research*.
- Wentink, E.C. et al. (Feb. 2013). “Intention detection of gait initiation using EMG and kinematic data”. In: *Gait Posture* 37.2, pp. 223–228.
- Wentink, E.C. et al. (Jan. 2014). “Detection of the onset of gait initiation using kinematic sensors and EMG in transfemoral amputees”. In: *Gait Posture* 39.1, pp. 391–396.
- Winter, David A., Gordon K. Ruder, and Colum D. MacKinnon (1990). “Control of Balance of Upper Body During Gait”. In: *Multiple Muscle Systems*. Springer New York, pp. 534–541.
- Wolpaw, Jonathan and Elizabeth Winter Wolpaw (2012). *Brain-computer interfaces: principles and practice*. OUP USA.
- World Health Organization (2021). *Spinal Cord Injury*. URL: <https://www.who.int/news-room/fact-sheets/detail/spinal-cord-injury> (visited on 03/31/2021).
- x-io Technologies (2021). *x-io Technologies website*. URL: <https://x-io.co.uk> (visited on 05/12/2021).
- Xu, Dongfang, Xiuhua Liu, and Qining Wang (2019). “Knee Exoskeleton Assistive Torque Control Based on Real-Time Gait Event Detection”. In: *IEEE Transactions on Medical Robotics and Bionics* 1.3, pp. 158–168.
- Yagn, Nicholas (July 2, 1889). “Apparatus to facilitate walking and running”. U.S. pat. 406,328. United States Patent Office.
- (Jan. 28, 1890a). “Apparatus for facilitating walking, running, and jumping”. U.S. pat. 420,178. United States Patent Office.
- (Nov. 18, 1890b). “Apparatus for facilitating walking, running, and jumping”. U.S. pat. 440,684. United States Patent Office.
- (Jan. 28, 1890c). “Apparatus for facilitating walking, running, and jumping”. U.S. pat. 420,179. United States Patent Office.

- Yan, Tingfang et al. (2015). “Review of assistive strategies in powered lower-limb orthoses and exoskeletons”. In: *Robotics and Autonomous Systems* 64, pp. 120–136.
- Yang, Wen Chieh et al. (2016). “Motion analysis of axial rotation and gait stability during turning in people with Parkinson’s disease”. In: *Gait and Posture* 44, pp. 83–88.
- Young, Aaron J. and Daniel P. Ferris (2017). “State of the art and future directions for lower limb robotic exoskeletons”. In: *IEEE Transactions on Neural Systems and Rehabilitation Engineering* 25.2, pp. 171–182.
- Zanotto, D, P Stegall, and S Agrawal (2013). “ALEX III: A Novel Robotic Platform for Gait Training”. In: *IEEE Intl. Conference on Robotics and Automation*, pp. 3914–3919.
- Zeilig, Gabi et al. (2012). “Safety and tolerance of the ReWalk™ exoskeleton suit for ambulation by people with complete spinal cord injury: A pilot study”. In: *Journal of Spinal Cord Medicine* 35.2, pp. 96–101.
- Zographos, S. et al. (2001). “Experimental study of the subtalar joint axis: Preliminary investigation”. In: *Surgical and Radiologic Anatomy* 22.5-6, pp. 271–276.
- Zoss, Adam, H. Kazerooni, and Andrew Chu (2005). “On the mechanical design of the Berkeley Lower Extremity Exoskeleton (BLEEX)”. In: *2005 IEEE/RSJ International Conference on Intelligent Robots and Systems, IROS*, pp. 3465–3472.
- Zwipp, Hans and Thorsten Randt (1994). “Ankle joint biomechanics”. In: *Foot and Ankle Surgery* 1.1, pp. 21–27.

